CHM7016W: DISSERTATION FOR THE DEGREE OF MASTER OF SCIENCE IN MEDICINE IN CARDIOTHORACIC SURGERY

The design and prototyping of a Transcatheter Aortic Valve Implantation training system specific for aortic valve regurgitation.

Prepared by:

Fadi Nkoma Fakih (NKMFAD001)

Supervisor : Dr.Chima Ofoegbu
Co-supervisor: Prof. Deon Bezuidenhout

Dissertation/Thesis/Project submitted in fulfilment of the requirements for the degree of "Master of Science in Medicine"

Department of Surgery
Division of Cardiothoracic Surgery
Faculty of Health Sciences
University of Cape Town, Private Bag Rondebosch, 7700
South Africa 7700

Declaration

Plagiarism Declaration

1. I know that plagiarism is wrong. Plagiarism is using another's work and pretending it is one's own.
2. I have used the Harvard Convention for citation and referencing. Each significant contribution to and quotation in this report from the work or works of other people has been attributed and has been cited and referenced.
3. This report is my own work.
4. I have not allowed and will not allow anyone to copy my work with the intention of passing it as his or her own work.

Signed: Signed by candidate Date: 22-October-2023

Acknowledgments

I would like to thank my supervisor, Dr. Chima Ofoegbu, for his help and guidance, thank you for pushing me and guiding me through this journey. Thanks to my co-supervisor Prof. Deon Bezuidenhout, the experience he brought to this journey was priceless and greatly appreciated. Thanks to Prof Paul Human for his help with the statistical analysis of the data.

Thanks to my family, who allowed me to be here and motivated me to keep going. Thanks to my mom, Alice Fakih for her kind words and prayers, my dad Hani Fakih for the strength and the financial support, and my siblings for the encouraging messages and the laughs when needed.

My girlfriend Tais Soares for the moral support, the cooking, the relaxing time I needed to clear my mind, and a work buddy, who made it easier to work overnight.

My friends and colleagues, who are always here for me. Thank you for understanding that I did not ignore you but that I am just busy. I look forward to catching up with everyone.

Special thanks to Reno Chacko and Braden van Breda my friends, colleagues, and mentors without whom I would probably not be here. Thank you for your friendship and advice that made me a better engineer, scientist, and human being. To Robin Smith, Dr Harish Appa, and Willie Rabie for their assistance, expertise, and friendship. Their essential insight played a huge role in the completion of this thesis.

And a final thanks you to Strait Access Technologies, the company where I work, that enabled me to pursue this degree, they motivated and encouraged me to do it. Thanks to all members of the management team and to all the staff members.

Abstract

Aortic regurgitation (AR) caused by rheumatic heart disease is a significant cause of mortality in developing countries. The replacement of the regurgitant aortic valve was historically performed by surgical insertion of a bioprosthetic or mechanical heart valve.

Transcatheter Aortic Valve Implantation (TAVI) has become a common surgical procedure to replace defective aortic valves. The balloon-expandable (BE) transapical TAVI technique involves, a replacement valve crimped onto an inflatable medical balloon and delivered in the aortic valve by making a small incision in the chest and going through the apex of the heart. Once the crimped replacement valve is in position the balloon is inflated, expanding the replacement valve in the native aortic valve, and pushing the native leaflet onto the side. The balloon is then deflated and removed from the heart leaving the prosthetic valve in position.

Strait Access Technologies (SAT), a South-African start-up has developed an in innovative low-cost BE transapical TAVI for people suffering from AR. The delivery device consists of a non-occlusive balloon, allowing blood to flow freely during the entire procedure, and uses three locating arms called trunks for easy implantation through temporary anchoring tactile feedback. Compared to majority of the delivery system in the market the heart of the patient doesn't need to be stopped when the SAT delivery device is being used and minimal imaging system is required during the implantation procedure. After determining the optimal orthogonal projection of the aortic root using fluoroscopy and following the right cusps rule, each trunk is positioned in an aortic leaflet cusp to keep relative motion between the delivery device and the heart, and to locate the valve axially and rotationally. Once the trunks are in position the surgeons apply a small force and get tactile feedback to confirm positioning. The force applied during the tactile feedback procedure causes the native leaflets to droop. The droop can be defined as the displacement of the leaflet in the axial direction due to the pull force of the trunks. The amount of droop affects the axial positioning of the valve which is critical as is can led to regurgitation or valve embolization which can potentially be fatal.
It has been shown that the complication rate during TAVI reduces drastically after the first 100 implantation, hospitals with high volumes of TAVI have better outcomes. Surgeon proficiency in TAVI procedures can be achieved in multiple ways including workshops, course, simulation and animal trial. Training is important when surgeons are introduced to new technologies. The training methods and the repeat practice can drastically improve their clinical outcome. Most training systems currently available do not indicate the droop of the leaflet based on the force applied.

This study aims to define the relationship between the force applied during anchoring of the trunks and the native leaflet droop, to determine and quantify the force required to accurately position the valve, and, to develop a training rig to train surgeons in the correct use of the device.

To do so a pull-force tool replicating the trunks of the delivery device was designed and coupled to a force gauge. Three radiopaque markers were inserted into cadaveric pig hearts connected to a pulsatile pump replicating the blood flow. The pull-force tool was inserted in the pumping heart anchored in the native leaflet and pulled to cause droop. The forces applied on the native leaflet and the droops were recorded under fluoroscopy. Three equations defining the relationship between the droop and the force applied per leaflet were then defined. The force required to position the valve accurately was calculated. A training rig was also developed to train surgeons on the use of the delivery device and was divided into three main parts: an imaging system, a circulatory loop, and a force indication device. The imaging system was designed based on the Phillips BV Pulsera C-arm. It was designed to have similar dimensions, and the same degrees of movement as the image needs to be in a specific orientation for follow the right cusps rule, and to hold a standard security camera that projects the images on a screen to replicate the fluoroscopy imaging the surgeon will see during the procedure. The circulatory loop was designed using 3D printed clear materials and replicating the native anatomy dimensions. The data from the first part of the study was used to develop a force indicator, designed to be a replica of the TAVI delivery device, and uses a colour light system to indicate to the surgeon if adequate force is being applied to accurately position the valve.

The three equations derived after measuring the droop test of all leaflets are F_{L1} = -3.4831 x $Droop_{L1}$ - 1.94, F_{L2} = -4.5872 x $Droop_{L2}$ - 1.88, and F_{L3} = -4.7007 x $Droop_{L3}$ – 1.70, fot the Right Coronary Cusps (RCC), Non-Coronary Cusps (NCC) and the Left Coronary Cusps (LCC) respectively. The forces required to position the valve accurately was calculated to be between 7.39N and 17.96N, for a minimum droop of 1.2mm and a maximum droop of 4.6mm. The C section of the C-arm is made of aluminium, the C arm can move and be locked into position when the adequate image is obtained using 2 different locking mechanisms. It is designed to hold a camera that can project images into a screen, replicating fluoroscopy images. The circulation loop was 3D printed, using parts made of clear silicone and clear rigid material, a valve was deployed inside using a delivery device de-aired with a solution mixed with food colouring to confirm visibility during the procedure without the use of X-ray. Images were taken during the deployment and compared to the X-ray images and the images obtains could be used as substitute of fluoroscopy images to train surgeons. The force indicator was designed with a light that shines blue when the force applied is less than 7.39N the light shines green when the force applied is between 7.39N and 17.96N and the light shines red when the force applied is greater than 17.39N. majority of the parts were 3D printed. The force indicator was built and tested to confirm that the light shined as designed. This will give a good tactile feedback indication to the surgeon to know when adequate force is applied.

The three systems designed, used in conjunction, can be used to train surgeons on the TAVI without being exposed to any radiation, obtain adequate imaging, and apply the appropriate force to accurately position the valve.

Table of contents

List of tables

List of Figures

Acronyms and abbreviations

SAT	Strait Access Technologies
TAVI	Transcatheter Aortic Valve Implant
RF	Rheumatic Fever
RHD	Rheumatic Heart Disease
CT	Computed Tomography
WHO	World Health Organisation
AS	Aortic Stenosis
HICs	High-Income Countries
AR	Aortic Regurgitation
SDGs	Sustainable Development Goals
UN	United Nation
AEC	Animal Ethics Committee
LCC	Left Coronary Cusp
NCC	Non-Coronary Cusp
RCC	Right Coronary Cusp
PX	Pixel
IPA	Isopropyl alcohol
VIVIDR	Valve in Valve International Data Registry
VR	Virtual Reality
FEA	Finite Element Analysis
MRI	Master Record Index
CAD	Computer Aided Design
USB	Universal Serial Bus
BE	Balloon Expandable
SE	Self-Expandable
PET	Polyethylene Terephthalate
SOV	Sinus of Valsalva
SJ	Sinotubular Junction
VAJ	Ventriculo-Arterial Junction
LV	Left Ventricle

1. Introduction

1.1 Background/ Motivation

Rheumatic Heart Disease (RHD) is one of the most under-estimated yet deadly disease affecting more than 33 million people around the world and causing 320 000 deaths annually (1). It is also the most common cause of acquired heart disease in children and young adults globally (2). In 2017 the World Health Organisation (WHO) declared it to be a global health threat.

Although it is largely eradicated in developed countries, RHD is a silent killer in Africa, the Middle East, Central and South Asia, the South Pacific, and in impoverished pockets of developed nations. If detected on time, Rheumatic Fever (RF) can be treated by receiving penicillin injections regularly. With proper care and regular antibiotic treatment, most children with RF lead a normal life (3). Multiple episodes of acute RF cause more damage to the heart valve if not taken care of accordingly (4) and if not treated appropriately, rheumatic fever causes RHD. Current management options for rheumatic heart disease include valve repair and/or replacement which is done by open heart surgery or various minimally invasive surgery methods including transcatheter device implantation. However, open heart surgery is both not easily accessible and very expensive for patients in low and middle-income countries (MIC).

Transcatheter aortic valve implantation (TAVI) is a minimally invasive surgical procedure that replaces the aortic valve without removing the native one. For balloon expandable TAVI, a new valve is crimped onto an inflatable balloon and delivered to the aorta accessing the femoral artery (transfemoral approach) or by making a small incision in the chest and accessing through the apex of the left ventricle (transapical approach).

Transcatheter aortic valves were developed for calcific aortic stenosis (AS) which is prevalent in the ageing population of North America and Europe. Most contemporary valves used for TAVI need the crushed calcium deposits for anchorage, but these calcium/mineral deposits are lacking in non-calcified, compliant roots seen in aortic regurgitation (AR) (5). In high-income countries (HICs) four to five times more patients suffer from calcific AS than AR (6). Consequently, when the contemporary TAVI valves are used in non-calcified roots, they need to be oversized (relative to the aortic root) for appropriate valve insertion and seating. This is important for our South African population (a MIC) where four times more patients are affected by non-calcific AR than calcific AS (7) due to the prevalence of RHD (8).

Strait Access Technologies (SAT), a South African start-up company affiliated with the University of Cape Town, is designing, and testing a new valve for AR patients. This valve will be delivered transapically in a unique way. The delivery system includes a non-occlusive balloon,

locating arms (trunks) that help position the valve and help to reduce the cost of surgery as complex imaging is not required.

During the procedure, those locating arms (trunks) are anchored in the aortic leaflet. The operating surgeon needs to apply a certain force to keep the device in place during the operation. If the force applied is too great there is a risk of damaging the native leaflet and the positioning of the valve will be incorrect. If the force is too low, the valve will be placed high. As current training, the surgeons deploy a valve in an explanted heart model and later on in a living animal. A good method of replacing and reducing animal trials is to develop a training rig that will simulate the leaflet strength and give the operating surgeon a feel of the tactile feedback required to position the SAT Valve.

This project resonates with one of the 17 Sustainable Development Goals (SDGs) set by the UN in 2016. The third goal has the objective of ensuring healthy lives and promoting well-being for all at all ages (9). By developing a training device that will help surgeons sharpen their skills, one target of this goal which is to "Substantially increase health financing and the recruitment, development, training, and retention of the health workforce in developing countries, especially in the least developed countries and small island developing States", is achieved (9).

There is only one cardiac centre per 33 million people in Africa compared to the United States which has 1 cardiac centre per 120,000 people (10). The number of registered cardiologists in South Africa in 2016 was approximately 200 for 52 million South Africans (one for 260 000). Brazil in the same period (with similar cardiovascular health issues to South Africa) has 8 000 board-certified specialists in cardiology for a population of 185 million (1 for 23 000) (11). In 2018, surgeons from all over the world signed the Cape Town Declaration on Access to Cardiac Surgery in the Developing World. The second aim of this declaration is: "To advocate for the training of cardiac surgeons and other key specialized caregivers at identified and endorsed centres in low- to middle-income countries" (10). There is a need for more surgeons in the field of cardiothoracic surgery in Africa. In a bid to accelerate the acquisition of technical knowledge and implantation skills to safely implant the unique SAT device, a realistic simulator was designed and applied from various scientifically derived data and variables. The training device will replicate all the steps presented in a TAVI and give the surgeons a realistic simulation.

1.2 Thesis outline

Chapter 2 provides a literature review of the human heart, more specifically on the aortic valve situated in the left chamber of the heart. It gives a summary of the different methods for replacing a malfunctioning aortic valve. It also gives some examples of training devices used. It finally gives us a summary of different processes used in training.

Chapter 3 describes the TAVI procedure by illustrating the valve implantation procedure step by step, defines the problem observed during the procedure, propose a solution to the problem, and defines the aims and objectives of the thesis.

Chapter 4 presents the methodologies used to define the pull force, it explains how the droop tests were prepared and carried out and how the data was analysed. It presents the guideline followed in the design of each section of the training device which are the imaging system, the circulatory loop, and the force indicator.

Chapter 5 provides us with the results of the droop test and the data analysis done. It describes the design choices and manufacturing process selected to make the training rig. It explains why certain materials were selected as well as the human factor assessed during the design of the imaging equipment. It shows the different iterations of the circulation loop as well as the reason why the design was changed. It explains how the force indicator was designed as well as shows its performance.

Chapter 6 concludes the report and Chapter 7 gives recommendations on what to do to take the project further. It explains how to carry on with the droop test and what to do to validate the data. It also explains how to translate the data to humans, and how to upgrade each component of the training rig.

2. Literature Review

2.1 Anatomy overview

2.1.1 Physiology of the heart

The human heart is a muscular pump divided into two sides, containing four chambers that circulate blood around the body. The purpose of the four heart valves is to control the direction of blood flow, allowing forward flow and preventing backward flow (12).

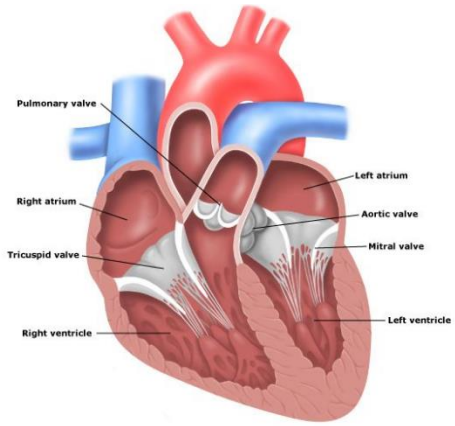

Figure 2-1 The Heart and its chamber (13)

The blood flow to the heart enters from the right atrium passing through the tricuspid valve to go to the right ventricle. From the right ventricle, it flows through the pulmonary valve, going via the right and left pulmonary arteries to the lungs where it gets oxygenated. The oxygenated blood flows back to the heart through the pulmonary veins into the left atrium. From the left atrium, the blood flows through the mitral valve into the left ventricle. The left ventricle contracts and pushes the blood through the aortic valve into the ascending aorta and is then distributed to the rest of the body from the aorta.

2.1.2 Aortic valve

The aortic valve is a valve in the heart, situated between the left ventricle and the aorta that prevents blood to return to the ventricle from the aorta (14). The aortic valve is normally tricuspid and consist of an annulus, three delicate leaflets commissure posts and sinuses of Valsalva. The aortic sinuses are dilated pockets of the aortic root that form the outer component of the three cuplike closing structures of the aortic valve (15). An illustration of an aortic root can be seen in Figure 2-2.

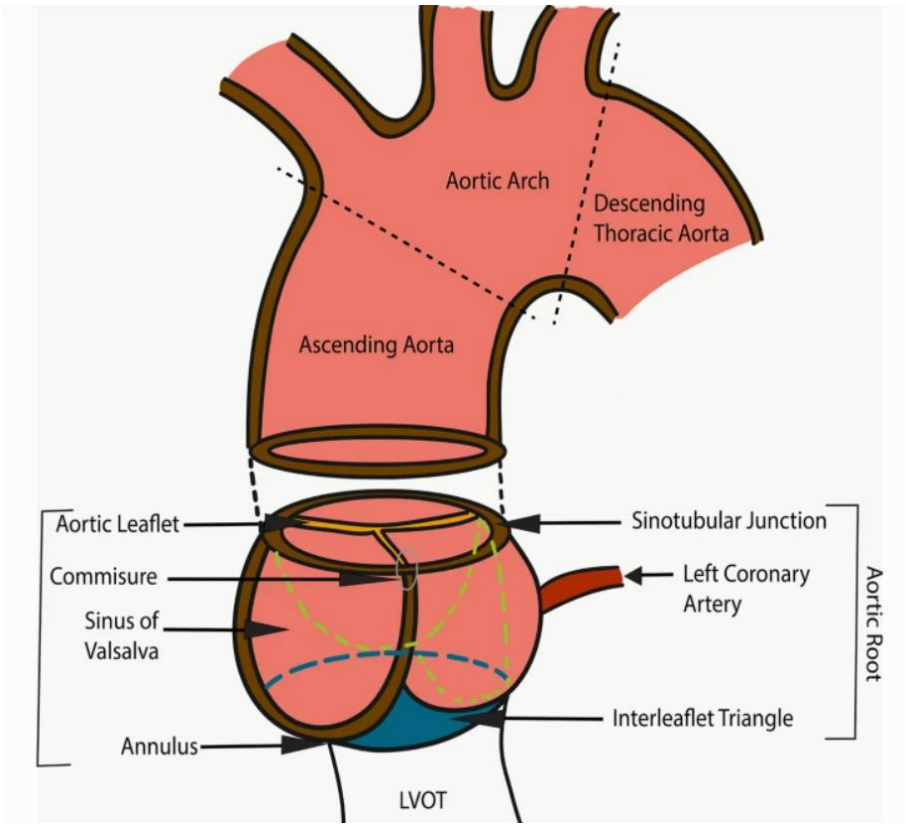

Figure 2-2 Illustration of an aortic root (16)

Rankin et al. (2013) show a better understanding of the aortic root geometry. The study was done using computer tomographic angiograms from 10 patients. The aortic valve geometry can be seen in Figure 2-3.

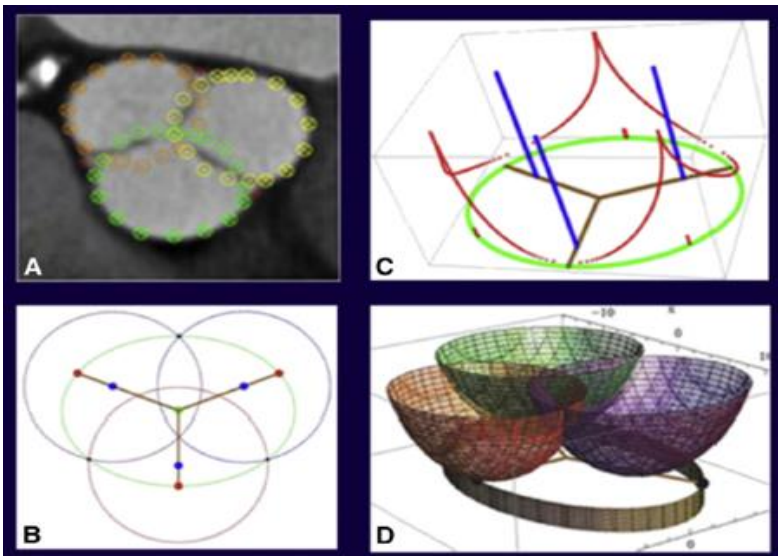

Figure 2-3 Aortic valve geometry (17)

Figure 2-3 shows that the valve base has an elliptic shape. Image A shows a computed tomographic (CT) image of a normal valve while image B shows the average dimensions of the analysed valves. Image C shows the centrums of the leaflet-sinus complexes, and the leaflet aortic junction, and image D is a representation of the reconstructed valve (Rankin et al., 2013).

2.1.3 Aortic leaflet

The aortic leaflets are three flaps of the aortic valve. In aortic insufficiency, the leaflets do not close tightly, allowing blood to leak back into the left ventricle (18). Rankin et al. (2013) shows that the vertical leaflet height was greater than represented by hemispheres. It shows that the leaflet–sinus cross sections were not circular. The geometric shapes, dimensions, areas, and volumes of all three leaflets are similar except for the right coronary leaflet being approximately 10% larger than the non-coronary leaflet and the left coronary leaflet (Rankin et al., 2013).

2.1.4 Biomechanics of leaflets

The result of a biaxial test shows that the leaflets from different species, human, ovine, and porcine, have different mechanical properties (19). The main difference found was that the human leaflet biomechanical properties decreased in the circumferential extensibility compared to the porcine and ovine one. The human leaflet did not stretch at all during the test. Ageing may account for the differences seen between species. The porcine species was shown to have an increase in AV thickness from 6 weeks to 6 months old (20); a similar observation was made by McDonald et al. (2002) in the human AV, where they show that the human leaflet increases significantly in area and thickness with age.

2.1.5 Frozen heart characteristic

Clark R. (1973) studied the stress-strain difference between fresh and frozen human aortic and mitral leaflets. The aortic leaflets were cut between 24 to 48h after death without freezing the hearts. Fresh tissues were preserved in 5 to 10 ml of a saline solution maintained at 4°C while the frozen leaflets were kept at a temperature of -70°C. The samples were cut and tested using a uniaxial tensile tester. The results can be seen in Table 2-1.

Table 2-1 Average Values for aortic leaflets (n=50) (22)**.**

Parameter	Fresh				Frozen			
	Circumferential		Radial		Circumferential		Radial	
	Average	SD	Average	SD	Average	SD	Average	SD
Pre-transition modulus (g/mm^2)	1.987	0.692	1.125	0.46	1.41	0.412	1.155	0.8
Stress at transition (g/mm^2)	0.701	0.242	0.752	0.329	472	0.095	0.359	0.11
Elongation at transition (%)	12.8	5.6	23.85	8.275	12	4.9	9.575	1.375
Post-transition Modulus (g/mm^2)	598	301	174	69.8	846	20.4	244	89
Elastic recovery (%)	99.1	0.545	98.57	3.36	98.4	0.463	99.35	3.53
Thickness (mm)	0.6	0.07	0.62	0.06	0.51	0.05	0.53	0.05

It can be noticed that the fresh aortic leaflets are more elastic and have a lower tensile strength in the radial direction. From the results, it was noted that freezing aortic tissue altered the mechanical behaviour of the aortic valve tissue resulting in a generalised stiffening (22).

2.1.6 The Aorta

The aortic arch is the top part of the main artery carrying oxygenated blood away from the heart (14). It is the segment of the aorta that helps distribute blood to the head and upper extremities via the brachiocephalic trunk, the left common carotid, and the left subclavian artery (23). The size of the aortic arch varies in humans due to different trauma, diseases, age, and in congenital conditions. Figure 2-4 shows an aorta, the ascending part, the arch, and the descending part.

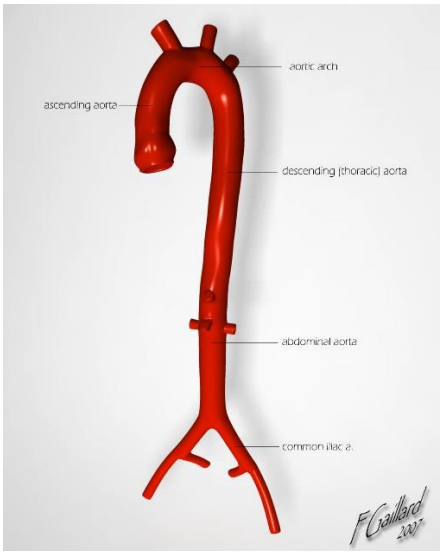

Figure 2-4 Aorta illustration (24)

The aortic arch dimensions are different in each person. There are many studies that measured the sizes of the aortic arch. Alberta et al., (2013) measured the proximal diameter of the arch, the distal diameter, and the aortic arch radius of curvature of patients with trauma, and, of patients with aneurysms. Redheuil et al. (2011) measured the same parameters for patients of different ages. Table 2-2 tabulates the results of those studies.

Table 2-2 Aorta Dimension

Study	Patient category	Aortic arch radius of curvature (mm)	STDEV (mm)	Ascending aorta diameter (mm)	Descending aorta diameter (mm)
H.B. Alberta et al.	Patient with trauma	40.38	11.29	25.1	23.8
H.B. Alberta et al.	Patient with aneurysm	59.82	14.99	33.5	33.6
A.Redheuil et al	For younger than 30 years	29.4	0.002	27.5	18.3
A.Redheuil et al	For over 70-year-olds	37	0.003	33.2	21.5

The data shows that that the radius of curvature increase with age. It shows that aneurysm causes the radius of curvature to increase more significantly than age and trauma.

2.1.7 Left ventricle anatomy relevant to transapical TAVI implantation.

The entry angle, during a transapical TAVI, can be defined as the angle between the entry point situated in the left ventricular apex of the heart to the aortic annular plane. The ideal location is not in the true apex but rather lateral to the left anterior descending coronary artery and toward the base (27). Figure 2-5 below illustrate the angle between the entry point and the annular plane.

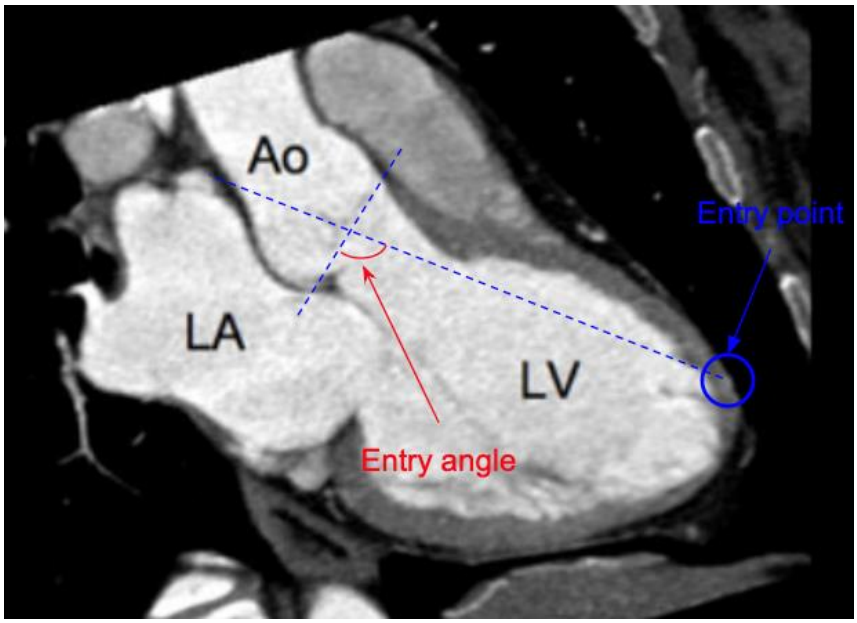

Figure 2-5 Entry angle illustration (28)

The effect of the entry angle can be seen in the study done by Falk et al., (2011), with 30 patients, to test the feasibility of implanting a self-expanding TAVI. One of the concerns was the high rate of aortic dissections that was happening due to the angle. The stiff device was thereafter redesigned to be more flexible and less traumatic to the anatomy while being pushed through the annular plan to position the valve (29). Figure 2-6 shows an illustration of their stiff devices crossing the native aortic valve, and it can be seen that the device is hitting on the aortic root.

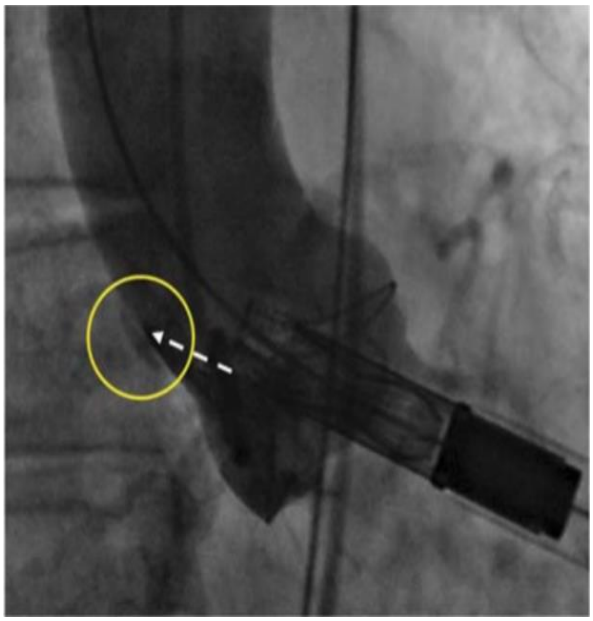

Figure 2-6 Implication of aortic angle (29)

2.2 Rheumatic Heart Disease pathology

2.2.1 Description of Rheumatic Heart disease

The aortic valve is also affected in RHD, though with a less incidence than mitral valve disease. The aortic valve becomes increasingly affected with increasing patient age in RHD (30). Rheumatic aortic stenosis (AS) or regurgitation (AR) is diagnosed based on presence of commissural fusion, leaflet thickening/shortening and increased echogenicity along the leaflet edges (31). The AR component (37%) in RHD is usually more significant than the AS component (9%) in a study by Sliwa et al. (31) while isolated AS is quite uncommon in RHD and usually takes decades to occur. (31,32) . Moderate to severe aortic regurgitation often remains stable for years until the left ventricle (LV) starts to fail after chronic volume overload (systolic and diastolic) (33,34). The current European Society of Cardiology (ESC) and European Association for Cardiothoracic Surgery (EACTS) guidelines for the management of valvular heart disease (VHD) suggest these indications for surgery in patients with severe AR; symptomatic patients regardless of LV function, asymptomatic patients with LV dilation (LV end-systolic dimension > 50mm or LV end-systolic dimension > 25mm/m2) or dysfunction (left ventricle ejection fraction ≤ 50%) and symptomatic/asymptomatic patients undergoing coronary artery bypass grafting (CABG) or surgery of the ascending aorta (35). A study by Scherman et al, showed that 50% surgery rate (repair/replacement) patients with RHD aortic valve disease (36).

2.2.2 Different mechanism observed in aortic regurgitation.

Morphological changes in the aortic valve may include leaflet tip prolapse involving in descending frequency order the left coronary cusp (LCC), the right coronary cusp (RCC) and the non-coronary cusp (NCC)(33). These features may then lead to central non-coaptation or eccentric AR between retracted or rolled cusps. This combination of leaflet thickening, retraction and rolled up edges result in the mixed effect of AS and AR(33). The Carpentier classification has been used in the characterization of AR and may affect the decision making regarding options for managing AR and also outcomes of aortic valve repairs(37);

- Type Ia: dilation of the sinotubular junction (SJ)
- Type Ib: dilation of the sinus of Valsalva (SOV) and SJ
- Type Ic: dilation of the ventriculo-arterial junction (VAJ)
- Type II: Excessive leaflet motion (prolapse) or loss of commissural integrity.
- Type III: Leaflet restriction ± commissural fusion (seen in RHD).

Table 2-3, Figure 2-7, Figure 2-8, Figure 2-9, Figure 2-10, Figure 2-11, and Figure 2-12 accentuate the above text(8).

Table 2-3 Carpentier classification of aortic regurgitation (37)

AR Type	Aortic Annulus	Sinus of Valsalva	Sinotubular Junction	Ascending Aorta	Other
Normal Leaflets					
Type Ia	↔	↔	↑↑	↑↑	-
Type Ib	↔	↑↑	↑↑	↔	-
Type Ic	↑↑	↔	↔	↔	-
Type Id	↔	↔	↔	↔	Perforation
Type II	↔	↔	↔	↔	Cusp prolapse
Type III	↔	↔	↔	↔	Cusp restriction

↔ Denotes that the measurement could be increased/decreased or normal.
AR = aortic regurgitation.

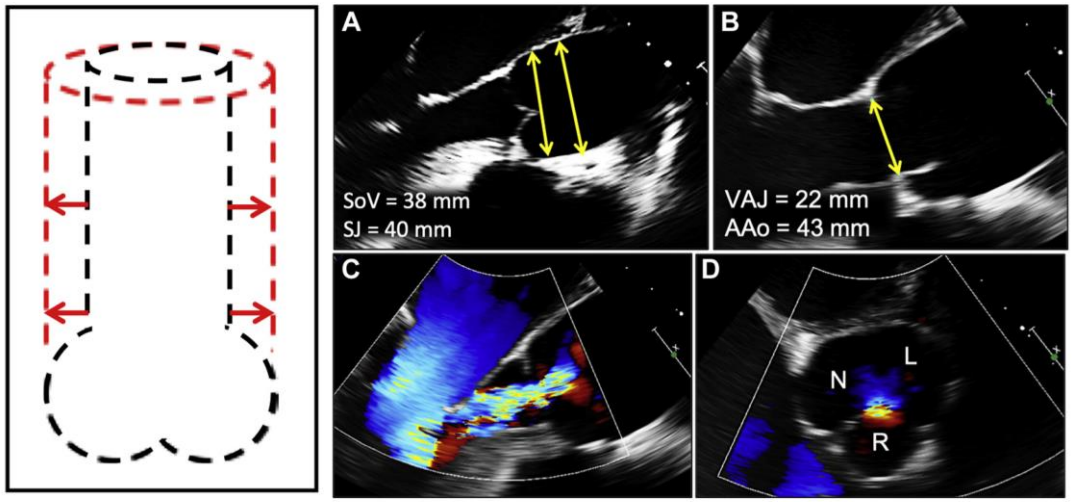

Schematic showing the outline of a normal aortic root and ascending aorta **(black)** and changes expected in Type Ia aortic regurgitation (AR) (i.e., a dilated sinotubular junction [SJ] and ascending aorta [AAo]) **(left panel)**. On the **right**, 2-dimensional and color Doppler images of the aortic root in a patient with Type 1a AR **(A to D)**. See text for details. L = left coronary cusp; N = non-coronary cusp; R = right coronary cusp; SoV = sinus of Valsalva; VAJ = ventriculoaortic junction.

Figure 2-7: Type Ia AR is associated with dilation of the Aao and SJ (37)

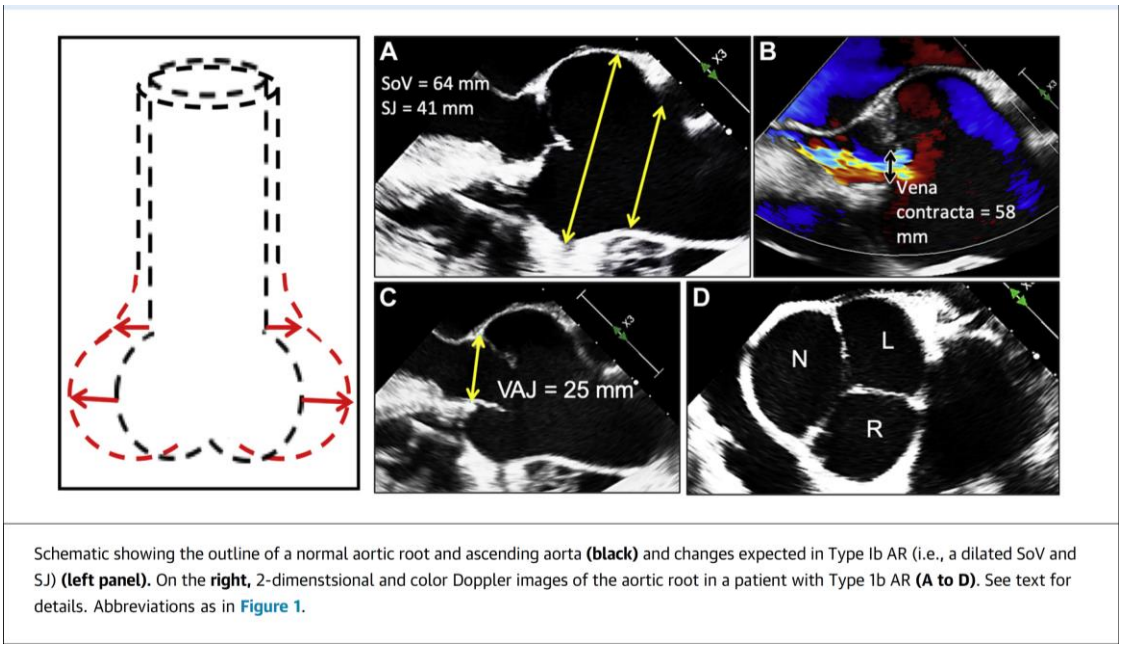

Schematic showing the outline of a normal aortic root and ascending aorta **(black)** and changes expected in Type Ib AR (i.e., a dilated SoV and SJ) **(left panel).** On the **right,** 2-dimenstsional and color Doppler images of the aortic root in a patient with Type 1b AR **(A to D)**. See text for details. Abbreviations as in Figure 1.

Figure 2-8: Type Ib AR is associated with dilation of the SoV and SJ (37)

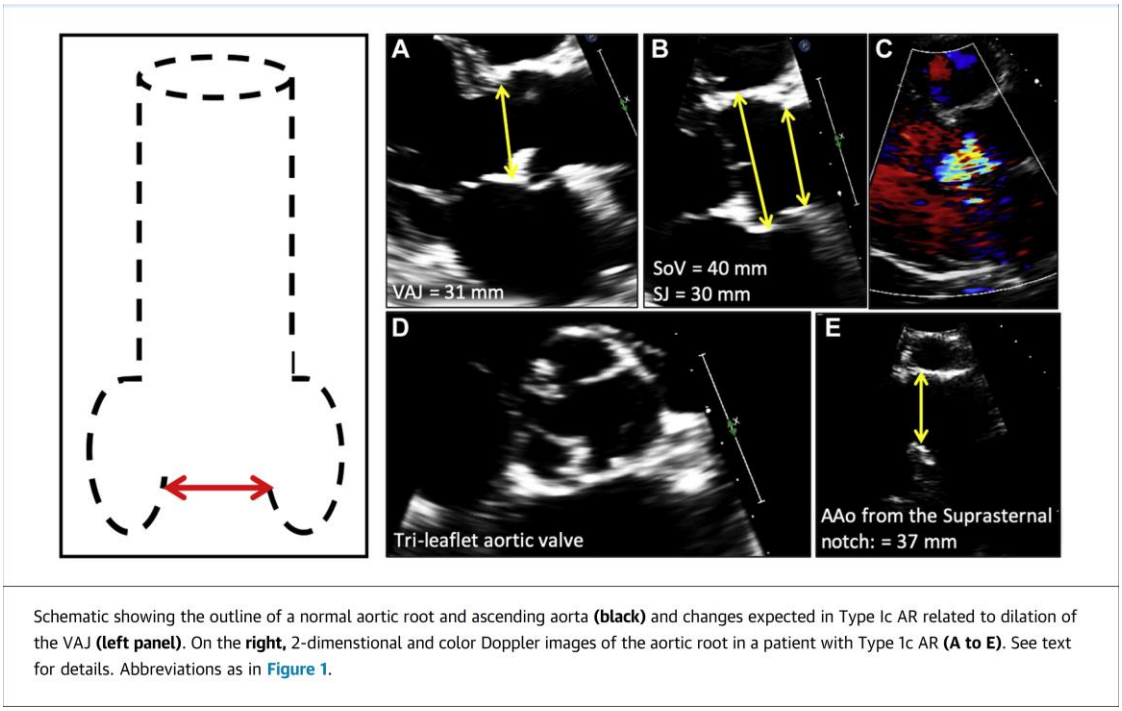

Schematic showing the outline of a normal aortic root and ascending aorta **(black)** and changes expected in Type Ic AR related to dilation of the VAJ **(left panel)**. On the **right,** 2-dimenstional and color Doppler images of the aortic root in a patient with Type 1c AR **(A to E)**. See text for details. Abbreviations as in Figure 1.

Figure 2-9: Type Ic AR is associated with dilation of the VAJ (37)

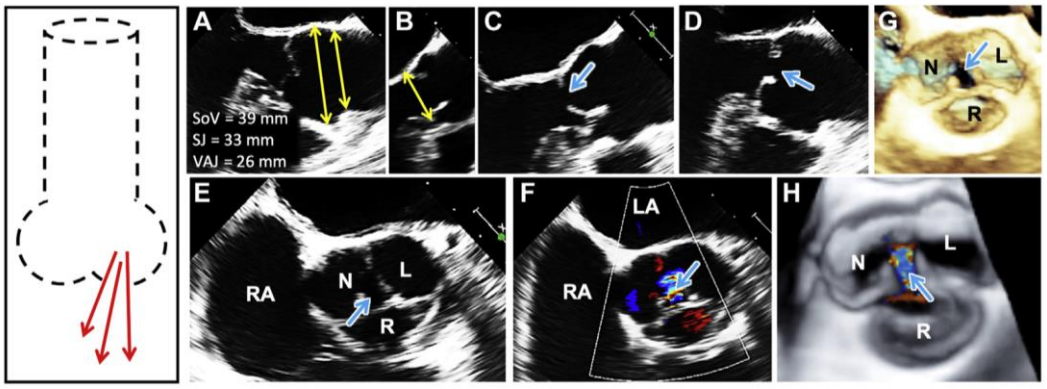

Schematic showing the outline of the aortic root and ascending aorta **(black)** and changes expected in Type Id AR (i.e., perforation of the aortic valve leaflet) **(left panel)**. On the **right,** 2-dimensional, 2-dimensional color Doppler, 3-dimensional narrow-angle, and 3-dimensional color Doppler images of the aortic root are depicted in a patient with Type 1d AR **(A to H)**. **Blue arrows** identify the area of leaflet perforation in the noncoronary cusp. See text for details. Abbreviations as in Figure 1.

Figure 2-10: Type Id AR is associated with left perforation (37)

FIGURE 5 Type II AR Is Associated With Excessive Leaflet Motion

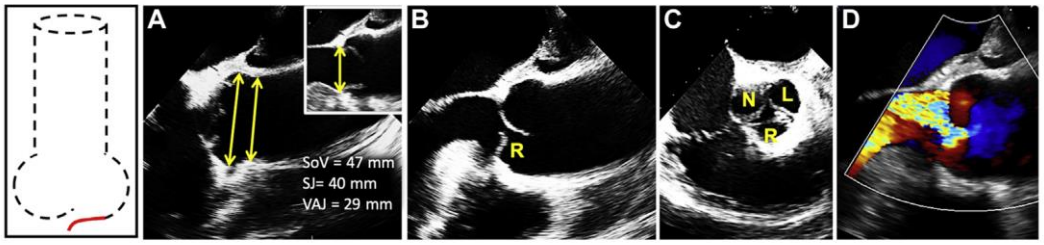

Schematic showing the outline of the aortic root and ascending aorta **(black)** and changes expected in Type II AR (i.e., leaflet prolapse) in **red (left panel)**. On the **right,** 2D and color Doppler images of the aortic root are depicted in a patient with Type II AR **(A to D).** See text for details. Abbreviations as in Figure 1.

Figure 2-11: Type II AR is associated with excessive leaflet motion (37)

The lack of calcium in AR may pose a considerable challenge for TAVI application which increases the risk of TAVI device dislodgement, malposition and embolization (38). The post-inflammatory changes in RHD lead to leaflet fusion and fixed obstruction with the aortic valve in a constantly open position resulting in AS/AR and disruption of the valve architecture with fibrosis and collagen deposition (39). This lack of calcium may also result in higher rates of paravalvular leak (PVL) as compared to the AS cohorts (38). Furthermore, the AR valves are more elastic than the AS valves and can expand to a greater degree during valve implantation meaning TAVI valves used for AR need significant oversizing (38).

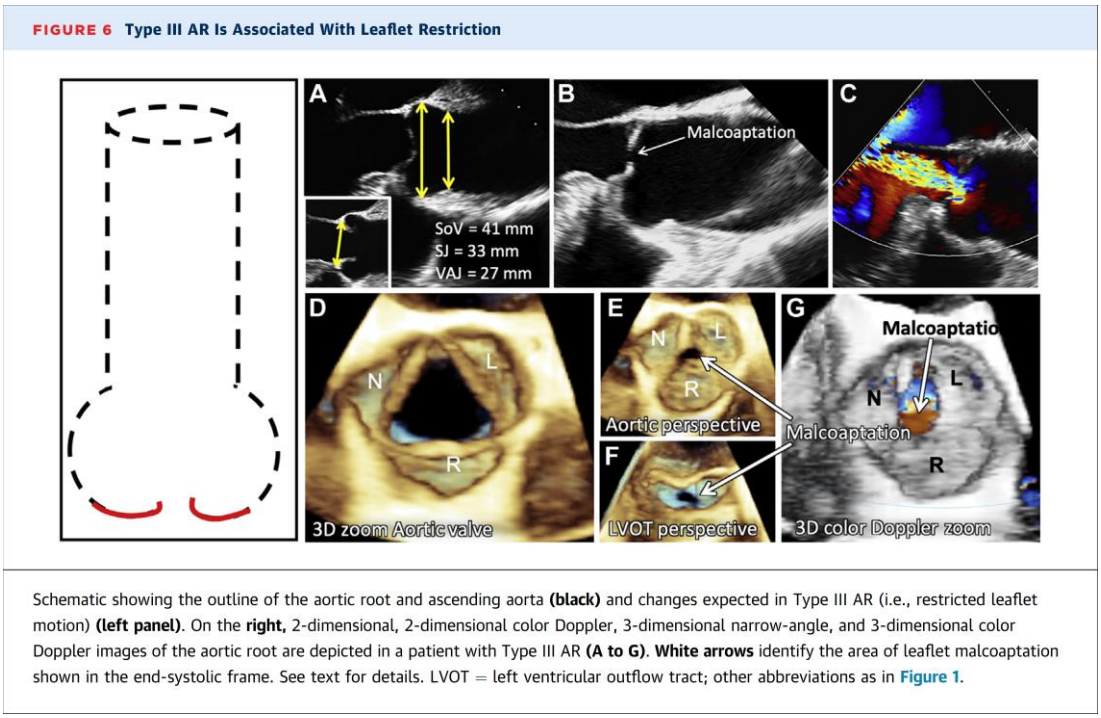

Figure 2-12: Type III AR is associated with leaflet restriction (37)

2.3 Aortic Valve Replacement

2.3.1 Open Heart Surgery (Aortic Valve)

Open heart surgery has been performed since the 10th of September 1896 (40). During open-heart surgery, the patient is connected to a heart-lung bypass machine, which keeps blood moving through the body during the procedure while the heart is cut open and the leaflets are replaced by a prosthesis or repaired (41). There are many surgical approaches that can be used to repair the aortic valve such as open or minimally invasive surgery. Surgery was the only option for all types of valvular heart disease until 1984 where the first transseptal percutaneous mitral balloon commissurotomy in mitral rheumatic disease was published (42). As far as aortic regurgitation is concerned, most patients are treated with surgery, and TAVI remains at a preliminary stage (42)

2.3.2 Transcatheter Aortic Valve Implantation

The field of medicine is evolving every day with new surgery methods being developed. One of the most recent cardiothoracic procedures is a TAVI, a minimally invasive surgical procedure that replaces a malfunctioning aortic valve with an artificial valve without having to remove the malfunctioning valve. Recent studies show positive results for TAVI compared with surgical aortic valve replacement. Surgical risk has been removed from the decision consideration (43). TAVI is now done for low, intermediate, and high risk patients (44). The management of VHD

including AR/AS usually involves the input of the heart team in the decision of the most appropriate management (35).

The current guidelines for management of VHD suggest the use of TAVI in these patient cohort (35);

- Age > 75 years
- Unsuitable/high risk for surgical AVR as indicated by Society of Thoracic Surgeons - predicted risk of mortality (STS-PROM) and European System for Cardiac Operative Risk Evaluation II (EuroSCORE II) of >8%.
- Suitability for transfemoral TAVI

2.3.3 Different type of aortic TAVI valve

There are two main TAVI valves, Balloon expandable (BE) valves and self-expandable (SE) valves. BE valves are made of a metal frame, crimped over a medical balloon, and inserted in the heart through an artery. Once the valve is in the correct position, the balloon is inflated, causing the valve to expand and anchor in the right position. SE valves are made of a shape memory metal frame such as nitinol. The valve is crimped onto a delivery catheter, kept into its crimped shaped by an outer sheath, and inserted through an artery, usually the transapical or transaortic approach, and guided up to the heart. Once in position the outer sheath is retracted, and the valve springs back to its set shape. The choice of valve depends on several factors, including the patient's anatomy and medical history, the preference and experience of the treating physician, and the availability of specific valves at the hospital where the procedure is being performed. Some of the valves used are:

Self-Expanding TAVI Valves:

- Medtronic CoreValve and Evolut R
- Boston Scientific Lotus and Acurate Neo
- JenaValve
- Abbott Portico

Balloon-Expandable TAVI Valves:

- Edwards SAPIEN 3 and SAPIEN 3 Ultra
- J-Valve

There is a difference in TAVI valves for AS and AR as the two conditions require different treatment approaches. TAVI is done on AS patients to replace the native narrowed valve, which restricts the blood flow output, with a new prosthetic valve that opens the orifice and allows for

a better blood flow out of the heart. TAVI is done on AR patients to replace the leaking native valve, with a prosthetic valve that seals around the native orifice, preventing blood from flowing back in the ventricle. There are only 2 TAVI valves dedicated to treating AR, the J-valve and the JenaValve. Both have been successfully used via transapical approach(45).

All of the TAVI valves mentioned are made with bioprosthetic leaflets, made of animal tissues, such as cow or pigs' tissues, that are treated and cut to create the leaflets of the implant valves. Those valves are limited by structural valve degeneration which requires reoperation or the need for lifelong anticoagulation(46). To overcome those issues, multiple new polymer leaflet technologies have been developed in recent years (46). From all the polymer valves currently being developed, only one has completed in-human trials which is the Foldax Tria surgical valve, a surgically implanted Polymer leaflet valve (47); no TAVI valve made from polymeric material has completed in-human trials.

2.3.4 SAT Aortic Valve

SAT is developing 3 iterations of a TAVI valve for the treatment of AR. The valves are made of 3 main components. A skirt, three leaflets and a stent. The stent is made of nickel-cobalt-chromium alloy MP35N the leaflet was designed based on Bézier curves shape, and the skirt was made of electro spun polymer (48). The valve can be crimped over a medical balloon and restored to its original shape by inflating and expanding the balloon (48). The valve has three self-elevating anchoring arms based on geometric changes due to plastic deformation occurring after crimping during deployment (48). It has an hourglass shape and its waist seats in the annulus plane of the native valve (48). 3 valves are currently being develop following the same design, a bioprosthetic valve, using bovine leaflet, a universal valve using either polymer and bioprosthetic leaflets, and a polymer valve using polymer leaflets. Figure 2-13 shows the 3 different designs of the valve with A being the bioprosthetic valve, B a universal valve and C a Polymer valve.

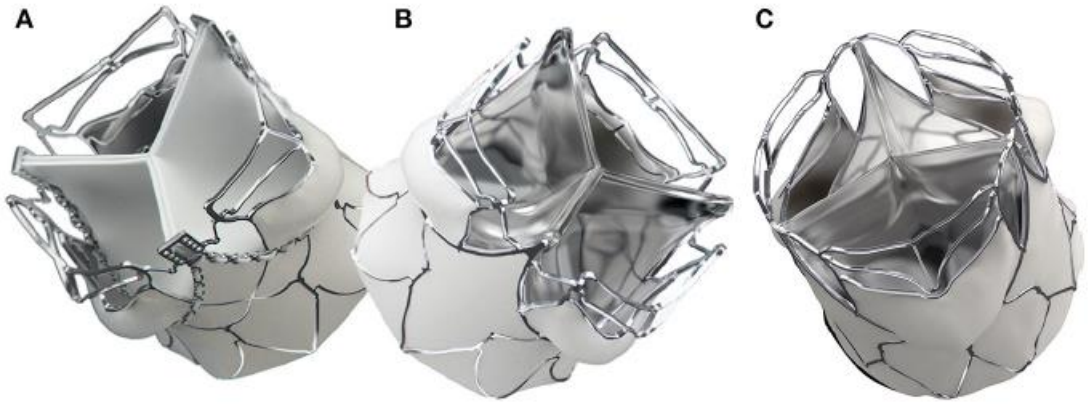

Figure 2-13 SAT Valve (48)

2.3.5 Different delivery systems

Catheter based delivery devices are used to deliver and position the valve during TAVI. As there are 2 main types of valves BE and SE, there are 2 main types of devices to deliver such valves. Each device can be delivered in the heart in different approaches which are transfemoral approach, transapical approach, transaortic approach and trans subclavian approach. The transfemoral approach is the most common approach used in TAVI (49), it is done by inserting the delivery system entering from the femoral artery in the groin and guided to the heart over a guide wire. The transapical approach is done by making a small incision on the chest, exposing the heart, and inserting the delivery device directly through the apex of the heart. The Transaortic approach is done by delivering the valve through an incision on the aorta. The trans subclavian approach is done by inserting the delivery device through the subclavian artery. Figure 2-14 illustrates the different access point on the human body.

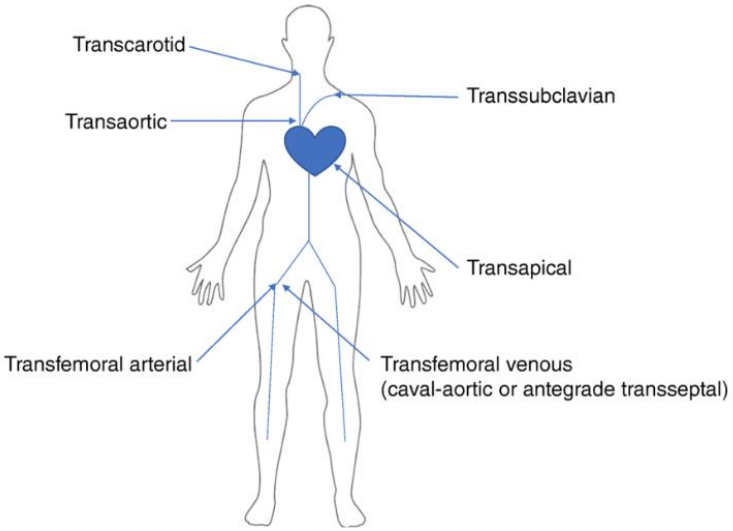

Figure 2-14 Access route for TAVI (50)

At the early age of TAVI only 57.1% were done using the femoral artery access due to the size of the delivery device (51). By 2019 95.3% of TAVI were done using the transfemoral approach (51).

2.3.6 SAT delivery device

The delivery device is a BE using the transapical approach. Two of the main parts of the delivery device are a non-occlusive helical balloon and a tactile placement and stabilization balloon with retractable feelers called trunks (48). The hollow balloon is made of a tube woven through a nitinol frame mesh in a helix shape. The trunk balloons were based on a balloon tube that could retract through invagination. Both trunks and helical balloons are made of thin wall polyethylene terephthalate (PET) (48). Figure 2-15 shows the delivery device. Image A shows the helical

balloon and the trunks, image B shows the helical balloon woven into the nitinol frame and image C shows a valve position over the helical balloon.

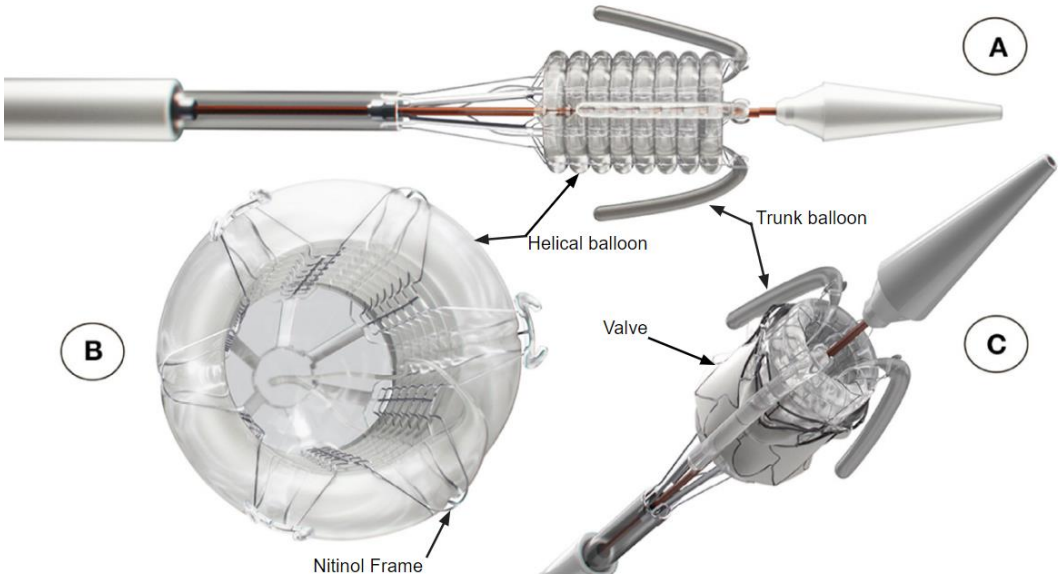

Figure 2-15 SAT delivery device (48)

The TAVI system (device and valve) was deployed in 10 sheep successfully and none of the valves migrated, dislodges or embolized (5). Figure 2-16 shows the illustration of the deployment as well as fluoroscopy images.

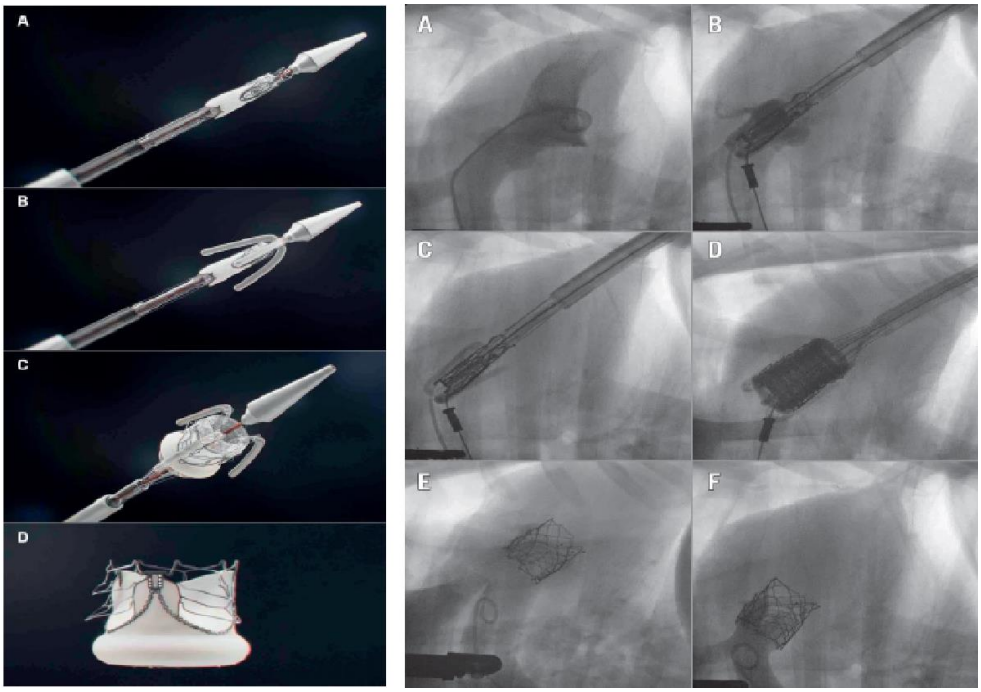

Figure 2-16 TAVI deployment (5)

The images on the left show the delivery device at each step during the implantation. Image A shows the SAT delivery device with a crimped valve. Image B shows the 3 trunks extended. Image C shows the helical balloon inflated and the valve expanded. Image D shows the valve.

The images on the right show Fluoroscopy-guided transapical insertion of the SAT-TAVI valve. The images were taken during an animal study done. Images A and B, shows a visualisation of the root under fluoroscopy. Image C shows the trunks extended. It is at this step that the force (F) is applied to position and stabilize the root. Image D shows the valve being deployed. Image E and F shows the valve final position (5).

2.3.7 Animal Trials

Clinical trials to confirm the safety and efficacy of medical devices are done after investigators conduct preclinical research using animal models (52). These animal trials are mostly to validate the valve design or assess its performance. Large animals such as sheep and pigs whose heart size, anatomy, material degradation, and endogenous tissue growth closely resemble humans are often employed (53). It is essential to ensure that the implant position of a transcatheter heart valve within a given surgical heart valve is in its ideal position, as too low a position can lead to suboptimal function or paravalvular regurgitation and too high a position may lead to coronary artery obstruction or valve migration (54). Initial results from the VIVIDR (Valve in Valve International Data Registry) reported mal positioning in 15% of cases resulting in the need for additional procedures (54).

2.4 Training

2.4.1 Training methods

All procedures have a learning curve, and the United States Transcatheter Valve Therapy registry shows that the complication rate reduces drastically after the first 100 TAVI (55). Outcomes of TAVI operations depend on the hospital volumes with better outcomes seen with larger volumes. If an apparatus is developed to help the surgeons practice TAVIs, the outcome of the procedures might improve. Surgeon proficiency in TAVI procedures can be achieved in multiple ways including workshops, course, simulation and animal trial.

There are several training simulation methods that can be used for TAVI procedural training, Virtual reality (VR) simulation is one. VR simulations use computer-generated environments to simulate a TAVI procedure, allowing surgeons to practice the procedure in a safe and controlled environment. A study was done on 11 patients to evaluate the impact of VR tool in procedural planning (56). In this study all cases survived with good clinical outcome and no major clinical complication was observed.

Another training method that can be used are Phantom models. Phantom models are specialized training aids that are designed to simulate the anatomy and physiology of the heart allowing the surgeon to practice TAVI procedure in a controlled environment.

Animal model can be used to train surgeons on TAVI as the animal can provide a more realistic simulation of the procedure. A cadaveric heart may also be used.

2.4.2 Training Rigs

There are multiple training rigs for TAVI available on the market.

An example of software simulation for TAVI training is ANGIO Mentor; this was developed in 2008 and involved usage of a replica of the deployment handle to simulate TAVI procedure (57). Their system includes a C-arm fluoroscopy machine to create a more realistic environment.

Figure 2-17 Angio Mentor (57)

Mentis Visit is a VR trainer for medical professionals focusing on image guided procedural. A study was done to compare the face-to-face teaching with a simulator-based teaching, using the mentis, for coronary anatomy knowledge (58). This study suggested that student knowledge of coronary anatomy could potentially be improved by simulator-based teaching. Figure 2-18 shows an image of the Mentis Visit.

Figure 2-18 Mentis Visit (58)

Another example is a cardiac bio simulator platform which can be used to train surgeon by using a combination of an animal or human heart connected to a circulatory system. It can be used to train surgeons, cardiologist, and radiologist virtually in a high realistic setting (59).

Figure 2-19 Cardiac Biosimulator Platform (59)

Most training systems available are not indicating the droop of the leaflet based on the force applied.

2.5 Modalities and techniques to plan transapical TAVI access and device implantation.

2.5.1 CT-scan data

Computer tomography (CT) which uses X-rays to assess specific areas of the body has become an important tool in medical imaging since its introduction (60). Though the amount of radiation used is larger than for a routine chest radiograph, safe doses have been determined for humans (61). Intravenous contrast agents which usually contain iodine are used to visualize the vascular tissues in an X-Ray or CT scan (62). The CT scans are used in TAVI to determine the patient aortic root dimensions (annulus, sinotubular junction, sinus of Valsalva, coronary artery heights) and then correlate this with the appropriate valve prosthesis for insertion.

2.5.2 Right cusps rule

The right cusp rule is a method used in TAVI to determine the optimal orthogonal projection of the aortic root using fluoroscopy by aligning the right coronary cusp (RCC) between the left coronary cusp (LCC) and non-coronary cusp (NCC) (63). The methods used to determine the right cusp rule was described in detail in an article publish by Kasel et al. (2013).The pigtail catheter is placed in the right cusp and contrast is injected. The C-arm is rotated in the left or right anterior oblique projection to move the RCC toward the NCC or LCC respectively and rotated in the caudal or cranial direction to bring the RCC up or down respectively. An illustration of the procedure can be seen in Figure 2-20.

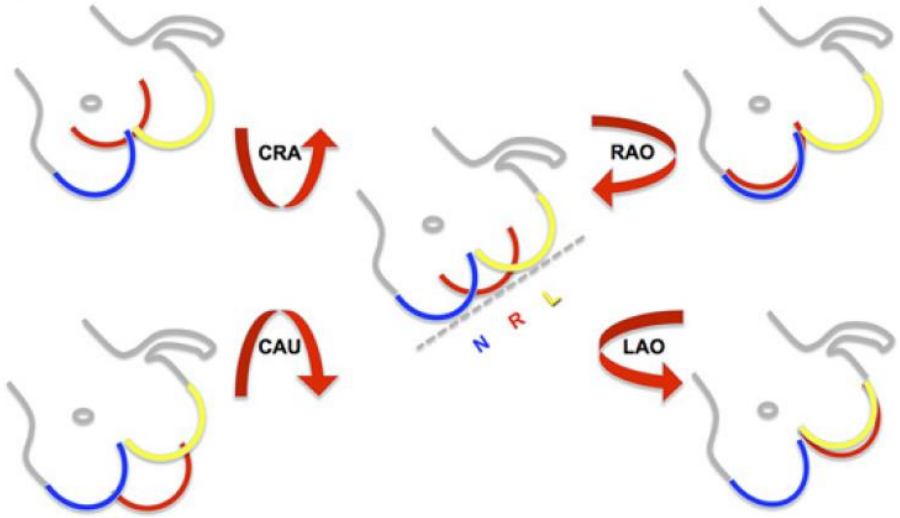

Figure 2-20 Right cusp rule positioning (63)

Kasel et al. (2014) speculated that the technique describes above contribute to the reduction of the contrast volume injected in the patient and the reduction of the procedural time, it also demonstrated that TAVI can be successfully performed under fluoroscopy guidance only (64).

2.5.3 3D printing

Three-dimensional (3D) printing is an impressive manufacturing tool which usage has increased over the past 20 years in biomedical engineering. 3D printing has enabled the easy manufacturing of complex shapes in a short time and at a lower cost (65). 3D printing can be used for preoperative planning by creating a patient specific model to help the surgeon plan the procedure in advance. Due to its affordability, it can be used to create prototype faster and test them, it can also be used to print patient specific implant using biomaterials. The different applications of 3D printing in medicine can be seen in Figure 2-21.

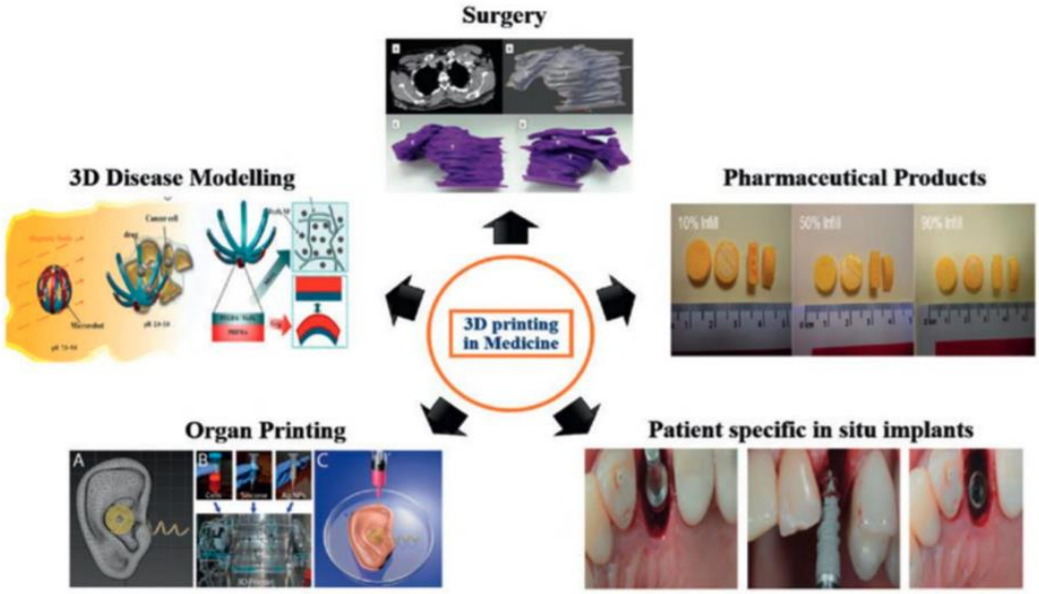

Figure 2-21 3D printing applications (Kalaskar, 2017)

In an article published by the Sydney university, Dr Carmine Gentile states that they are developing an approach that uses biological material taken from the patient to replace damaged heart tissue (66).

Redondo et al. (2021) showed the patient's aortic valve and leaflet were 3D printed to confirm the rotational orientation of the valve before implantation. It was shown that this method can potentially be used for all other kind of TAVI devices. Figure 2-22 shows the steps taken to extract the scan print and test the device.

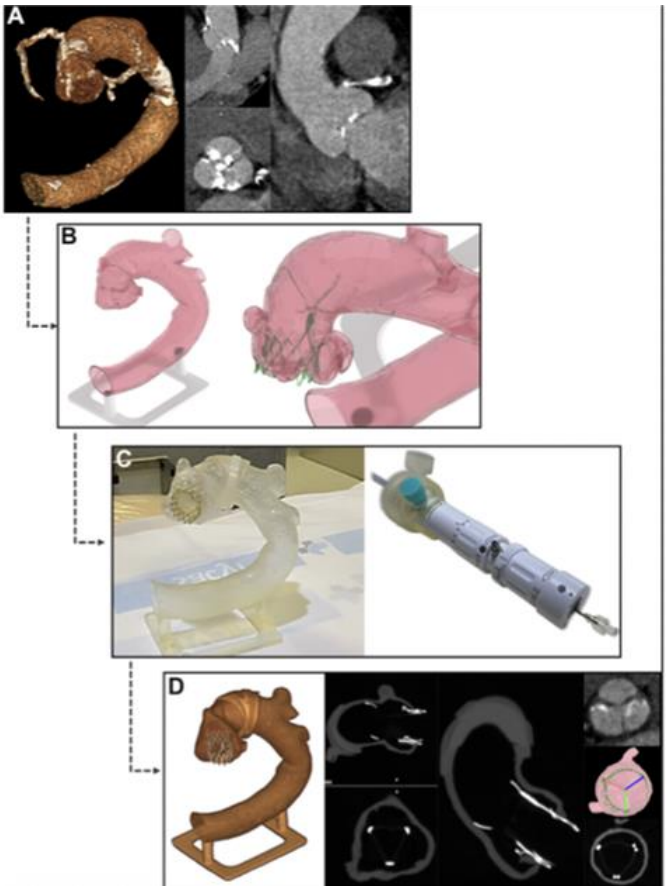

Figure 2-22 Usage of 3D printing for TAVI (67)

Image A is the CT scan image taken before the valve was implanted. The second image (image B) is the in silico simulated prosthesis implant. On the left of image C, the 3D-printed root from the CT scan images can be seen. The last image is the post-implant CT showing that the position of the valve is as predicted in the model (67).

2.6 Current Procedure

The illustrations bellow (Figure 2-23, Figure 2-24, and Figure 2-25) can be used as reference to describe the TAVI procedure, the whole procedure is done under fluoroscopy imaging. The steps taken during a TAVI using the delivery device and balloon are as follow:

1. The delivery device is inserted through the apex of the left ventricle and aortic valve to a supra-annular position (A)
2. The outer sheath is retracted to expose the head of the device (B)
3. The trunks are extended (C)
4. The delivery device is slightly pulled back to engage the trunks to the native leaflet and confirming positioning (C)

5. The helical balloon and valve are deployed while maintaining the pull force F on the device (D)
6. Invaginate the trunks so that they retract from the leaflets (E)
7. Collapse the helical balloon (F)
8. Retrieve the device head with the sheath (G)
9. Remove the delivery device, leaving the correctly aligned implant in the native anatomy (H)

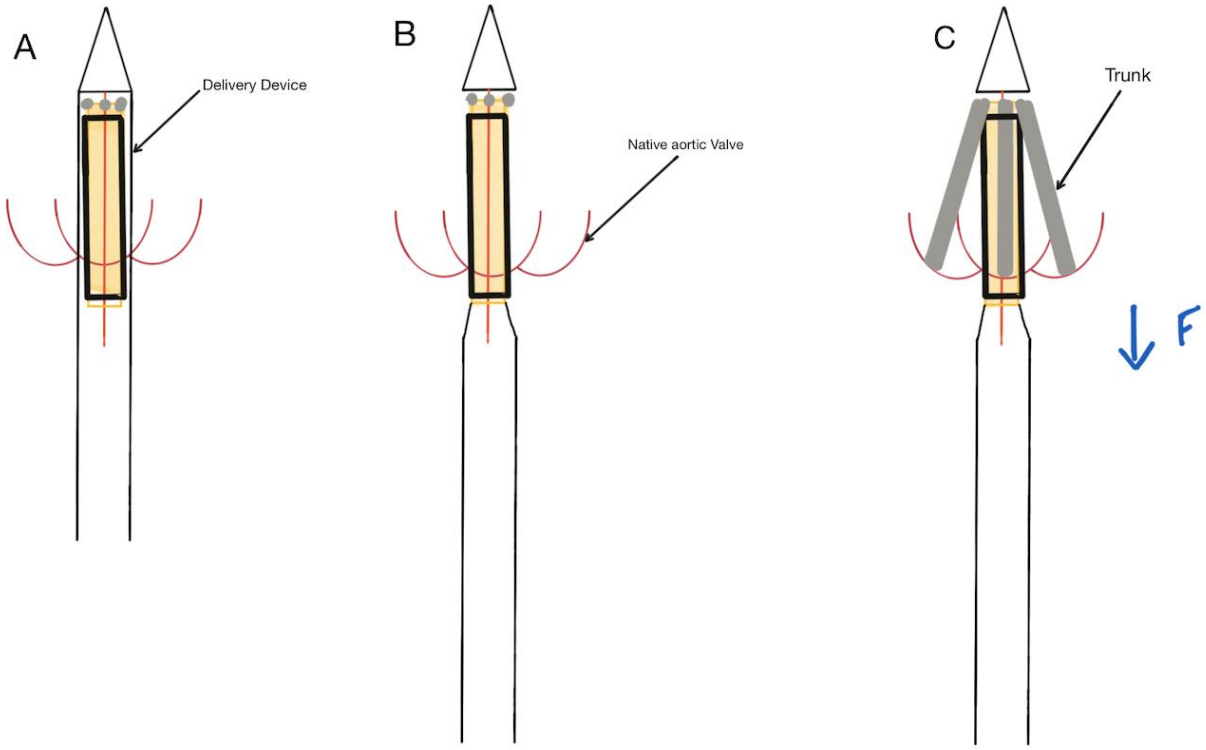

Figure 2-23 SAT Valve Implant illustration steps A, B, and C

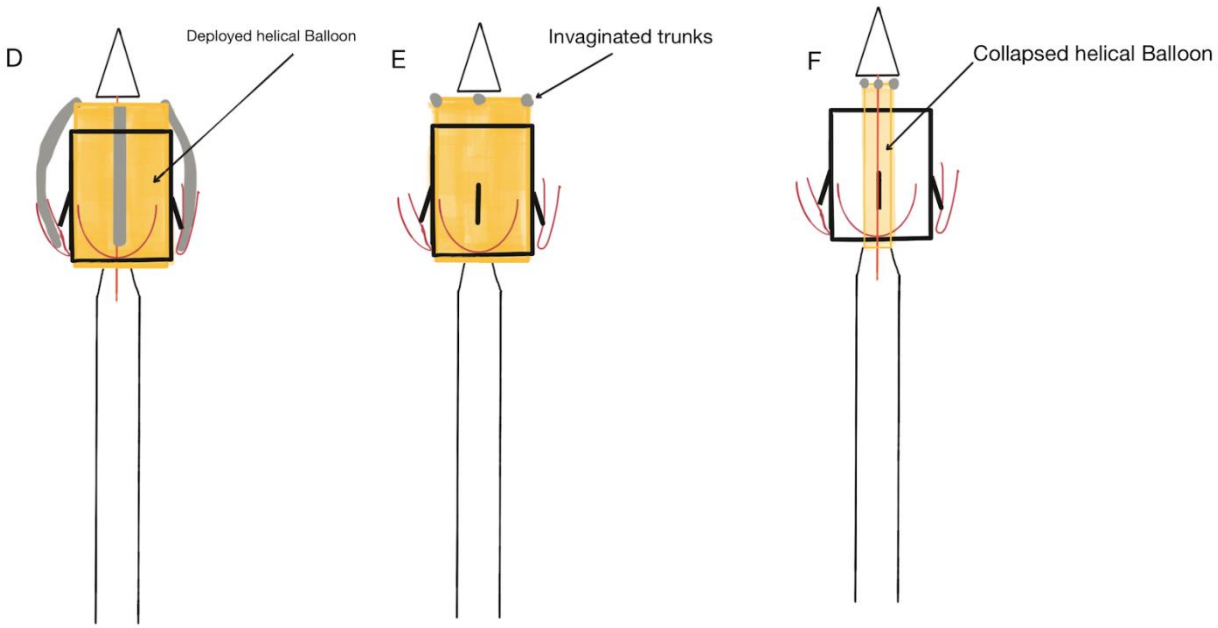

Figure 2-24 SAT Valve Implant illustration steps D, E, and F

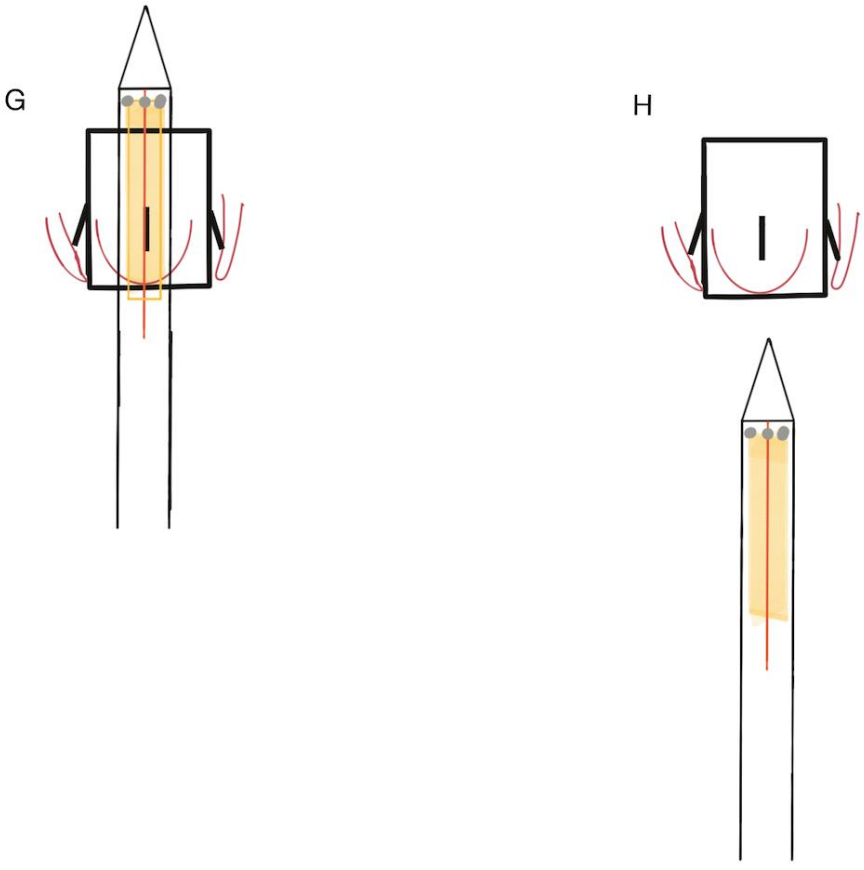

Figure 2-25 SAT Valve Implant illustration Steps G and H

3. Aims and objectives.

3.1 Problem statement

The unknown during the procedure is the force (F) required to position the valve accurately. This force (F) has two anatomical impacts. The first impact is to manipulate the annular plane to the desired position (Figure 3-1). The second is that it may cause the native leaflet to droop (Figure 3-2).

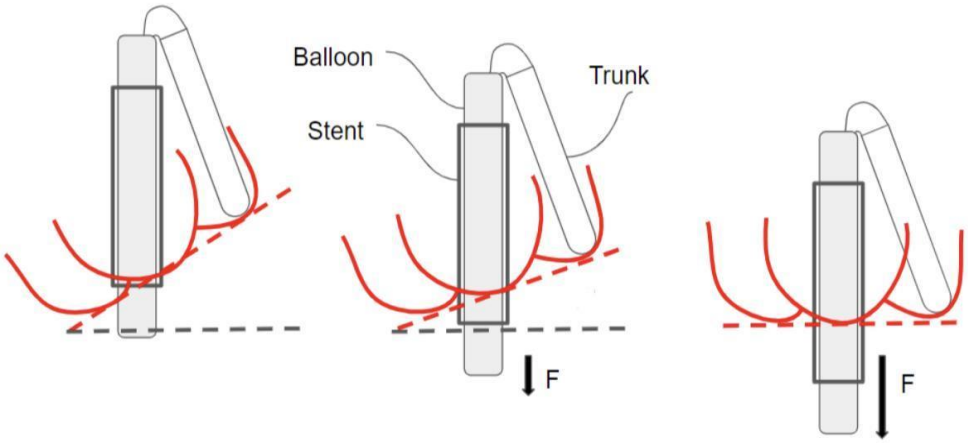

Figure 3-1 Annular plane manipulation illustration

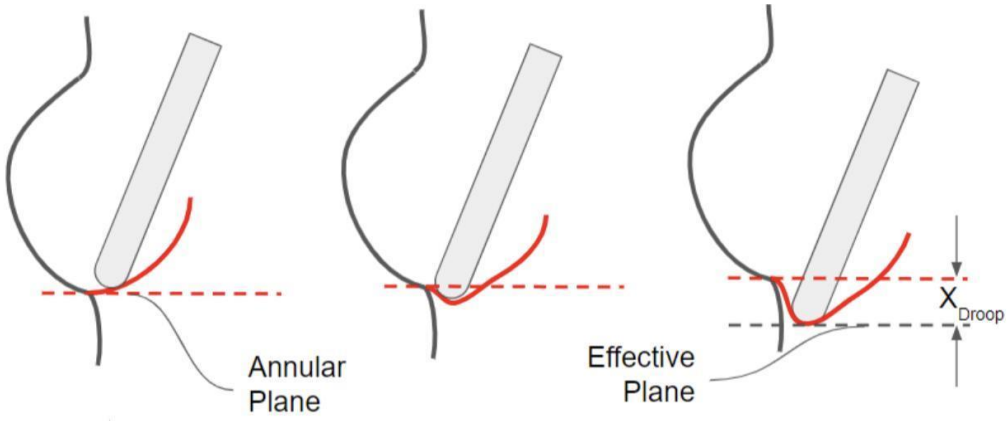

Figure 3-2 Leaflet Droop illustration.

The force required to deploy the SAT delivery device is unknown. Currently, to train surgeons, multiple animal trials and ex-vivo tests are required. Those exercises are costly and exposing the operating team to radiation.

3.2 Proposed solution

The proposed solution is to develop a training rig that will replicate all aspect of the TAVI, the training rig should enable the surgeon to practice valve positioning in an environment free of radiation and indicating when adequate force is applied to accurately position the valve.

3.2.1 Research aims.

The aims of this research are:

1. To determine the force required to accurately position the valve.
2. To develop a training device to train surgeons on the use of the delivery device.

3.2.2 Research objectives.

The research objectives are:

1. To determine a relation between the force applied and the leaflet droop.
2. To calculate the force range required to accurately position the valve.
3. To develop an imaging system that will be used to train surgeons.
4. To develop a circulatory loop model to implant valve during training.
5. To develop a force indicator tool that indicates if adequate force is applied during the valve positioning phase.
6. To test the force indicator tool and evaluate its effectiveness.
7. To provide recommendation for the use of the training rig and suggest areas for further research.

4. Materials and Methods

4.1 3D Printing procedure

The printer used was a Formlabs Form 2 printer, a stereolithography printer using a laser that cures the liquid resin to make the 3D object needed, with a printing bed of 150 x 150 x 170mm as seen in Figure 4-1

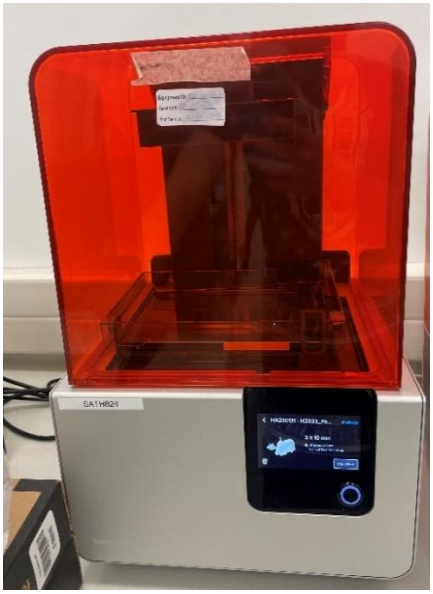

Figure 4-1 FormLabs Form 2 printer.

The parts were designed using SolidWorks 2022 then saved in STL format. The files were then uploaded onto the preform software that got the model ready for printing. Once the parts were done printing, they were removed from the printing bed then washed in IPA. The parts were left to dry then cure using a curing chamber called Form Cure (part number FH-CU-01) see Figure 4-2.

Figure 4-2 FormLabs Form Cure

There is a wild range of materials that can be printed but the three resins used are white resin, clear resin, and elastic resin. The resins information can be seen in Table 4-1.

Table 4-1 Resin post-printing settings

Resin name	Product code	Wash time	Drying time	Curing time	Curing temp
White	RS-F2-GPWH-04	2 x 10 min	1h	60 min	60°C
Clear	RS-F2-GPCL-04	20 min	1h	30 min	80°C
Elastic	RS-F2-ELCL-01	20 min	1h	60 min	60°C

To keep the part clear and non-sticky, the elastic resin was cured soaked in a 60°C water container.

The clear resin was used when a see-through material was required, the elastic resin has a 50A shore hardness and was used when a flexible material was needed, for all other applications, the white resin was used.

4.2 Leaflet Droop test

4.2.1 Test set-up

The droop can be defined as the displacement of the leaflet in the axial direction due to the pull force of the trunks.

Fifty (50) pig hearts were collected from a local abattoir for this purpose, only the hearts with minimal tissue damage were taken. This number of pig hearts was chosen empirically as there were no previous studies to reference regarding this concept. The requisite animal ethics committee (AEC) applications for using animal material for scientific studies approval was obtained before the commencement of the study (AEC reference number 021_022). The approval letter can be seen in appendix A.

The pigs were landrace pigs breed for food consumption; they were between 5 to 6 months old at the time of slaughter. The hearts were cut leaving approximately 20cm of the aortic arch intact. The hearts were cleaned by trimming all excess fat and tissue from the heart can be seen in Figure 4-3. The heart on the left was a fresh-cut heart and the one on the right was cleaned.

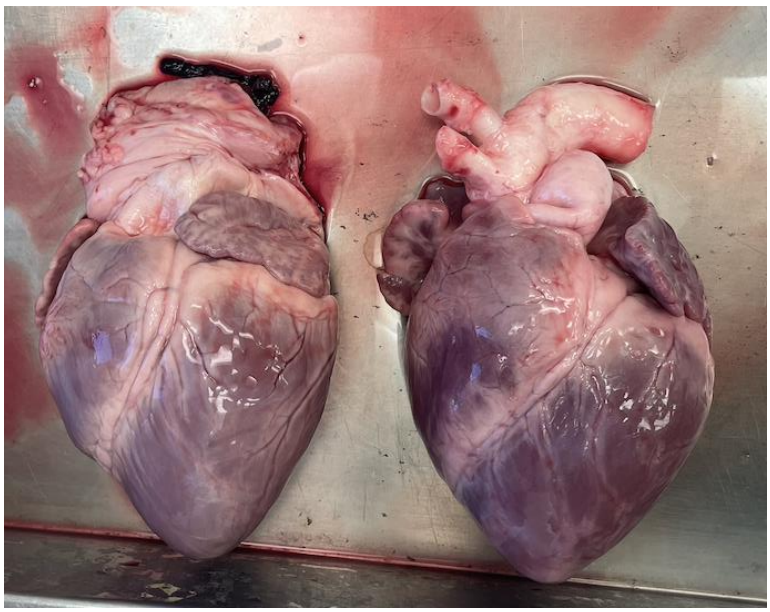

Figure 4-3 Freshly cut and cleaned hearts.

The hearts were cannulated as follow; two ports were inserted in the aortic arch branch (left subclavian artery and brachiocephalic trunk). One of the ports was used to insert the endoscope to see inside the heart and the other to insert the pigtail catheter that delivered the contrast medium. The apex of the heart was punctured, and 4 purse-string sutures were placed to seal the hole. A hole was cut in the left ventricle and a modified 3D-printed screw was inserted; the screw was used to connect the heart to the pulsatile pump. An image of the setup can be seen in Figure 4-4.

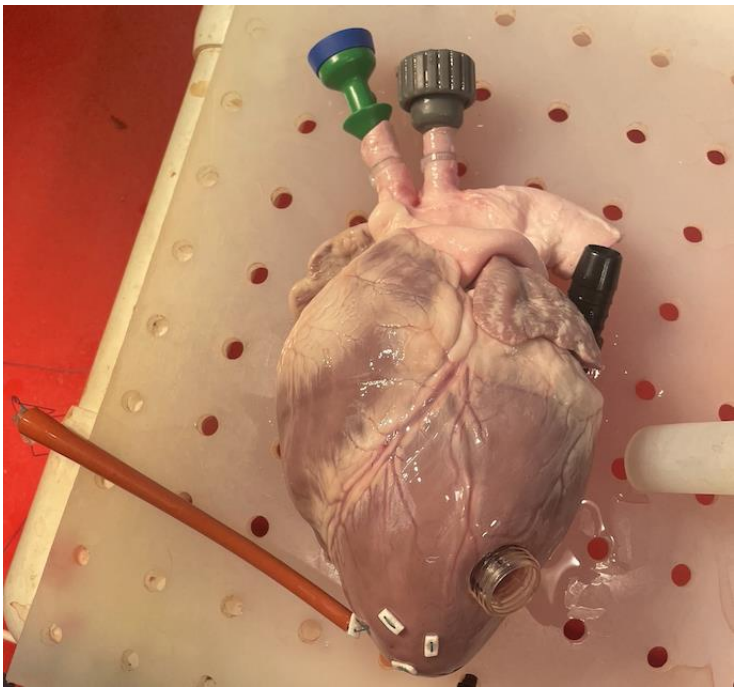

Figure 4-4 Cannulated heart

Three radiopaque markers were used as reference to measure the droop, the markers consist of a barium iridium marker band bonded onto a nitinol harpoon (see Figure 4-5). The markers were positioned in the heart on the attachment between each leaflet and the SOV, as shown in Figure 4-6.

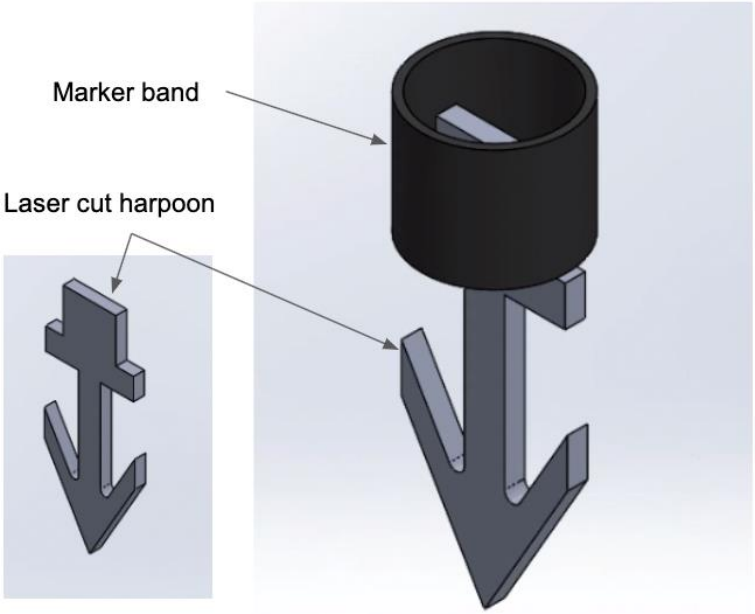

Figure 4-5 Radiopaque Marker

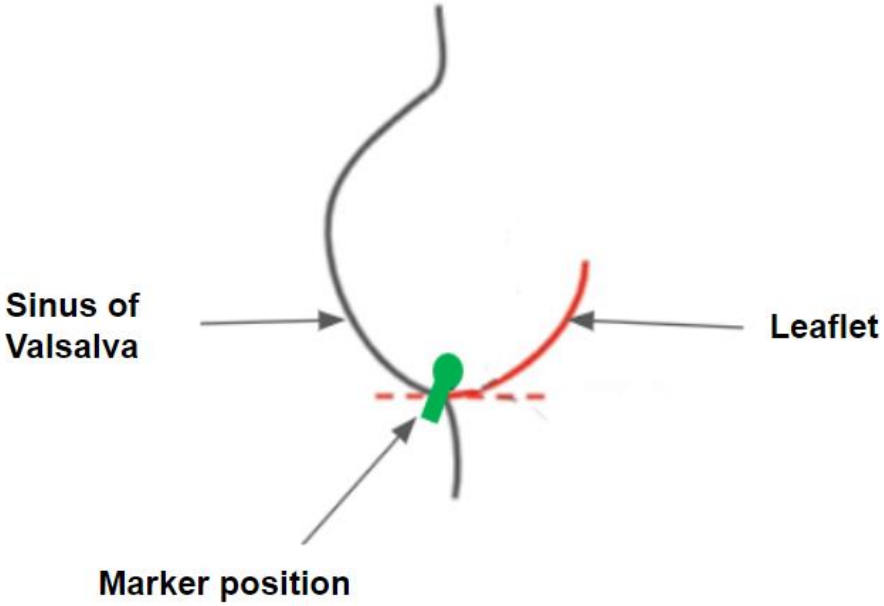

Figure 4-6 Marker position design

A pull force tool was designed to replicate the 3 trunks of the delivery device (Figure 4-7). The pull force tool was 3D printed using the FormLabs white resin. As the 3D printed material used was not radiopaque, stainless-steel rods were inserted into each of the pull force tools' cavities to make them visible under fluoroscopy.

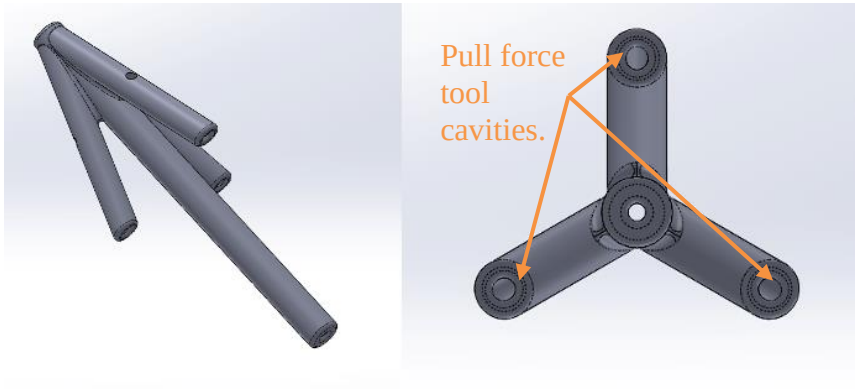

Figure 4-7 Pull Force Tool

The pull force tool was then introduced into the heart from the opening in the aortic arch and slid down until each of the 3 arms of the pull force tool was positioned in a leaflet. The end of the pull force tool was guided out of the heart from the entry side using a metallic rod. The metal rod was inserted into the heart from the left aortic apex entry point all the way until it came out of the aortic arch. Once the pull force is in position the heart was connected to the pump. The final setup can be seen in Figure 4-8.

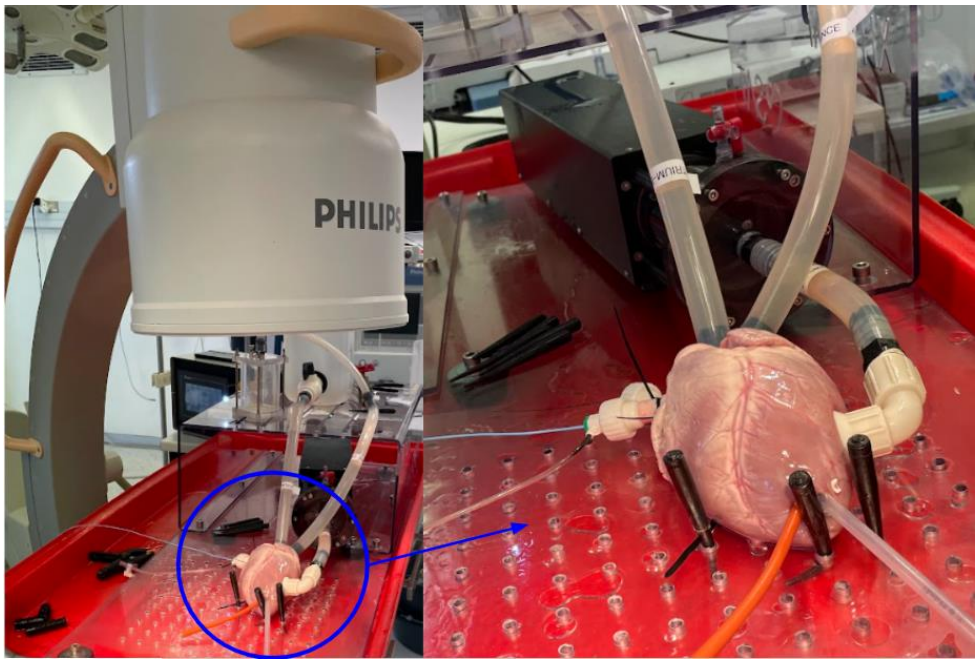

Figure 4-8 Test set-up.

The pig hearts were connected to a pulse duplicator pump which replicated the blood flow and the pressure gradient across the aortic valve. Once connected the pump was started and a contrast medium was injected, under fluoroscopy, to position the C-arm following the right cusps rule. However, due to the position of the hearts and the location of the connection ports, the NCC was positioned in the centre of the image instead of the RCC. The RCC was positioned on the left, and the LCC on the right of the fluoroscopy image. Figure 4-9 shows an illustration of the difference between the position of the leaflets following the right cusps rule and the modified version used.

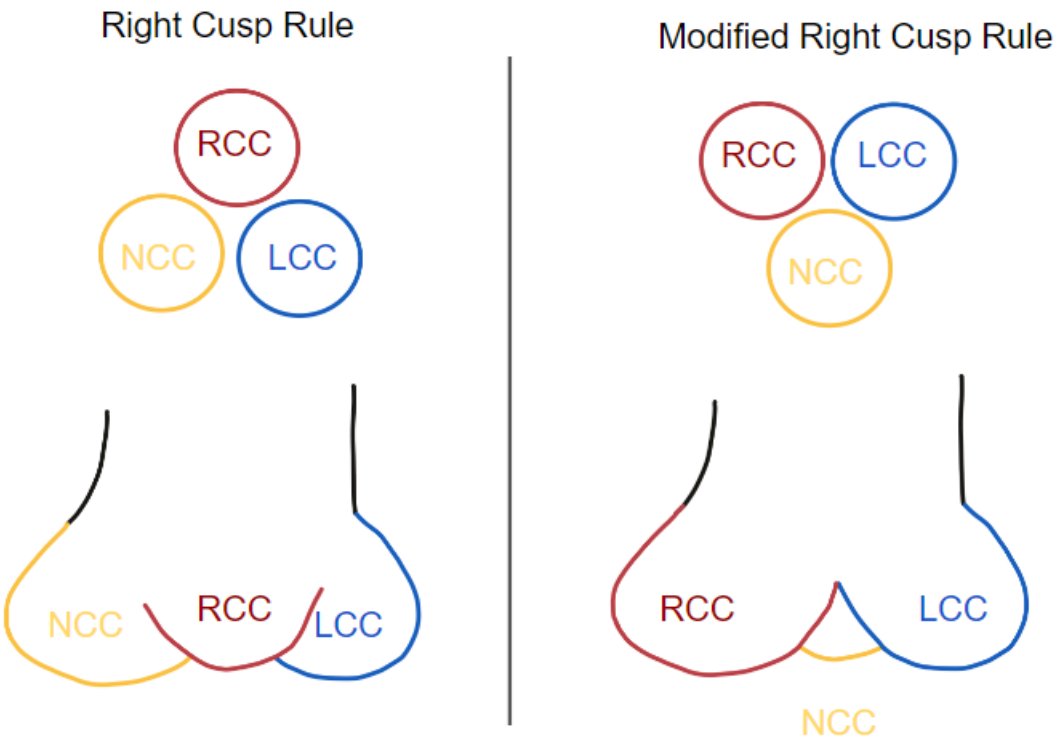

Figure 4-9 Aortic cusps position comparison during the right cusp rule and the modified method.

Despite the small deviation from conventional methods, the measurement of the leaflet droop was not impacted. The data obtained from the rotated images were still valid as they accurately reflected the force applied and the leaflet droop during the procedure.

A force gauge was connected to the pull force tool. The force gauge used was a LUTRON FG-6005SD. A force was applied incrementally, pulling the pull force tool inside the aortic leaflet causing the leaflet to droop and manipulating the annular plane. An illustration of the procedure can be seen in Figure 4-10:

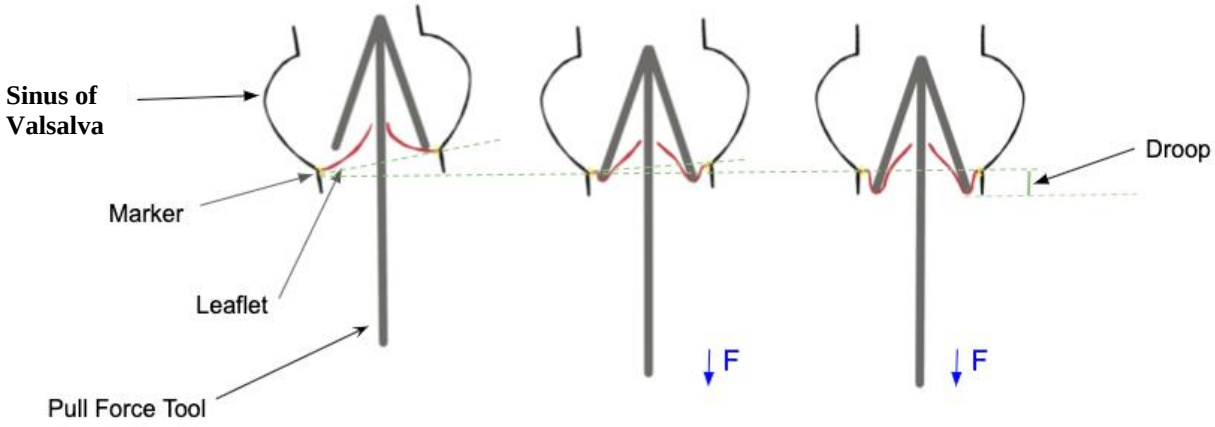

Figure 4-10 Test illustration

The following equipment were used for the tests.

Table 4-2 Test Apparatus

Quantity	Name	Description
50	Pig hearts	Hearts used for the tests
30	Leaflet harpoon	Laser cut harpoon with marker band used to locate the connection between aortic leaflet and aortic root
1	Pull force tool	A 3D-printed tool replicating the position of the SAT delivery device trunk
1	Force gauge	Used to measure the pull forced
1	Pulse duplicator pump	A pump pushing and drawing water are used to pump the pigs' hearts and replicate the blood flow.
1	Fluoroscopy machine	An imaging device used to visualise and determine the leaflet droop
1	Surgical plier	A tool used to position the harpoon in the right position
1	Endoscope	Used to position the harpoon in the right position
1	Syringe	A syringe filled with contrast medium to visualize the inside of the heart using fluoroscopy
50	Sutures	Used to seal the heart entry point (left ventricle apex) to prevent leak
2.5L	Contrast medium	Mixed solution made of 50% contrast and 50% saline

250	Cable ties	Use to connect the hearts
1	Scissors	Used to clean the heart
1	Pigtail catheter	Used to inject contrast in the heart

4.2.2 Data Analysis

During the tests 2 data sets were recorded, the fluoroscopy images and the pull force from the force gauge. The fluoroscopy images were analysed using the MICRO DICOM Software. The recordings were saved as a series of images and transferred to a computer for data analysis. Using the images from the fluoroscopy, the droop and the angles were measured in five different images, the first time at the start of the test, the last one at the lowest droop, and 3 in between. To keep consistent data, the 3 images selected were the last image during the diastole phase. The values measured were in pixels (px) and converted to mm by using the diameter of the endoscope as reference. The droop of the 3 leaflets, NCC, LCC and RCC were kept separated in the data analysis. Leaflet 1 is the RCC (most left in the image) leaflet 2 is the NCC (leaflet in the centre of the image), and leaflet 3 is the LCC (leaflet on the right in the image). Once all images were analysed, they were saved as a video keeping each image in order (the images are numbered from first to last). The time at which each image appears in the video is recorded. An example of the droop data obtained for heart 15 can be seen in Table 4-3.

Table 4-3 Droop values measured example

Image Number	Droop L1 (mm)	Droop L2 (mm)	Droop L3 (mm)	Time (s)
1	0.856474	-2.43292	-1.21111	0
37	-2.13025	-7.7805	-3.47636	2.346
64	-3.02576	-10.1706	-5.52426	4.147
81	-4.27907	-11.4756	-5.67711	5.268
96	-4.63101	-12.4306	-6.34259	6.278

As the force gauge recorded only one value per second, it was not possible to directly obtain the force values for the droop selected. The forces for the droops obtained had to be calculated. As the pull test was stopped when the lowest droop and higher force was obtained, the timeframe of the forces recorded relative to images saved could be determined. The highest force time was matched to the time of the lowest droop and the previous force recorded was thus obtained by subtracting one second per entry for each force values recorded preceding the maximum force. An example of the force recorded at one second interval for heart 15 can be seen in Table 4-4.

Table 4-4 Force vs Time example

Force (N)	Time (S)
4.61	1.278
7.96	2.278

11.73	3.278
13.81	4.278
15.46	5.278
16.16	6.278

The forces for each droop values were interpolated using the 2 closed time values. The interpolation formula used to calculate the forces can be seen in equation 1. Table 4-5 shows three forces and times. Force A and C are measured from the pull force and B is the force required at a specific droop measured at time X. Note A<B<C

Table 4-5 Force and time example

Force	Time
A	w
B	X
C	y

$$\boldsymbol{B = A + \frac{C-A}{y-w}(X - w)} \qquad \textbf{Equation 1}$$

Once all the forces have been calculated for each droop, a graph is drawn using excel to represent the force vs droop.

The results were following a linear trend. To compare and analyse the droop of all the hearts, a model was developed by calculating the droop of each leaflet at 2.5N, 5N, 7.5N, 10N and 12.5N using the trend line equation generated, as the force recorded per droop differs from heart to heart.

Once all 50 tests were done, the values calculated were analysed. The outliers were removed from the data set before starting with the analysis. The Bivariate Fit of the droop by force was calculated for each leaflet and the linear fit of was obtained per leaflet.

It was shown empirically that during the TAVI there is 3.6 mm leaflet droop caused by the trunks. Thus, the design of the trunk lengths has an additional 3.6mm length included to cater for this droop. Furthermore, in the TAVI the valve can be deployed 1mm lower or 2.4mm higher that its desired position. In order to account for these different tolerances, the forces causing a droop of 3.6mm, 1.2mm and 4.6mm on all three leaflets were calculated using the linear fit equations. Those three forces are the minimum, maximum and expected force required to accurately position the implanted valve during the TAVI in a cadaveric porcine heart.

4.3 Training Rig Design Methodology

During the design of the rig, each part was given a unique identifier. The identifier (item numbers) was sequentially generated on a Master Record Index (MRI) spreadsheet starting from 0001. Every custom-made part drawn was given a drawing number. The format of the drawing number was NKMFADXXXX-RX with XXXX being the item number of the parts. RX was the revision of the file, starting at R0.

The components used that were not designed, that were available to be purchased in-store, had as drawing number “Bought Out” in the bill of materials table in the assembly drawing,

Each item designed had a unique name, item number, and revision number. For each new item created a new line was populated on the MRI spreadsheet. Each line on the MRI spreadsheet gave more detail about the part. Each line of the MRI spreadsheet had the generated item number, the drawing number, the part name, a detailed description of the part, the manufacturing method of the part, its material, the part’s latest revision, and the supplier of the part raw material (or of the part). The MRI spreadsheet can be seen attached in Appendix B.

The training rig was designed following the user need and design input mentioned in Table 4-6.

Table 4-6 User need and Design Input

N	User need	N	Design input
1	The rig should be used to train new surgeons on the SAT TAVI Procedure	1.1	The training rig should include left ventricle apex suturing training
		1.2	The training rig should include an imaging of the device positioning during the procedure
		1.3	The training rig should include tactile feedback indication
		1.4	The training rig should include rotational alignment (device marker and C-arm positioning)
		1.5	The training should include axial positioning evaluation
		1.6	The training should include rotational positioning evaluation
2	The rig should be able to evaluate the deployment of a new valve/ delivery device	2.1	The training should evaluate for coronary occlusion
		2.2	The training rig should include the distance between the entry point the and landing zone

To achieve all design inputs, the design of the training rig was split into 3 main systems which are, an imaging system, a circulation loop, and a pull force indicator.

4.3.1 Imaging system

During a TAVI, the surgeon looks at a screen, displaying live fluoroscopic images, while manoeuvring the device. To reduce radiation exposure, an imaging system was designed and

incorporated into the training rig. The imaging system is composed of a C-arm, a camera, and a screen. The C-arm was designed with similar dimensions to the Phillips BV Pulsera shown in Figure 4-11. It was designed to have the same degree of movement and locking mechanism to hold the selected position. The camera will project live images to the screen in black and white to replicate fluoroscopy images.

Figure 4-11 Philips BV Pulsera C-arm

4.3.2 Circulatory loop

The circulatory loop will replicate the heart and the blood flow. The circulatory loop had a heart model made from clear, see-through material to allow the camera to record what was happening inside. A mix of water and food colouring was used instead of contrast to see the delivery device under the camera. The circulatory loop can be used to train surgeons or evaluate the performance of new devices. The circulatory loop consists of 12 parts which are:

1- The ventricular connection: The ventricular connection was 3D printed using the clear resin. Due to its hard property, a compliance chamber was needed to mimic ventricular function. The ventricular connection was connected to the pump, the aortic root, and the mitral valve replicate. The ventricular connection also includes an entry point section.
2- A pulsatile pump: The pulsatile pump used is connected to a computer-controlled pump which both pumps water forward through the ventricle into the aorta (systole) and draws back pulling water from the atrium into the ventricle (diastole)
3- Mitral valve replica: It is a one-way valve used to replace the mitral valve. The valve was positioned to close when the pulsatile pump pushes water into the system and open during the drawback.
4- Compliance chamber: The compliance chamber replicates the compliant nature of the arterial system. The volume of air in the chamber compresses during systole, due to the increase of

pressure from the pump and expands when the pressure drops during diastole. Expanding air increases the diastolic pressure of the system and aids the forward flow of water whilst the ventricle refills from the atrium. It follows that increasing the volume of air in the chamber increases the compliance of the system.

5- Aortic root: The aortic root was printed from the elastic material. The design of the root was taken from a patient's CT scan. The aortic root was connected to the aortic arch and the ventricular connection. The connections were sealed and able to resist water flow without leaking.

6- Aortic arch: The aortic arch was printed using the formal clear resin. The design of the arch was taken from a patient's CT scan. The model of the aortic arch was modified to include a connection point to the aortic root and the compliance chamber.

7- Subclavian compliance**:** A compliance chamber used to replicate the subclavian compliance

8- Resistance valve: The resistance valve is a simple brass gate valve that can adjust the flow using the screw on the flow resistor. The mean arterial pressure of the system increases by increasing the resistance of the system.

9- Atrial reservoir: The atrial reservoir is a water bath reservoir that has a heating element to reach 37 degrees

10- Femoral compliance: A compliance chamber used to replicate the femoral compliance

11- Transfemoral entry point: An entry point was introduced for the transfemoral approach.

12- Aortic entry point: The aortic entry point is the part where the device will be introduced into the system. It contains a silicone material that the training surgeon will puncture and suture as training for the TAVI.

A sketch of the circulation loop can be seen in Figure 4-12.

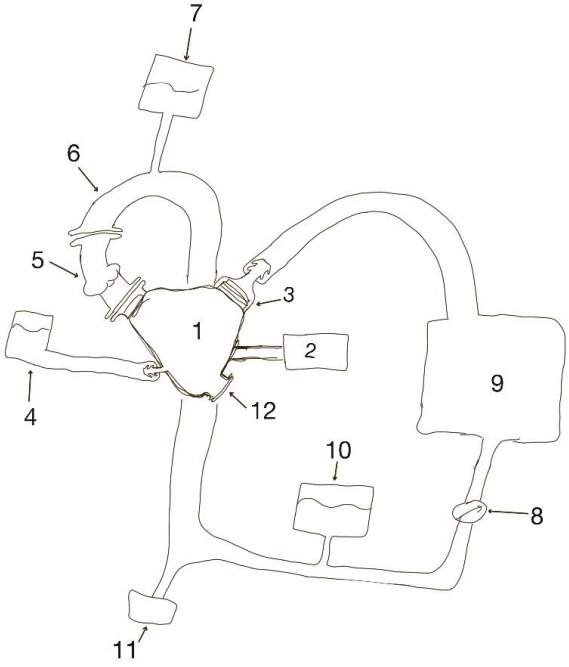

Figure 4-12 Circulatory loop illustration

4.3.3 Force indicator

The force indication device was designed using the current delivery device geometry as design input and the values of the force obtained during the leaflet droop test as force indication. The handle diameter of the delivery device is 45mm and 283mm long. The distance between the trunks and the distal end of the handle is 261mm. The force indicator device has a force sensor included. When the force applied by the surgeon is within the desired force range the light will shine green. When the force applied is greater than the required force, the light will shine red. When the force applied is less than the required force, the light will shine blue.

An illustration of the training rig setup can be seen in Figure 4-13.

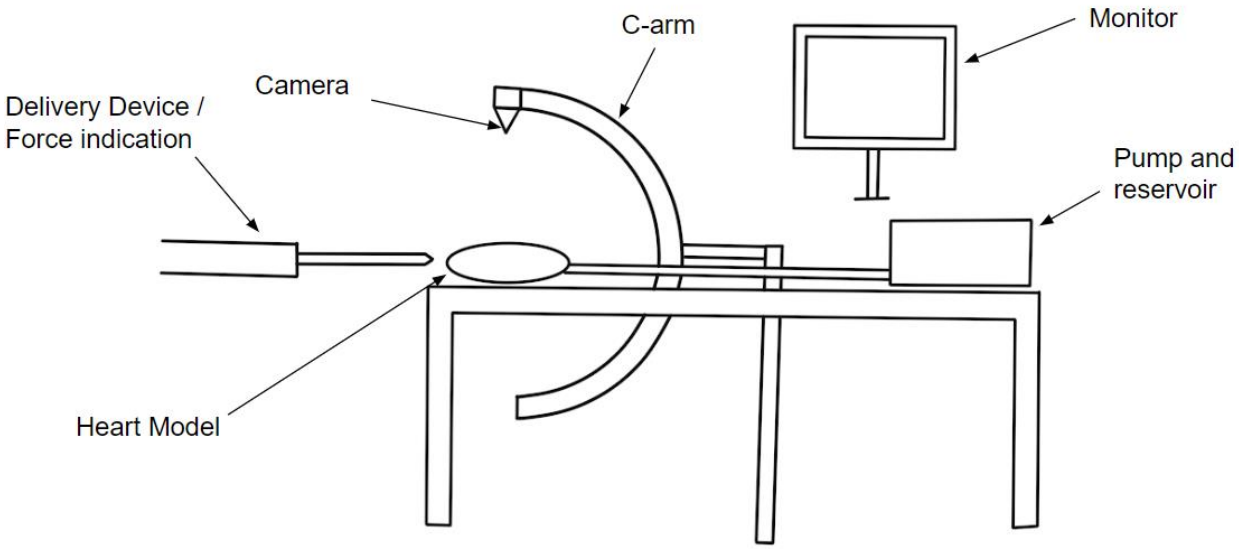

Figure 4-13 Training rig set-up

4.4 Scope and limitations

The leaflet droop test study will be limited to cadaveric porcine hearts, no human nor other animal species heart will be used. No living animal will be used for testing at this point either. The porcine hearts allow for conducting a controlled and ethical study while still providing valuable insight in the relationship between the force applied and the droop. The use of explanted hearts ensures that the specimens were ethically obtained and minimizes any potential harm to live animals. This study provides a foundation for further research.

The force gauge used to record the force during the droop test could only record one value per second, to get the force required multiple calculations were necessary.

The training device was developed to train the surgeon on the procedure pertaining to the SAT delivery device only, which are, device insertion, trunk positioning under fluoroscopy, and tactile feedback system.

The imaging equipment was fully designed but not manufactured as not in the scope of this thesis.

The circulatory loop was designed, and a prototype was build.

The force indication device was fully designed, build, and tested.

5. Results and Discussion

5.1 Leaflet Droop test results

During the test, some markers dislodged from their positions, making it impossible to measure the droops. In some cases, the pull force tool hooked onto the marker resulting in a 0mm droop recorded. Those values measured were removed from the data making the sample size slightly less than 50. Figure 5-1 shows an endoscopic image of the position of the 3 markers in the hearts after they have been positioned. Figure 5-2 shows the pull force tool inside a heart while the heart being pumped. The marker on the left in Figure 5-2 was starting to dislodge but did not leave its position during the test. This was caused during the marker insertion in the leaflet which sometimes causes a small tear in the native anatomy.

Figure 5-1 Markers position

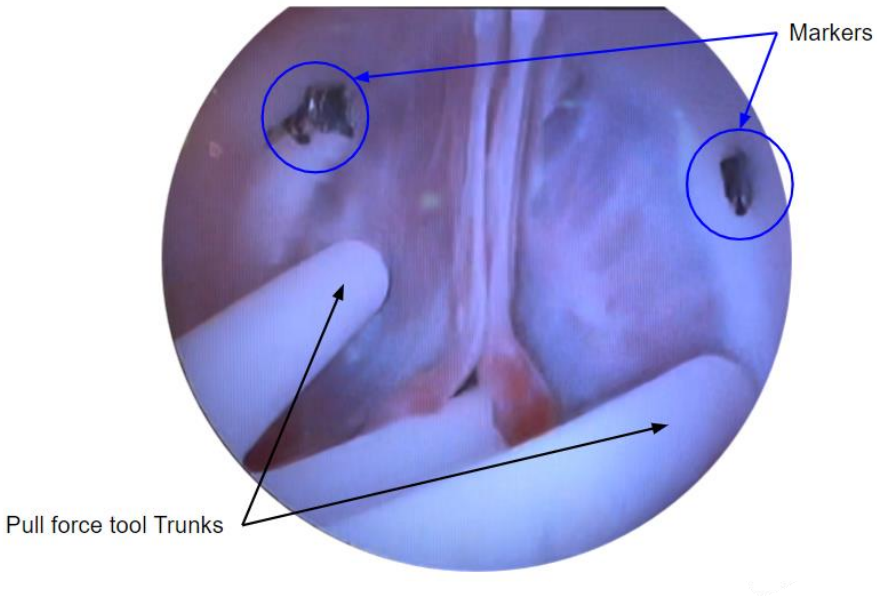

Figure 5-2 Pull force tool trunks and marker in the heart.

Figure 5-3 shows some of the fluoroscopy images obtained during the test. The first image (A) shows the positioning of the cusps before starting the test following the modified right cusp rule. The black arrow shows the pigtail catheter used to inject contrast. The second image (B) shows the angle between the pull force tool (yellow line) and the aortic angle (red line) and the initial position of the tool and the marker (the green line between the two red lines for each leaflet). The black arrow on the second image shows the endoscope used for measurement. The 3rd and 4th images (C and D) show the different angles and droop obtained by applying more force.

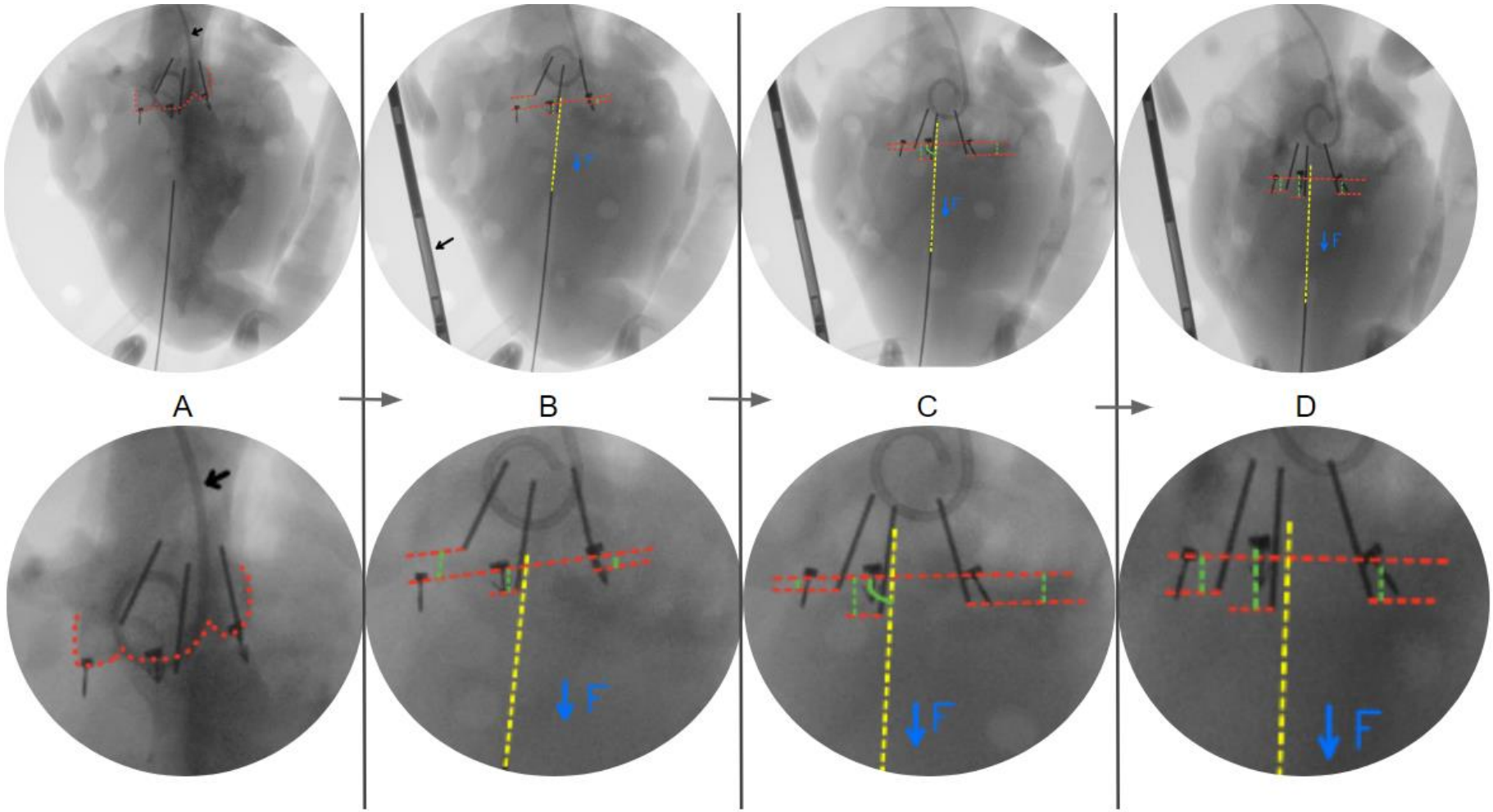

Figure 5-3 Fluoroscopy images obtained

Once the tests are done, the hearts are cut open and the markers are removed, Figure 5-4 shows a cut heart with the market still in position.

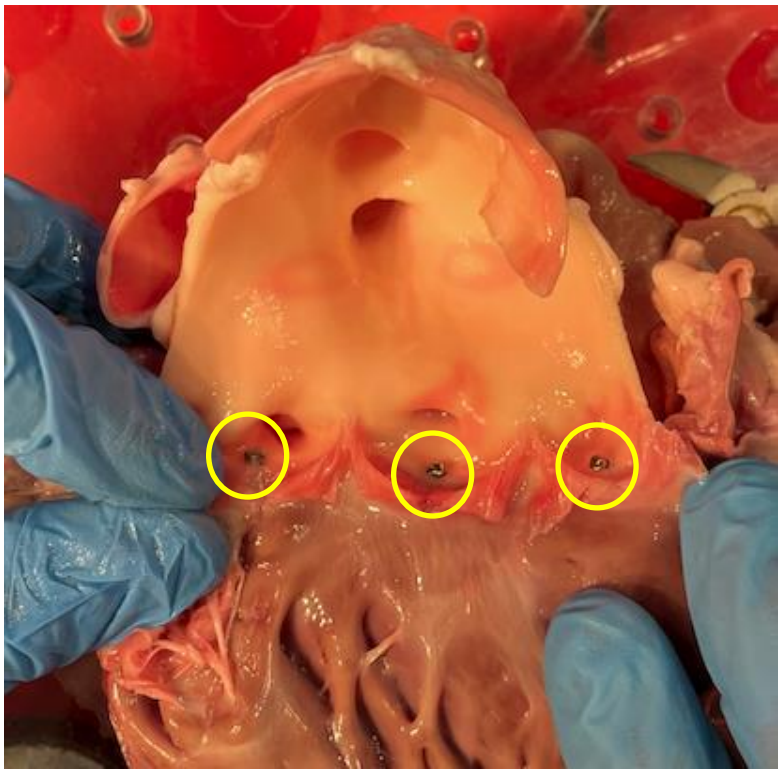

Figure 5-4 Heart cut open.

The graphs on Figure 5-5 and Figure 5-6 show the droop and force measured per leaflet, for heart 5 and heart 10 respectively.

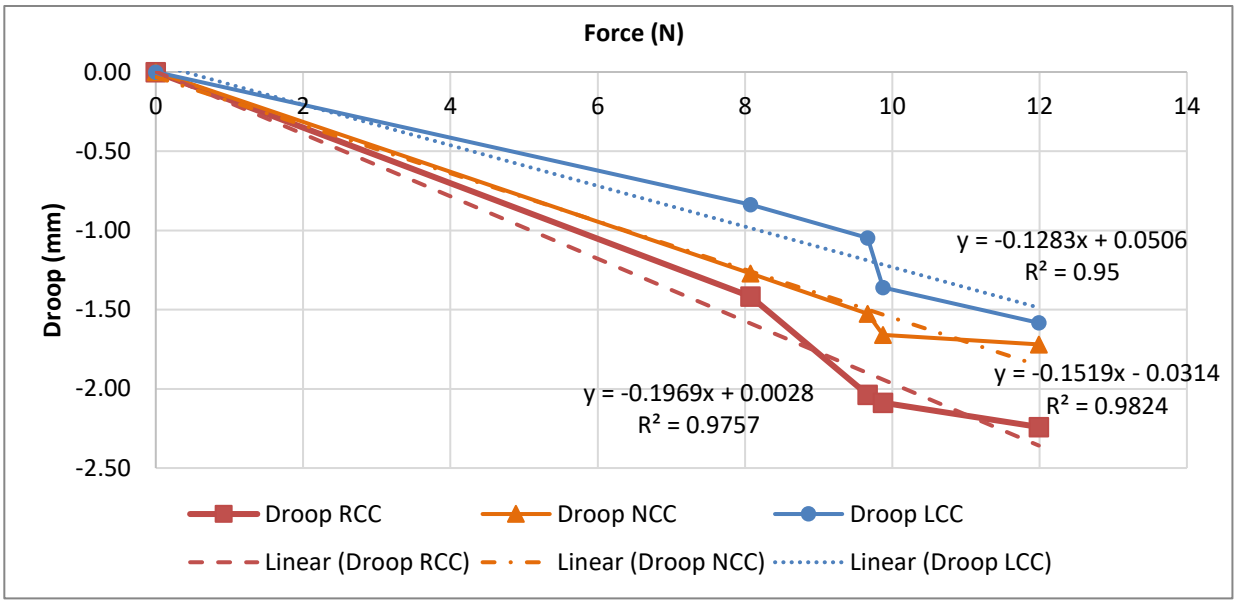

Figure 5-5 Droop vs force graph for heart 5's leaflets.

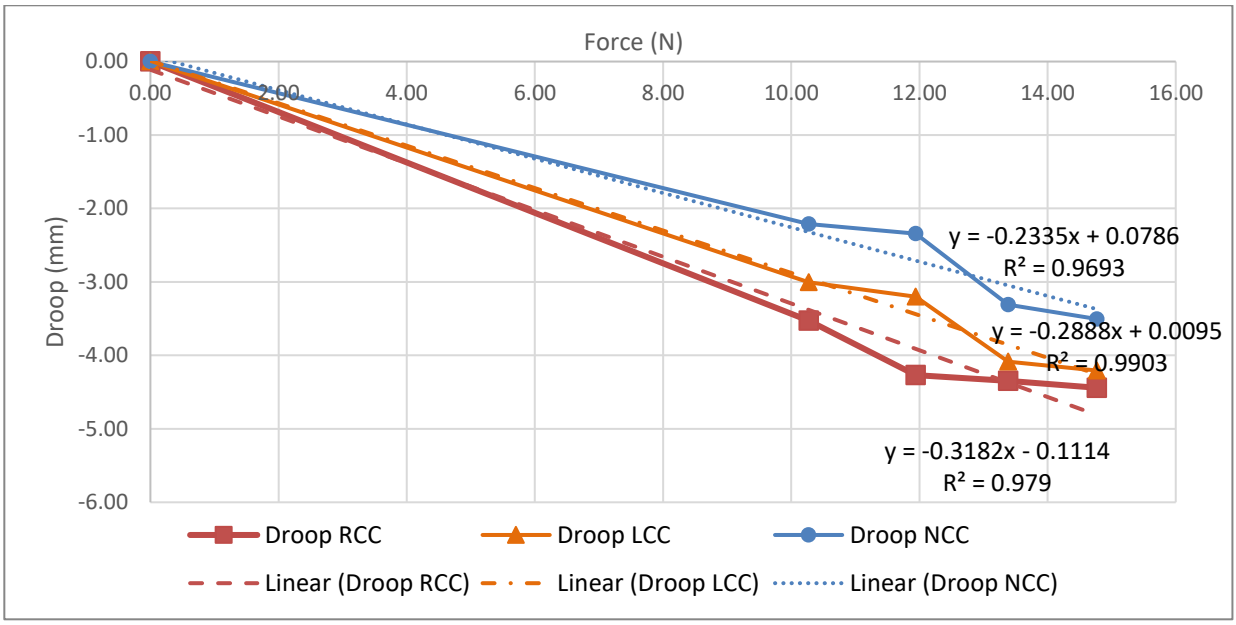

Figure 5-6 Droop vs force graph for heart 10's leaflets.

On those 2 graphs the droop is linear, with R^2 of the liner trendline over 0.95 and the RCC droops more than the LCC and the NCC which is representative of the entire data set.

The linear trendline have a R^2 values over 0.7 on 93.9% of the measurement. The distribution of R square can be seen in the chart on Figure 5-7 for the entire measured data set. 0.8% of the trendlines have a R^2 value less than 0.5, 5.3% are between 0.6 and 0.7, 9.8% are between 0.7 and 0.8, 23.5% are between 0.8 and 0.9, and 60.6% of R^2 values are above 0.9.

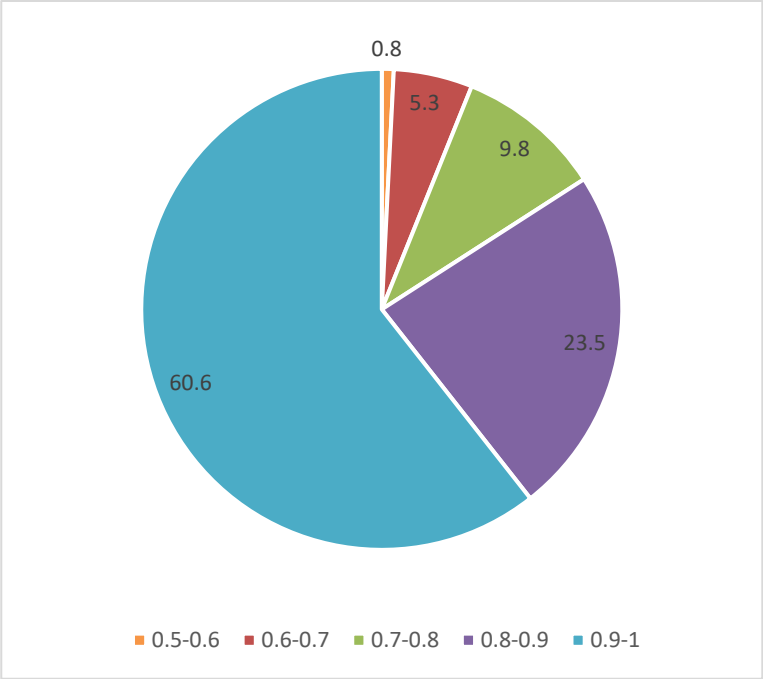

Figure 5-7 R^2 distribution

There was a total of 16 cases one harpoon either dislodged from its position or one of the pull force's trunks was positioned on top of one marker, making it only possible to measure 2 leaflets and one heart was not measurable. In all 34 cases where all three leaflets were measured the 47% of the time, the LCC had the lowest droop following by the NCC who had the lowest droop 41% of the time and the RCC having the lowest droop 12% of the time, for similar force applied.
The RCC was the leaflet with the highest droop 71% of the times following by the NCC 18% of the time and the LCC 11% of the times. The results can be seen in Table 5-1

Table 5-1 Leaflets droop position relative to the two others per test (N=36)

	Highest droop observed (compared to the other 2)	Lowest droop observed (compared to the other 2)
LCC	11%	41%
NCC	18%	47%
RCC	71%	12%

The NCC was the cusps with the most unmeasurable droop (12 times) compared to the LCC (1 time) and the RCC (2 times). Figure 5-8 below shows us heart 39 with one marker dislodged, the marker can be seen moving in the ascending aorta with the flow. The dislodgment of the marker can be caused by the soft tissue tearing when the heart is pumped or by not positioning them deep enough in the tissue.

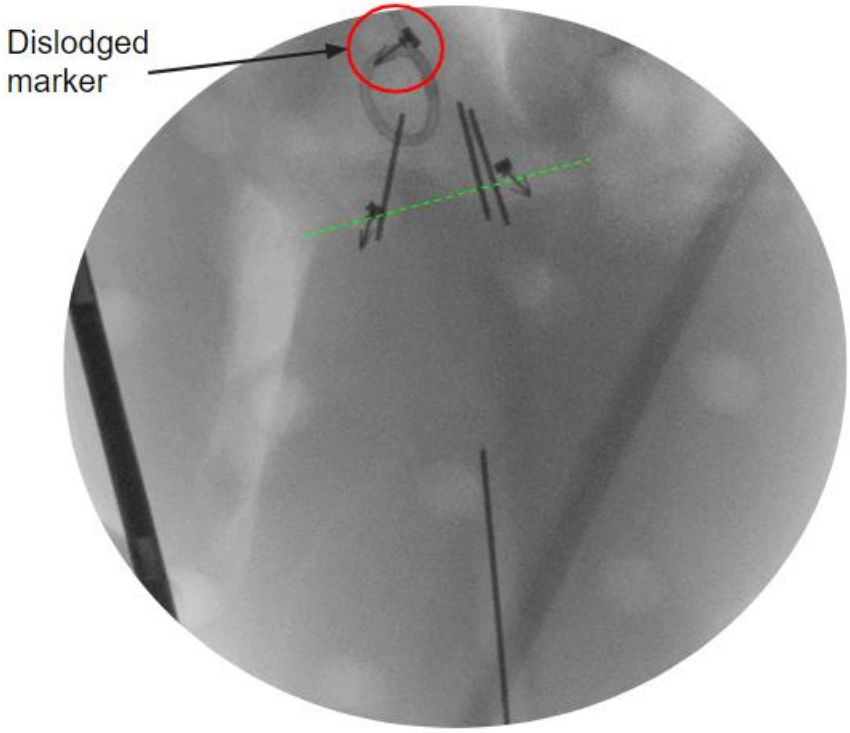

Figure 5-8 Dislodged marker in heat 39.

Figure 5-9 shows the pull force trunks positioned on top of the marker. It is difficult to see it prior to the test as the image obtained from the fluoroscopy is in 2D.

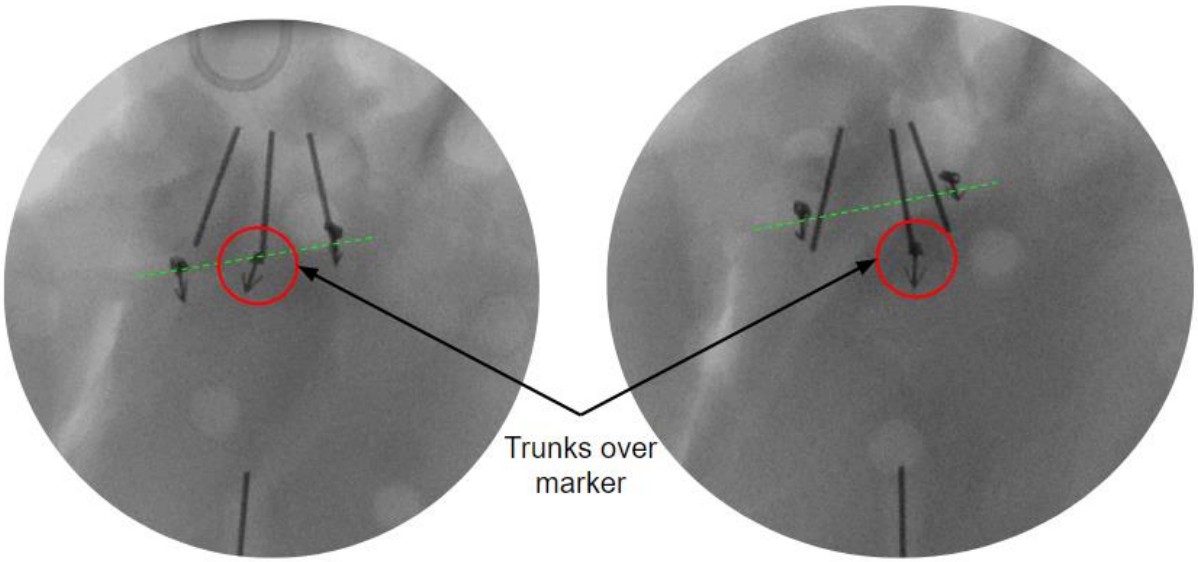

Figure 5-9 Pull force positioned over marker.

Table 5-2, Table 5-3, and Table 5-4 show the average values and the standard deviation for each leaflet obtained for the whole set. The full data set can be seen in Appendix C attached.

Table 5-2 Test result for L1 (RCC)

Force (N)	Average Droop (mm)	STDEV	Droop max (mm)	Droop min (mm)	N
2.5	-1.24	0.72	-2.70	1.35	48
5	-1.97	0.77	-3.34	-0.29	48
7.5	-2.70	0.95	-4.29	-0.42	48
10	-3.43	1.20	-5.59	-0.55	48
12.5	-4.16	1.49	-7.91	-0.67	48

Table 5-3 Test result for L2 (NCC)

Force (N)	Average Droop (mm)	STDEV	Droop max (mm)	Droop min (mm)	N
2.5	-1.08	1.02	-5.44	0.02	37
5	-1.64	1.31	-6.87	-0.08	37
7.5	-2.21	1.62	-8.30	-0.19	37
10	-2.78	1.94	-9.73	-0.29	37
12.5	-3.35	2.28	-11.17	-0.39	37

Table 5-4 Test result for L3 (LCC)

Force (N)	Average Droop (mm)	STDEV	Droop max (mm)	Droop min (mm)	N
2.5	-0.97	0.69	-3.71	-0.11	47
5	-1.49	0.84	-4.66	-0.29	47
7.5	-2.01	1.02	-5.62	-0.47	47
10	-2.54	1.22	-6.58	-0.65	47
12.5	-3.06	1.43	-7.53	-0.83	47

A visual representation of the droop of each leaflet by force can be seen in Figure 5-10. Each dot represents a value obtained.

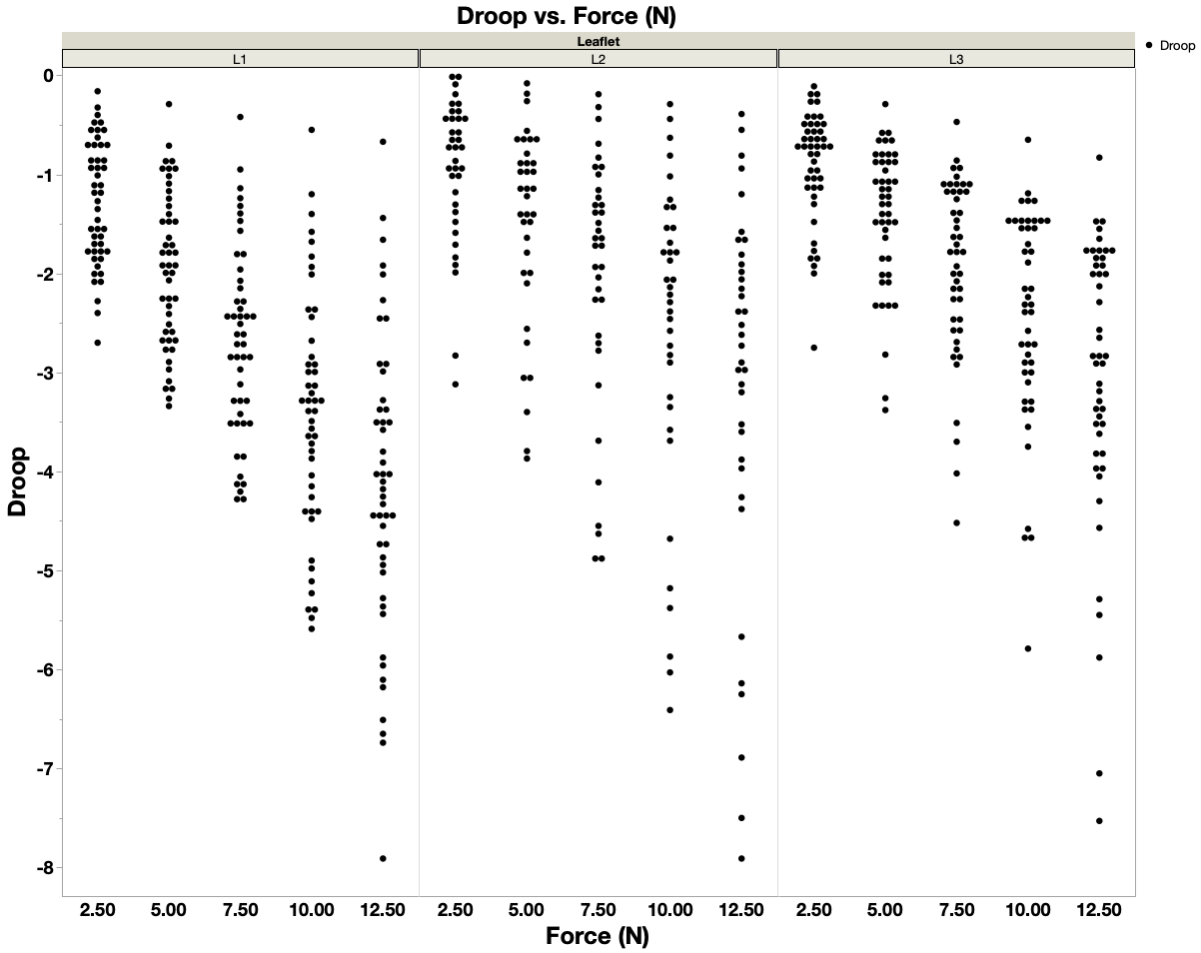

Figure 5-10 Droop vs Force result per leaflet.

A one-way analysis of the leaflet droop by per leaflet was done at each force. Figure 5-11 shows the droop of each leaflet at force of 2.5N.

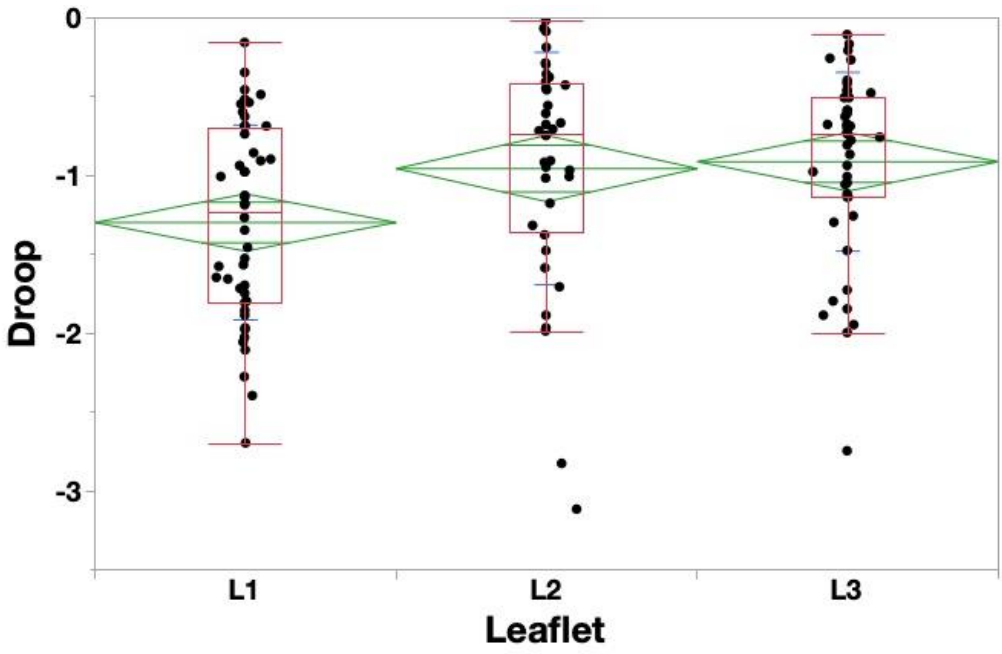

Figure 5-11 One way analysis at 2.5N.

The graph shown in Figure 5-11 above shows us that the droop of the second and third leaflets react similarly compared to the first leaflet which droops more at a lower force. The graphs for all other forces can be seen in Appendix C attached.

The linear regression graph per leaflet can be seen in Figure 5-12

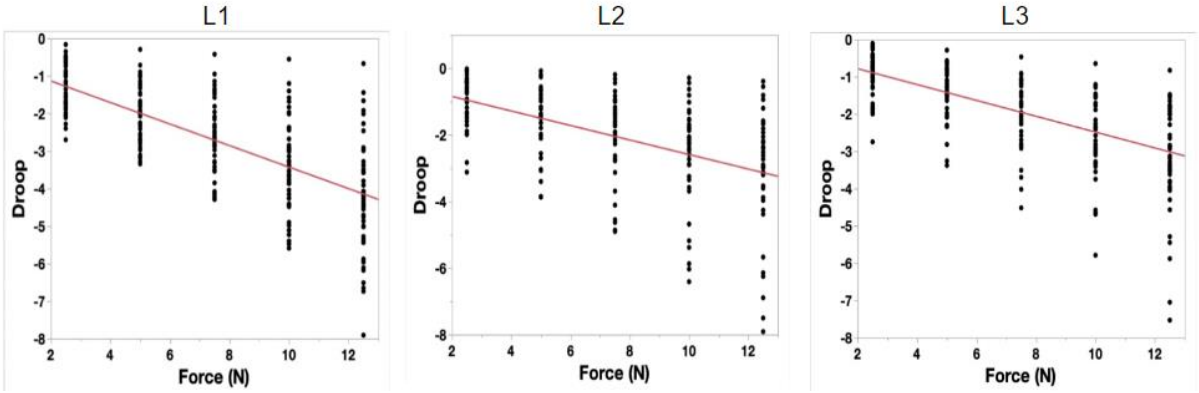

Figure 5-12 Linear regression per leaflet.

Table 5-5 was obtained showing the summary of fit for the graph presented in Figure 5-12

Table 5-5 Summary of fits

	L1 (RCC)	L2 (NCC)	L3 (LCC)
R-Square	0.481869	0.243136	0.370934
R-Square Adjusted	0.479692	0.238884	0.368187
Root Mean Square Error	1.056966	1.367483	0.985753
Mean of Response	-2.71029	-2.04539	-1.96078

To obtain the values needed the 3 linear equations needed are:

$F_{L1} = -3.4831 \times Droop_{L1} - 1.94$
$F_{L2} = -4.5872 \times Droop_{L2} - 1.88$
$F_{L3} = -4.7007 \times Droop_{L3} - 1.70$

Using the equations mentioned above the force required to cause a droop of 1.2mm, 3.6mm and 4.6mm were calculated and Table 5-6 was obtained.

Table 5-6 Calculated force at 1.2mm 3.6mm and 4.6mm droop

Leaflet	Force at 1.2mm droop (N)	Force at 3.6mm droop (N)	Force at 4.6mm droop (N)
L1 (RCC)	6.12	14.48	17.96
L2 (NCC)	7.39	18.40	22.98
L3 (LCC)	7.34	18.62	23.32

The forces calculated are represented in Figure 5-13.

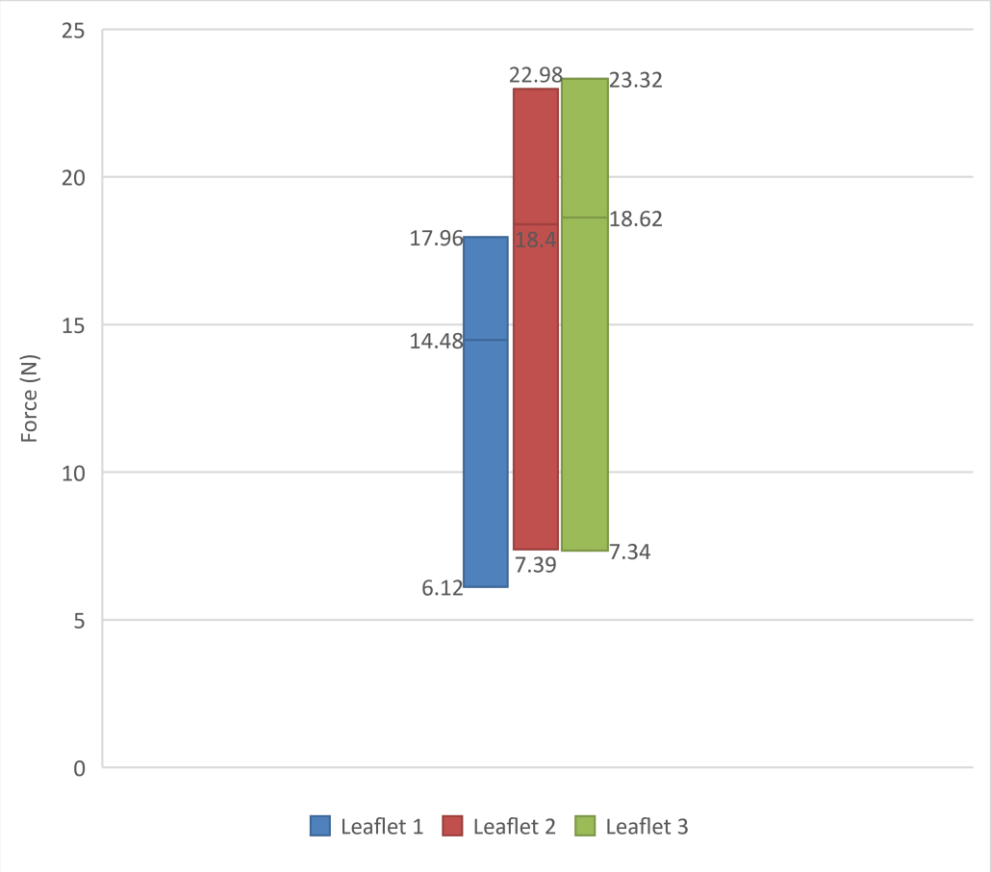

Figure 5-13 Calculated force at 1.2mm 3.6mm and 4.6mm droop per leaflet illustration.

The pull force required to accurately position the SAT delivery device within the valve should be between 7.39N and 17.96N to cater a droop of 1.2mm and 4.6mm on all 3 leaflets.

The values obtained for the Leaflet 1 (RCC) are different compared to the two others which are close. This could be explained by the fact that the L1 is the last leaflet in contact with the pull force tool causing it to move first before drooping. In a study done by Rankin et al. (2013), it was shown that the right coronary cusp is 10% larger than the non-coronary leaflet, and the left coronary leaflet.

The full data set can be seen in Appendix C as well as more statistical analysis done.

5.2 Training Rig Design and manufacturing

5.2.1 Imaging system design

5.2.1.1 Design overview

The imaging system concept was design such that the C section was be able to rotate in 4 different directions indicated in Figure 5-14. The C section was able to rotate on direction 1 and 2 indicated in Figure 5-14 around the rotational axis A and pivot point A. I was able to rotate in direction 3 and 4 around the rotational axis B and pivot point B.

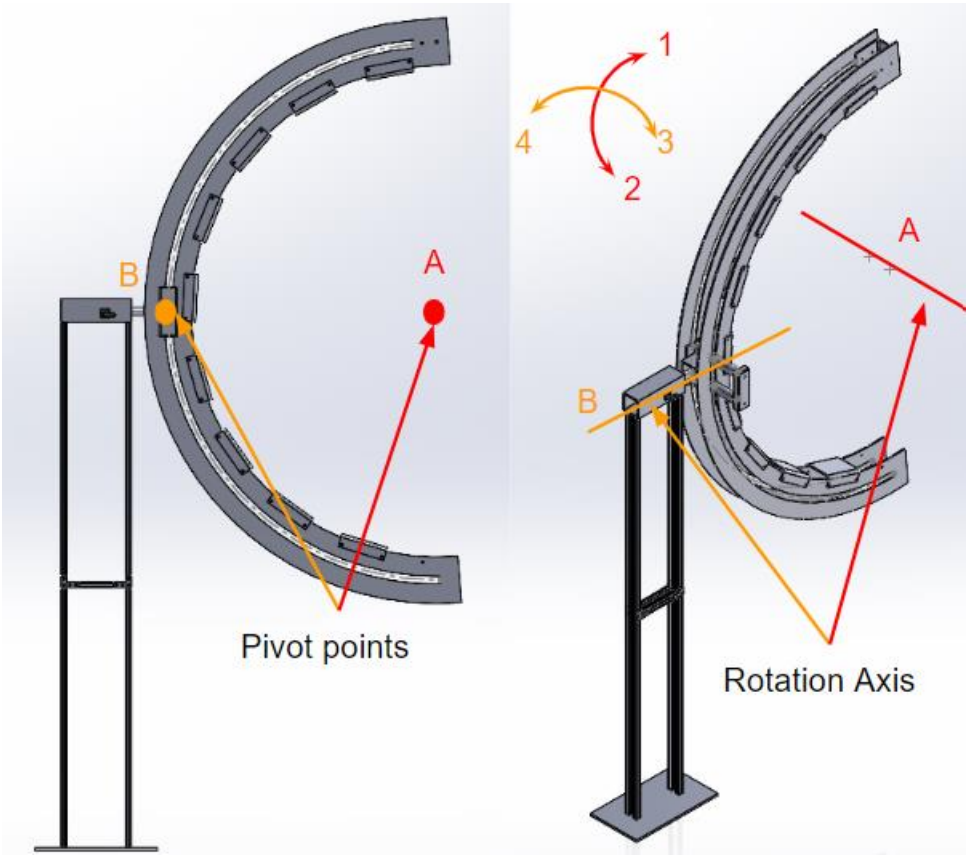

Figure 5-14 C-arm Assembly

Two locking mechanisms were introduced to lock the C arm in position once the most appropriate visualization angles are found. A handle was designed with two compression spring inside to prevent the C arm to rotate in direction 1 and 2. A quick release lock mechanism was purchased to prevent the C arm from rotating in direction 3 and 4. Figure 5-15 shows the position of the two mechanisms.

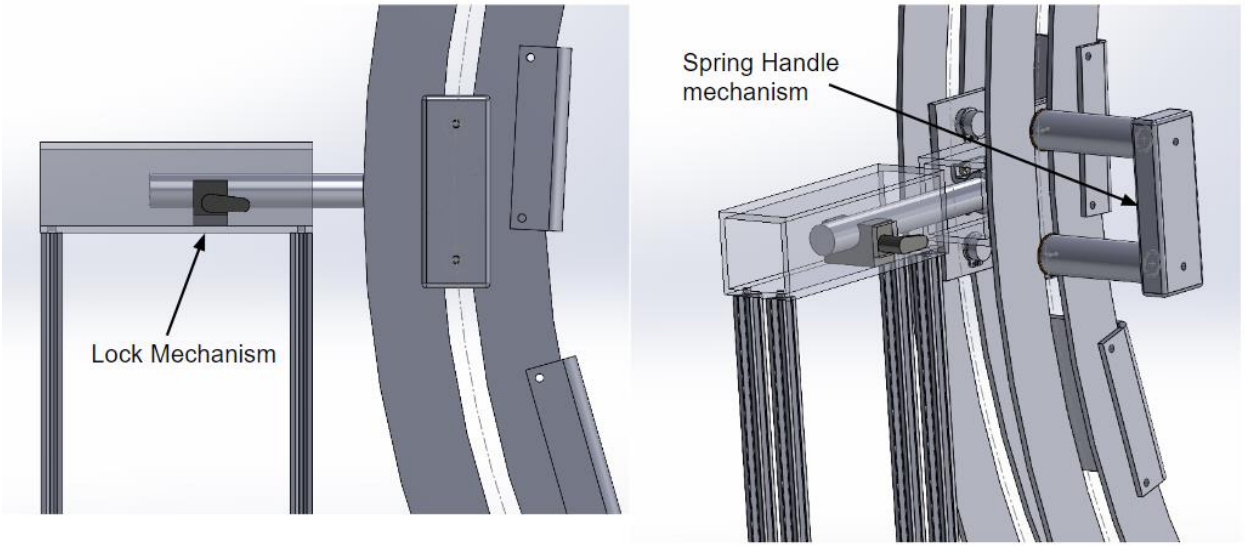

Figure 5-15 C-arm locking mechanisms.

5.2.1.2 Design, Material selection, and calculation

5.2.1.2.1 C arm

The C section designed has an overall diameter of 1 m and was made 3mm thick. It was decided to put 2 of each per imaging module for more stability. It contained 22 holes of 3.5mm diameter and a 13.2mm thick slot. The hold will be used to connect the two C arm with a connector part. The connector will be a designed part. The slot will be used to connect the C arm to the main body and allow for rotation. An individual C section volume is 304722.25 mm^3 ($304.722x10^{-6}$ m^3). The volume was obtained from the model part on solid work. The C-arm design can be seen in the Figure 5-16.

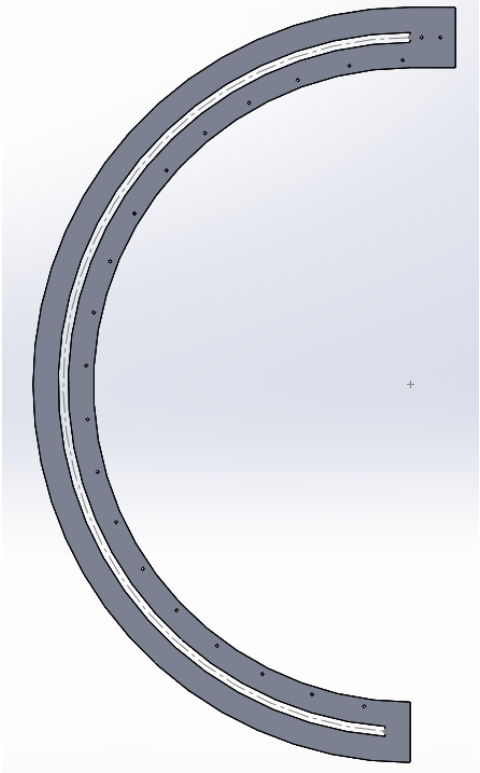

Figure 5-16 C-arm section

A wild range of materials were available to be selected for this part. The factor taken into consideration to select the material were the density (for the weight), ease of manufacturing, and ease of cleaning. The materials considered were stainless steel, aluminium, and polycarbonate. Table 5-7 shows the material property and comparison of the three materials for the design selected.

Table 5-7 C-arm material selection

Material	Density (Kg/m^3)	Weight in kg (at $304.72x10^{-6}$ m^3)	Manufacturability comment	Cleaning comment
Stainless steel	8000	2.434	Easy but Expensive	Compatible with common solvent
Aluminium	2712	0.826	Easy and affordable	Compatible with common solvent
Polycarbonate	1200	0.365	Easy and afordable	Crack with IPA

The manufacturability comment was decided based on the previous quotes obtained for other previous experiments.
The weight was calculated using the following formula.

$$m = \rho V$$

With
m = mass in Kg
ρ = density in Kg/m^3
V = Volume in m^3

Polycarbonate is the lightest material available, but it is not compatible with isopropyl alcohol (IPA). IPA is a common solvent used in some cleaning agents and hand sanitizers. Polycarbonate was not considered for this reason.

Stainless steel is the most used metal in medical tools (68). Stainless steel was the primary choice for the C-arm design, but its high density was a negative point. It is also a more expensive material to manufacture than aluminium.

Aluminium has the second lowest weight and advantages include compatibility with most common solvents and cleaning agents used in labs, easy of manufacture and affordability. Aluminium is also the most widespread metal on earth (69) making it easily accessible.

Aluminium was then selected for its weight, cost, manufacturability, and accessibility.

5.2.1.2.2 Horizontal shaft

The horizontal shaft will be connecting the C arm assembly on the front end to the back end of the imaging module. It will hold the weight of the whole c-arm assembly and provide it with the rotational movement required to position the camera in the correct direction. Figure 5-17 illustrate the position of the horizontal shaft in the assembly.

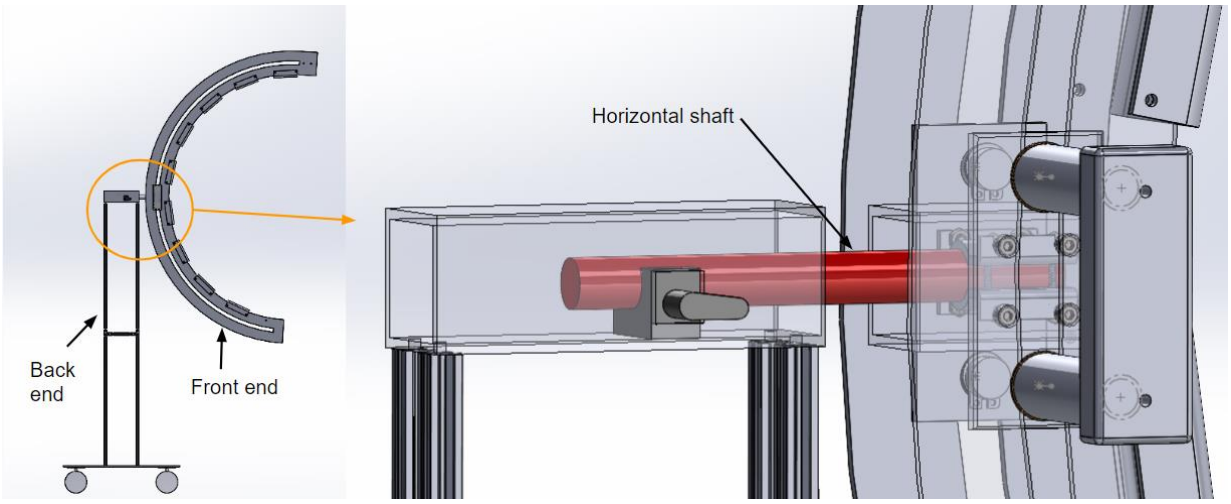

Figure 5-17 Horizontal shaft position

The weight of the parts attached to it, on the front end, can be seen in Table 5-8:

Table 5-8 C-arm parts weight

Name	Quantity	Volume (m^3)	Density (kg/m^3)	Total Mass (Kg)
C arm	2	$304.722x10^{-6}$	2712	1.652
C arm connector	9	$23.920\ x10^{-6}$	2712	0.581
Spring base	2	$15.110\ x10^{-6}$	8000	0.242
C arm Central joint	1	$30.849\ x10^{-6}$	8000	0.247
C arm rod support	2	$2.81\ x10^{-6}$	2712	0.015
Handle assembly	1	$66.688\ x10^{-6}$	2712	0.181
Camera stand	1	$18.931\ x10^{-6}$	2712	0.051
Camera	1	-	-	0.2
Bolts	52	-	-	0.47
Nuts	52	-	-	0.197

The total mass on the table was obtained by multiplying the quantity of each item with its volume and density The volume was obtained on each parts model.

The handle assembly is made of aluminium but most of the parts will be 3D printed and made from silicone.

The mass of the bolt was estimated from the largest bolt present in the assembly. The largest bolt used is an M3x10 and a single unit has for weight 9 grams.

The mass of a single M3 nut was measured and the value obtained is approximately 3.8grams

The total weight of the part on top of the rod is 3.836kg for safety 5kg will be used in the calculation.

The horizontal shaft is considered as a cantilever shaft with a 5kg weight acting on it as a uniform distributed load of 30mm long at the tip of it. The shaft was designed to be 15mm in diameter and 122.5mm long (total length of 150) based on the initial design length.

A finite element analysis (FEA) of the horizontal shaft, done on Abaqus, shows that the maximum deflexion point will be of $23.28x10^{-6}$ mm and the maximum stress in the material will be 13.75 MPa. The result can be seen in Figure 5-18. The stress caused by the weight of the C arm section will not cause damage to the shaft.

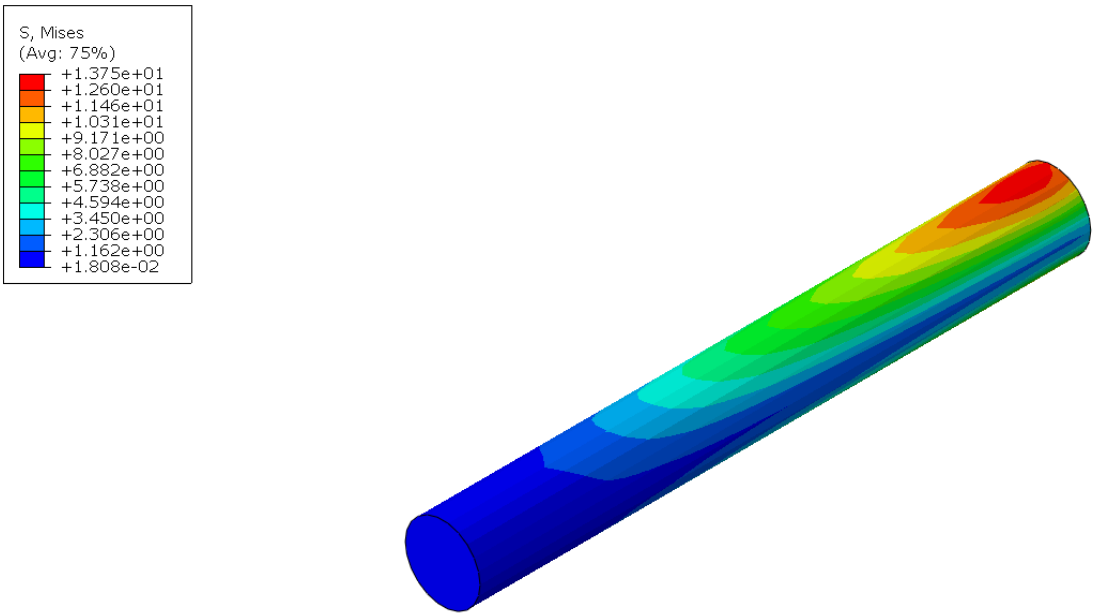

Figure 5-18 FEA Analysis result

5.2.1.2.3 Spring and handle system

The spring selected should provide enough force to hold the C arm section stationary when the correct position is found. Figure 5-19 shows the position of the springs as well as the force direction.

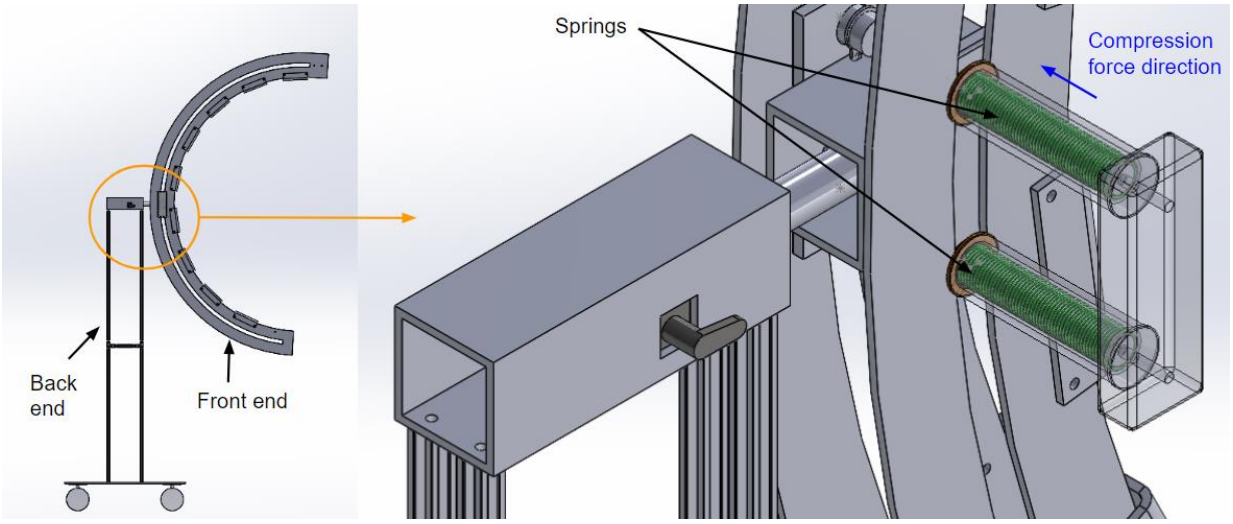

Figure 5-19 Spring position

The weight of the C arm section was calculated to be approximately 5 Kg, and the force required to hold the spring stationary is 49.05N, the force was calculated using the following formula.

F=mg with g=9.81m/s^2.

The average pull strength of a standing woman and standing man was determined to be 85.09N 147.58N respectively (70).

The spring selected should have a force between 49.05N and 85.09N based on the above criteria which are the force required to hold the C-arm in position and the average pull force of a woman.

The spring identified was a steel extension spring with an initial tension force of 42.2N. the spring has a free length of 66.2mm and a maximum extended length of 178.2mm. It has an outside diameter of 13mm, a wire diameter of 1.2mm, and a spring constant of 0.32N/mm. The handle system was designed to have two springs, mounted in series, making the total force of the handle system 84.4N.

5.2.1.2.4 Back-end legs and assembly

The legs are assembled from 4 modular assembly profile struts (part number 100078). It has a laser-cut housing which will hold the horizontal shaft. The shaft will rotate, and once the correct position is found, it can be locked using a clamp. The clamp selected is a 15mm single rod clamp with red ratchet locking knob and can be seen in Figure 5-20.

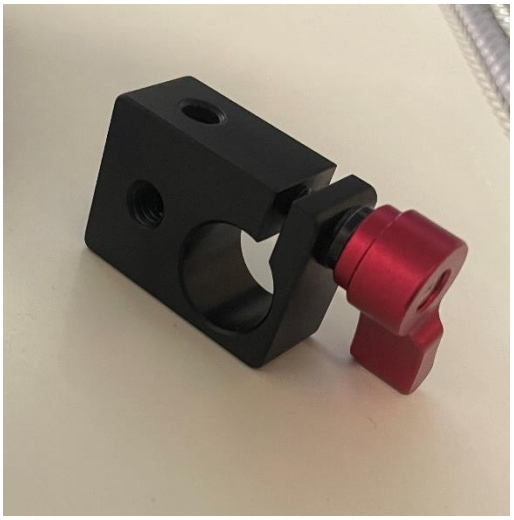

Figure 5-20 Clamp selected.

The base of the back end consists of a stainless-steel block mounted on 4 wheels making the part easily movable. The wheels selected are, tente braked swivel castor wheel, which can hold a maximum load of 75kg, has a wheel diameter of 75mm, and can be locked in position. The base plat has a mass of 3.2Kg holding the whole assembly on the ground and preventing it from toppling.

5.2.1.2.5 Discussion

The C-arm was designed to be safe to use by anyone, it is easy to assemble and the parts necessary to build a C-arm should be available worldwide. The part more prone to fail first is the horizontal shaft as all the load will be transmitted through it, but based on the FEA model it should not fail.

The C-arm design in this section, coupled with a camera projecting the images on a screen, could be used to train the surgeons on the imaging part of the TAVI without being exposed to radiation.

5.2.2 Circulatory loop design

Two concepts were designed. The 2 concepts are similar and using the same pulsatile pump and materials, the differences are the design of the ventricle connection, the design of the aortic root and the design of the aortic arch.

5.2.2.1 Pilot Rig

An initial test was done to confirm the possibility of using the Formlabs Elastic resin as the aortic root material. A simple stand was designed, and the root was not connected to any pump. Figure 5-21 shows the setup.

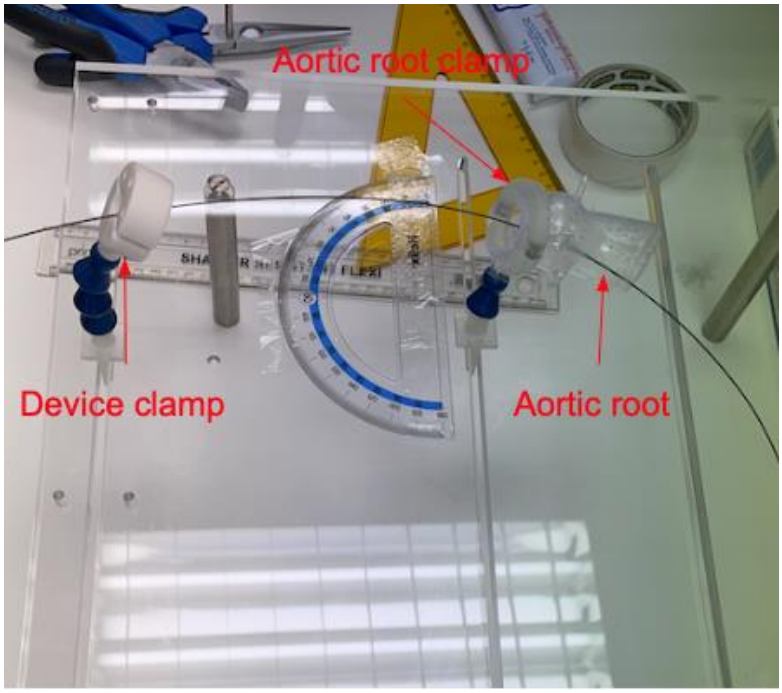

Figure 5-21 Feasibility study

The device was introduced through the device clamp. Going through the printed aortic root at a specific angle. The device was able to deliver the valve to the right position. Figure 5-22 shows the deployment and the results of the deployment.

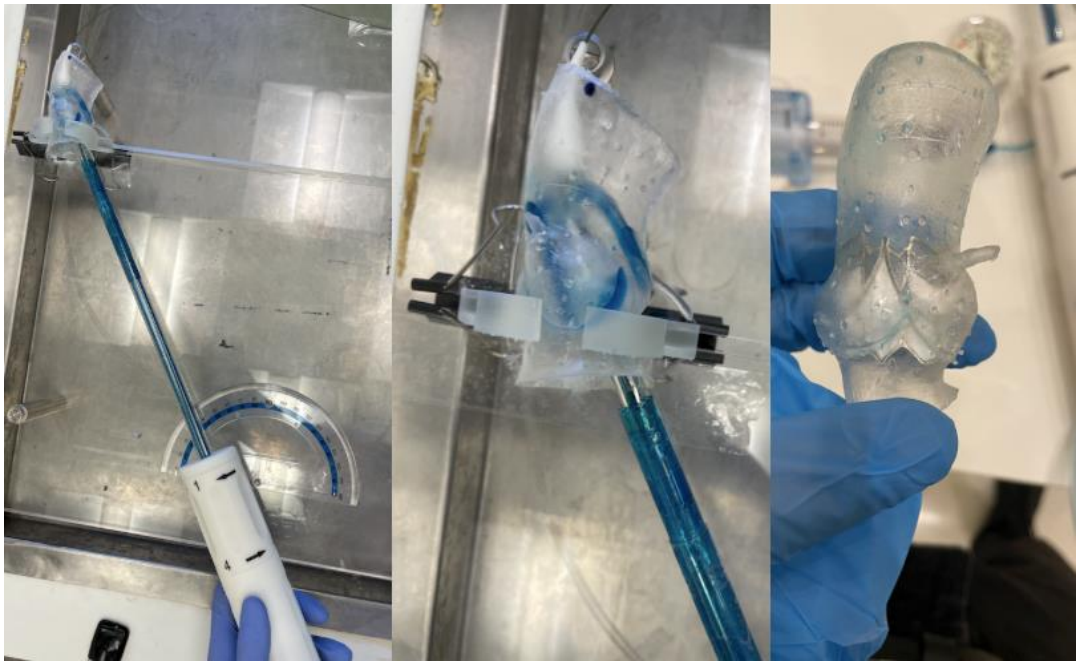

Figure 5-22 Feasibility study result

Figure 5-22 above shows that the delivery device was able to deliver the implant valve into the printed aortic root. The valve was positioned slightly high compared to the annulus and the rotational positioning was slightly off. The following test could be achieved from this test:

- Testing the effect of the device and valve size variation
- Checking for coronary occlusion
- Evaluating deployment at different entry angles
- Confirming rotational positioning of the valve
- Confirming axial positioning of the valve

The current setup was not able to give us an indication of the leaflet droop as expected. The leaflet used were 3D printed alongside the aortic root and was not optimized for it.

5.2.2.2 Concept 1

The first concept was design using an aortic arch and aortic root extracted from patient data (see ethics approval in appendix A). Concept 1 was designed such that the angle between the aortic root and the entry point can be changed. To do so an articulated ball and socket mechanism was included. Figure 5-23 shows the Computer Aided Design (CAD) model of the aortic root, aortic arch, ventricle, the connection points and the position of the ball lock mechanism.

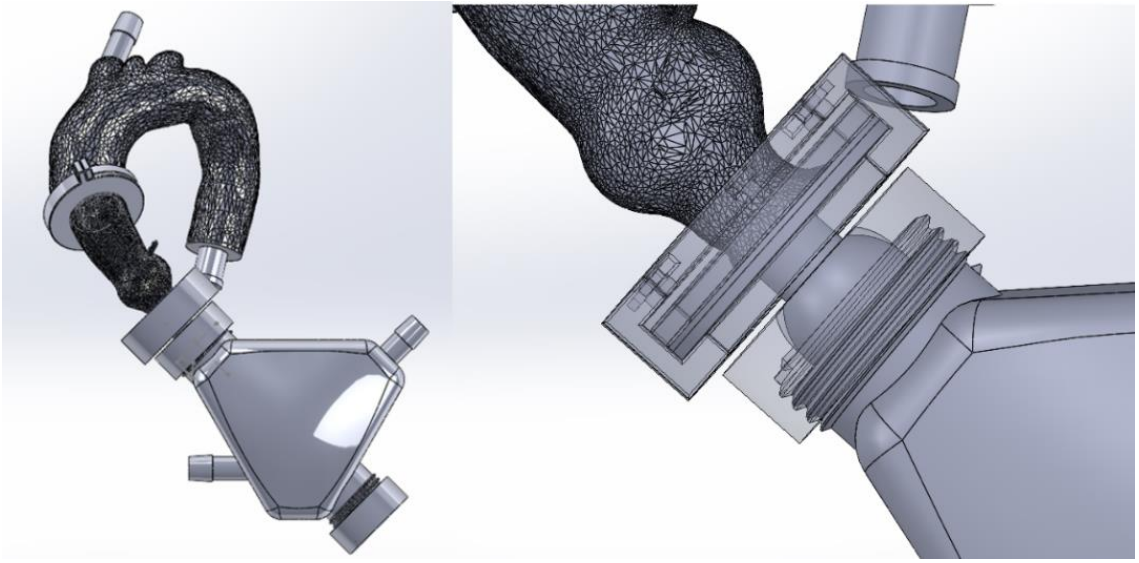

Figure 5-23 Concept 1 design

The ball cap can be loosened to move the aortic root to the desired angle then the ball cap gets tightened to lock it in position. This design would assist in changing the angle without having to redesign or print a new adapter. The printed aortic root is connected to the ventricle by sitting on top of the ball pin then encapsulated by the root clamp. The root clamp has screws on its top surface that pushed the root clamp insert over the root creating a clamping force. To connect the aortic root and aortic arch, a connector was designed. The aortic arch sits over the connector and a clamp is bolted to it prevent it from moving, the connector is then slid inside the aortic rood and tighten together using a cable tie. Figure 5-24 shows an exploded view of the assembly and identify all component.

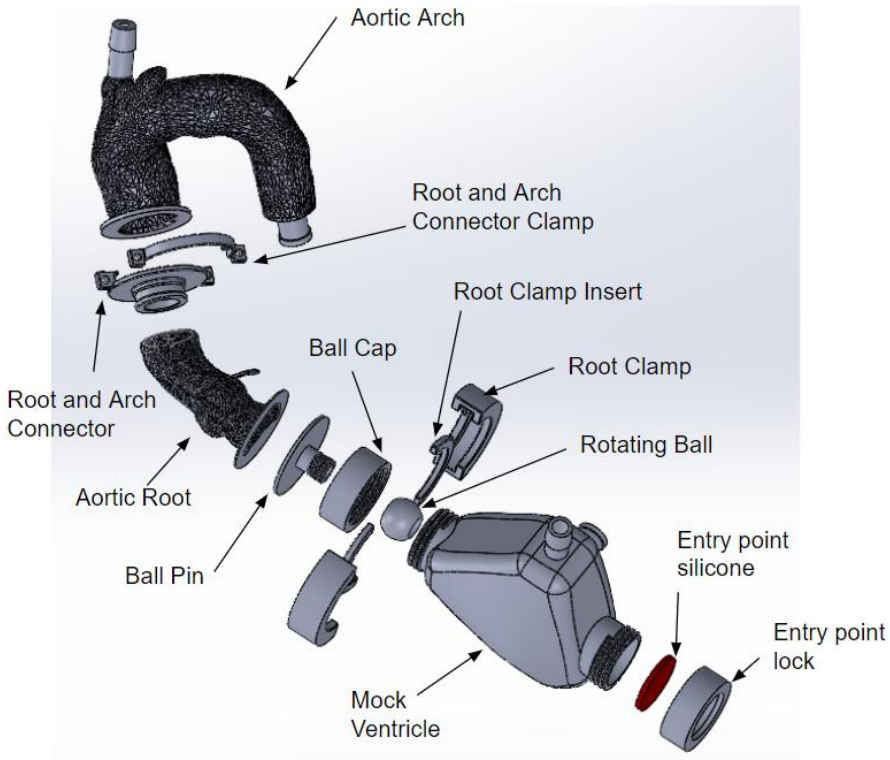

Figure 5-24 Concept 1 exploded view

The aortic root and aortic arch were 3D printed from a patient CT scan. The aortic arch and ventricle were printed using the Formlabs clear resin. The aortic root was 3D printed using the Formlabs elastic resin. The printed parts can be seen in Figure 5-25.

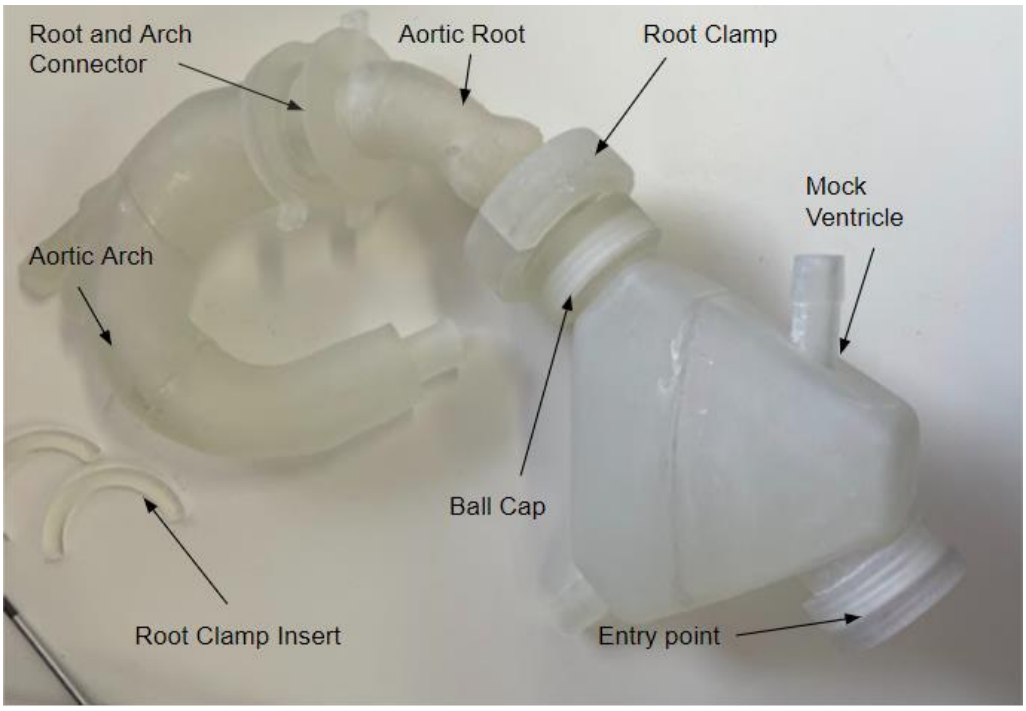

Figure 5-25 Concept 1 physical parts

An aortic valve was used as mitral valve replica, it was encapsulated in a silicon chamber to prevent leaks and connected to the ventricle. The ventricle was connected to a pump and the design was tested, see Figure 5-26. Few issues were found. The main one is that the ball lock mechanism was taking up a lot of space reducing the space which in the device could move in. By moving the root, it was also needed to reposition the whole system making it more complex to position before any test. It was not possible to pump water through the systems as there was leak at the connection between the aortic arch and aortic root, and between the aortic root and ventricle.

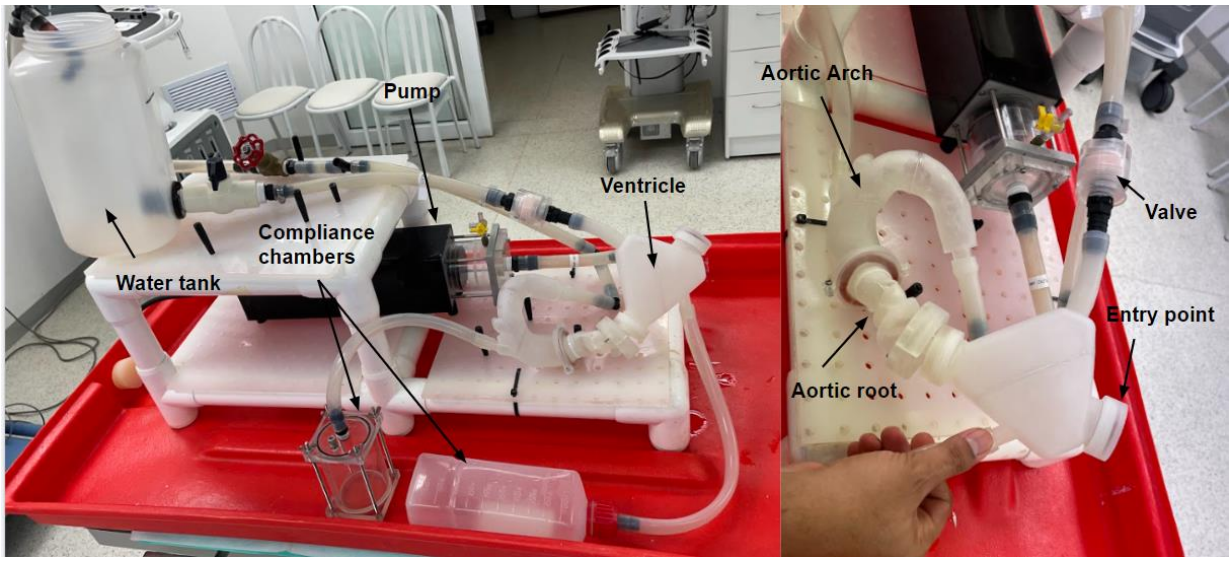

Figure 5-26 Concept 1 circulation loop

5.2.2.3 Concept 2

The second iteration was designed to only have one angle between the entry point and the aortic root. It also has less parts that the first iteration and simpler connection points to reduce leak when being pumped. The aortic root and arch were designed using simple geometry instead of using a model extracted form CT scan. Figure 5-27 shows CAD models off the concept.

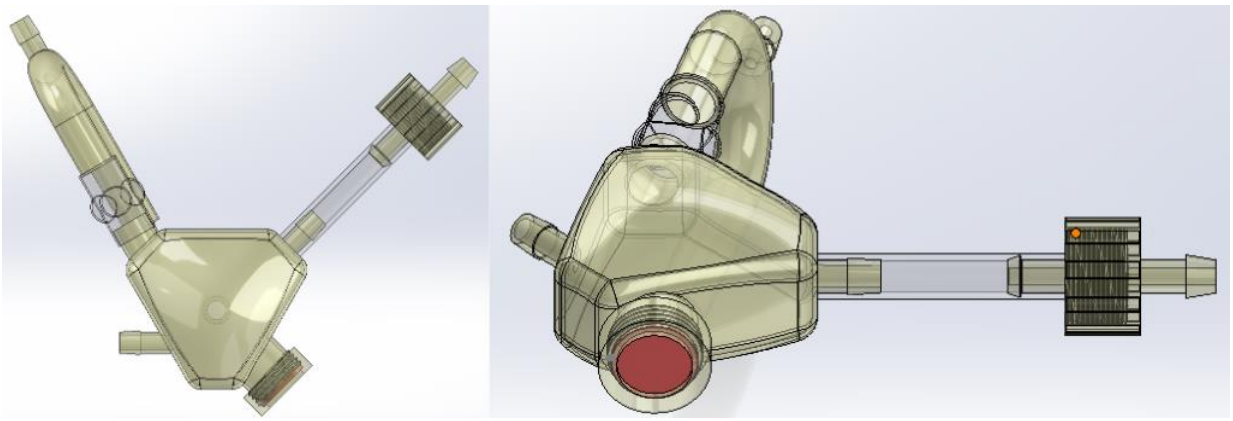

Figure 5-27 Concept 2 design

Aortic root is slid over the ventricle and kept in place using a cable tie, the aortic arch is slid inside the aortic root and connected using a cable tie. Figure 5-28 shows an exploded view of the assembly and identify all component.

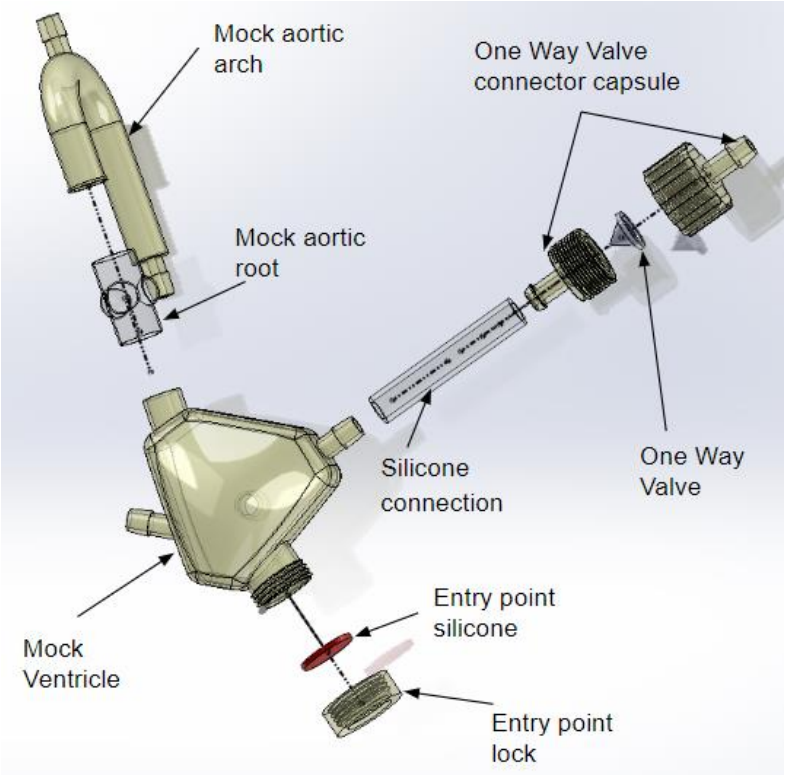

Figure 5-28 Concept 2 exploded view.

The mock aortic arch and ventricle were printed using FormLabs clear resin and the mock aortic root was printed using the FormLabs elastic resin. The one-way valve selected is a cross slit one way valve (part number is CR200.002) and was obtained from MiniValve, a one-way valve

manufacturer based in Cleveland, USA. The one-way valve was encapsulated in a part printed using the FormLab clear resin The parts were printed and can be seen in Figure 5-29:

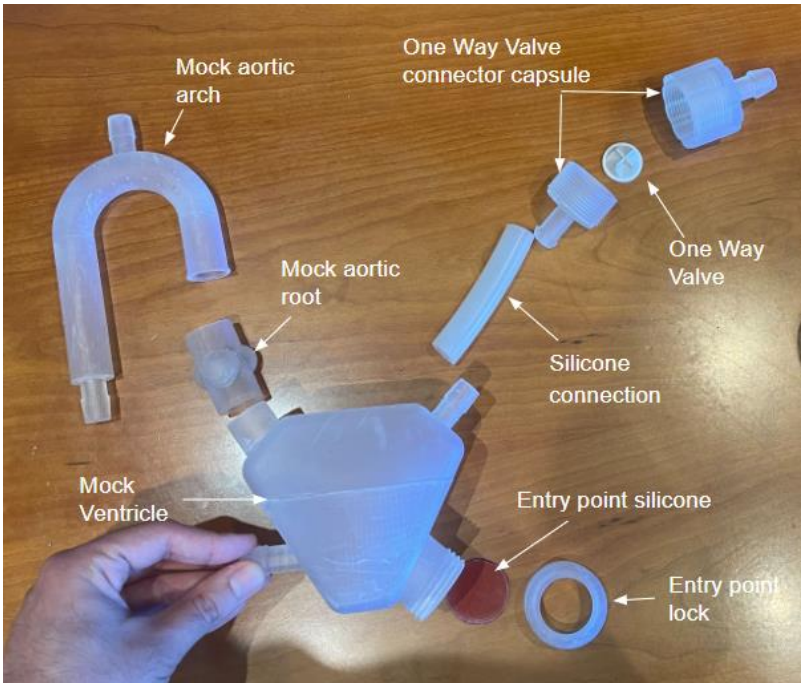

Figure 5-29 Concept physical 2 parts

A transfemoral entry point was not included as the delivery device on hand is part of a transapical approach TAVI system. The parts were connected to the pulsatile pump as seen in Figure 5-30. The delivery device was prepared, and the heart model pumped, unfortunately the aortic root tore. The elastic resin from Formlabs was not holding the pressure generated by the pulsatile pump. The test could not be done under pressure as the root kept tearing.

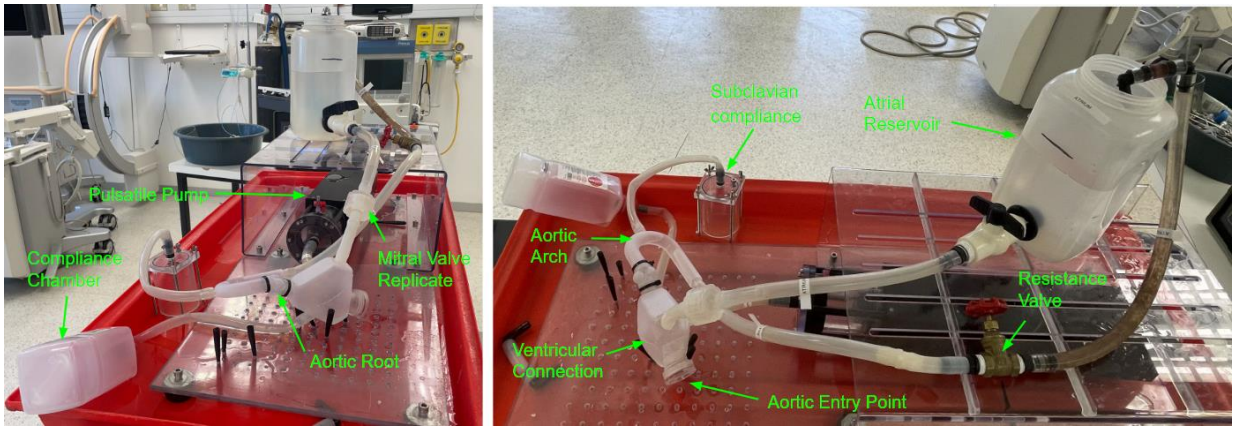

Figure 5-30 Concept 2 Circulation Loop

As the parts could not be pumped, the part was soaked under water as the 3D printed parts are clearer under water. The device was de-aired with water mixed with food colouring to help with visibility. The device was introduced from the entry point of the mock ventricle and advanced through the printed root, the retrieval sheath was retracted, and the trunk extended, the valve was deployed, the trunks were retracted, and the helical balloon vacuumed. The device was re-sheathed and removed from the part. Figure 5-31 shows on image A the device being inserted and positioned, on image B the trunks are extended and on image C the helical balloon is inflated, deploying the valve.

Figure 5-31 Device Deployment in concept 2.

By changing the colour to black a white, similar images are obtained to the fluoroscopic images obtained during the TAVI. Figure 5-32 and Figure 5-33 show the comparison of the black and white images of the test done (images on the left) with the fluoroscopic images obtained during a TAVI done on pigs (images on the right). Figure 5-32 shows the comparison of images during trunks extension and tactile feedback phase and Figure 5-33 shows the comparison of images during the balloon inflation phase.

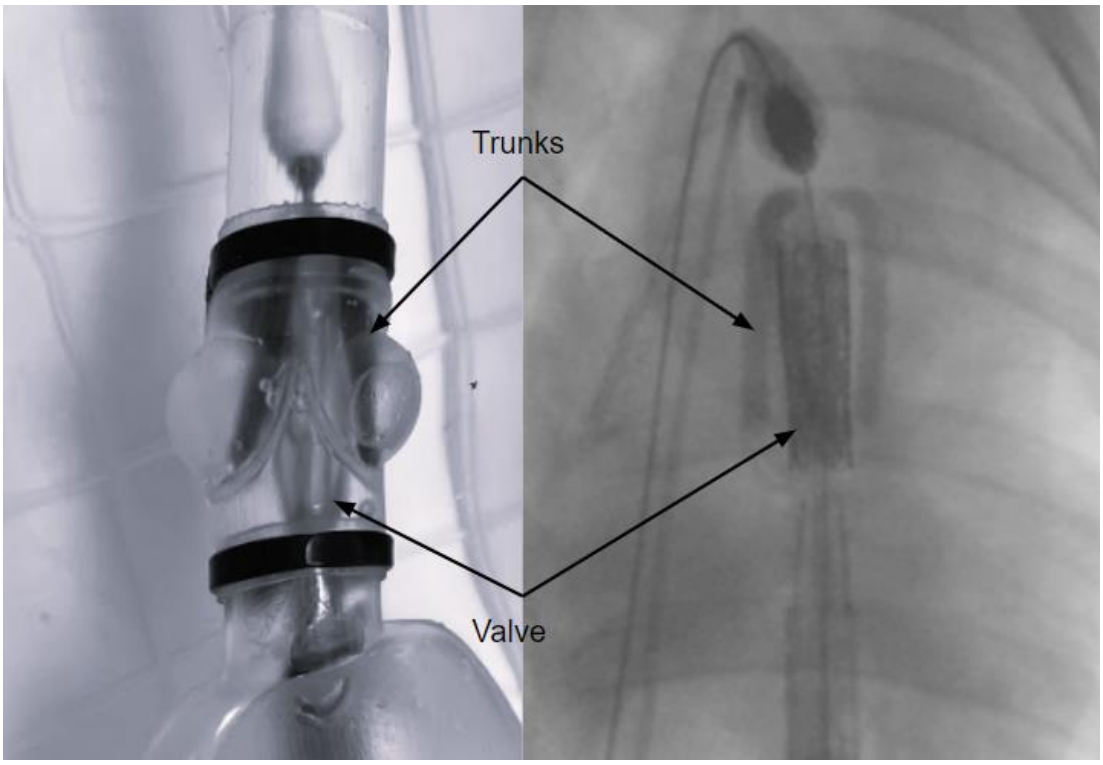

Figure 5-32 Trunks visibility on test images compared to fluoroscopy images.

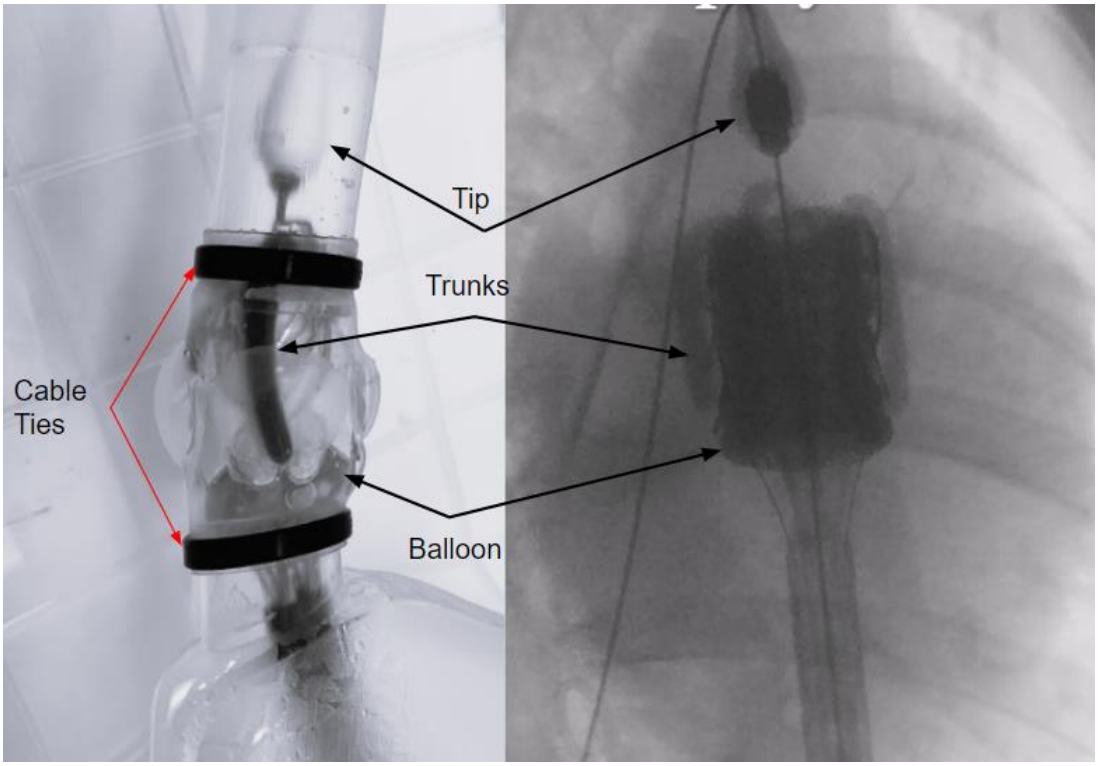

Figure 5-33 Device visibility on test images compared to fluoroscopy images.

The trunks, the crimped valve, the inflated valve, and the tips can be seen in both images. Too much food colouring was used in the medium used to deair the delivery device making it more visible during the test, a more diluted concentration should be defined to replicate similar visibility of the trunks and be more representative of the fluoroscopy images. The cable ties are too visible in the images obstructing the views.

The diameter of the printed aortic root was too small, constricting the valve, the material was not elastic enough and tore but the positioning could still be evaluated after deployment. As seen in Figure 5-34 the rotational alignment could still be assessed by comparing the position of the valve arm and the printed part Sinus of Valsalva, it can also be evaluated by comparing the position of the valve commissure post to the printed part commissure post. The axial positioning can be evaluated by measuring the distance between the bottom of the valve and the bottom of the printed root cusp. As seen in Figure 5-34 the valve is positioned slightly higher than expected, this due to the printed leaflet stiffness, they are not drooping when the trunks are inflated.

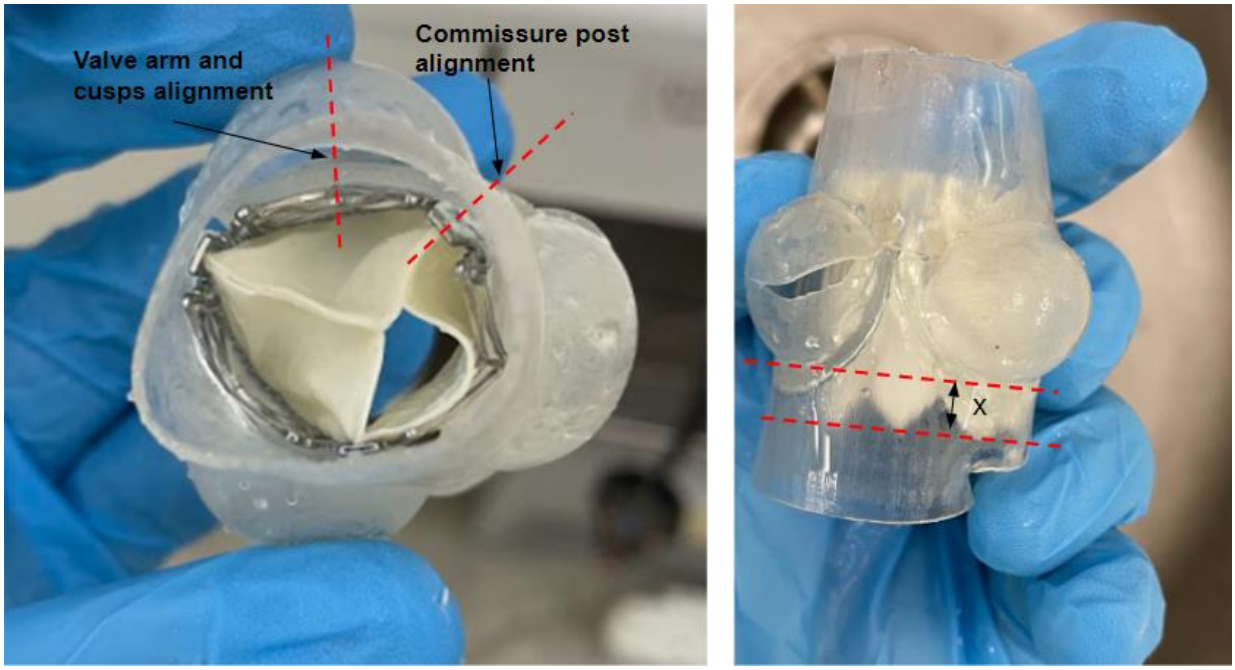

Figure 5-34 Valve position assessment after deployment.

5.2.3 Force indication Device

5.2.3.1 Detail design

The force sensor selected is The Grove-Round Force Sensor (FSR402). It has a round force sensitivity resistor at the end of the sensor, the higher the force is applied on the resistor the smaller the resistance gets. It has a force sensitivity range of 0.2N to 20N with a repeatability of ±2%. The force sensor was connected to a micro controller. The micro controller selected was the ADAFRUIT INDUSTRIES Feather M0 basic proto, which was designed for low power and

portable project. A light was connected to the controller. The Figure 5-35 below shows the connection between the force sensor, the micro controller, and the light.

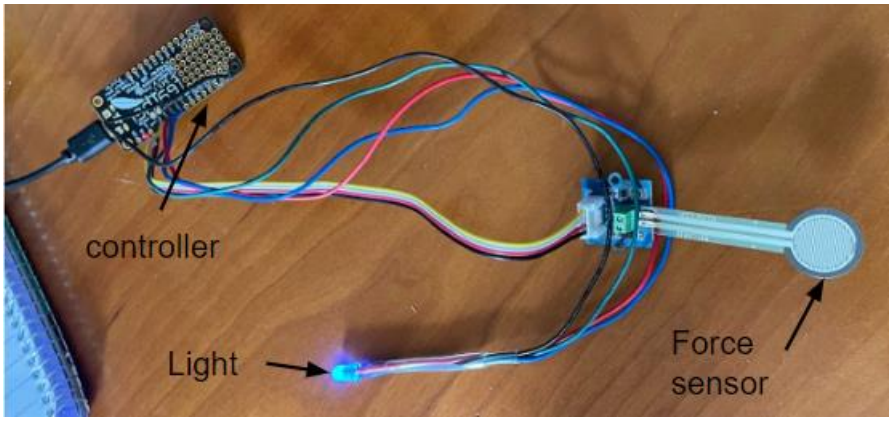

Figure 5-35 Controller Connection

The code used to make the light shine in a specific colour based on the force applied can be seen in Appendix E. The code was written on Arduino.

Before assembling the parts, the force sensor was tested using a force gauge. When a force less than 7.39N was applied, the light shone blue. The light shone green when the force was between 7.39N and 17.96N and it shone red when the force applied was greater than 17.96N. Figure 5-36 shows multiple images taken at different force and the light shining at those forces.

Figure 5-36 Initial Sensor Test

On image A the force was 5.00N and the light was blue, on image B the force was 6.61N and the light was blue, on C the force was 13.74N and the light was green, on D the force was 16.63 and the light was green, on E the force was 19.01 and the light was red, on F the force was 21.10N and the light was red. Figure 5-37 is a CAD image of the force indicator device design.

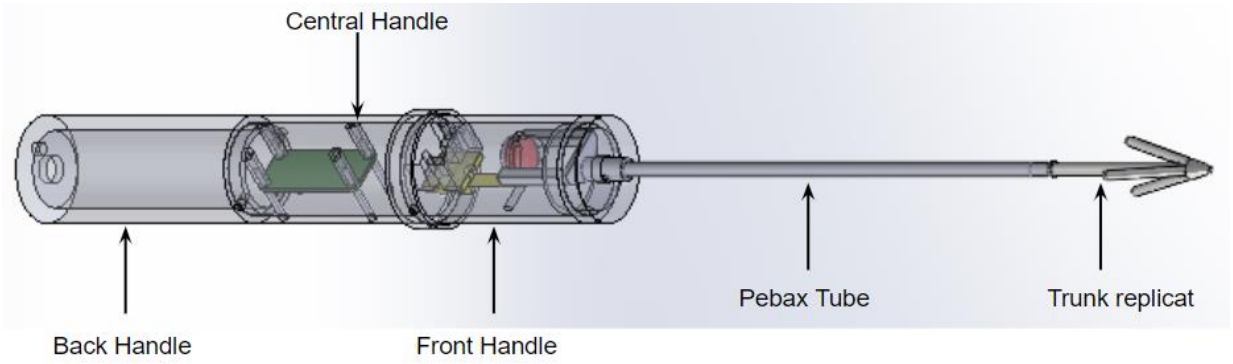

Figure 5-37 force indicator Design

Figure 5-37 above shows that the training device consists of 5 main sections, the back handle, the central handle, the front handle, the Pebax tube, and the trunk replica. The front handle contains the force sensor, the central handle has the microcontroller, and the light is positioned in the back handle. To connect the handle to the trunk replica, a Pebax tube was used, it has a 72D durometer.

Figure 5-38 shows the front handle on the left and the central handle on the right. It shows the parts and the design aspect included in the handle.

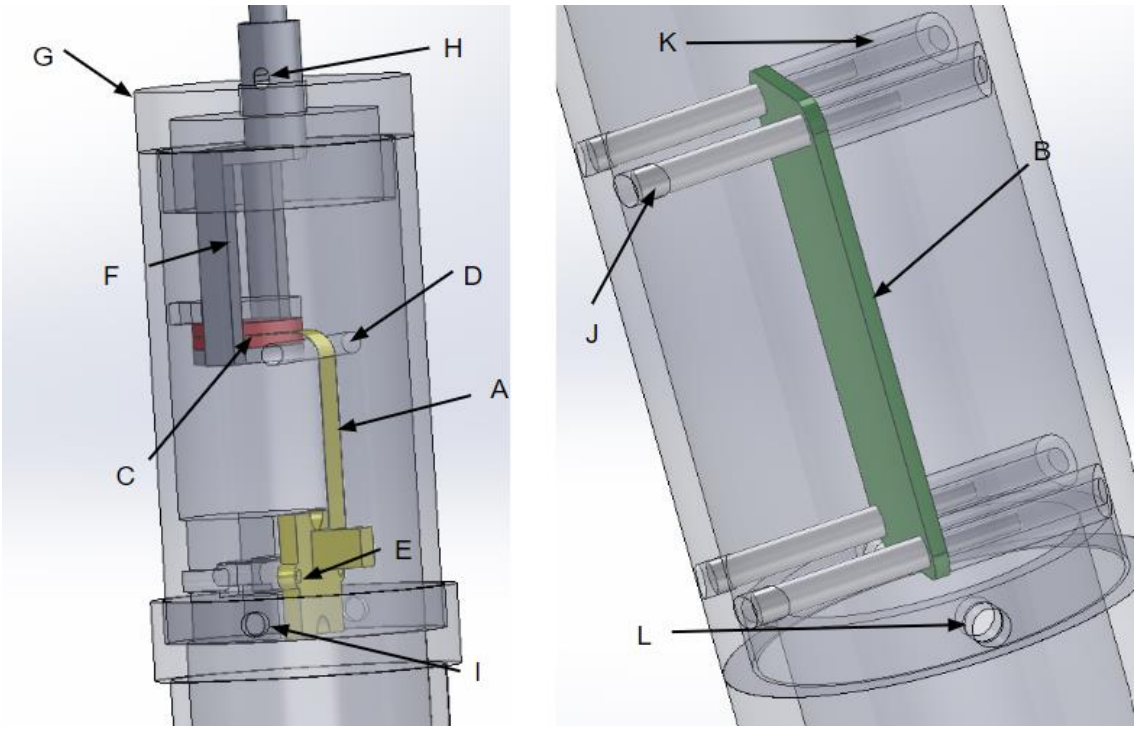

Figure 5-38 Front and Central Handle Design

Part A is the force sensor, positioned in the front handle. Part B is the micro controller. The force sensor is sandwiched in between two silicone disk, part C in the image above. Part D is a tube placed in the front handle to secure the sensor and prevent kinking. The sensor is bolded in the handle using the hole shown as E. The part F is in an independent part transferring the force to the sensor. It is inserted inside the handle and is prevented from moving down by a pin inserted in the hole H. Part G is a cap guiding part F up and down and preventing its fall. A grab screw is inserted in the hole I to connect the front and central handle. To hold the microcontroller in the handle. 4 pins (part J) are inserted in the handle in the part K which are 4 guide and support for the microcontroller.

5.2.3.2 Part manufacturing and testing

The handles were 3D printed using the FormLabs White Resin. The front handle was printed in two parts for ease of assembly. The sensor was bolted to it. The part transferring the pull force to the sensor was place in position and the silicon pads were glued in position. The second part of the front handle was slid over, and the sensor placed in position. Those steps can be seen in Figure 5-39.

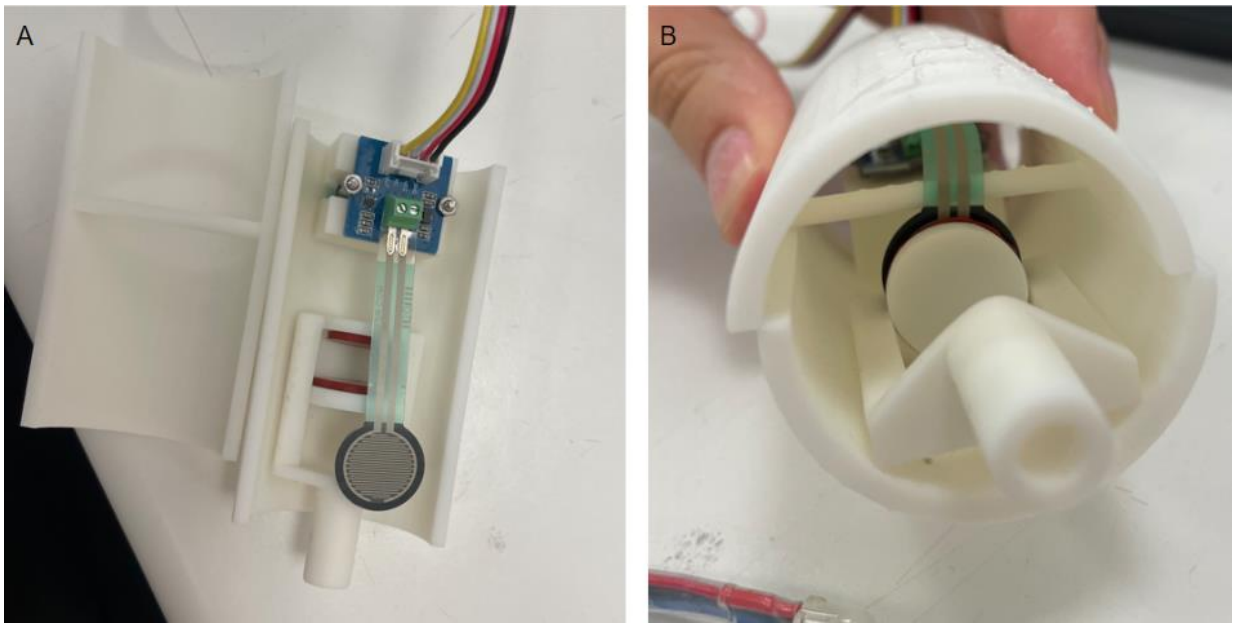

Figure 5-39 Front Handle Assembly

The microcontroller was slid in the central handle and positioned using the 4 locating pins as seen in Figure 5-40.

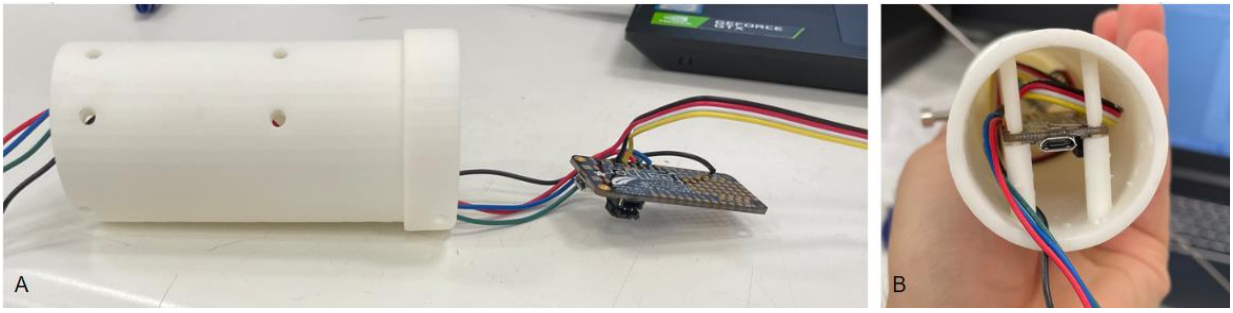

Figure 5-40 Central Handle Assembly

A USB cable is connected to the micro controller and comes out of the back end, it was used to power the microcontroller the light and the sensor, as no batterie was included. The light was inserted in the back-end handle. The front and central handle were connected using screws as there was no grubscrew available. The central and the back handle were connected using screws are there was no grubscrew available. The cap was inserted in the front handle and the pin was put in place. The Pebax tube and the trunk replica are bonded to the assembly using glue.

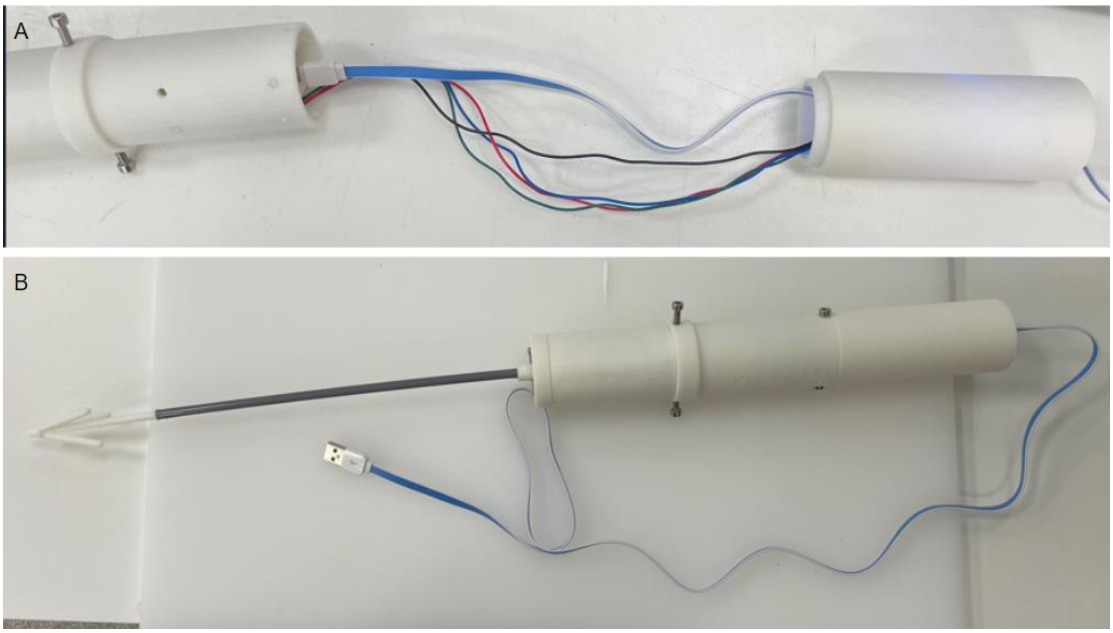

Figure 5-41 Back End and full Assembly

After assembly of the tactile feedback training device, it was connected to the force gauge to confirm its reliability. Figure 5-42 shows the light shining in different colours as the force increases.

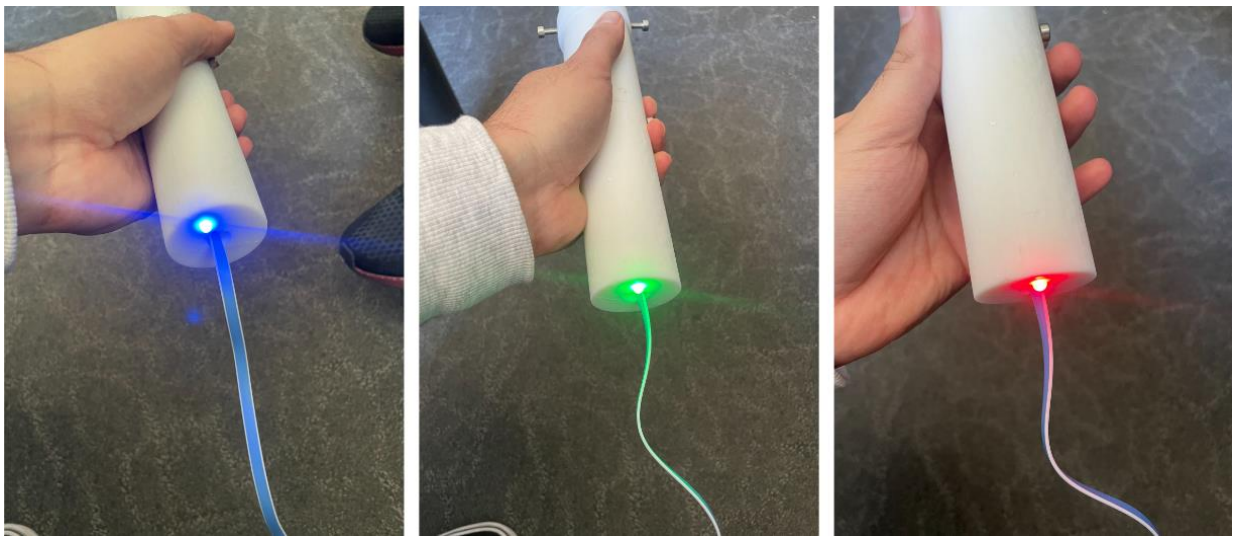

Figure 5-42 Working device.

The device was connected to the force gauge using a Kevlar rope and pulled. Figure 5-43 shows the force and the light at different pull. On A the light shone blue, and the force indicated is 6.33N, on image B the light shone green and the force is 7.59N, on image C the light shone green and the force shows 17.21N, an on image D the light shone red and the force shown was 18.29N.

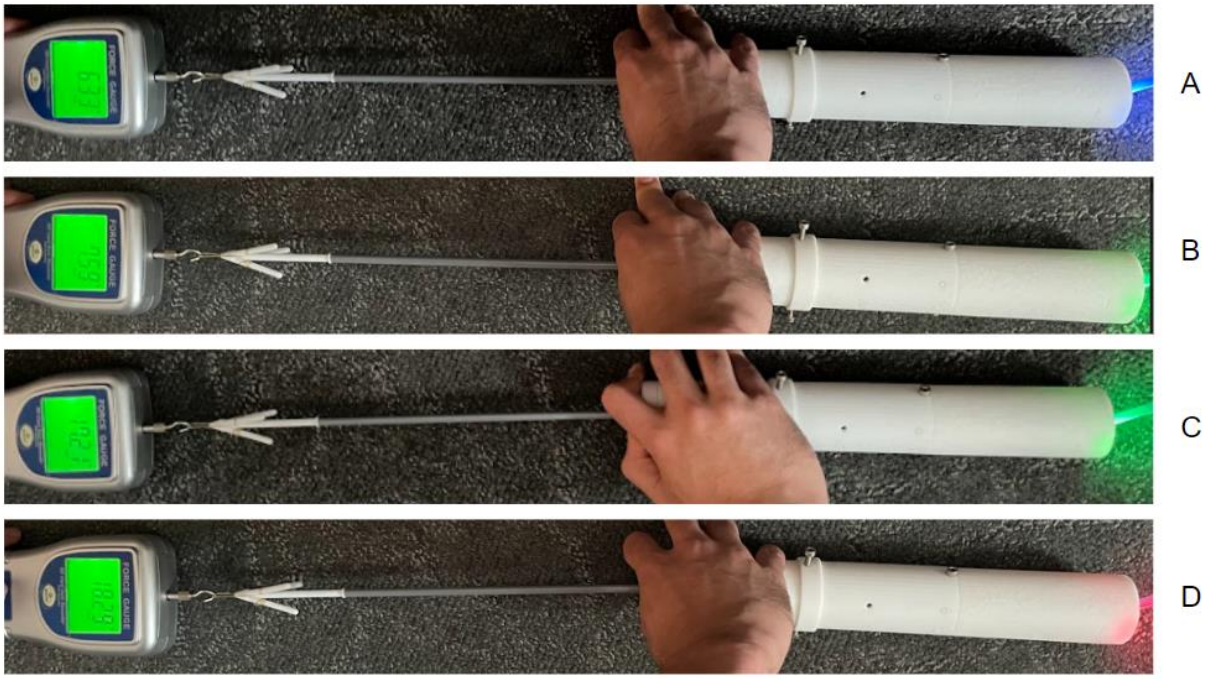

Figure 5-43 Forces and light indication

The forces indicated are relating to the force calculated during the droop test. The device can be used to train surgeons on accurately positioning the valve in cadaveric pig heart.

5.3 Study limitation

The force gauge used to record the droop force during the droop test had a low resolution and could only record one value per second. This slow resolution was the reason for the interpolation calculation and could be the cause of the high standard deviation. By using a force gauge with a higher resolution, the reading of the force could be directly obtained at the desired droop value.

Due to the COVID-19 pandemic the time needed to collect the porcine hearts from the local abattoir and to start the experiment was longer than expected delaying the whole project. The measure taken to prevent the spread of the COVID-19 prevented us to go and cut the hears to the desired dimensions.

The droop and the corresponding force were only measured using cadaveric pigs' heart, more tests need to be done to validate the test method. Once the test method has been validated, it can be reproduced using cadaveric human hearts.

There was only one type of 3D printed available and there not too many different materials available to use. The prototypes could only be made from one material which wasn't suitable for the application.

6. Conclusion

TAVI has become a common surgical procedure to replace defective aortic valves. During the TAVI using the SAT delivery device, 3 trunks are positioned in the native aortic leaflet to provide axial positioning, and to keep relative movement between the heart and the delivery device a force is exerted, pulling the trunks into the native leaflet causing them to droop.

In this thesis the relationship between the pull force applied and the leaflet droop is determined in cadaveric porcine hearts. This force is then used to design a training system for the TAVI kit.

Three equations defining the relationship between the droop and the force were obtained, one equation per leaflet, by inserting three markers in an explanted porcine heart, which was connected to a pulse duplicator pump, a tool replicating the trunks was inserted in the heart and coupled to a force gauge. A force was applied on the pull force tool causing each native leaflet to droop, which was measured under fluoroscopy by comparing the distance between each marker to the corresponding pull force tool. The three equations obtained are F_{L1} = -3.4831 x $Droop_{L1}$ - 1.94, F_{L2} = -4.5872 x $Droop_{L2}$ - 1.88, and F_{L3} = -4.7007 x $Droop_{L3}$ – 1.70, the forces required to position the valve accurately was calculated to be between 7.39N and 17.96N.

The procedure is done under fluoroscopy to obtain the desired rotational orientation, guide the device, and to have real time images of the procedure when the device is in the heart. The surgeon is exposed to radiation during the procedure when the images are requires and the position of the C-arm impact the rotational positioning of the valve. An imaging system comprising a C-arm replica was designed to train surgeons and by using a standard security camera, images similar to the fluoroscopy images can be obtained during training.

A circulatory loop was designed to deploy and test a delivery device and valve when needed, to train surgeons without need of animal materials, and to see clear images using the C-arm designed. The circulatory loop uses a pulsatile pump developed by SAT, connected to a mock ventricle, a mock aortic ach and aortic root, connected using cables ties. The parts are 3d printed using the FormLabs clear resin for the arch, and ventricle and the Formlabs elastic resin for the aortic root. The root tore during the test as the material could not handle the pressure. A valve was deployed in the root without using the pulsatile pump and photos were taken during the procedure. The images obtained resembled the one obtained under fluoroscopy and the axial and rotational positioning of the valve after deployment could be assessed.

A force indicator device was developed using colour changing light as indication of according to the force applied. To measure the force applied the Grove-Round Force Sensor (FSR402) was used and connected to the ADAFRUIT INDUSTRIES Feather M0 basic proto which was used as microcontroller. The force indicator has the same dimension as the delivery device and was designed such as when a force is applied on the trunks a light situated on the proximal side of the device shines according to the force applied. the light shone blue when a force less than 7.39N was applied. The light shone green when the force was between 7.39N and 17.96N and it shone

red when the force applied was greater than 17.96N. The force indicator was tested using a force gauges, the trunks were tied to the force sensor using Kevlar and the light shone as expected.

Once all the parts are manufactured, the training system described in this thesis can be used to train a new surgeon on the TAVI procedure in a porcine model. It will also be possible to evaluate the positioning of a new revision of the TAVI kit using this rig.

7. Recommendation

The following improvements can be implemented:

- Droop Data Validation and Human Translation

The values obtained during the tests on the explanted pig hearts must be validated and translated into human values. To do so the following method is suggested.

-Firstly, validate the data for a pig model, this can be done by repeating the experiment using a bigger sample size to allow statical models/tendencies to be established.

-Secondly, initiate live animals testing. This step will give the corelation between the droop using fresh tissue and rigoured tissued on pig hearts, and how the rigour mortis factor affects droop.

-Thirdly, repeat the test using cadaveric human heart. This will give us the value of the droop using cadaveric human hearts.

-Finally, convert values obtained in cadaveric human hearts to live humans using the pig experiment as reference knowing the effect of rigour mortis on leaflet droop.

- Imaging system

The C-arm system should be built and tested.

A specific camera and screen must be selected and connected to the designed C arm. The camera must be able to record images and videos, to replay them, and, to broadcast on the connected screen live visual of the test while it is happening.

- Circulation loop

The circulating loop can be improved by replacing the aortic root material to a more compliant silicon material.

Other methods of manufacturing the aortic root can be tested such as dipping or casting if a more compliant 3D printed material is not found. In both cases a mould should be design and new materials should be investigated.

- Force indicator

A different force sensor can be used for more accuracy in the readings.

The mock trunks can be designed to be retractable, by doing this the device can be use in a cadaveric heart.

A battery can be included in the handle to eliminate the need of a USB cable.

The force sensor can be included in the aortic leaflet of the circulation loop. By doing that the surgeon can use an actual delivery device to deploy the valve and get training on the force positioning at the same time

References

1. World Heart Federation. Cardiac Surgery Intersociety Alliance - World Heart Federation [Internet]. 2023 [cited 2023 Jan 14]. Available from: https://world-heart-federation.org/cardiac-surgery-intersociety-alliance/
2. Noubiap JJ, Agbor VN, Bigna JJ, Kaze AD, Nyaga UF, Mayosi BM. Prevalence and progression of rheumatic heart disease: a global systematic review and meta-analysis of population-based echocardiographic studies. Sci Rep. 2019 Dec 1;9(1).
3. RHD Australia. Individuals, Families & Communities | Rheumatic Heart Disease Australia [Internet]. 2020 [cited 2023 Jan 14]. Available from: https://www.rhdaustralia.org.au/individuals-families-communities
4. Beggs S, Peterson G, Tompson A. Antibiotic use for the Prevention and Treatment of Rheumatic Fever and Rheumatic Heart Disease in Children. 2008.
5. Scherman J, Ofoegbu C, Myburgh A, Swanevelder J, van Breda B, Appa H, et al. Preclinical evaluation of a transcatheter aortic valve replacement system for patients with rheumatic heart disease. EuroIntervention. 2019 Dec 1;15(11):E975–82.
6. Iung B, Baron G, Butchart EG, Delahaye F, Gohlke-Bärwolf C, Levang OW, et al. A prospective survey of patients with valvular heart disease in Europe: The Euro Heart Survey on Valvular Heart Disease. Eur Heart J [Internet]. 2003 Jul [cited 2023 Jan 14];24(13):1231–43. Available from: https://pubmed.ncbi.nlm.nih.gov/12831818/
7. Pan W, Zhou D, Cheng L, Ge J. Aortic regurgitation is more prevalent than aortic stenosis in Chinese elderly population: Implications for transcatheter aortic valve replacement. Int J Cardiol [Internet]. 2015 Oct 10 [cited 2023 Jan 14];201:547–8. Available from: https://pubmed.ncbi.nlm.nih.gov/26325436/
8. Zilla P, Yacoub M, Zühlke L, Beyersdorf F, Sliwa K, Khubulava G, et al. Global Unmet Needs in Cardiac Surgery. Glob Heart [Internet]. 2018 Dec 1 [cited 2023 Jan 14];13(4):293–303. Available from: https://pubmed.ncbi.nlm.nih.gov/30245177/
9. United Nation. Global indicator framework for the Sustainable Development Goals and targets of the 2030. 2016;
10. Zilla P, Bolman RM, Yacoub MH, Beyersdorf F, Sliwa K, Zühlke L, et al. The Cape Town Declaration on Access to Cardiac Surgery in the Developing World. Annals of Thoracic Surgery. 2018 Sep 1;106(3):930–3.
11. Sliwa K, Zühlke L, Kleinloog R, Doubell A, Ebrahim I, Essop M, et al. Cardiology–cardiothoracic subspeciality training in South Africa: a position paper of the South Africa Heart Association. Cardiovasc J Afr [Internet]. 2016 Jul 6 [cited 2021 Nov 2];27(3):188. Available from: /pmc/articles/PMC5783290/
12. University of Rochester Medical Center. Anatomy and Function of the Heart Valves - Health Encyclopedia [Internet]. 2023 [cited 2023 Jan 15]. Available from: https://www.urmc.rochester.edu/encyclopedia/content.aspx?ContentTypeID=90&ContentID=P03059
13. UpToDate. Heart chamber anatomy PI - UpToDate [Internet]. 2023 [cited 2023 Jan 14]. Available from: https://www.uptodate.com/contents/image?imageKey=PI%2F58389
14. Law J, Martin EA (Elizabeth A). Concise medical dictionary. Tenth edition. Oxford: Oxford University Press; 2020.
15. Kouchoukos NT, Blackstone EH, Hanley FL, Kirklin JK. Anatomy, Dimensions, and Terminology - ClinicalKey. In: Cardiac Surgery [Internet]. Fourth. 2013 [cited 2021 Nov 1]. p. 1–66. Available from: https://www-clinicalkey-

com.ezproxy.uct.ac.za/#!/content/book/3-s2.0-B9781416063919000012?scrollTo=%23hl0004046
16. Nagpal P, Agrawal MD, Saboo SS, Hedgire S, Priya S, Steigner ML. Imaging of the aortic root on high-pitch non-gated and ECG-gated CT: awareness is the key! Insights Imaging [Internet]. 2020 Dec 1 [cited 2023 Oct 5];11(1):1–14. Available from: https://insightsimaging.springeropen.com/articles/10.1186/s13244-020-00855-w
17. Rankin JS, Bone MC, Fries PM, Aicher D, Schäfers HJ, Crooke PS. A refined hemispheric model of normal human aortic valve and root geometry. Journal of Thoracic and Cardiovascular Surgery. 2013;146(1).
18. SSM Health. SSM Health . 2021 [cited 2021 Nov 1]. Aortic Insufficiency: Causes, Symptoms & Treatment. Available from: https://www.ssmhealth.com/heart-vascular-health/valvular-disease/aortic-insufficiency
19. Martin C, Sun W. Biomechanical characterization of aortic valve tissue in humans and common animal models. J Biomed Mater Res A. 2012 Jun;100 A(6):1591–9.
20. Stephens EH, Grande-Allen KJ. Age-related changes in collagen synthesis and turnover in porcine heart valves. J Heart Valve Dis [Internet]. 2007 Nov [cited 2023 Jan 14];16(6):672–82. Available from: https://pubmed.ncbi.nlm.nih.gov/18095519/
21. McDonald PC, Wilson JE, McNeill S, Gao M, Spinelli JJ, Rosenberg F, et al. The challenge of defining normality for human mitral and aortic valves: Geometrical and compositional analysis. Cardiovascular Pathology [Internet]. 2002 [cited 2023 Jan 14];11(4):193–209. Available from: https://pubmed.ncbi.nlm.nih.gov/12140125/
22. Clark RE. Stress-strain characteristics of fresh and frozen human aortic and mitral leaflets and chordae tendineae. Implications for clinical use. J Thorac Cardiovasc Surg [Internet]. 1973 [cited 2023 Jan 14];66(2):202–8. Available from: https://pubmed.ncbi.nlm.nih.gov/4720973/
23. Kelley JD, Kerndt CC, Ashurst J V. Anatomy, Thorax, Aortic Arch. StatPearls [Internet]. 2022 Aug 8 [cited 2023 Jan 14]; Available from: https://www.ncbi.nlm.nih.gov/books/NBK499911/
24. Gaillard F. Aorta (illustration) [Internet]. 2007 [cited 2023 Jan 14]. Available from: https://radiopaedia.org/images/955?case_id=8881
25. Alberta HB, Secor JL, Smits TC, Farber MA, Jordan WD, Matsumura JS. Differences in aortic arch radius of curvature, neck size, and taper in patients with traumatic and aortic disease. Journal of Surgical Research. 2013;184(1):613–8.
26. Redheuil A, Yu WC, Mousseaux E, Harouni AA, Kachenoura N, Wu CO, et al. Age-related changes in aortic arch geometry: Relationship with proximal aortic function and left ventricular mass and remodeling. J Am Coll Cardiol. 2011 Sep 13;58(12):1262–70.
27. Ben-Gal Y, Williams M. Transapical Transcatheter Aortic Valve Implantation. Operative Techniques in Thoracic and Cardiovascular Surgery. 2011;16(1):41–61.
28. Tineke W, Marieke H. The Radiology Assistant. 2009 [cited 2023 May 5]. Cardiac Anatomy. Available from: https://radiologyassistant.nl/cardiovascular/anatomy/cardiac-anatomy
29. Falk V, Walther T, Schwammenthal E, Strauch J, Aicher D, Wahlers T, et al. Transapical aortic valve implantation with a self-expanding anatomically oriented valve. Eur Heart J. 2011 Apr;32(7):878–87.
30. Scherman J, Zilla P. Poorly suited heart valve prostheses heighten the plight of patients with rheumatic heart disease. Int J Cardiol [Internet]. 2020 Nov 1 [cited 2023 Oct 5];318:104–14. Available from: https://pubmed.ncbi.nlm.nih.gov/32464247/

31. Sliwa K, Carrington M, Mayosi BM, Zigiriadis E, Mvungi R, Stewart S. Incidence and characteristics of newly diagnosed rheumatic heart disease in urban African adults: insights from the heart of Soweto study. Eur Heart J [Internet]. 2010 Mar [cited 2023 Oct 5];31(6):719–27. Available from: https://pubmed.ncbi.nlm.nih.gov/19995873/
32. Zühlke L, Karthikeyan G, Engel ME, Rangarajan S, Mackie P, Cupido-Katya Mauff B, et al. Clinical Outcomes in 3343 Children and Adults With Rheumatic Heart Disease From 14 Low- and Middle-Income Countries: Two-Year Follow-Up of the Global Rheumatic Heart Disease Registry (the REMEDY Study). Circulation [Internet]. 2016 Nov 8 [cited 2023 Oct 5];134(19):1456–66. Available from: https://pubmed.ncbi.nlm.nih.gov/27702773/
33. Dougherty S, Zuhlke L, Wilson N. Acute rheumatic fever and rheumatic heart disease. Elsevier Health Sciences; 2022.
34. Carabello BA. Assessment of the patient with valvular heart disease: An integrative approach. Aswan Heart Cent Sci Pract Ser. 2011 Dec 29;2011(2):15.
35. Vahanian A, Beyersdorf F, Praz F, Milojevic M, Baldus S, Bauersachs J, et al. Guidelines for the management of valvular heart disease. Eur Heart J [Internet]. 2022 Feb 14 [cited 2023 Oct 5];43(7):561–632. Available from: https://pubmed.ncbi.nlm.nih.gov/34453165/
36. Scherman J, Manganyi R, Human P, Pennel T, Brooks A, Brink J, et al. Isolated mechanical aortic valve replacement in rheumatic patients in a low- to middle-income country. J Thorac Cardiovasc Surg [Internet]. 2019 Mar 1 [cited 2023 Oct 5];157(3):886–93. Available from: https://pubmed.ncbi.nlm.nih.gov/30107929/
37. Addetia K, Lang RM. Roadmap to the Mechanisms of Aortic Regurgitation on Echocardiography. JACC Case Rep [Internet]. 2020 Aug [cited 2023 Oct 5];2(10):1589. Available from: /pmc/articles/PMC8302201/
38. Markham R, Ghodsian M, Sharma R. TAVR in Patients with Pure Aortic Regurgitation: Ready to Use? Curr Cardiol Rep [Internet]. 2020 Sep 1 [cited 2023 Oct 5];22(9). Available from: https://pubmed.ncbi.nlm.nih.gov/32725310/
39. Fernandes ADF, Fernandes GC, Grant J, Knijnik L, Cardoso R, Cohen MG, et al. Transcatheter Aortic Valve Replacement for Severe Symptomatic Aortic Stenosis in Rheumatic Heart Disease: A Systematic Review. Cardiol Rev [Internet]. 2022 Nov 1 [cited 2023 Oct 5];30(6):318–23. Available from: https://pubmed.ncbi.nlm.nih.gov/36201243/
40. Shucker H. B. The Journal of cardiovascular surgery. 1989 [cited 2021 Nov 1]. When did cardiac surgery begin? - PubMed. Available from: https://pubmed.ncbi.nlm.nih.gov/2651455/
41. Mayo Clinic Staff. Mayo Clinic. 2021. Heart valve surgery.
42. Overtchouk P, Vahanian A, Modine T. Valvular heart disease: when does surgery remain the best option? EuroIntervention. 2019 Nov;15(10):831–2.
43. Reardon MJ, Leon MB, Popma JJ, Mack MJ. Heart team 2.0. EuroIntervention. 2019 Nov;15(10):825–7.
44. Voigtländer L, Seiffert M. Expanding TAVI to Low and Intermediate Risk Patients. Front Cardiovasc Med [Internet]. 2018 Jul 12 [cited 2023 Feb 7];5. Available from: /pmc/articles/PMC6052659/
45. Costanzo P, Bamborough P, Peterson M, Deva DJ, Ong G, Fam N. Transcatheter Aortic Valve Implantation for Severe Pure Aortic Regurgitation With Dedicated Devices. Interventional Cardiology: Reviews, Research, Resources. 2022;17.

46. Singh SK, Kachel M, Castillero E, Xue Y, Kalfa D, Ferrari G, et al. Polymeric prosthetic heart valves: A review of current technologies and future directions. Front Cardiovasc Med. 2023 Mar 9;10:271.
47. Kereiakes DJ, Answini GA, Yakubov SJ, Rai B, Smith JM, Duff S, et al. Preliminary Evaluation of a Novel Polymeric Valve Following Surgical Implantation for Symptomatic Aortic Valve Disease. JACC Cardiovasc Interv. 2021 Dec 27;14(24):2754–6.
48. Appa H, Park K, Bezuidenhout D, van Breda B, de Jongh B, de Villiers J, et al. The Technological Basis of a Balloon-Expandable TAVR System: Non-occlusive Deployment, Anchorage in the Absence of Calcification and Polymer Leaflets. Front Cardiovasc Med. 2022 Mar 3;9.
49. Perrin N, Bonnet G, Leroux L, Ibrahim R, Modine T, Ali W Ben. Transcatheter Aortic Valve Implantation: All Transfemoral? Update on Peripheral Vascular Access and Closure. Front Cardiovasc Med [Internet]. 2021 Sep 29 [cited 2023 May 5];8:747583. Available from: /pmc/articles/PMC8511676/
50. Young MN, Singh V, Sakhuja R. A Review of Alternative Access for Transcatheter Aortic Valve Replacement. Curr Treat Options Cardiovasc Med [Internet]. 2018 Jul 1 [cited 2023 May 5];20(7). Available from: https://www.researchgate.net/publication/326181385_A_Review_of_Alternative_Access_for_Transcatheter_Aortic_Valve_Replacement
51. Carroll JD, Mack MJ, Vemulapalli S, Herrmann HC, Gleason TG, Hanzel G, et al. STS-ACC TVT Registry of Transcatheter Aortic Valve Replacement. Annals of Thoracic Surgery [Internet]. 2021 Feb 1 [cited 2023 May 5];111(2):701–22. Available from: http://www.annalsthoracicsurgery.org/article/S0003497520315149/fulltext
52. Seladi-Schulman J, Weatherspoon D. healthline . 2019 [cited 2021 Nov 1]. What Happens in a Clinical Trial. Available from: https://www.healthline.com/health/clinical-trial-phases
53. Kheradvar A, Zareian R, Kawauchi S, Goodwin RL, Rugonyi S. Animal models for heart valve research and development. Drug Discov Today Dis Models. 2017 Jun 1;24:55–62.
54. Noorani A, Radia R, Bapat V. Challenges in valve-in-valve therapy. J Thorac Dis [Internet]. 2015 [cited 2021 Nov 1];7(9):1501–8. Available from: https://jtd.amegroups.com/article/view/4844/html
55. Dawkins S, Prendergast B. Transcatheter aortic valve implantation - practice makes perfect. EuroIntervention. 2017 Nov;13(8):897–9.
56. Ruyra X, Permanyer E, Huguet M, Maldonado G. Use of virtual reality for procedural planning of transcatheter aortic valve replacement. Interact Cardiovasc Thorac Surg. 2022 Oct 10;35(5).
57. Simbionix. Training on ANGIO Mentor Helped Introduce TAVI Technology to Physicians Worldwide [Internet]. 2017 [cited 2021 Nov 1]. Available from: https://simbionix.com/training-on-angio-mentor-helped-introduce-tavi-technology-to-physicians-worldwide/
58. Fischer Q, Sbissa Y, Nhan P, Adjedj J, Picard F, Mignon A, et al. Use of Simulator-Based Teaching to Improve Medical Students' Knowledge and Competencies: Randomized Controlled Trial. J Med Internet Res [Internet]. 2018 Sep 1 [cited 2023 Feb 5];20(9). Available from: https://pubmed.ncbi.nlm.nih.gov/30249587/

59. Cocchieri R, van de Wetering B, Stijnen M, Riezebos R, de Mol B. The impact of biomedical engineering on the development of minimally invasive cardio-thoracic surgery. Vol. 10, Journal of Clinical Medicine. MDPI; 2021.
60. Mitra K. CT Scan. Journal of Undergraduate Medical Research [Internet]. 2021;3(1):49–50. Available from: https://www.researchgate.net/publication/353545789
61. Krans B, Sullivan D. healthline . 2018 [cited 2021 Nov 1]. Heart CT Scan. Available from: https://www.healthline.com/health/heart-ct-scan
62. National Institute of Biomedical Imaging and Bioengineering. National Institute of Biomedical Imaging and Bioengineering (NIBIB). 2021 [cited 2021 Nov 1]. Computed Tomography (CT). Available from: https://www.nibib.nih.gov/science-education/science-topics/computed-tomography-ct
63. Kasel AM, Cassese S, Leber AW, Von Scheidt W, Kastrati A. Fluoroscopy-guided aortic root imaging for TAVR: 'follow the right cusp' rule. Vol. 6, JACC: Cardiovascular Imaging. Elsevier Inc.; 2013. p. 274–5.
64. Kasel AM, Krapf S, Augsburg K, Deutsches AK, München H. Standardized Methodology for Transfemoral Transcatheter Aortic Valve Replacement With the Edwards Sapien XT Valve Under Fluoroscopy Guidance Bioresorbable vascular scaffolds View project Cardiogenic Shock View project [Internet]. Article in The Journal of invasive cardiology. 2014. Available from: https://www.researchgate.net/publication/265419559
65. Lai J, Wang C, Wang M. 3D printing in biomedical engineering: Processes, materials, and applications. Appl Phys Rev [Internet]. 2021 Jun 16 [cited 2021 Nov 1];8(2):021322. Available from: https://aip.scitation.org/doi/abs/10.1063/5.0024177
66. Hayden R. The University of Sydney. 2018 [cited 2021 Nov 1]. 3D printing moves into biomedical engineering. Available from: https://www.sydney.edu.au/news-opinion/news/2018/03/22/3d-printing-moves-into-biomedical-engineering.html
67. Redondo A, Valencia-Serrano F, Santos-Martínez S, Delgado-Arana JR, Barrero A, Serrador A, et al. Accurate commissural alignment during ACURATE neo TAVI procedure. Proof of concept. Revista Española de Cardiología (English Edition). 2021 Mar;
68. Bates Machine. Best Metals for Medical Device Manufacturing - Bates Machine Shop [Internet]. 2023 [cited 2023 Jan 14]. Available from: https://batesmachineonline.com/best-metals-for-medical-device-manufacturing/
69. All about aluminium. What is aluminium [Internet]. 2023 [cited 2023 Jan 14]. Available from: https://aluminiumleader.com/about_aluminium/what_is_aluminum/
70. Das B, Wang Y. Isometric pull-push strengths in workspace: 1. Strength profiles. Int J Occup Saf Ergon [Internet]. 2004 [cited 2023 Jan 14];10(1):43–58. Available from: https://pubmed.ncbi.nlm.nih.gov/15028193/

Appendix A : Ethics approval letters

UNIVERSITY OF CAPE TOWN
Faculty of Health Sciences
Animal Ethics Committee

Room G50 Old Main Building
Groote Schuur Hospital
Observatory 7925
Website: www.health.uct.ac.za/fhs/research/animalethics/forms

09 November 2021

Dr Chima Ofoegbu
Division of Cardiothoracic Surgery
Department of Surgergy
Faculty of Health Sciences
University of Cape Town

Dear Dr Ofoegbu

PROTOCOL TITLE: ***Transapical Transcatheter Aortic Valve Implantation (TAVI) In A Cadaveric Pig Heart Model: Determination Of Implantation Force (Student: Mr Fadi Nkoma Fakih)***

FHS AEC REF NO: 021_022

Thank you for submitting your request for authorisation of use of animal material for scientific purposes Faculty of Health Sciences (FHS) Animal Ethics Committee (AEC) for review.

I am pleased to inform you that the FHS AEC has **authorised** your protocol, which will terminate on **30 December 2024.**

Number of animals & species:

- 50 Pig Hearts

Please quote the FHS AEC REF NO (above) in all future correspondence.

Please note that the authorisation of this protocol imposes the following obligations on the principal investigator (PI):

1. To submit an annual mandatory progress report. The first annual report for this protocol is due on **28 February 2022**. The forms can be accessed from http://www.health.uct.ac.za/fhs/research/animalethics/forms
2. To submit a final mandatory report on the **30 December 2024**, please access the final report form from: http://www.health.uct.ac.za/fhs/research/animalethics/forms
3. Ensuring that all study participants perform within the confines of the procedures and experimental design of the protocol as authorised, or as amended.

4. Ensuring that all study participants comply with all applicable national legislation, UCT policies, FHS AEC policies and standard operating procedures (SOPs) and national standards (SANS 10386: 2008).
5. Ensuring compliance with DAFF Section 20 requirements.
6. Ensuring that you as the PI immediately alert the FHS AEC to any event involving the welfare of the animals which has occurred during the course of the study, as well as the actions that were taken to respond to these events.
7. Ensuring that you as the PI alert the FHS AEC to any new or unexpected ethical issues that arose during the course of the study, and how these issues were addressed.
8. Ensuring that all study participants are registered with or have been authorised by the South African Veterinary Council (SAVC) to perform the procedures on animals or will be performing the procedures under the direct and continuous supervision of SAVC-registered veterinary professionals or SAVC-registered para-veterinary professionals.
9. If the PI or any study participant is in any way uncertain how to respond to any of these obligations or deal with any of the issues referred to above, they must consult with FHS AEC.
10. All animals found dead must be reported to the RAF on the appropriate form: http://www.health.uct.ac.za/fhs/research/animalethics/forms
11. All animals found in distress must be reported to the RAF on the appropriate form.

My best wishes for successful research and /or teaching endeavour.

Yours sincerely

PROF G. LOUW
CHAIR, FHS AEC

AEC REF# 021_022

UNIVERSITY OF CAPE TOWN

Department of Surgery
Departmental Research Committee
A/Prof Maritz Laubscher
Groote Schuur Hospital
Observatory 7925
South Africa
Tel (021) 404 5108
Email: maritz.laubscher@uct.ac.za

8 Sep 2021

Mr F Nkoma Fakih

Department of Surgery
University of Cape Town

Dear Mr Nkoma Fakih

RE: Project 2021/241

PROJECT TITLE: Transapical Transcatheter Aortic Valve Implantation (Tavi) In A Cadaveric Pig Heart Model: Determination Of Implantation Force

The above protocol has been reviewed by the Department of Surgery Research Committee. I am pleased to inform you that the committee approved the scientific merit of the study, and endorse the protocol for submission to the relevant ethics committee.

Although this letter serves as confirmation that the above protocol has successfully passed through the surgical DRC, respective ethics committees still require DRC chair signature before submission.

Please use the above project number in all future correspondence,

Yours sincerely

A/PROF MARITZ LAUBSCHER
CHAIR SURGICAL DRC

"OUR MISSION is to be an outstanding teaching and research university, educating for life and addressing the challenges facing our society."

UNIVERSITY OF CAPE TOWN
Faculty of Health Sciences
Human Research Ethics Committee

Room G 50 Old Main Building
Groote Schuur Hospital
Observatory 7925
Email: hrec-enquiries@uct.ac.za
Website: www.health.uct.ac.za/fhs/research/humanethics/forms

04 December 2020

HREC REF: 826/2020

Dr H Appa
Strait Access Technologies
Cardiovascular Research Unit
313 Chris Barnard Building-FHS
Email: harish.appa@uct.ac.za
Student: fadi.nkomafakih@uct.ac.za

Dear Dr Appa

PROJECT TITLE: IN-VITRO AND IN-SILICO EVALUATION OF THREE-DIMENSIONAL COMPUTED TOMOGRAPHY GEOMETRY OF THE AORTIC ROOT IN PATIENTS SCREENED FOR TRANSCATHETER AORTIC VALVE IMPLANTATION-MASTER CANDIDATE-DR FADI N FAKIH

Thank you for submitting your study to the Faculty of Health Sciences Human Research Ethics Committee (HREC) for review.

It is a pleasure to inform you that the HREC has **formally approved** the above-mentioned study.

This approval is subject to strict adherence to the HREC recommendations regarding research involving human participants during COVID -19, dated 17 March 2020 & 06 July 2020.

Approval is granted for one year until the 30 December 2021.

Please submit a progress form, using the standardised Annual Report Form if the study continues beyond the approval period. Please submit a Standard Closure form if the study is completed within the approval period.
(Forms can be found on our website: www.health.uct.ac.za/fhs/research/humanethics/forms)

The HREC acknowledge that the student: - Dr Fadi Fakih will also be involved in this study.

Please quote the HREC REF in all your correspondence.

Please note that the ongoing ethical conduct of the study remains the responsibility of the principal investigator.

Please note that for all studies approved by the HREC, the principal investigator **must** obtain appropriate institutional approval, where necessary, before the research may occur.

Yours sincerely

PROFESSOR M BLOCKMAN
CHAIRPERSON, FHS HUMAN RESEARCH ETHICS COMMITTEE

Federal Wide Assurance Number: FWA00001637.
Institutional Review Board (IRB) number: IRB00001938
NHREC-registration number: REC-210208-007

This serves to confirm that the University of Cape Town Human Research Ethics Committee complies to the Ethics Standards for Clinical Research with a new drug in patients, based on the Medical Research Council (MRC-SA), Food and Drug Administration (FDA-USA), International Council for Harmonisation of Technical Requirements for Pharmaceuticals for Human Use: Good Clinical Practice (ICH GCP), South African Good Clinical Practice Guidelines (DoH 2006), based on the Association of the British Pharmaceutical Industry Guidelines (ABPI), and Declaration of Helsinki (2013) guidelines.
The Human Research Ethics Committee granting this approval is in compliance with the ICH Harmonised Tripartite Guidelines E6: Note for Guidance on Good Clinical Practice (CPMP/ICH/135/95) and FDA Code Federal Regulation Part 50, 56 and 312.

Appendix B: Item/Drawing Number Master Record Index

Item #	Drawing #	Name	Detailed Description	Manufacturing method	Material	Product	Latest revision	Supplier
0001	NKMFAD0001	C Arm	Laser cut C arm from aluminium used for the rotation of the camera	Laser cut	aluminium	Imaging	0	
0002	NKMFAD0002	Tube Clamp Half	3d printed part used to clamp the horizontal shaft and connect it to the c-arm	3D printing	tough	Imaging	0	
0003	NKMFAD0003	M2 Nut	fastening part	Bought	SS	Imaging	0	
0004	NKMFAD0004	Cheese Head Screw M2X16	fastening part	Bought	SS	Imaging	0	
0005	NKMFAD0005	Tube Clamp	Assembly of item 0002 0003 and 0004 used to hold the central tube	Assembly	-	Imaging	0	
0006	NKMFAD0006	C Arm Central joint	Housing holding the tube clamp	Machine	aluminium	Imaging	0	RS component
0007	NKMFAD0007	Spring	compressive spring used in the handle to lock the c-arm in position	Bought	steel	Imaging	0	RS component
0008	NKMFAD0008	Spring base	part of the handle holding the spring	Machine	aluminium	Imaging	0	
0009	NKMFAD0009	Spring stump	part of the handle holding the spring	3D printing	resin	Imaging	0	
0010	NKMFAD0010	Spring handle	part of the handle holding the spring	3D printing	resin	Imaging	0	
0011	NKMFAD0011	Spring Shell	part of the handle holding the spring	3D printing	resin	Imaging	0	
0012	NKMFAD0012	Rubber ring	part of the handle gripping the C-arm	Bought	silicone	Imaging	0	
0013	NKMFAD0013	Quick Release clamp	clamp locking the horizontal shaft in position	Bought	-	Imaging	0	Camvate
0014	NKMFAD0014	Horizontal Shaft	Horizontal shaft connecting the front and back part of the C-arm a	Bought	Steel	Imaging	0	

0015	NKMFAD0015	C Arm Front Join	Housing holding the horizontal shaft and the legs	Machine	aluminium	Imaging	0	RS component
0016	NKMFAD0016	Aluminium Leg Profile	Modular assembly legs used	Bought	aluminium	Imaging	0	Modular assembly
0017	NKMFAD0017	Base plate	Base of the legs connecting the wheels	Machine	SS	Imaging	0	
0018	NKMFAD0018	Wheel	Wheels attached to the based plate to move the assembly	Bought	-	Imaging	0	RS component
0019	NKMFAD0019	M3 Nut	fastening part	Bought	-	Imaging	0	
0020	NKMFAD0020	Socket screw M3x10	fastening part	Bought	-	Imaging	0	
0021	NKMFAD0021	Aluminium Leg support	legs supporting the C arm	Bought	aluminium	Imaging	0	Modular assembly
0022	NKMFAD0022	T-SLOT NUTS	fastening part	Bought	aluminium	Imaging	0	Modular assembly
0023	NKMFAD0023	90 DEGREE BRACKET	bracket used to connect the C arm legs	Bought	aluminium	Imaging	0	Modular assembly
0024	NKMFAD0024	(Wheel Nut) M6 Nut	fastening part for the wheel	Bought	-	Imaging	0	
0025	NKMFAD0025	(Wheel bolt) M6 Bolt	fastening part for the wheel	Bought	-	Imaging	0	
0026	NKMFAD0026	C arm Back End Sub Assembly	sub-assembly of the C arm	Assembly	-	Imaging	0	
0027	NKMFAD0027	90 degree sub assembly	sub-assembly	Assembly	-	Imaging	0	
0028	*NKMFAD0028*	C arm rod support	12mm Diameter rod	Machine	aluminium	Imaging	0	
0029	*NKMFAD0029*	circlip mock	For 12mm diameter	Bought	aluminium	Imaging	0	
0030	*NKMFAD0030*	Handle Sub Assembly	sub-assembly of the handle	Assembly	-	Imaging	0	
0031	NKMFAD0031	C arm Front End Sub Assembly	sub-assembly of the C-arm front end	Assembly	-	Imaging	0	
0032	NKMFAD0032	C arm connector	part used to connect both C-section	Laser cut	aluminium	Imaging	0	

0033	NKMFAD0033	Camera stand	Stand used to connect the Carm and the camera	Laser cut	aluminium	Imaging	0	
0034	NKMFAD0034	Camera	camera used to replicate X-ray	Bought	-	Imaging	0	
0035	NKMFAD0035	Mock Ventricle	3D printed part replicating the ventricle	3D printing	Clear	circulation loop	0	
0036	NKMFAD0036	Aortic arch	3D printed part replicating the aortic arch	3D printing	Clear	circulation loop	0	
0037	NKMFAD0037	Aortic root	3D printed part replicating the aortic root	3D printing	elastic	circulation loop	0	
0038	NKMFAD0038	Aortic valve leaflet	3D printed part replicating the aortic leaflet	3D printing	elastic	circulation loop	0	
0039	NKMFAD0039	Entry Cap	3D printed part used to lock and seal the entry point	3D printing	Clear	circulation loop	0	
0040	NKMFAD0040	Entry Silicone	silicone part used as entry point	Bought	Silicone	circulation loop	0	RS Component
0041	NKMFAD0041	One way valve	one way valve purchase from minivalve with item number CR 200.002-154.01	Bought	Silicone	circulation loop	0	Minivalve
0042	NKMFAD0042	One way valve holder Body	3D printed part used to hold the one-way valve	3D printing	Clear	circulation loop	0	
0043	NKMFAD0043	One way valve holder Head	3D printed part used to hold the one-way valve	3D printing	Clear	circulation loop	0	
0044	NKMFAD0044	Heart assembly	Assembly of the heart	Assembly	-	circulation loop	0	
0045	NKMFAD0045	silicone tube	use to guide/distribute water in the system	Bought	Silicon	circulation loop	0	
0046	NKMFAD0046	C-arm Full assembly	assembly of the full C-arm	Assembly	-	Imaging	0	
0047	NKMFAD0047	Microcontroller	microcontroller used to process the force and convert it to the led light	Bought	-	Force	0	RS Component

0048	NKMFAD0048	Force sensor	Sensor used to measure the force applied	Bought	-	Force	0	RS Component
0049	NKMFAD0049	LED Light	Led light used to indicate the force range applied by the surgeon	Bought	-	Force	0	Rs Component
0050	NKMFAD0050	force sensor silicon pad	Silicon pad used to protect the sensor	Bought	Silicon	Force	0	Rs Component
0051	NKMFAD0051	Handle Holder	Front handle part	3D printing	resin	Force	0	
0052	NKMFAD0052	Sensor press	Part transferring the force from the mock trunks to the sensor	3D printing	resin	Force	0	
0053	NKMFAD0053	Top seal	3D printed part used to hold the handle and the sensor press	3D printing	resin	Force	0	
0054	NKMFAD0054	Tactile feedback training device	Device used to train surgeon on the tactile feedback force	Assembly	resin	Force	0	
0055	NKMFAD0055	Microcontroller holder	Central part of the handle holding the microcontroller	3D printing	resin	Force	0	
0056	NKMFAD0056	Microcontroller pin	Pin used to locate the microcontroller in the handle	3D printing	resin	Force	0	
0057	NKMFAD0057	Back Handle	Back part of the handle	3D printing	resin	Force	0	
0058	NKMFAD0058	Pebax Shaft	Part connecting the handle to the mock trunks	Bought	Pebax	Force	0	Nordson
0059	NKMFAD0059	Mock Trunks	3D printed part used to replicate the SAT trunks	3D printing	resin	Force	0	

Appendix C : Test Data

Heart 1

Force (N)	Droop L1 RCC (mm)	Droop L2 NCC (mm)	Droop L3 LCC (mm)
0.00	0.00	0.00	0.00
3.28	-2.98	-2.86	0.00
4.55	-3.85	-3.58	-0.40
8.75	-4.57	-4.80	-0.46
11.83	-5.89	-5.42	-0.85

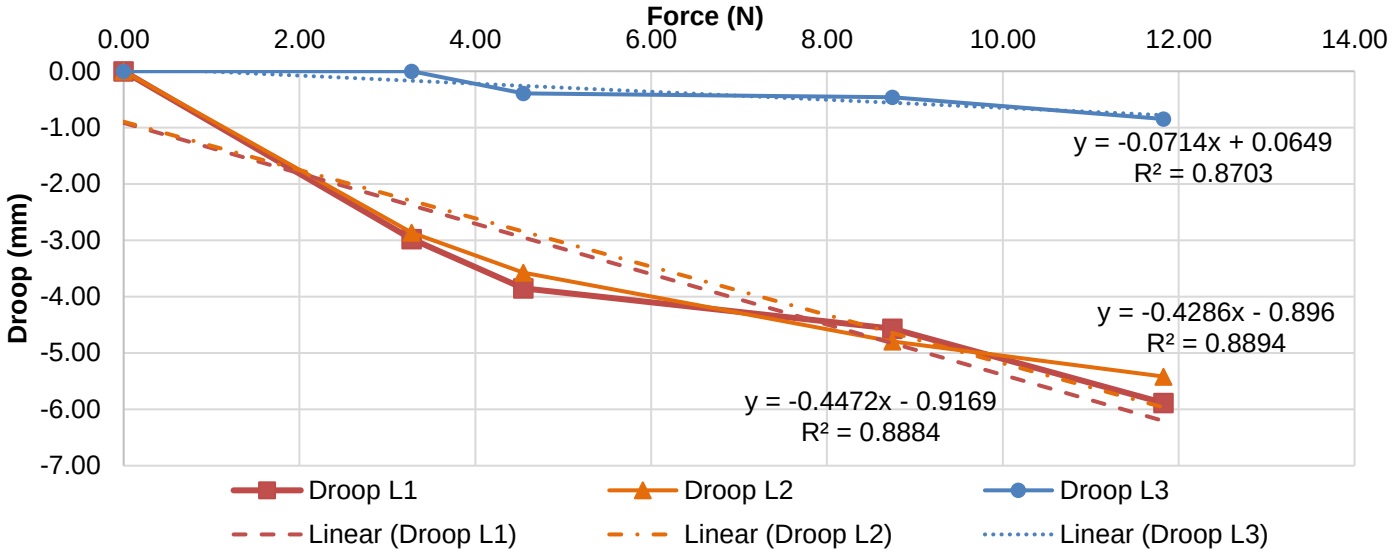

Heart 2

Force (N)	Droop L1 RCC (mm)	Droop L2 NCC (mm)	Droop L3 LCC (mm)
0.00	0.00	0.00	0.00
6.06	-1.06	-2.36	-1.55
7.13	-2.24	-2.34	-1.76
8.94	-2.99	-2.84	-1.80
12.72	-4.52	-3.13	-1.96

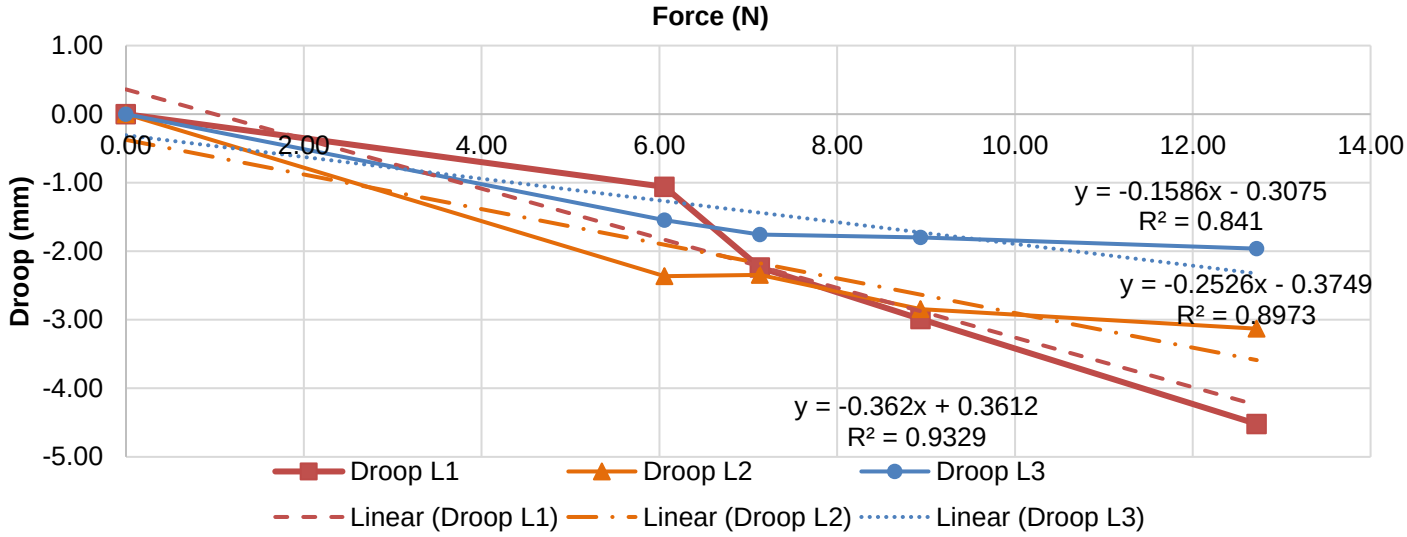

Heart 4

Force (N)	Droop L1 RCC (mm)	Droop L2 NCC (mm)	Droop L3 LCC (mm)
0.00	0.00	0.00	0.00
6.40	-3.90	-3.96	-2.24
7.60	-4.65	-4.24	-2.84
10.73	-5.48	-5.34	-3.06
14.09	-5.78	-5.41	-3.53

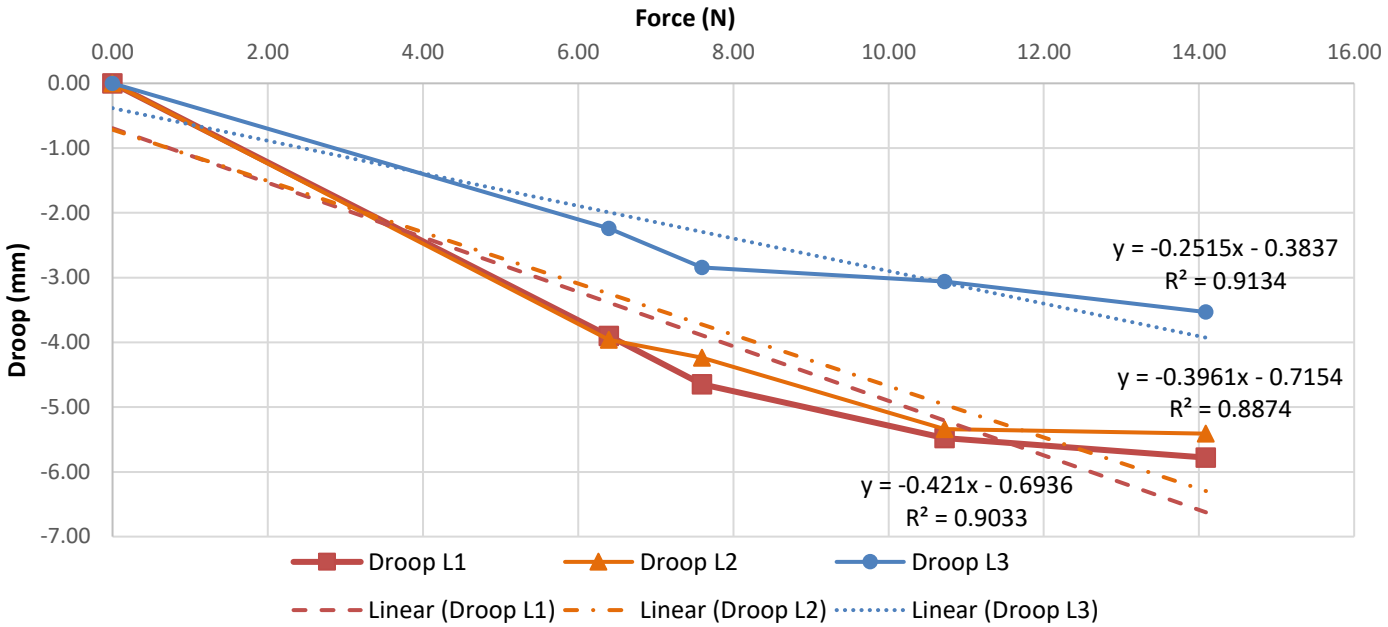

Heart 5

Force (N)	Droop L1 RCC (mm)	Droop L2 NCC (mm)	Droop L3 LCC (mm)
0	0.00	0.00	0.00
8.08	-1.42	-1.27	-0.84
9.67	-2.04	-1.53	-1.05
9.87	-2.09	-1.66	-1.36
11.99	-2.24	-1.72	-1.58

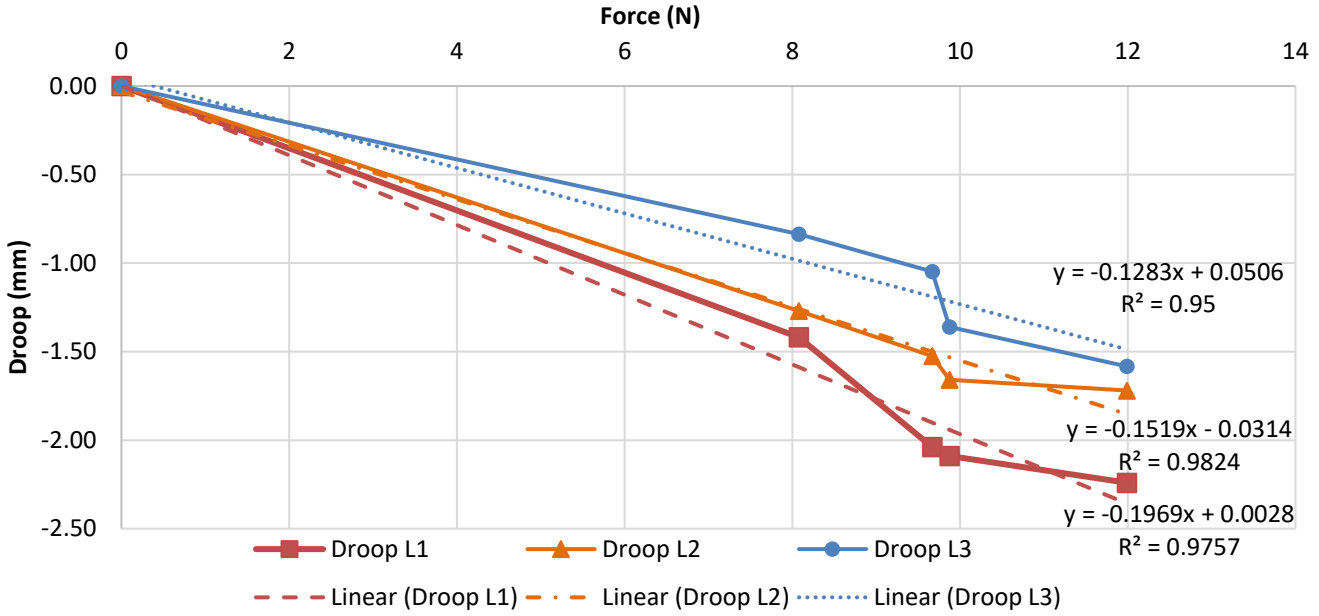

Heart 6

Force (N)	Droop L1 RCC (mm)	Droop L2 NCC (mm)	Droop L3 LCC (mm)
0.00	0.00	0.00	0.00
8.75	-2.56	-1.00	-2.54
9.75	-2.91	-1.96	-2.52
11.47	-3.07	-2.09	-3.05
11.26	-3.24	-2.54	-3.11

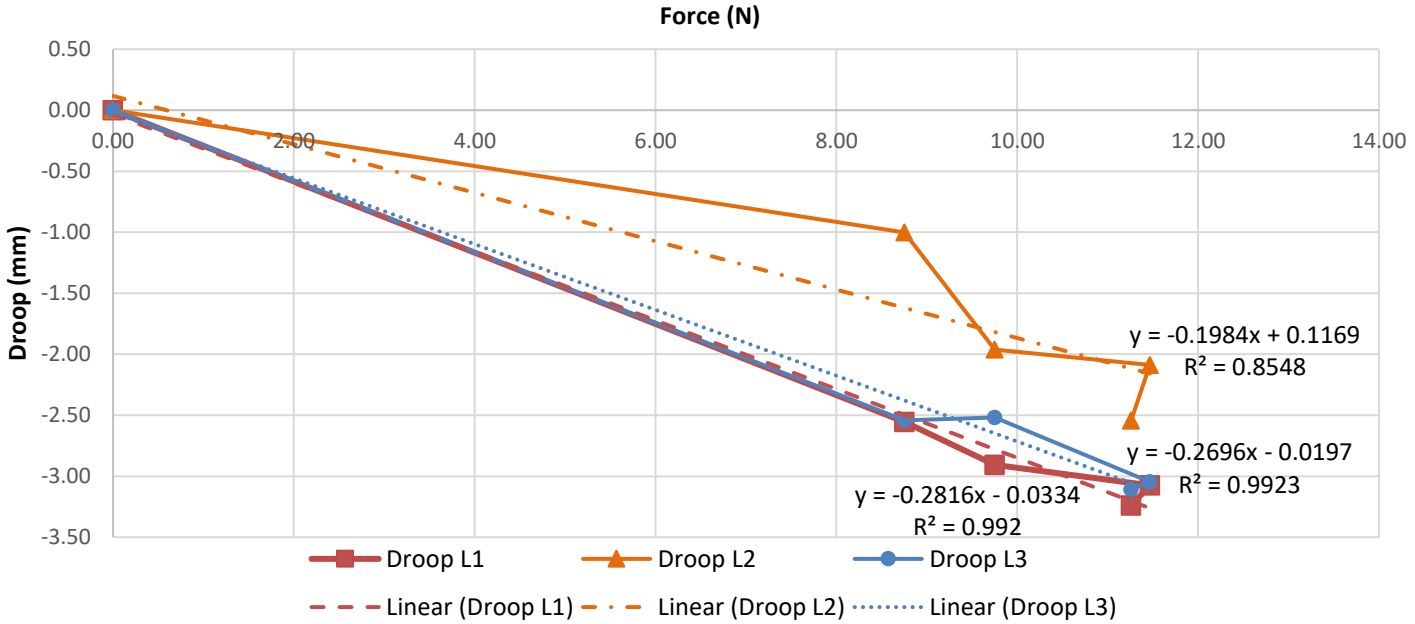

Heart 7

Force (N)	Droop L1 RCC (mm)	Droop L2 NCC (mm)	Droop L3 LCC (mm)
0.00	5.40	0.00	-2.64
4.78	-3.08	-3.80	-4.81
7.29	-3.73	-4.40	-5.30
8.76	-4.60	-6.40	-6.32
12.45	-6.49	-7.37	-7.41

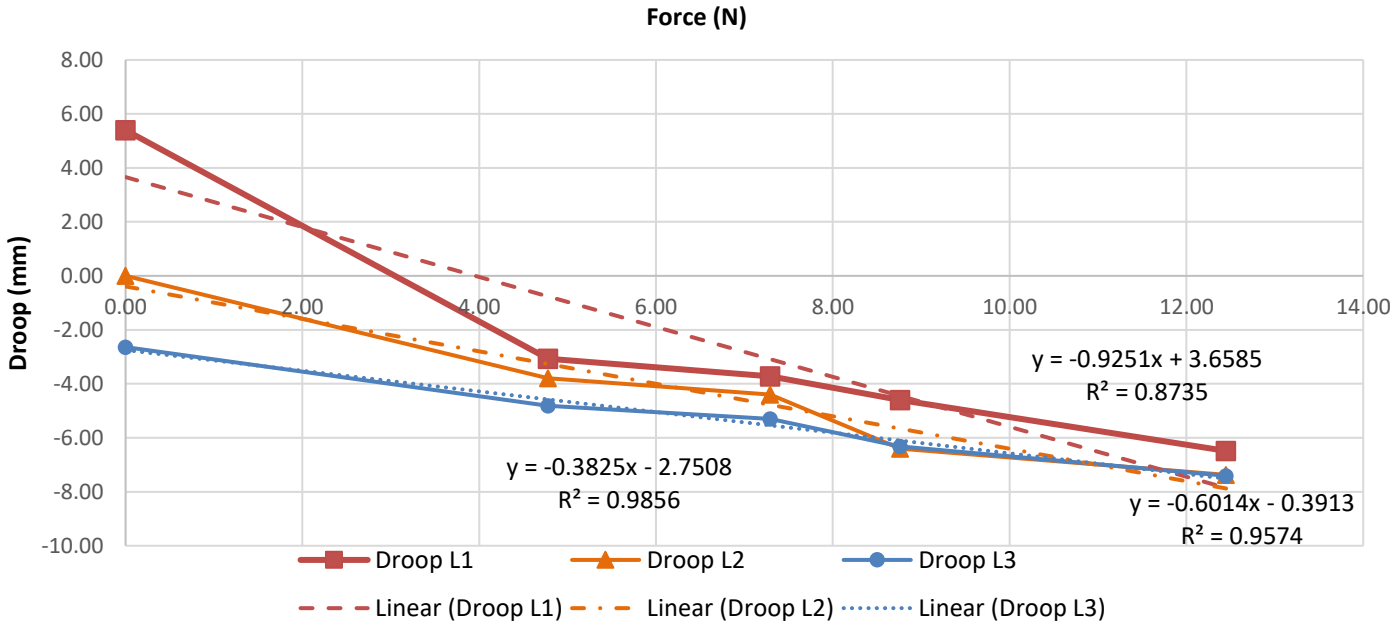

Heart 8

Force (N)	Droop L1 RCC (mm)	Droop L2 NCC (mm)	Droop L3 LCC (mm)
0.00	0.00	0.00	0.00
7.00	-3.65	0.00	-5.39
11.82	-3.90	0.00	-6.97
14.02	-5.14	0.00	-8.04
16.28	-5.35	0.00	-8.09

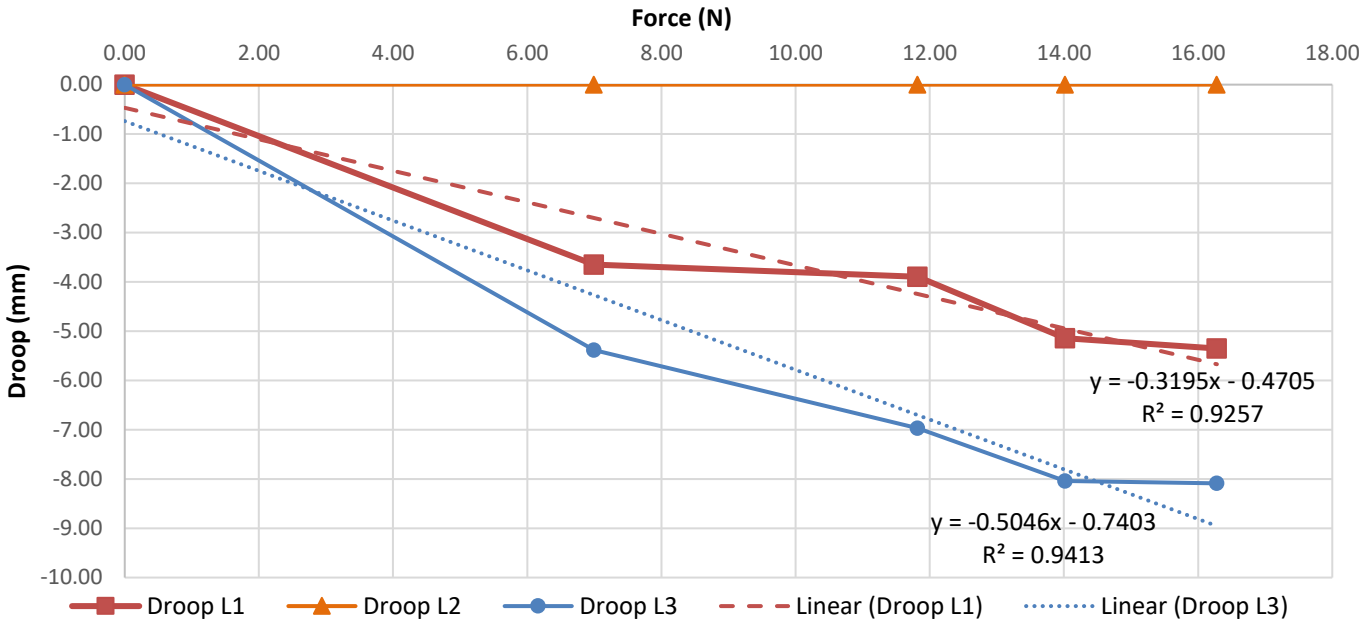

Heart 9

Force (N)	Droop L1 RCC (mm)	Droop L2 NCC (mm)	Droop L3 LCC (mm)
0.00	0.00	0.00	0.00
3.39	-2.48	-1.70	-1.43
9.42	-5.83	-2.42	-2.43
12.55	-6.75	-3.08	-2.61
14.54	-7.29	-3.09	-2.54

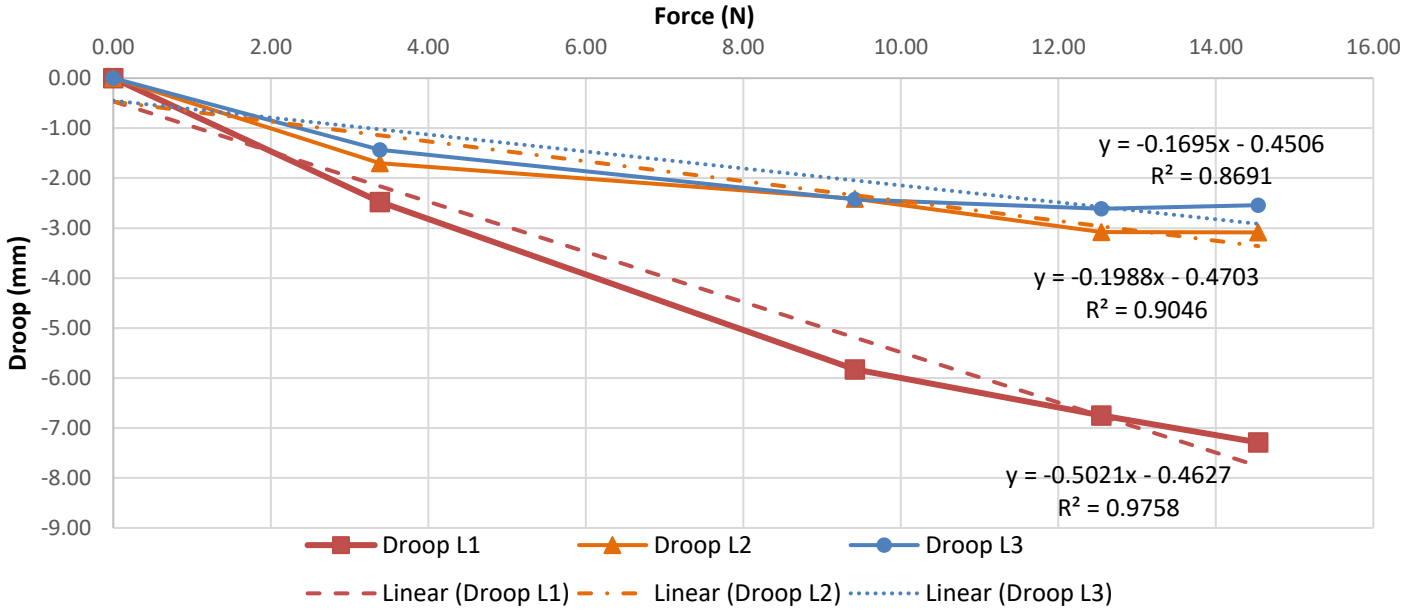

Heart 10

Force (N)	Droop L1 RCC (mm)	Droop L2 NCC (mm)	Droop L3 LCC (mm)
0.00	0.00	0.00	0.00
10.28	-3.53	-3.00	-2.21
11.94	-4.27	-3.20	-2.34
13.38	-4.35	-4.08	-3.31
14.77	-4.44	-4.21	-3.50

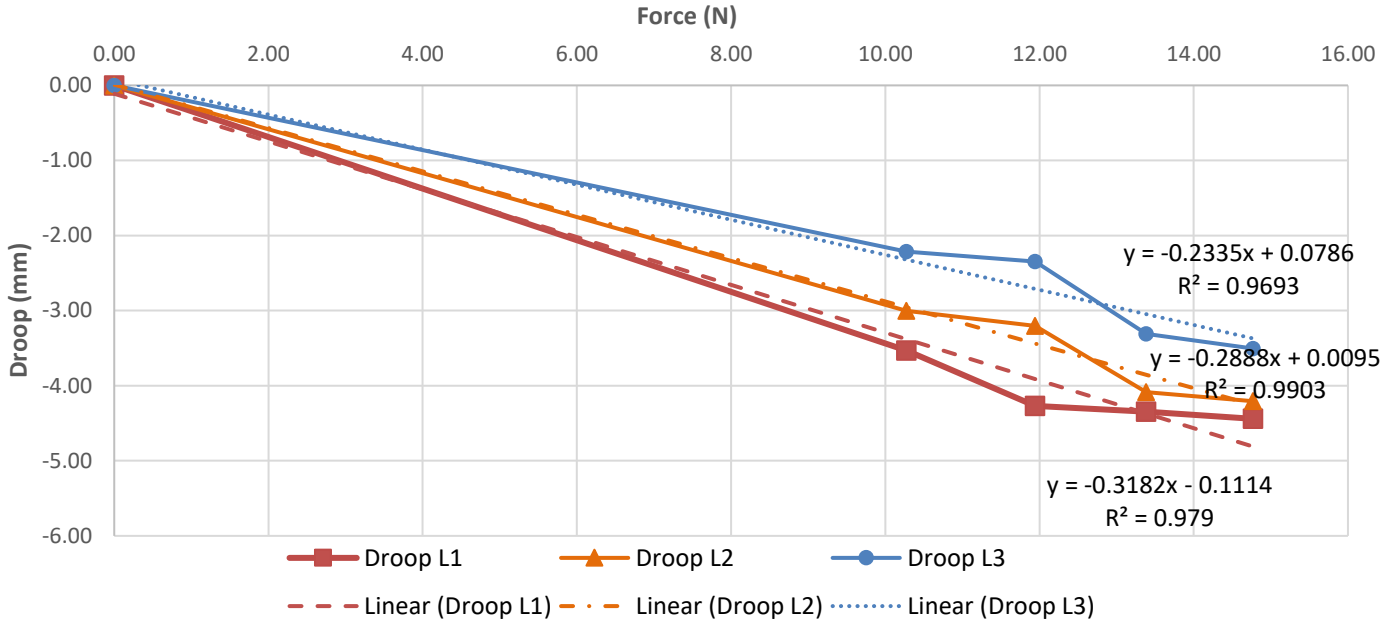

Heart 11

Force (N)	Droop L1 RCC (mm)	Droop L2 NCC (mm)	Droop L3 LCC (mm)
0.00	0.00	0.00	0.00
2.29	-2.53	-3.00	-2.21
5.30	-3.27	-3.20	-2.34
9.75	-3.35	-4.08	-3.31
15.14	-3.44	-4.21	-3.50

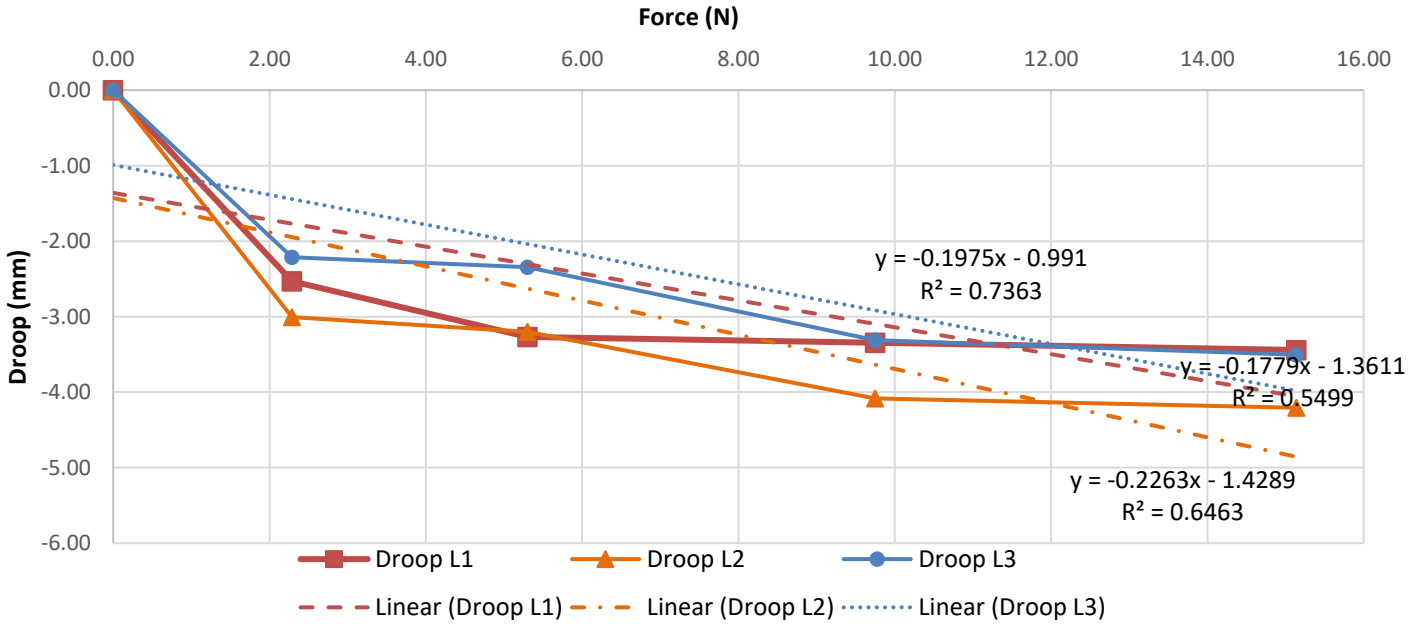

Heart 12

Force (N)	Droop L1 RCC (mm)	Droop L2 NCC (mm)	Droop L3 LCC (mm)
0.00	0.00	0.00	0.00
12.36	-5.60	-4.02	-1.97
15.78	-5.80	-4.67	-1.89
19.22	-7.43	-4.65	-2.36
26.64	-7.20	-4.81	-2.34

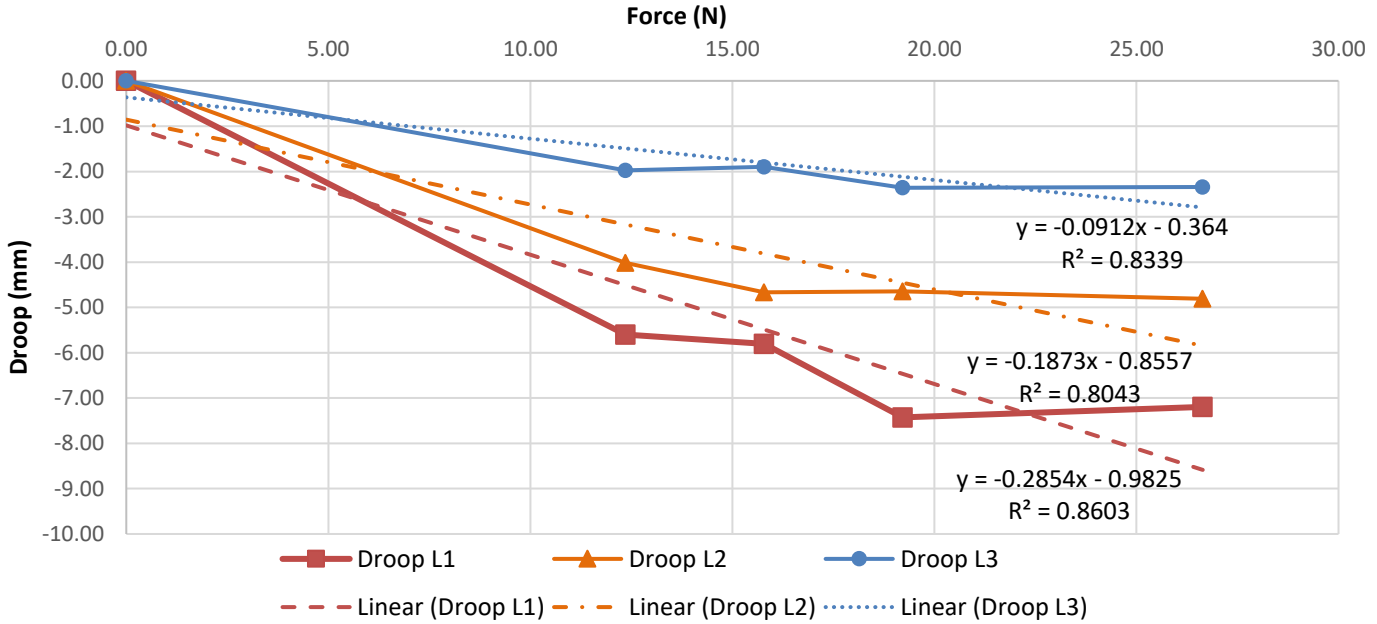

Heart 13

Force (N)	Droop L1 RCC (mm)	Droop L2 NCC (mm)	Droop L3 LCC (mm)
0.00	0.00	0.00	0.00
5.31	-3.27	-1.02	-2.39
9.46	-5.10	-1.08	-3.29
12.30	-5.45	-1.10	-4.17
15.40	-5.59	-1.30	-4.51

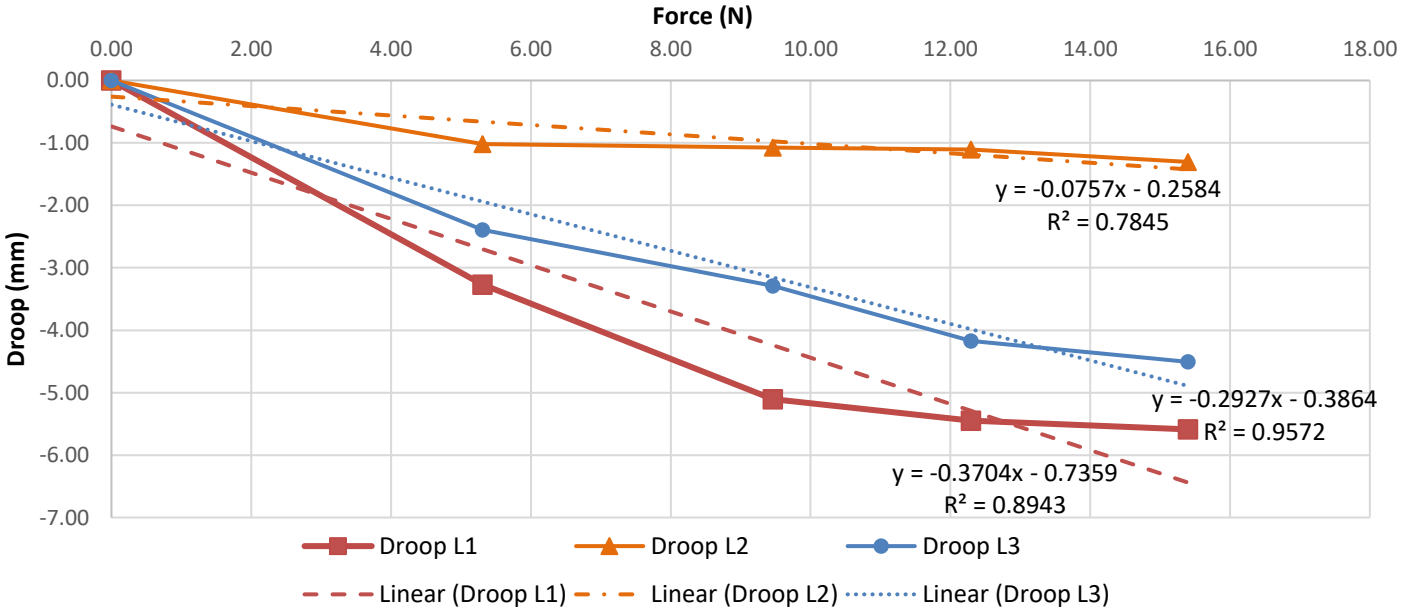

Heart 14

Force (N)	Droop L1 RCC (mm)	Droop L2 NCC (mm)	Droop L3 LCC (mm)
0.00	0.00	0.00	0.00
10.69	-2.66	0.00	-1.98
12.92	-3.09	0.00	-2.05
14.43	-3.17	0.00	-2.09
16.32	-4.07	0.00	-2.31

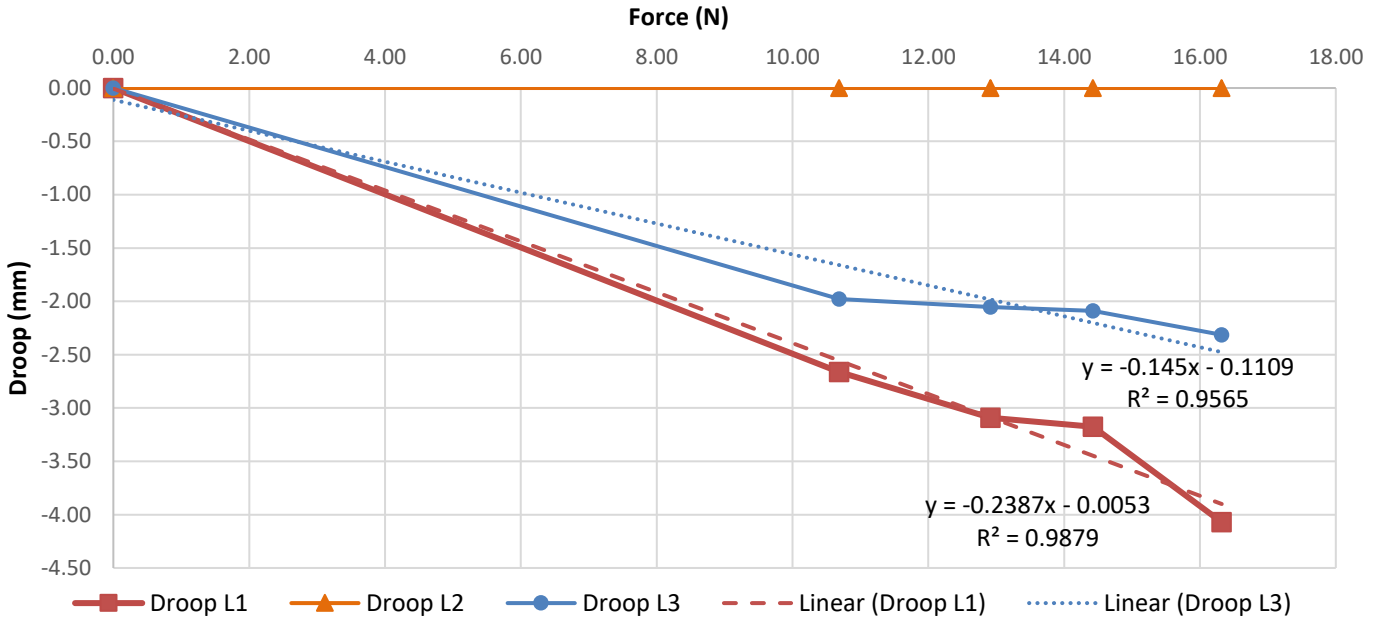

Heart 15

Force (N)	Droop L1 RCC (mm)	Droop L2 NCC (mm)	Droop L3 LCC (mm)
0.00	0.00	0.00	0.00
8.22	-2.99	-5.35	-2.27
13.54	-3.88	-7.74	-4.31
15.46	-5.14	-9.04	-4.47
16.16	-5.49	-10.00	-5.13

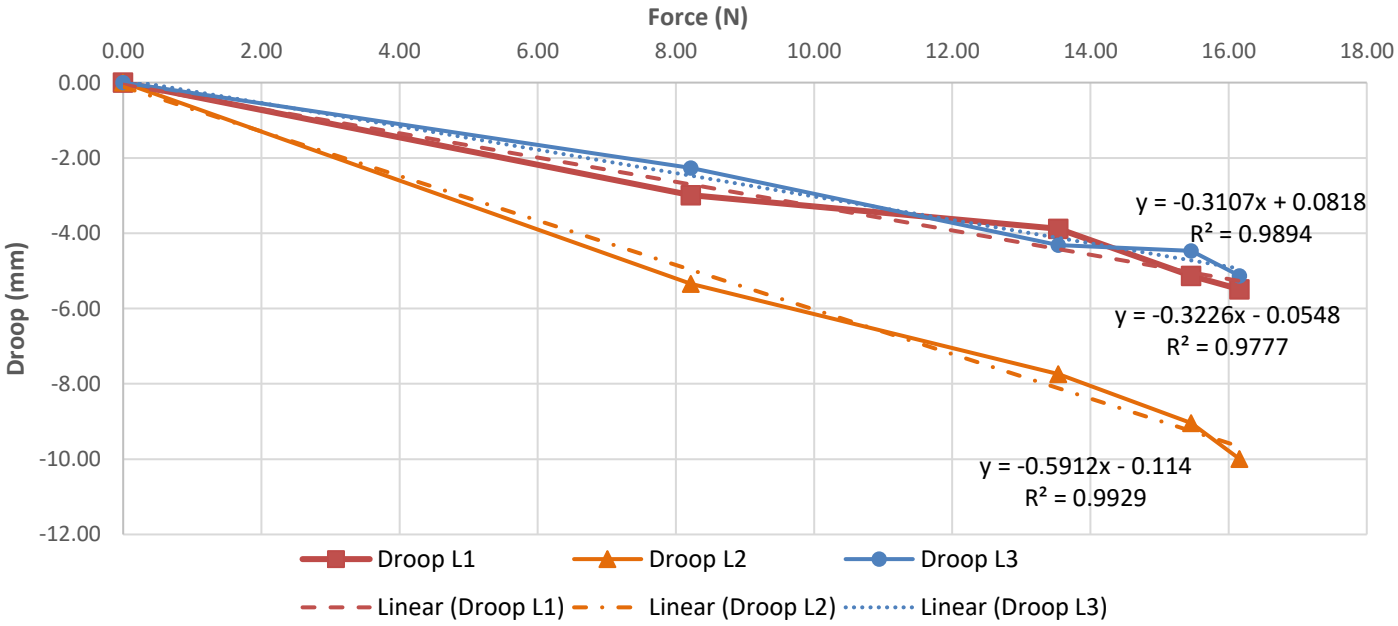

Heart 16

Force (N)	Droop L1 RCC (mm)	Droop L2 NCC (mm)	Droop L3 LCC (mm)
0.00	0.00	0.00	0.00
5.47	-1.35	-1.53	-1.79
12.50	-1.68	-2.64	-3.12
14.67	-2.30	-3.00	-4.19
17.06	-2.52	-3.46	-4.43

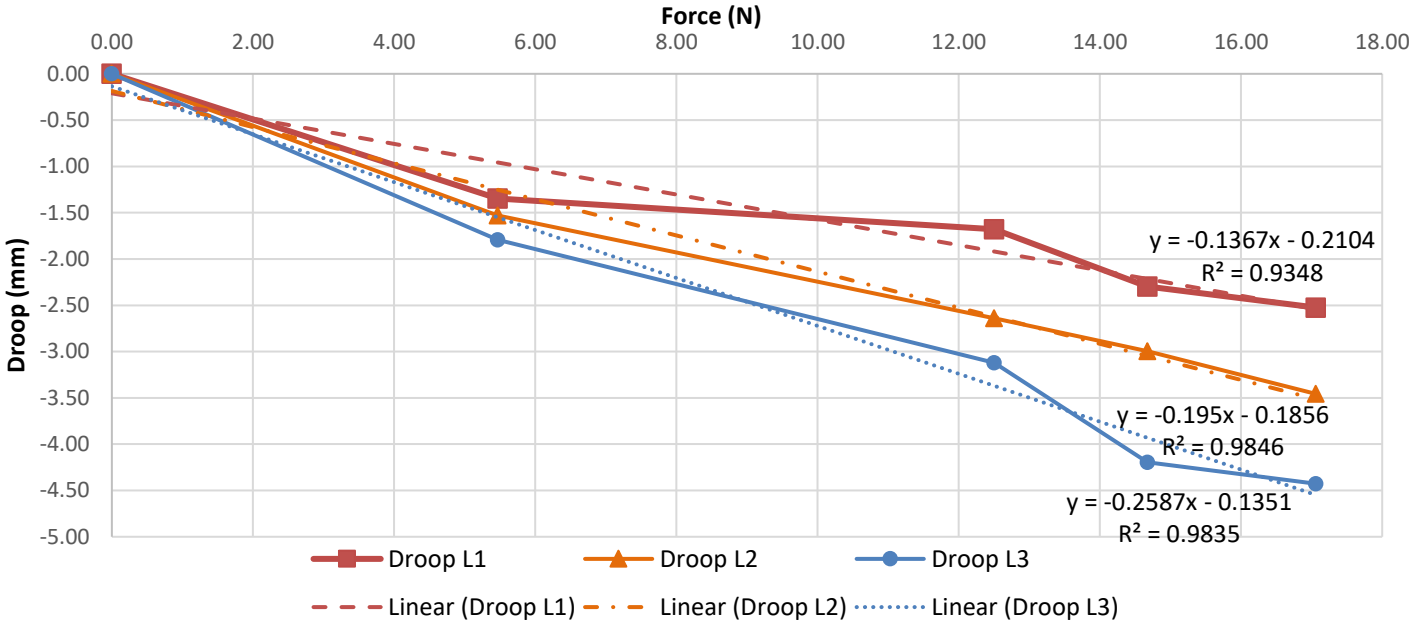

Heart 17

Force (N)	Droop L1 RCC (mm)	Droop L2 NCC (mm)	Droop L3 LCC (mm)
0.00	0.00	0.00	0.00
9.72	-4.21	-1.29	-0.97
13.18	-5.07	-1.57	-2.29
15.69	-5.16	-1.67	-2.49
17.47	-5.69	-2.55	-2.79

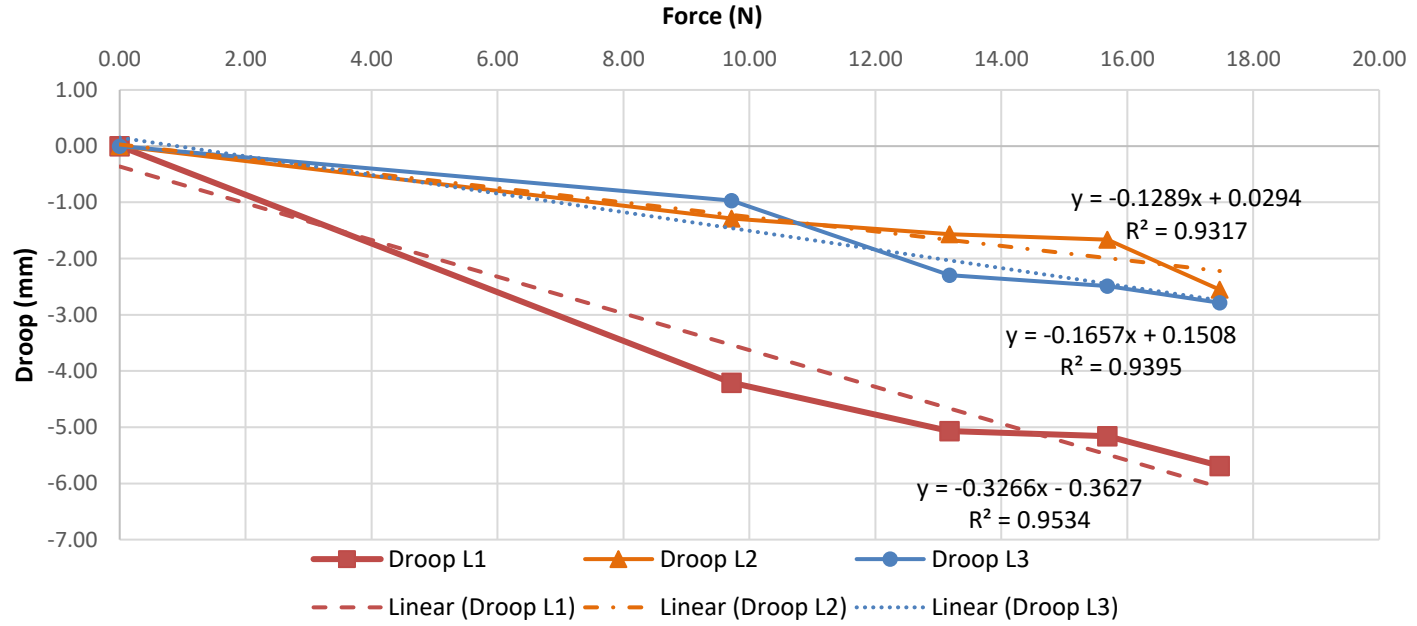

Heart 18

Force (N)	Droop L1 RCC (mm)	Droop L2 NCC (mm)	Droop L3 LCC (mm)
0.00	0.00	0.00	0.00
7.01	-4.52	-0.96	-4.13
9.53	-6.45	-2.49	-5.93
14.58	-7.06	-2.62	-6.07
18.06	-7.19	-2.87	-6.45

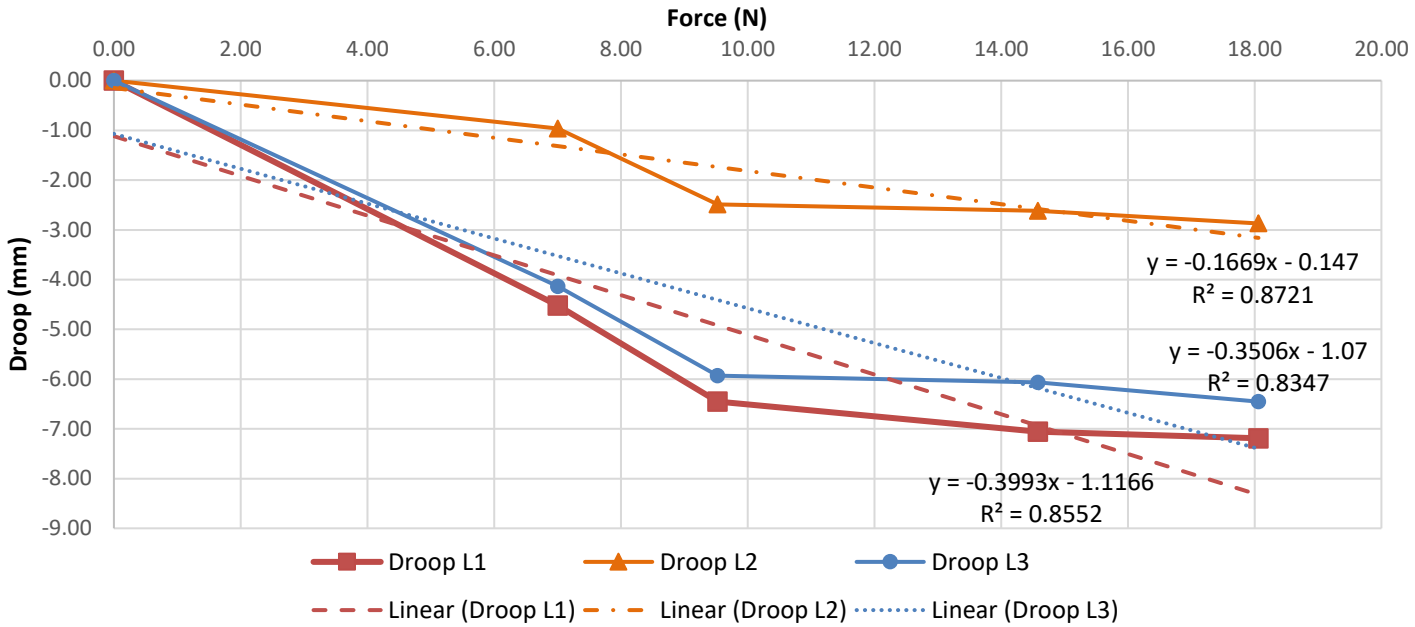

Heart 19

Force (N)	Droop L1 RCC (mm)	Droop L2 NCC (mm)	Droop L3 LCC (mm)
0.00	0.00	0.00	0.00
6.00	-0.81	0.00	-1.92
10.54	-5.64	0.00	-3.04
13.36	-5.96	0.00	-3.61
19.57	-6.26	0.00	-4.23

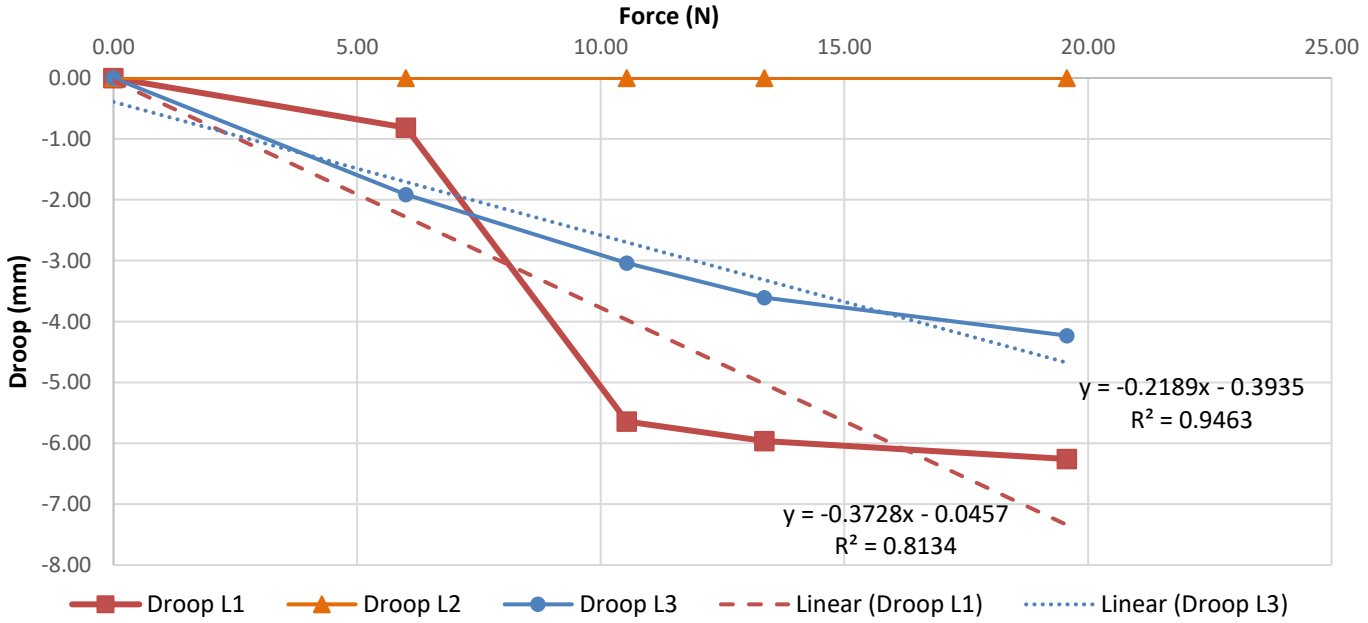

Heart 20

Force (N)	Droop L1 RCC (mm)	Droop L2 NCC (mm)	Droop L3 LCC (mm)
0.00	0.00	NA	0.00
13.34	-2.58	NA	-6.14
17.55	-3.17	NA	-8.12
19.25	-3.62	NA	-9.37
21.72	-3.62	NA	-10.18

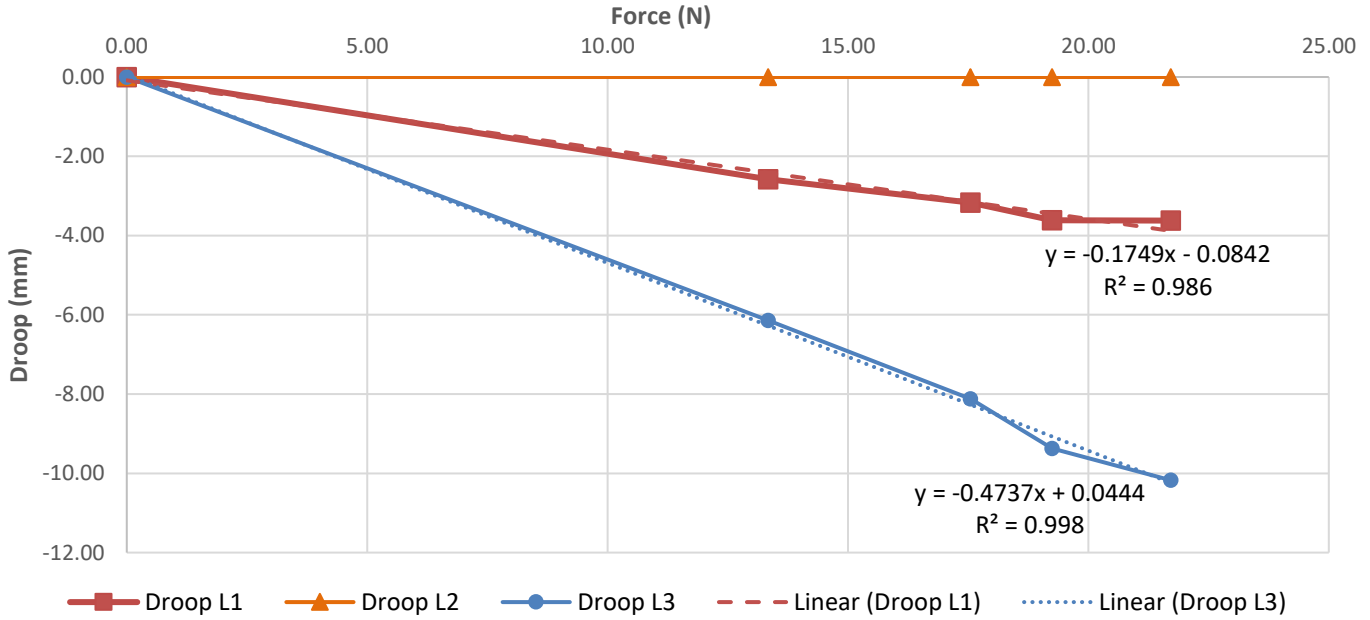

Heart 21

Force (N)	Droop L1 RCC (mm)	Droop L2 NCC (mm)	Droop L3 LCC (mm)
0.00	0.00	0.00	0.00
5.71	-4.08	-6.63	0.00
13.14	-5.94	-7.58	0.00
17.21	-6.77	-8.17	0.00
18.95	-7.03	-9.02	0.00

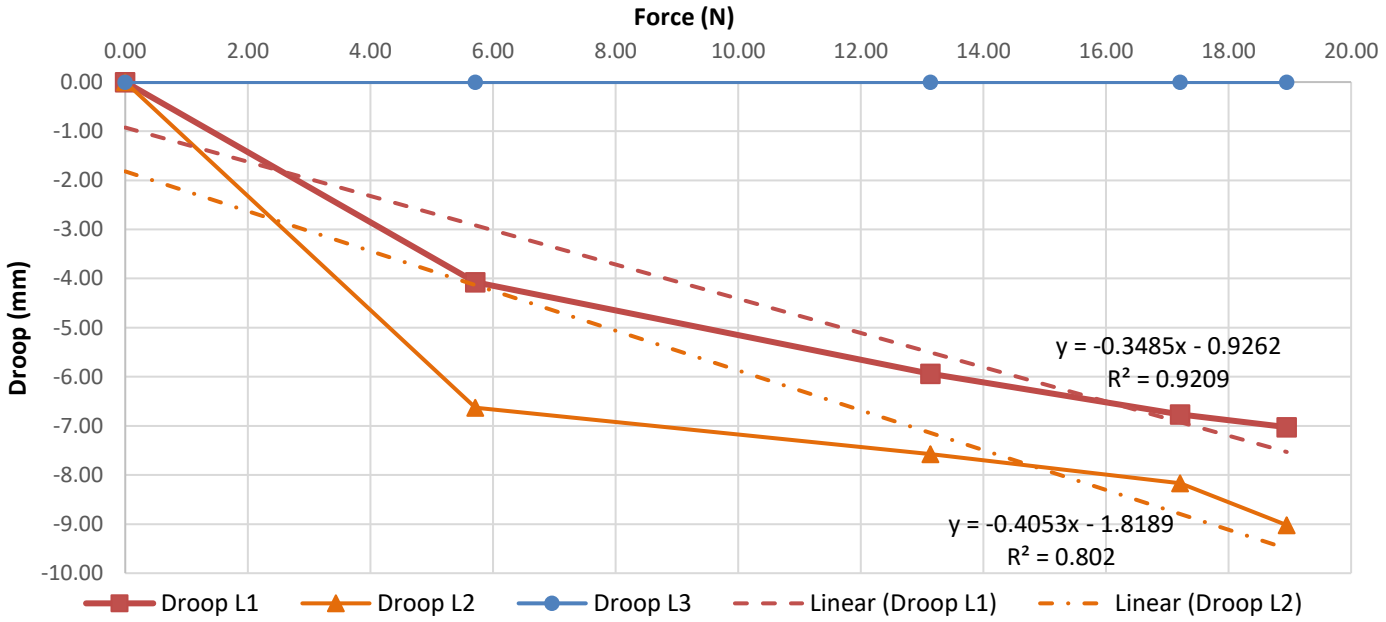

Heart 22

Force (N)	Droop L1 RCC (mm)	Droop L2 NCC (mm)	Droop L3 LCC (mm)
0	0.00	0.00	0.00
6.26	-2.52	-1.42	-1.39
13.70	-5.38	-2.48	-2.09
17.50	-5.76	-2.61	-2.40
21.07	-6.72	-3.19	-2.65

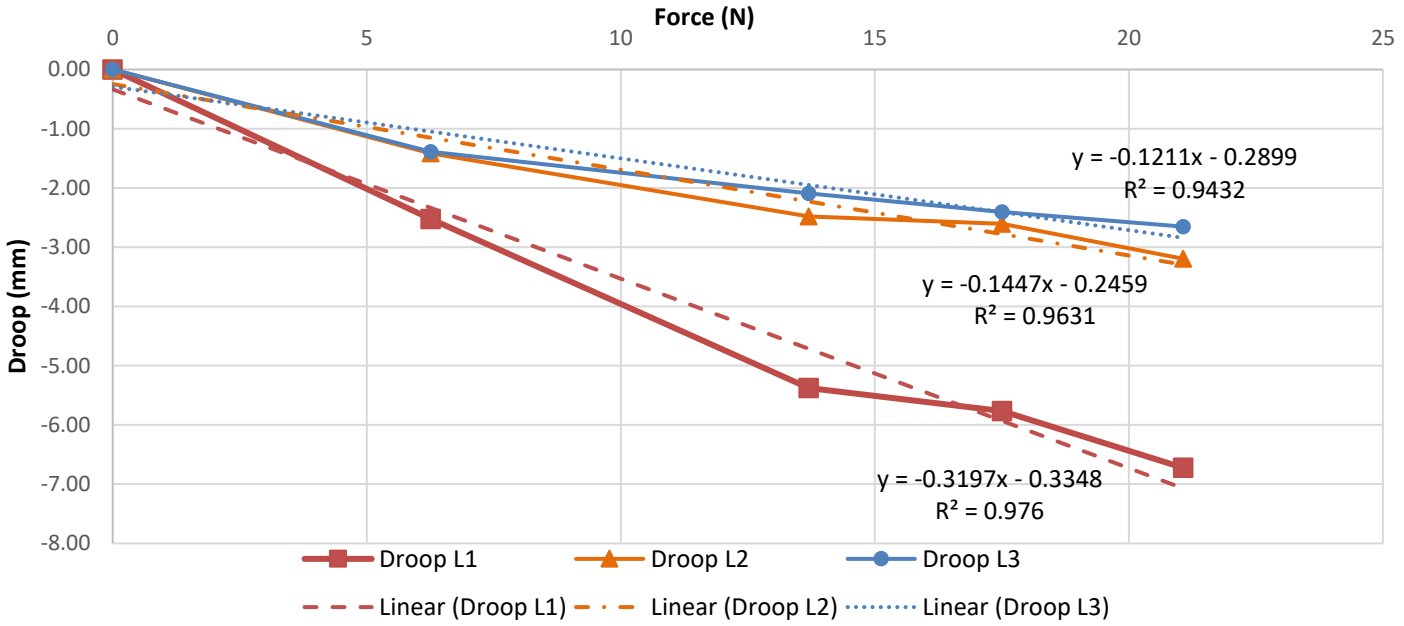

Heart 23

Force (N)	Droop L1 RCC (mm)	Droop L2 NCC (mm)	Droop L3 LCC (mm)
0	0.00	0.00	0.00
15.13	-5.71	-3.88	-2.47
18.24	-5.74	-4.00	-2.54
21.68	-5.74	-4.23	-3.00
23.11	-5.95	-4.73	-3.38

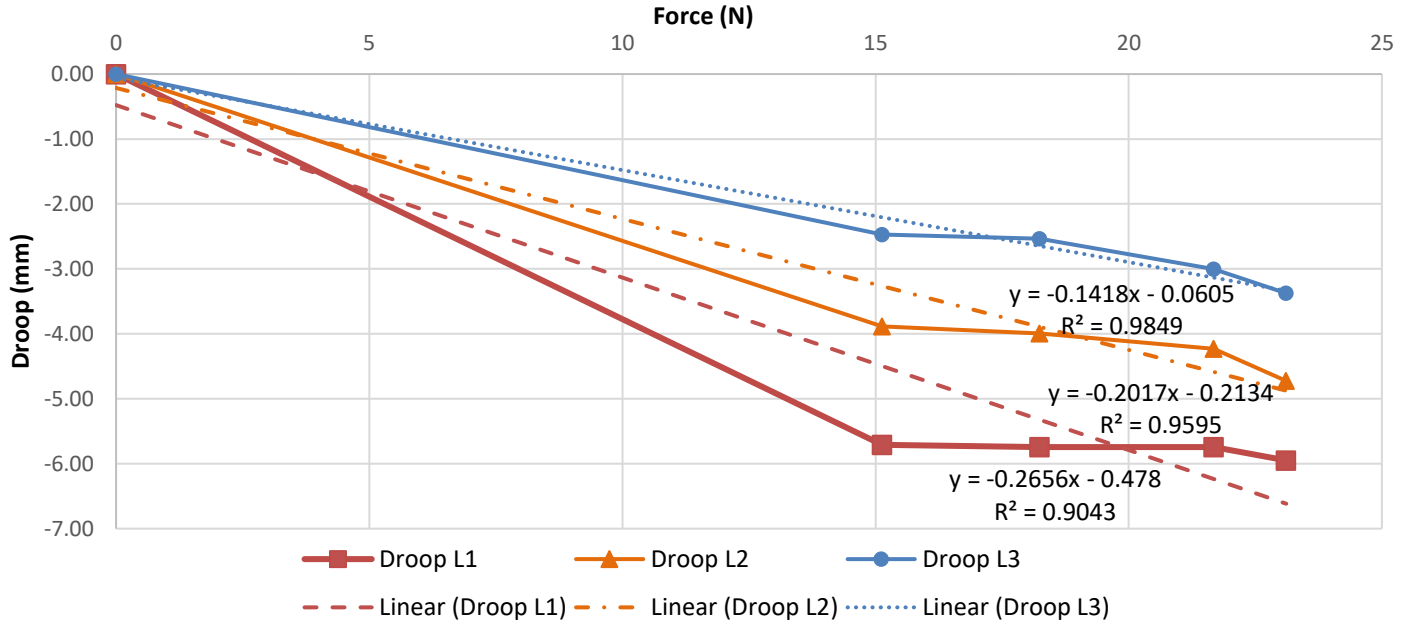

Heart 24

Force (N)	Droop L1 RCC (mm)	Droop L2 NCC (mm)	Droop L3 LCC (mm)
0.00	0.00	0.00	0.00
17.42	-6.32	-2.17	-2.88
20.68	-6.83	-2.77	-2.95
22.60	-7.53	-3.16	-3.07
25.36	-7.96	-3.46	-3.11

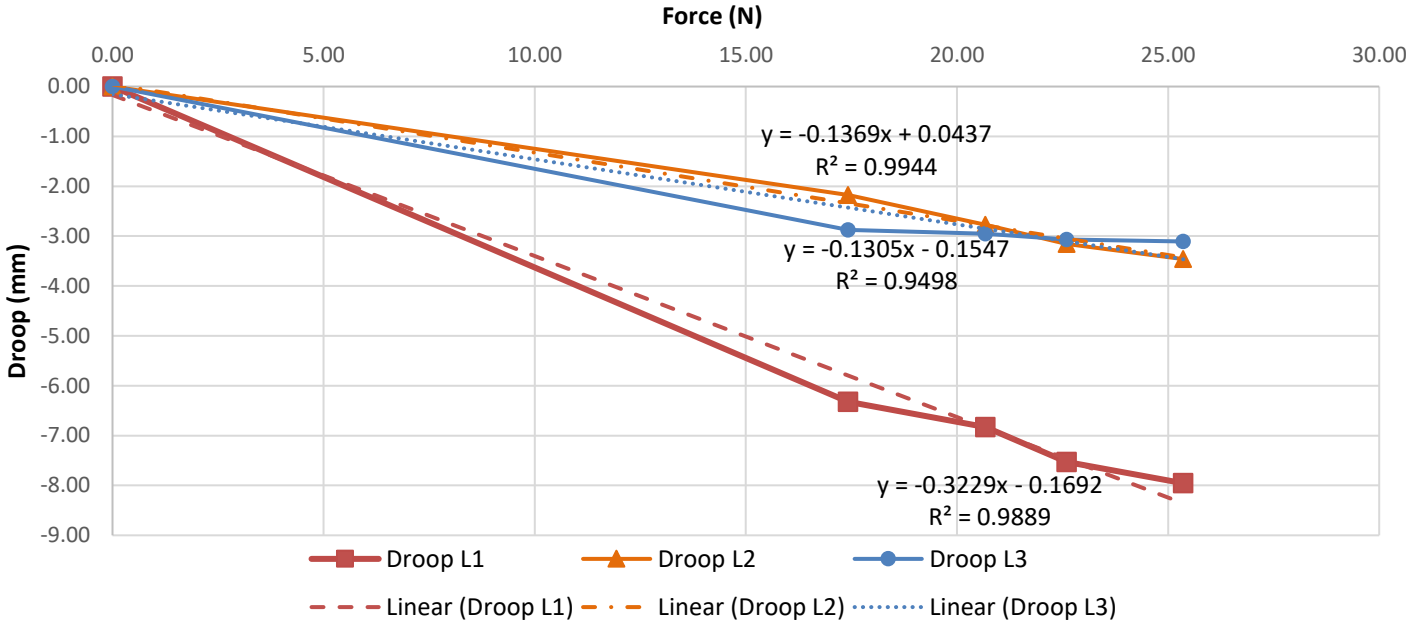

Heart 25

Force (N)	Droop L1 RCC (mm)	Droop L2 NCC (mm)	Droop L3 LCC (mm)
0	0.00	0.00	0.00
10.67	-1.73	-3.28	-2.81
16.72	-1.81	-3.63	-3.19
20.19	-2.12	-3.28	-4.09
20.96	-2.16	-2.69	-4.33

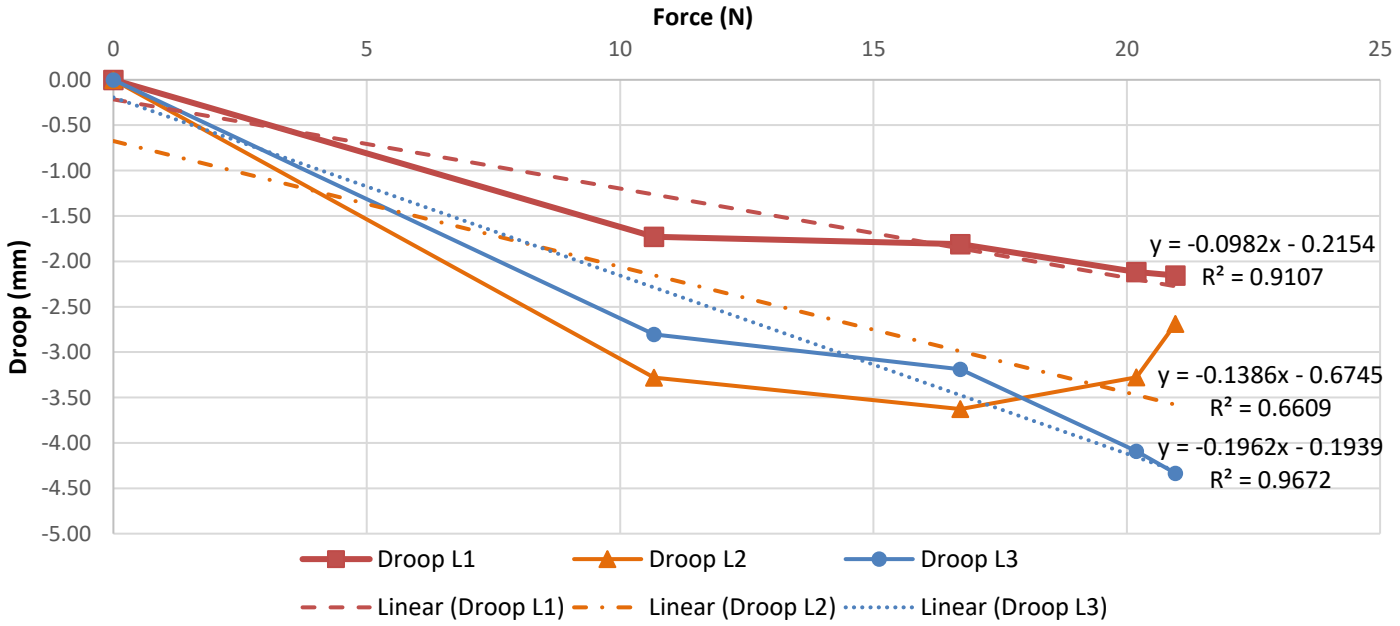

Heart 26

Force (N)	Droop L1 RCC (mm)	Droop L2 NCC (mm)	Droop L3 LCC (mm)
0.00	0.00	0.00	0.00
15.21	-5.31	-1.88	-3.53
15.71	-5.37	-2.31	-3.77
17.38	-5.67	-2.37	-3.98
19.92	-5.81	-2.46	-4.46

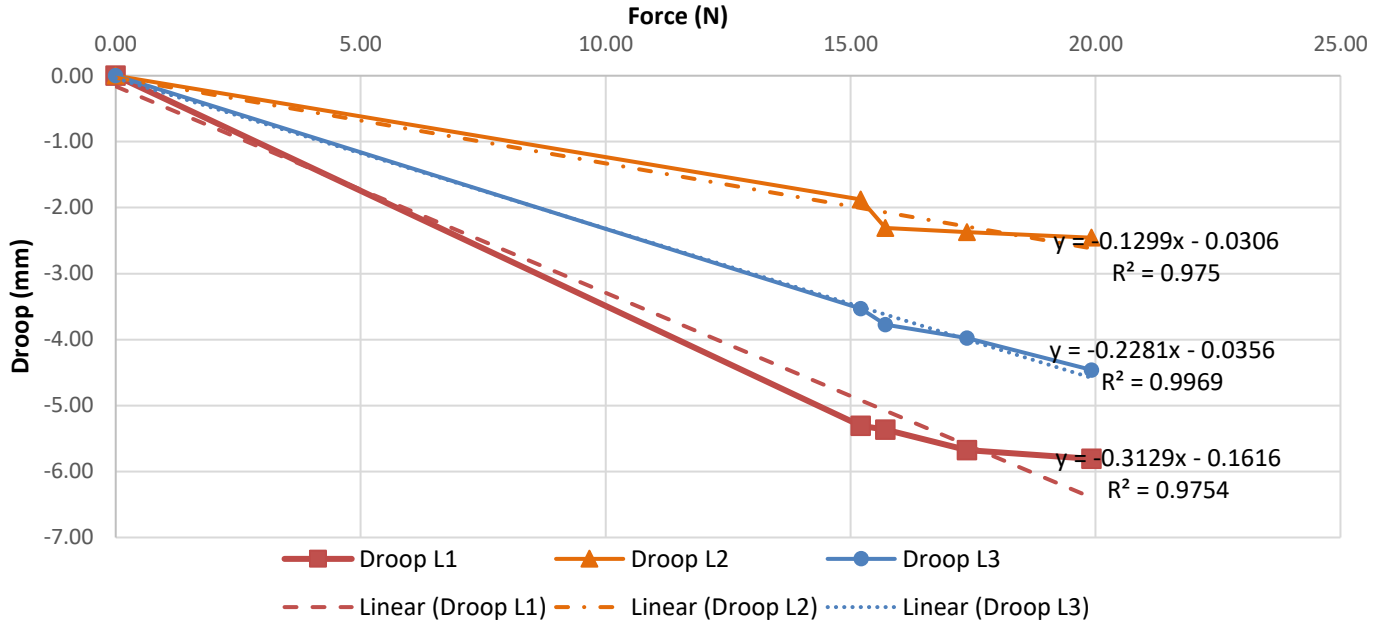

Heart 27

Force (N)	Droop L1 RCC (mm)	Droop L2 NCC (mm)	Droop L3 LCC (mm)
0.00	0.00	0.00	0.00
12.30	-3.43	-3.40	-2.04
14.81	-3.60	-3.71	-2.33
15.59	-3.98	-4.43	-2.37
23.90	-4.32	-4.95	-2.55

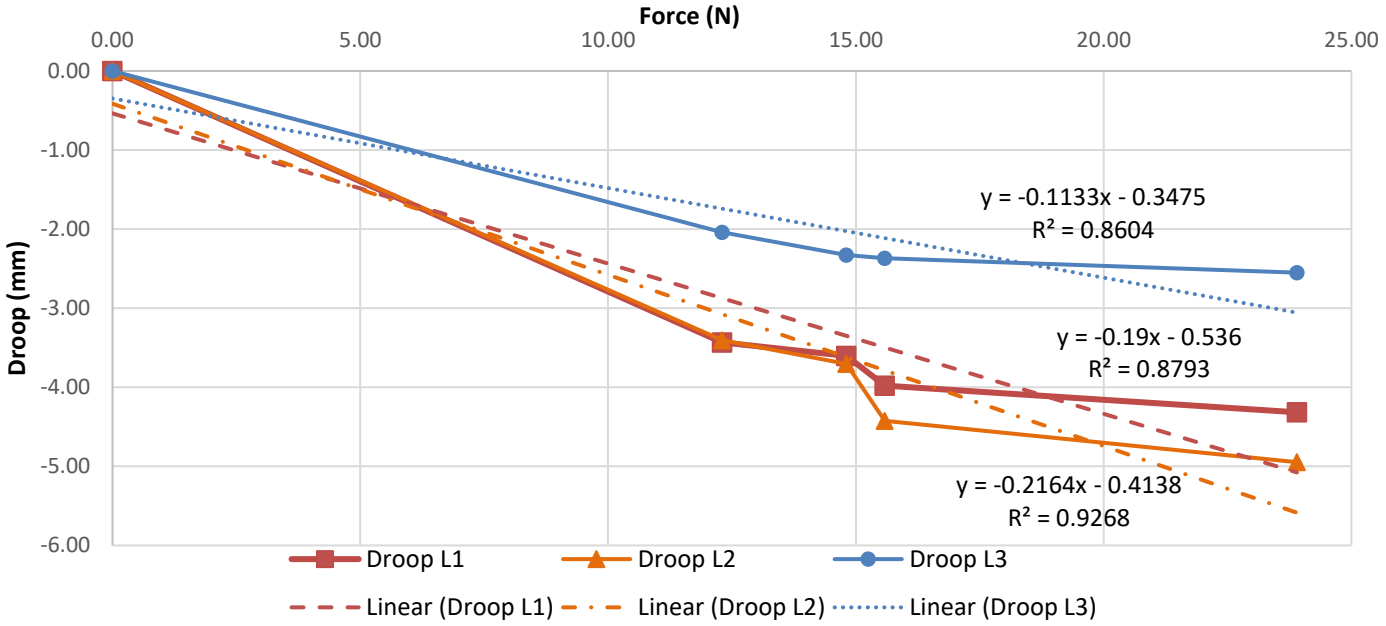

Heart 28

Force (N)	Droop L1 RCC (mm)	Droop L2 NCC (mm)	Droop L3 LCC (mm)
0.00	0.00	0.00	0.00
3.36	-3.25	-1.67	-3.24
12.15	-5.25	-1.91	-3.91
13.46	-6.01	-2.51	-4.76
20.30	-6.56	-2.70	-5.00

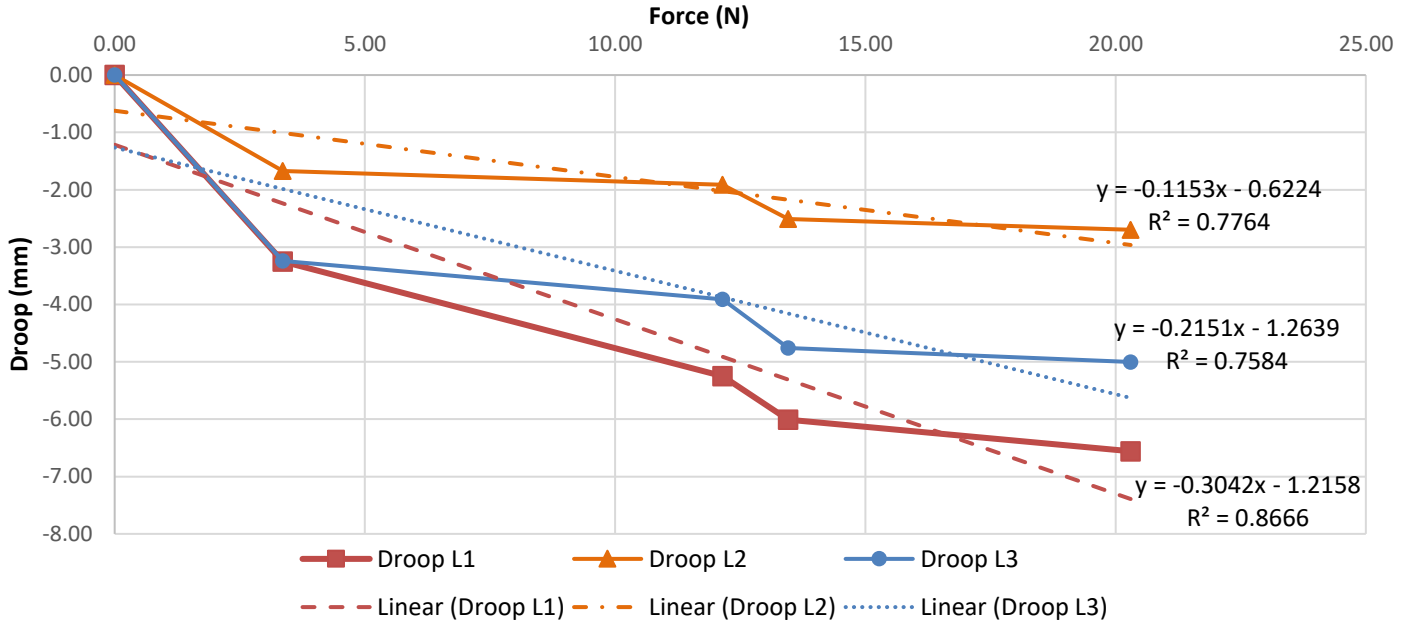

Heart 29

Force (N)	Droop L1 RCC (mm)	Droop L2 NCC (mm)	Droop L3 LCC (mm)
0.00	0.00	0.00	0.00
2.04	-4.83	0.00	-3.37
11.82	-5.13	0.00	-3.65
19.28	-6.27	0.00	-4.33
21.28	-6.93	0.00	-4.88

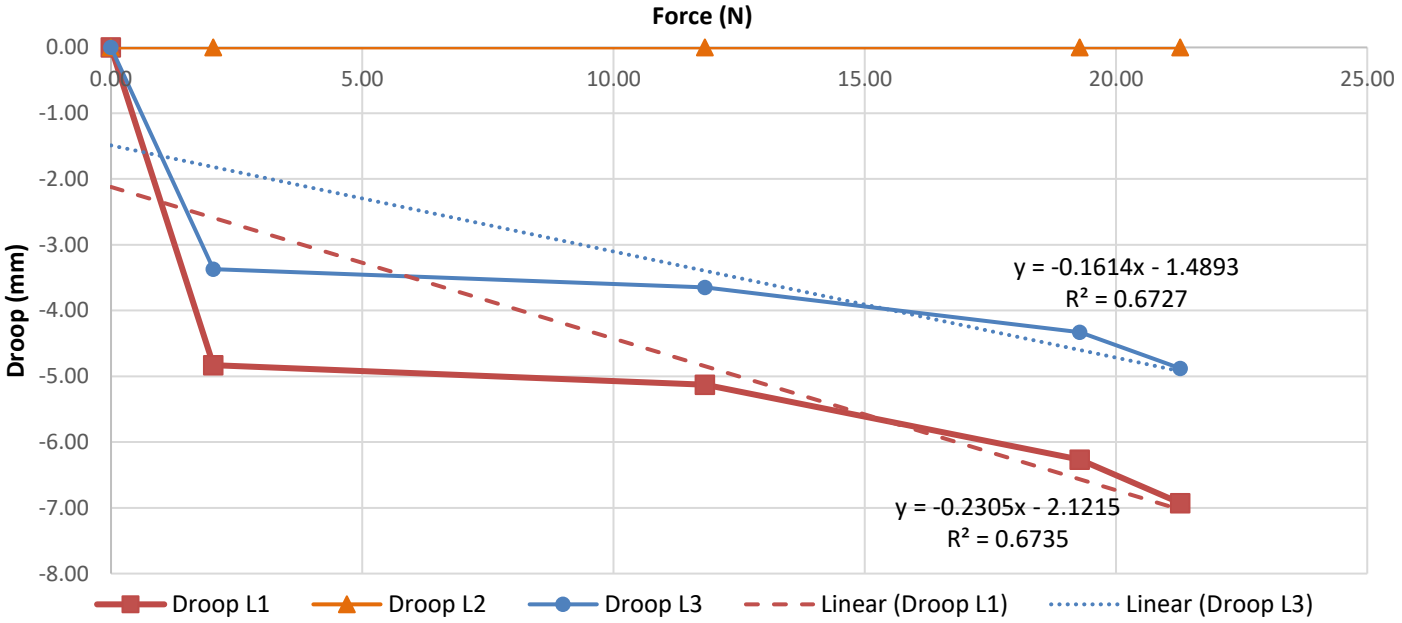

Heart 30

Force (N)	Droop L1 RCC (mm)	Droop L2 NCC (mm)	Droop L3 LCC (mm)
0.00	0.00	0.00	0.00
5.81	-5.53	-1.54	-2.88
13.75	-7.01	-2.92	-3.55
15.29	-7.41	-3.05	-5.27
19.20	-7.74	-3.25	-5.86

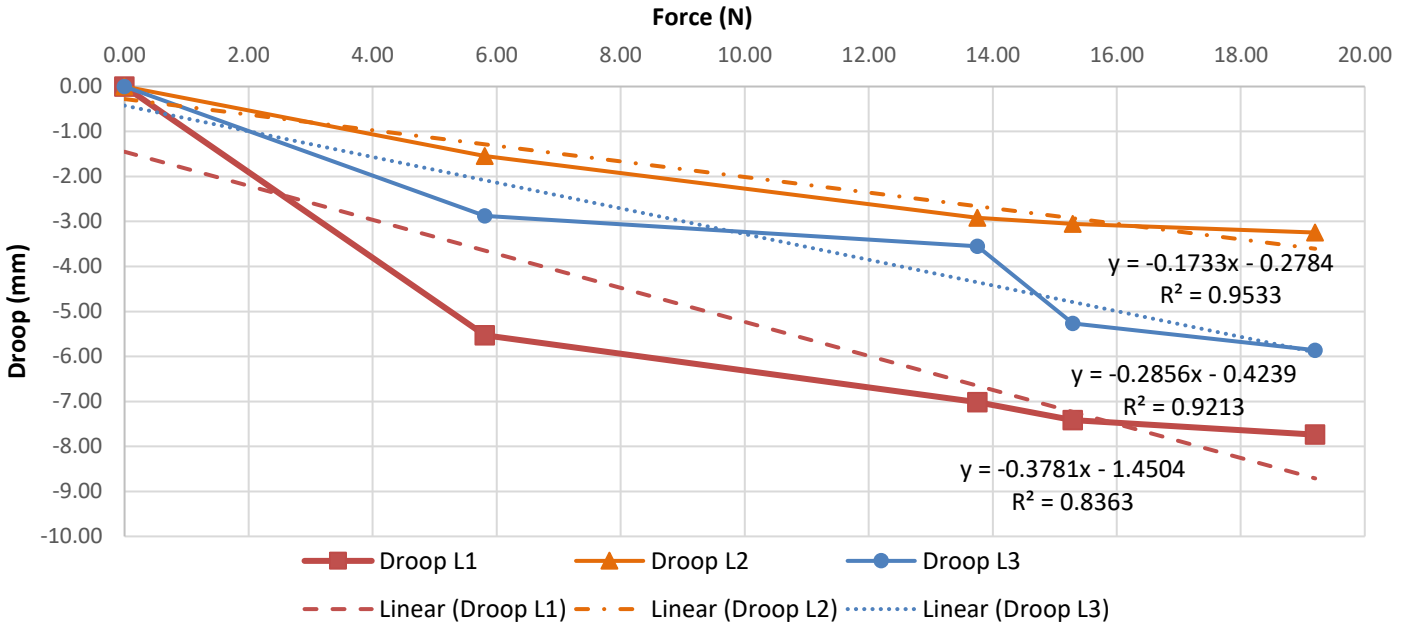

Heart 31

Force (N)	Droop L1 RCC (mm)	Droop L2 NCC (mm)	Droop L3 LCC (mm)
0.00	0.00	0.00	0.00
14.06	-0.79	-0.14	-3.60
17.55	-1.03	-0.61	-4.19
20.74	-1.05	-0.74	-4.42
23.49	-1.17	-1.01	-4.75

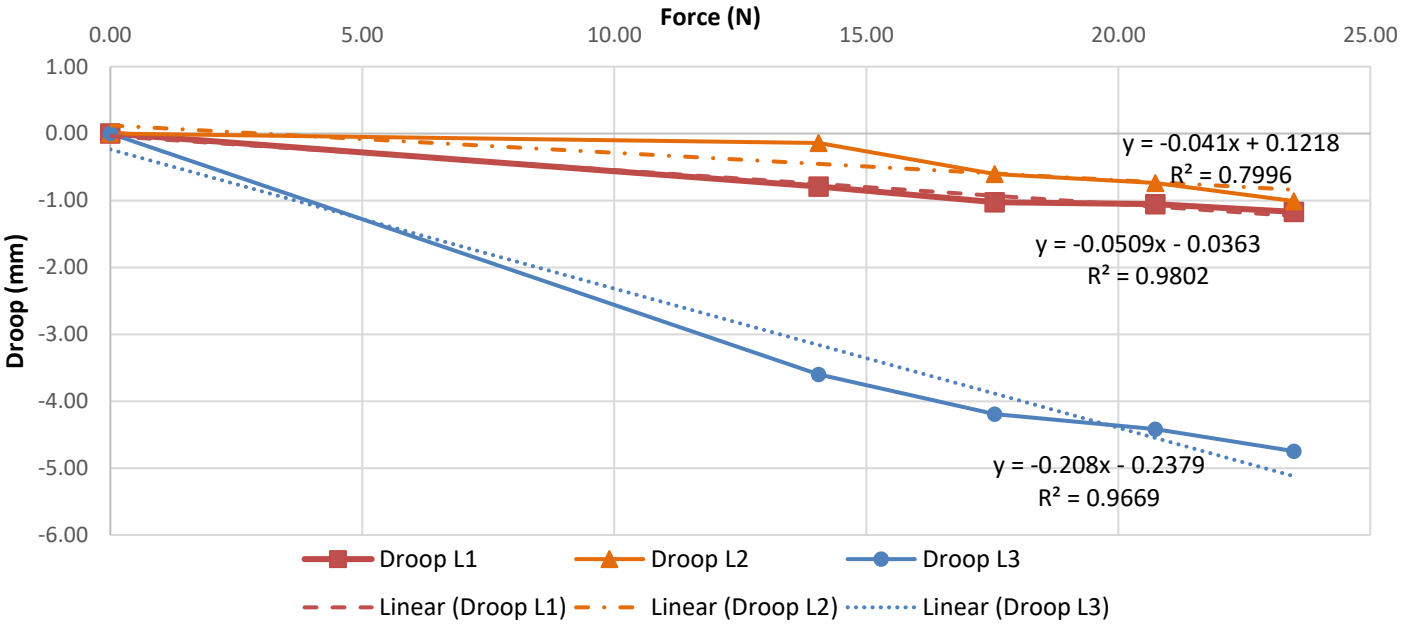

Heart 32

Force (N)	Droop L1 RCC (mm)	Droop L2 NCC (mm)	Droop L3 LCC (mm)
0.00	0.00	0.00	0.00
7.56	-4.63	-1.50	-3.40
12.35	-5.34	-2.26	-4.34
21.78	-6.70	-2.73	-4.84
26.91	-7.15	-3.28	-4.25

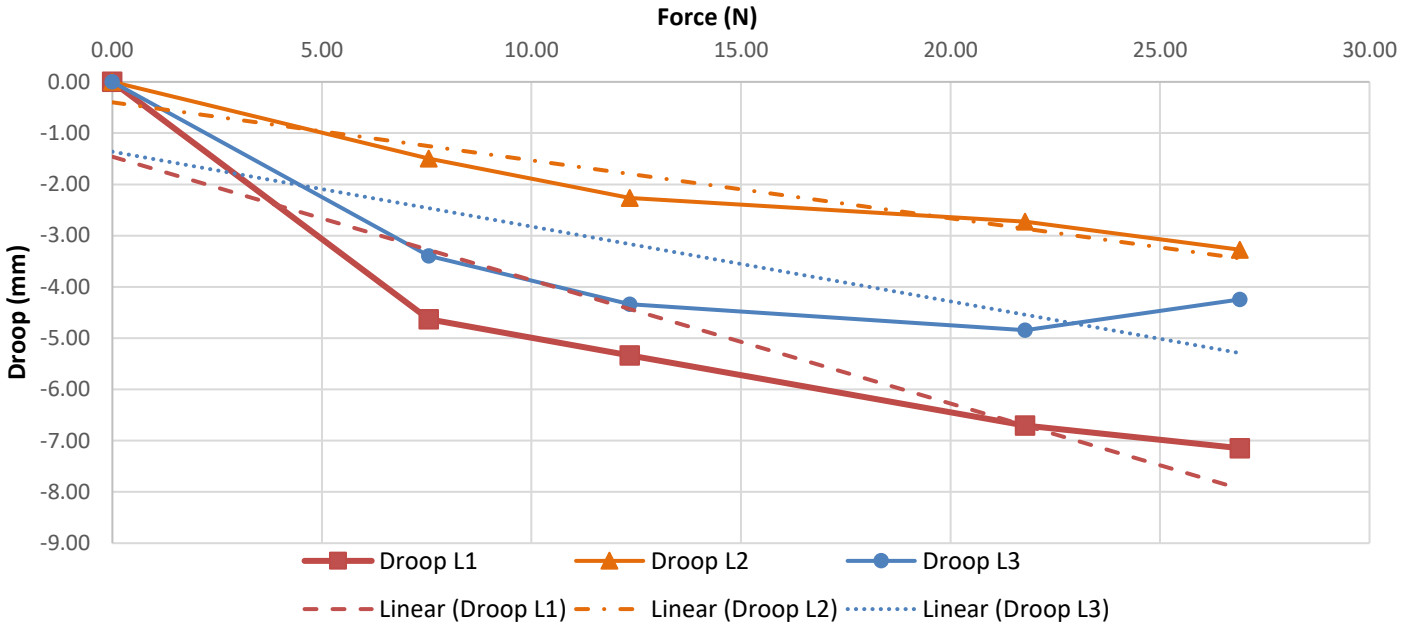

Heart 33

Force (N)	Droop L1 RCC (mm)	Droop L2 NCC (mm)	Droop L3 LCC (mm)
0.00	0.00	0.00	0.00
7.77	0.00	-6.91	-6.07
11.63	0.00	-7.45	-6.48
20.13	0.00	-8.40	-7.12
25.20	0.00	-8.60	-7.33

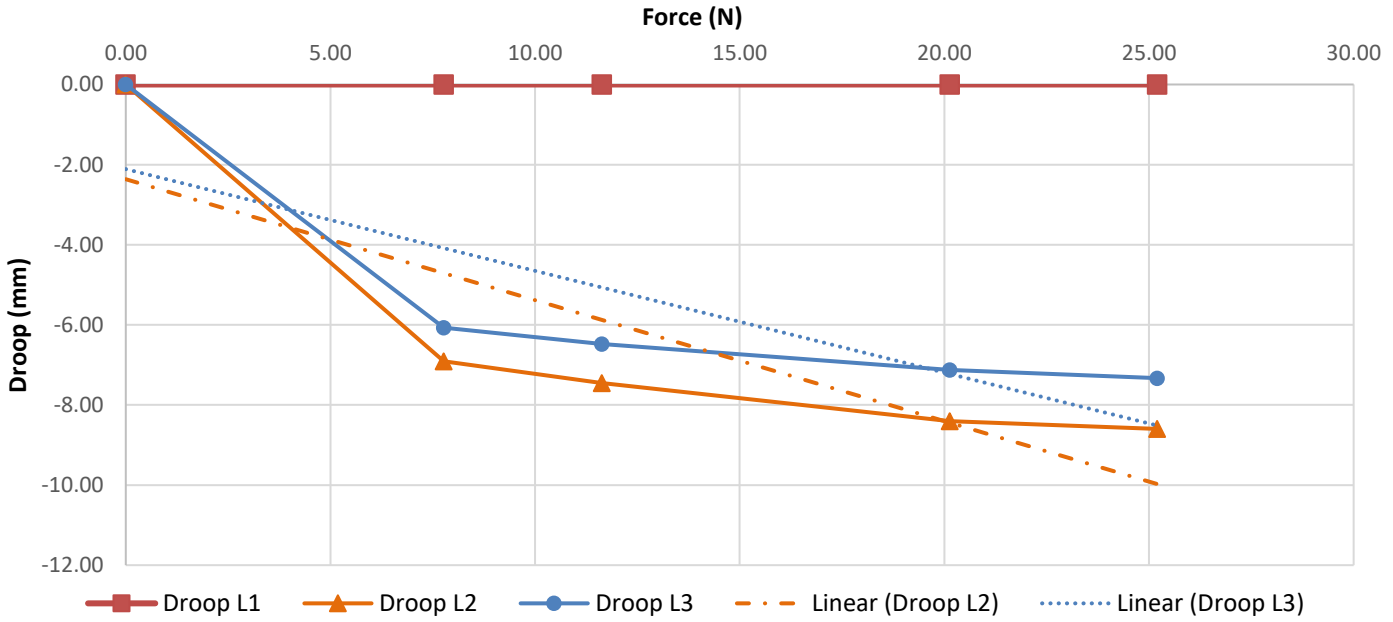

Heart 34

Force (N)	Droop L1 RCC (mm)	Droop L2 NCC (mm)	Droop L3 LCC (mm)
0.00	0.00	0.00	0.00
3.30	-1.72	-1.73	-0.84
6.62	-4.33	-2.93	-2.09
10.68	-4.82	-3.43	-3.12
17.23	-6.81		-4.93

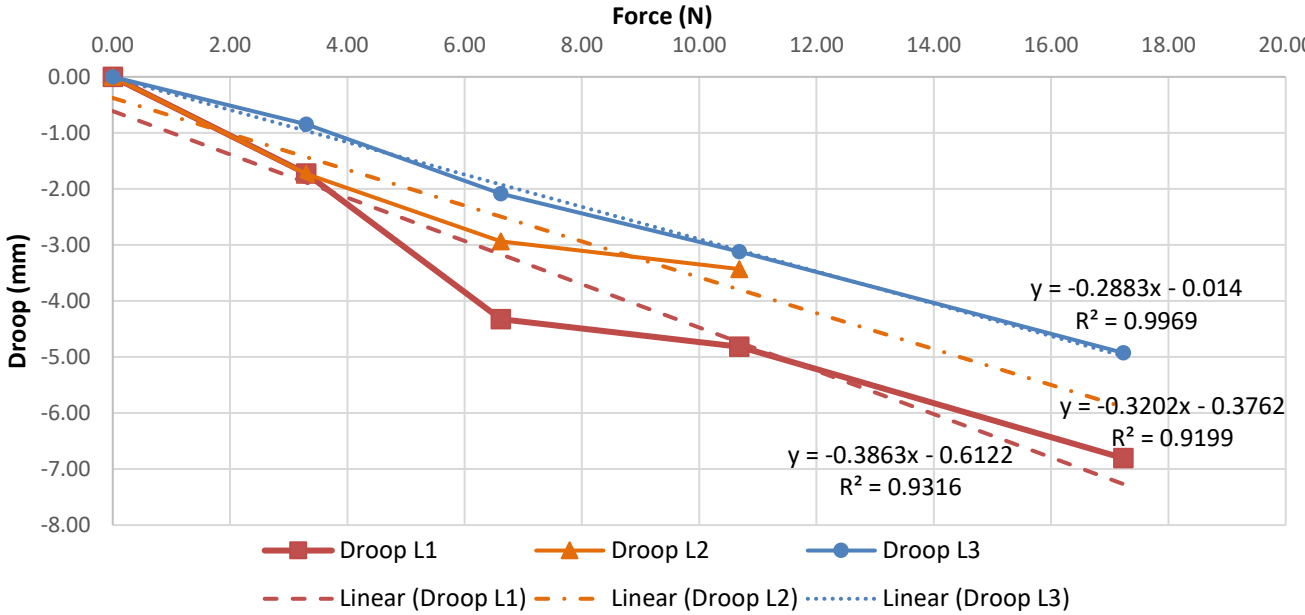

Heart 35

Force (N)	Droop L1 RCC (mm)	Droop L2 NCC (mm)	Droop L3 LCC (mm)
0.00	0.00	0.00	0.00
11.99	-5.37	-0.32	-4.03
11.63	-7.68	-0.56	-5.47
16.88	-9.71	-0.95	-6.28
21.27	-10.14	-0.90	-6.84

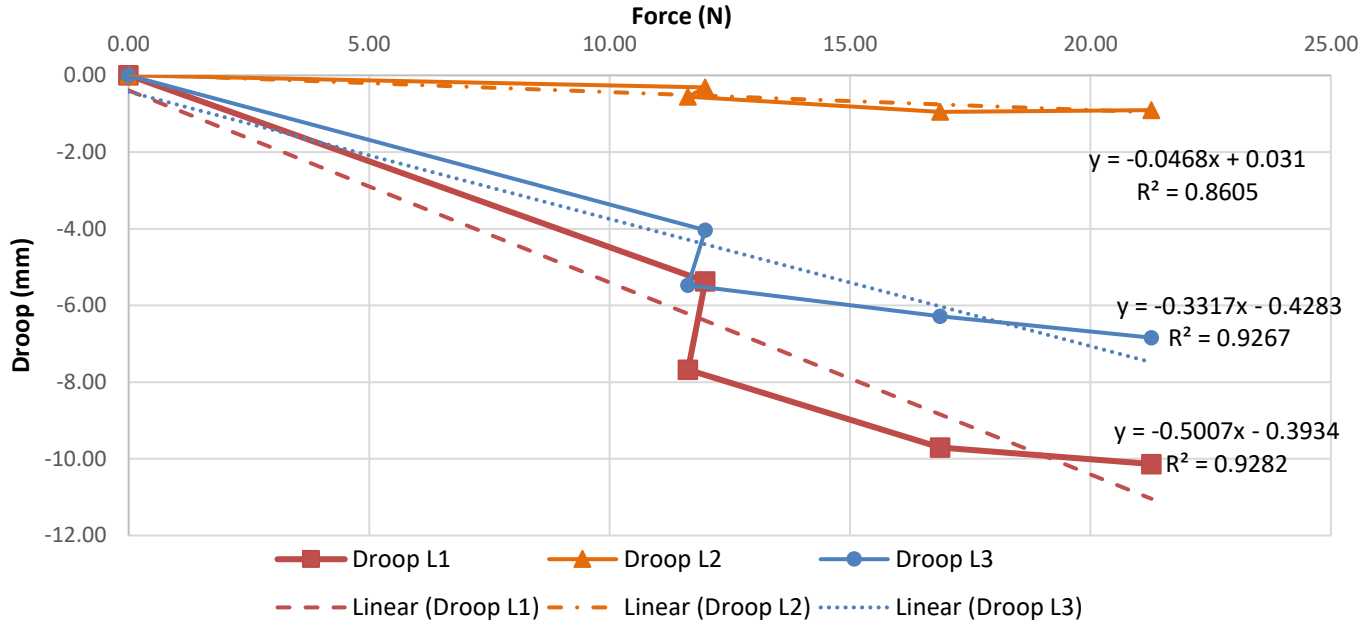

Heart 36

Force (N)	Droop L1 RCC (mm)	Droop L2 NCC (mm)	Droop L3 LCC (mm)
0.00	0.00	0.00	0.00
14.49	-3.06	-1.39	-3.42
18.37	-3.81	-1.79	-4.02
21.67	-4.09	-1.19	-5.78
27.69	-4.74	-1.31	-5.87

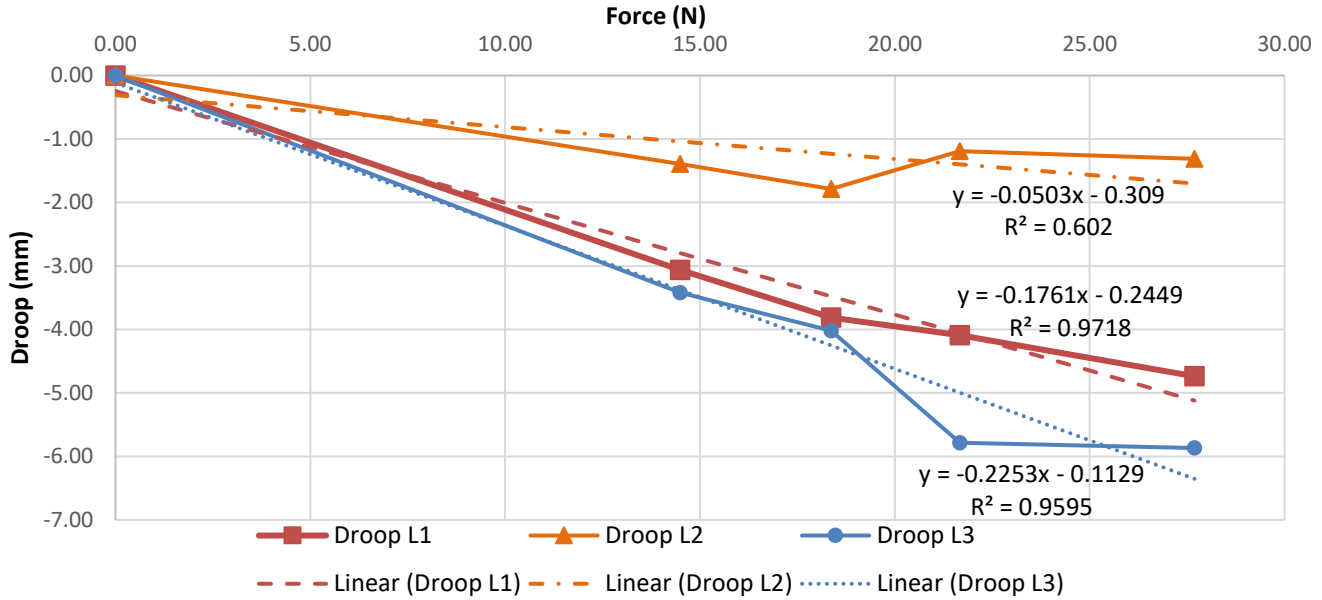

Heart 37

Force (N)	Droop L1 RCC (mm)	Droop L2 NCC (mm)	Droop L3 LCC (mm)
0.00	0.00	0.00	0.00
5.32	-4.35	0.00	-3.72
13.23	-7.01	0.00	-4.61
17.38	-8.15	0.00	-4.89
24.56	-9.14	0.00	-5.55

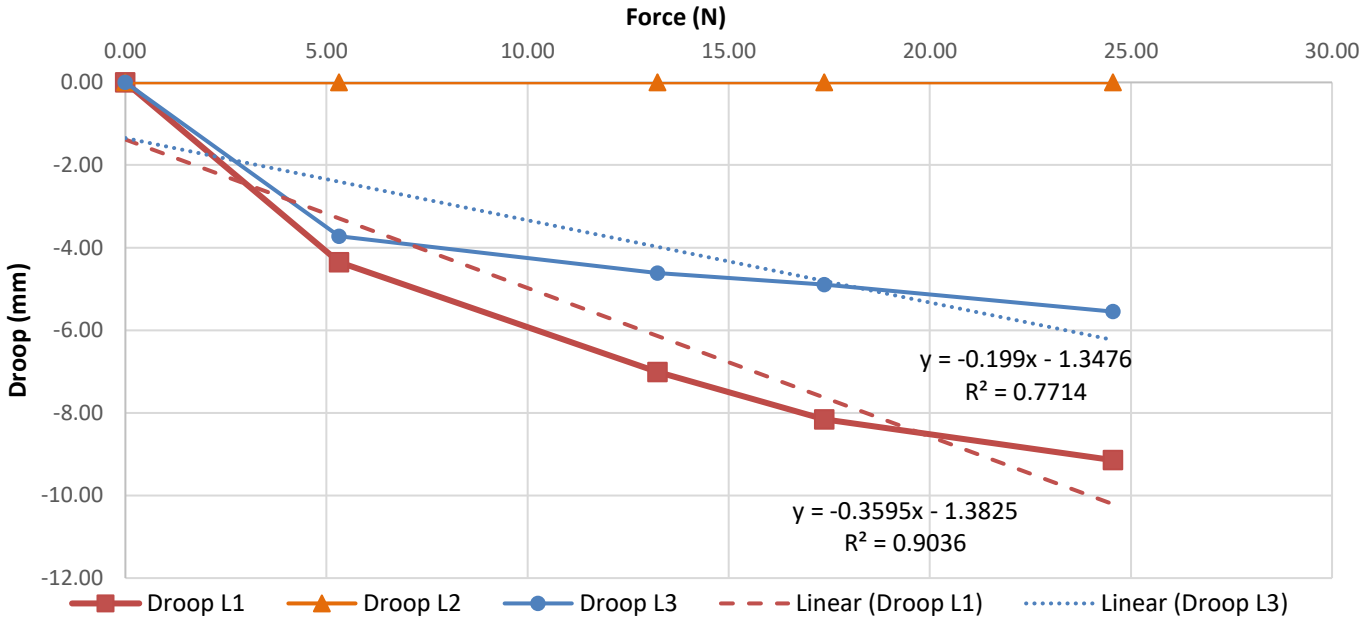

Heart 38

Force (N)	Droop L1 RCC (mm)	Droop L2 NCC (mm)	Droop L3 LCC (mm)
0.00	0.00	0.00	0.00
8.15	-1.70	-2.01	-1.89
15.87	-2.79	-3.44	-2.24
19.51	-3.23	-3.87	-2.66
24.51	-3.05	-4.27	-2.97

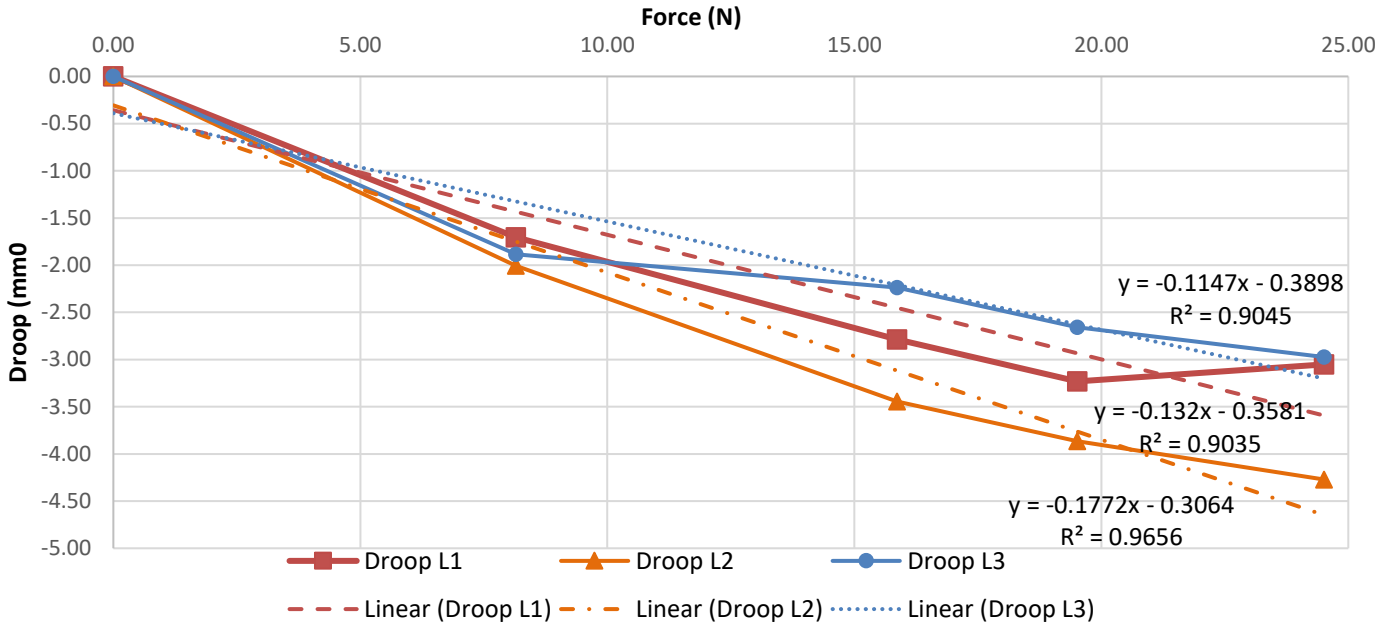

Heart 39

Force (N)	Droop L1 RCC (mm)	Droop L2 NCC (mm)	Droop L3 LCC (mm)
0.00	0.00	0.00	0.00
5.97	-2.48	0.00	-0.88
12.24	-3.99	0.00	-1.42
17.52	-4.86	0.00	-2.32
22.14	-5.28	0.00	-2.26

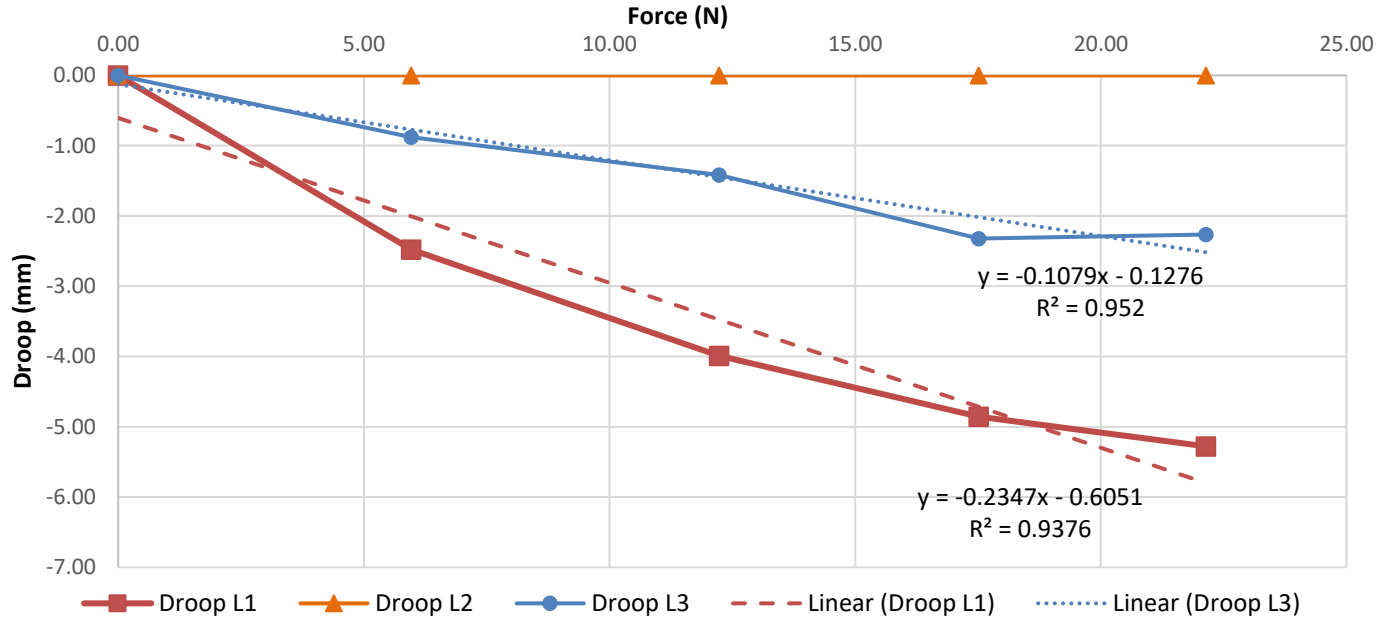

Heart 40

Force (N)	Droop L1 RCC (mm)	Droop L2 NCC (mm)	Droop L3 LCC (mm)
0.00	0.00	0.00	0.00
5.50	-0.63	-0.30	-0.29
15.20	-4.68	-3.70	-2.23
16.45	-6.70	-4.29	-3.12
23.79	-8.65	-6.22	-3.96

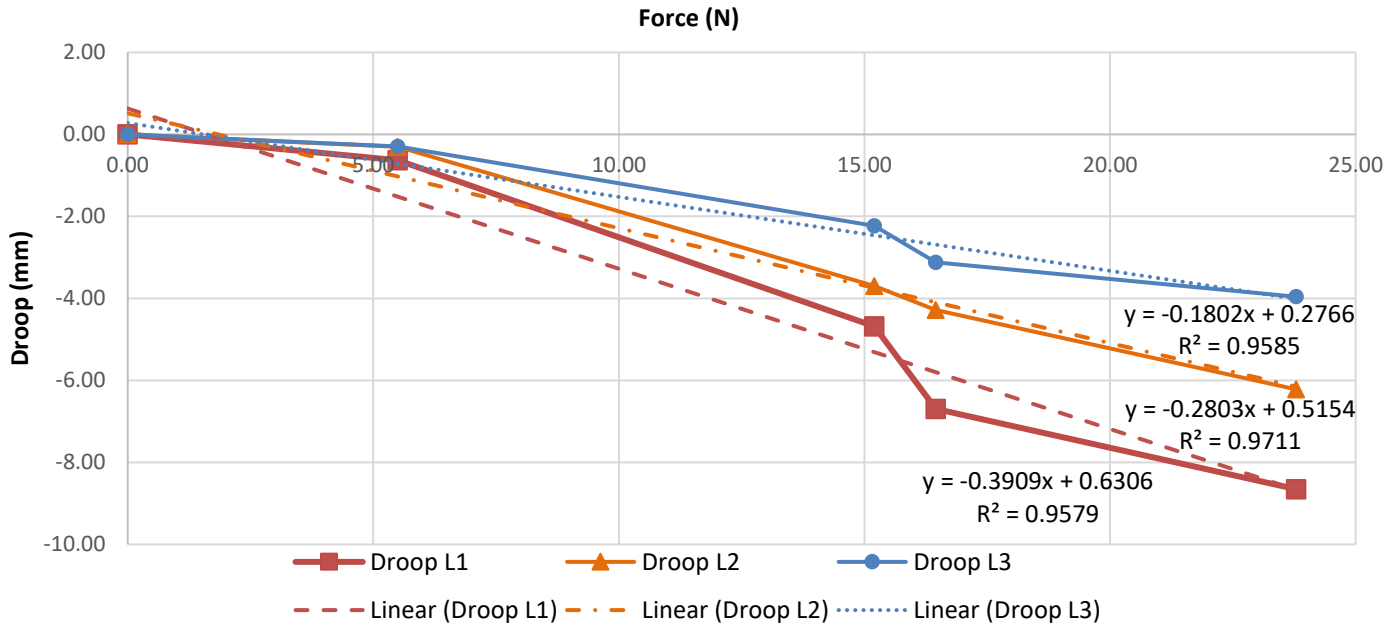

Heart 41

Force (N)	Droop L1 RCC (mm)	Droop L2 NCC (mm)	Droop L3 LCC (mm)
0.00	0.00	0.00	0.00
10.58	-5.15	-4.85	-2.51
16.54	-6.01	-5.50	-2.93
20.03	-6.43	-5.59	-2.99
23.18	-6.65	-5.83	-3.29

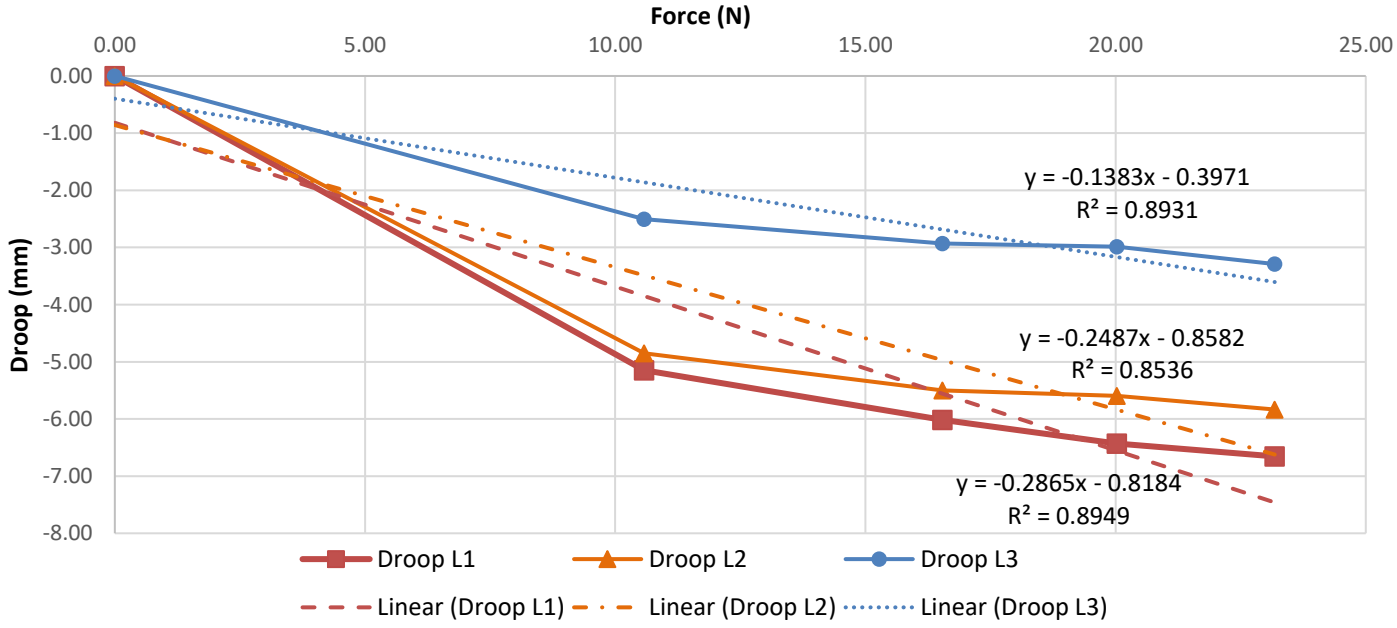

Heart 42

Force (N)	Droop L1 RCC (mm)	Droop L2 NCC (mm)	Droop L3 LCC (mm)
0.00	0.00	0.00	0.00
12.11	-3.92	0.00	-2.23
21.10	-4.80	0.00	-2.64
22.69	-5.79	0.00	-3.28

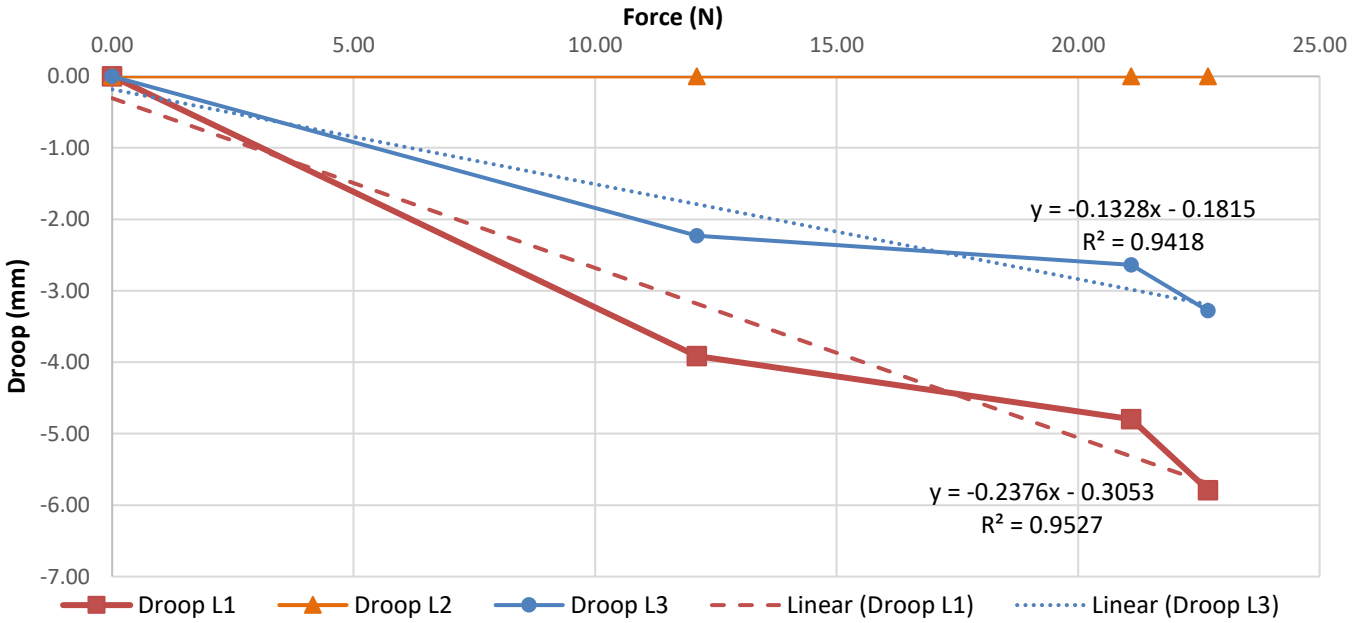

Heart 43

Force (N)	Droop L1 RCC (mm)	Droop L2 NCC (mm)	Droop L3 LCC (mm)
0.00	0.00	0.00	0.00
7.06	-4.51	-0.26	-0.86
17.59	-5.18	-1.17	-1.95
22.67	-5.83	-1.50	-2.86
24.34	-5.94	-1.79	-3.93

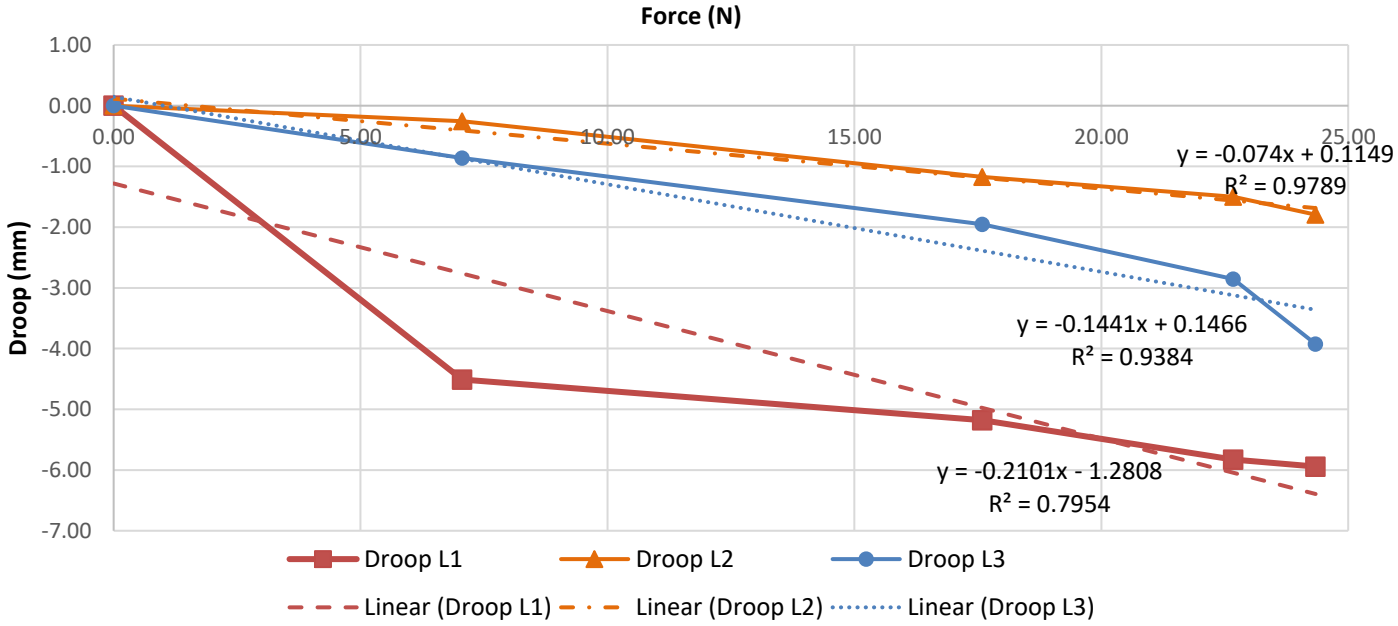

Heart 44

Force (N)	Droop L1 RCC (mm)	Droop L2 NCC (mm)	Droop L3 LCC (mm)
0.00	0.00	0.00	0.00
9.85	-4.12	-3.91	0.00
15.08	-4.28	-4.61	0.00
15.03	-4.46	-5.36	0.00
24.02	-4.90	-5.87	0.00

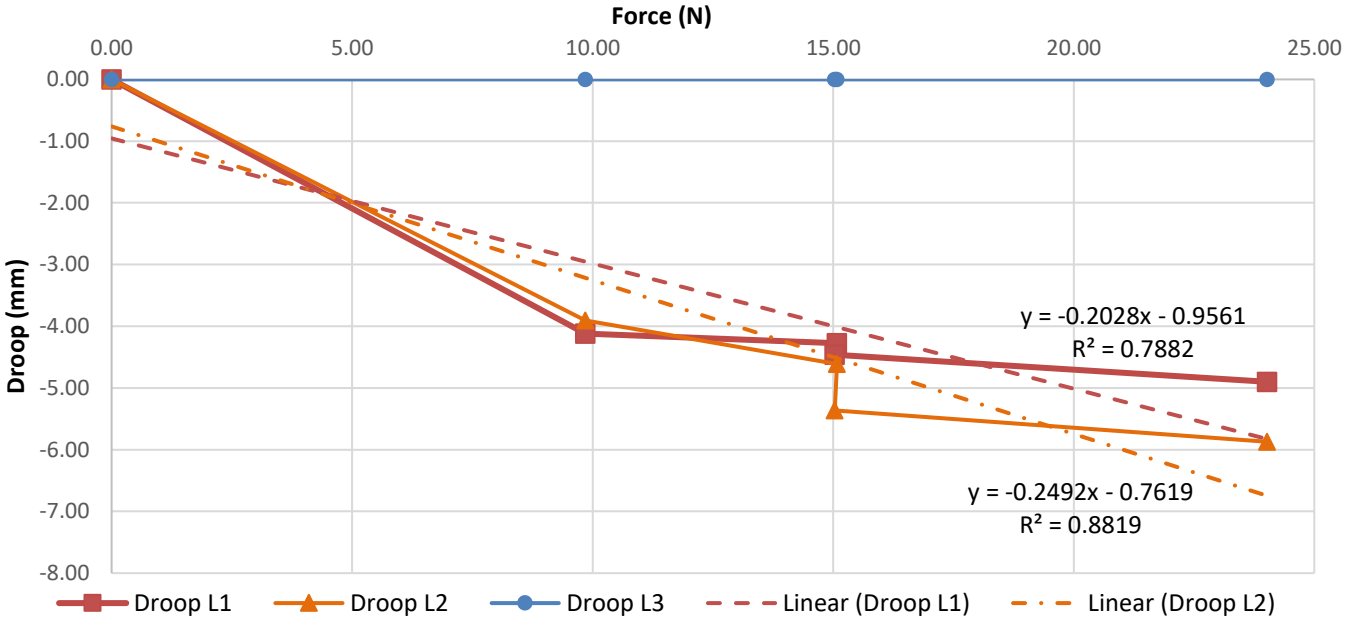

Heart 45

Force (N)	Droop L1 RCC (mm)	Droop L2 NCC (mm)	Droop L3 LCC (mm)
0.00	0.00	0.00	0.00
15.00	-2.20	-18.52	-3.83
19.48	-2.92	-17.33	-4.81
26.08	-3.05	-18.71	-5.58
32.42	-3.26	-18.72	-5.62

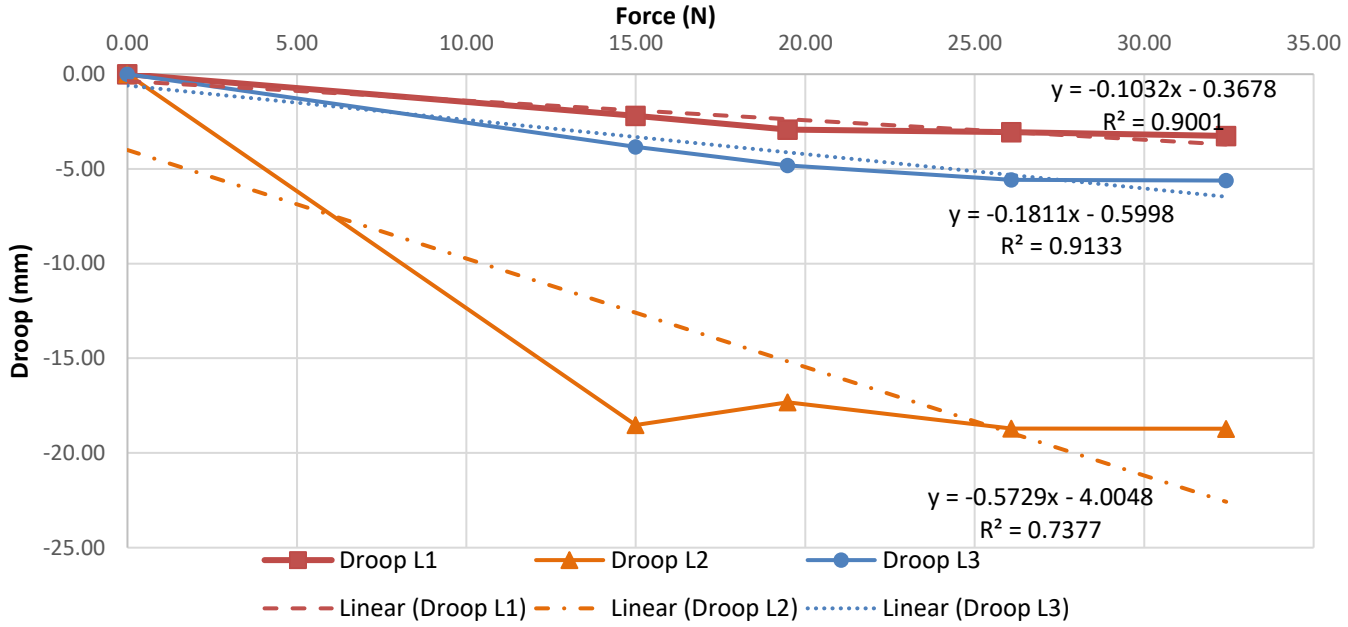

Heart 46

Force (N)	Droop L1 RCC (mm)	Droop L2 NCC (mm)	Droop L3 LCC (mm)
0.00	0.00	0.00	0.00
10.40	-4.12	0.00	-2.24
14.08	-5.06	0.00	-3.14
29.85	-5.49	0.00	-3.39
33.93	-6.04	0.00	-3.79

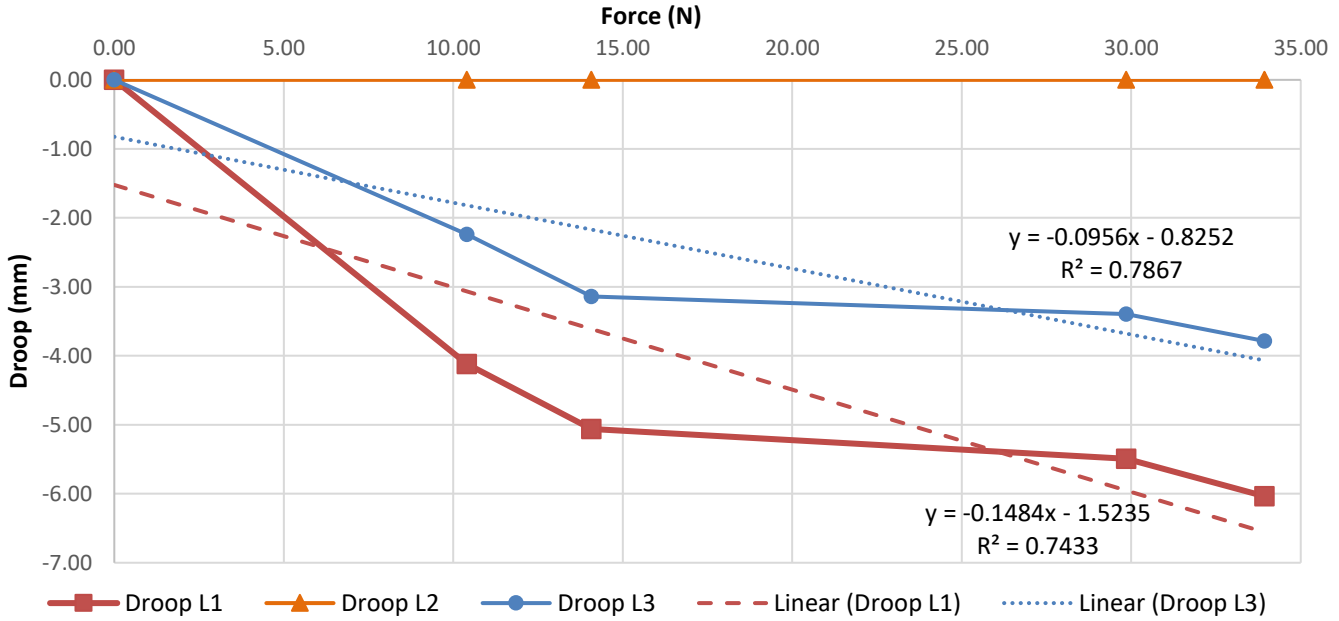

Heart 47

Force (N)	Droop L1 RCC (mm)	Droop L2 NCC (mm)	Droop L3 LCC (mm)
0.00	0.00	0.00	0.00
9.66	-5.77	0.00	-4.37
16.82	-6.73	0.00	-5.58
20.40	-7.02	0.00	-6.63
25.56	-7.72	0.00	-7.91

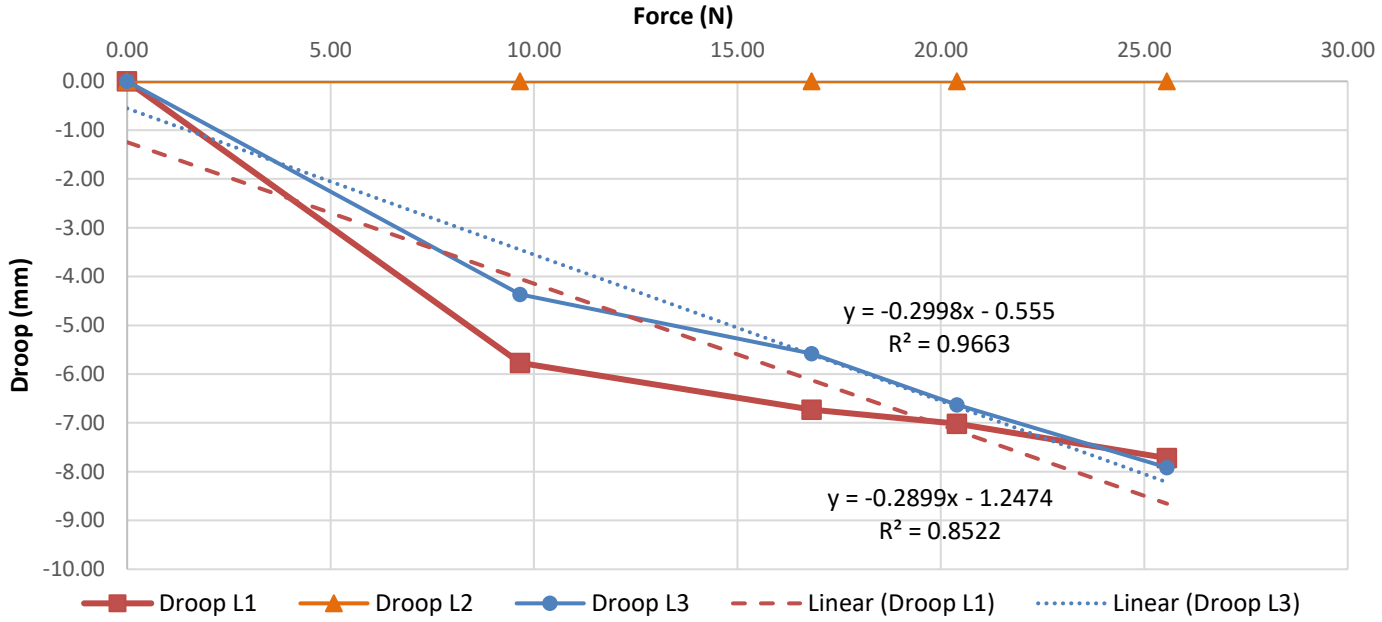

Heart 48

Force (N)	Droop L1 RCC (mm)	Droop L2 NCC (mm)	Droop L3 LCC (mm)
0.00	0.00	0.00	0.00
14.30	-3.59	0.00	-2.22
17.25	-4.07	0.00	-2.53
22.56	-5.10	0.00	-3.18
26.01	-5.82	0.00	-3.40

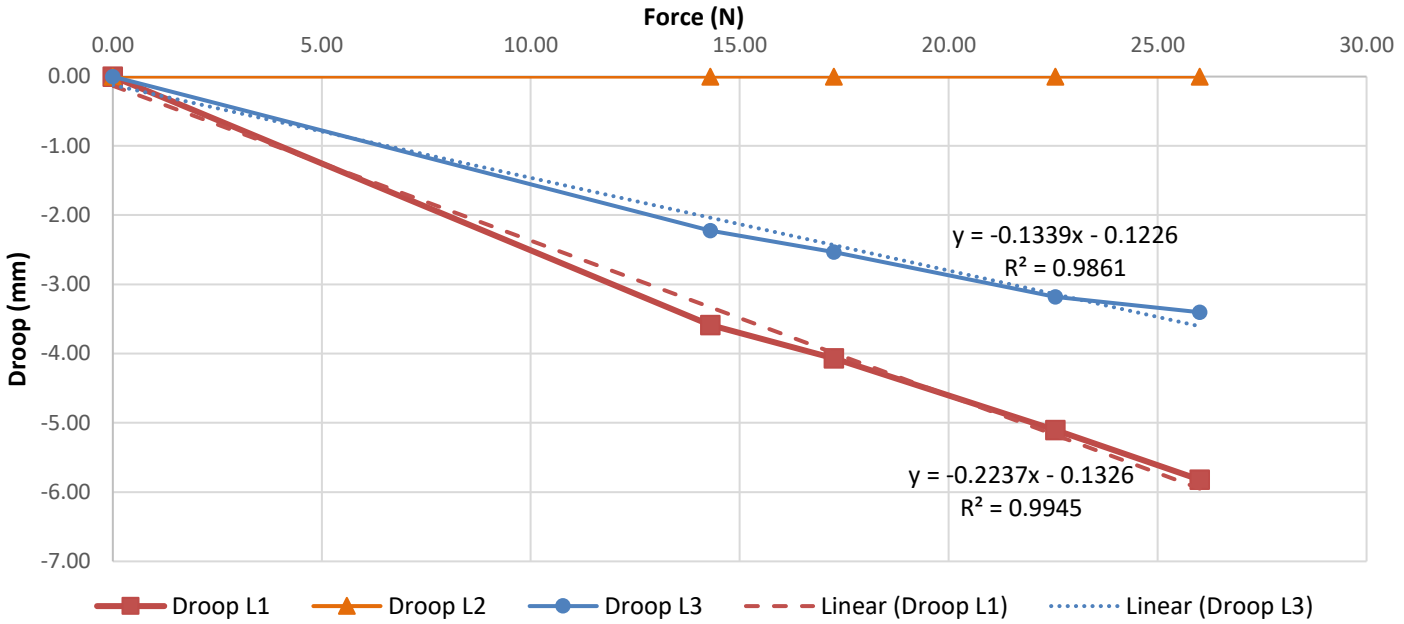

Heart 49

Force (N)	Droop L1 RCC (mm)	Droop L2 NCC (mm)	Droop L3 LCC (mm)
0.00	0.00	0.00	0.00
8.27	-3.99	0.00	-2.18
16.51	-4.57	0.00	-2.51
21.66	-4.89	0.00	-3.31
27.05	-5.35	0.00	-3.41

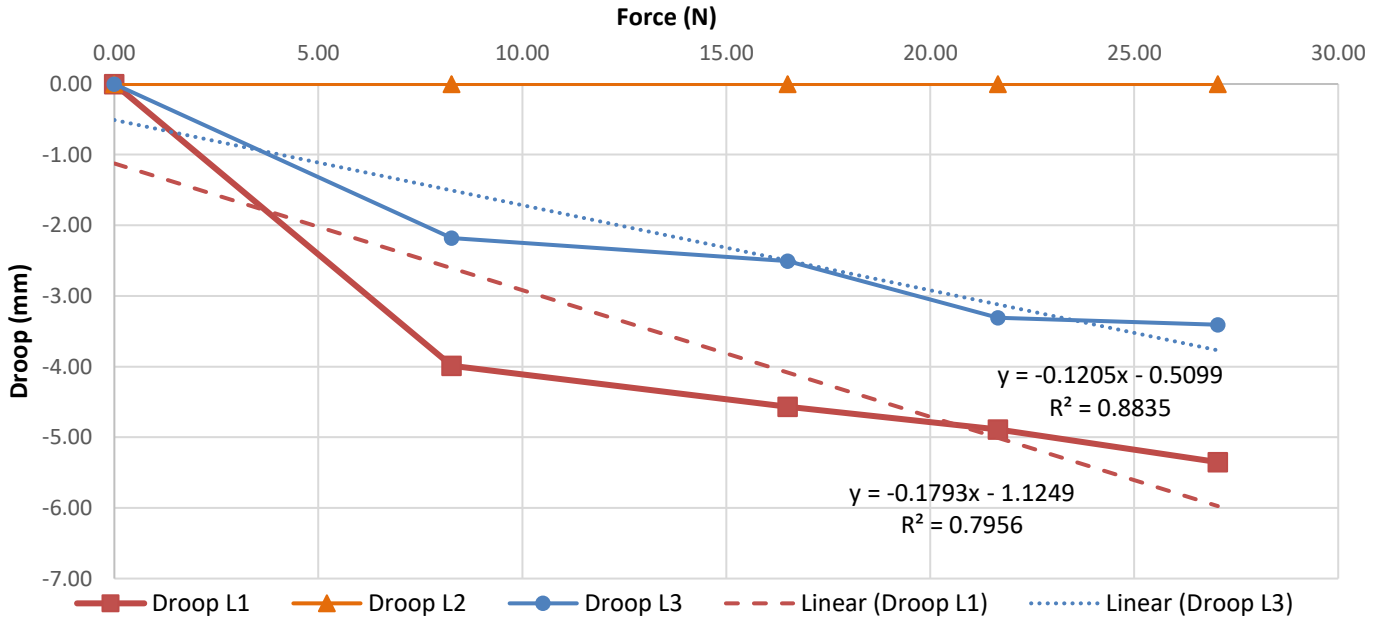

Heart 50

Force (N)	Droop L1 RCC (mm)	Droop L2 NCC (mm)	Droop L3 LCC (mm)
0.00	0.00	0.00	0.00
9.11	-4.76	-2.44	-2.62
15.01	-6.61	-4.01	-4.65
21.03	-7.24	-4.65	-5.20
26.67	-7.91	-5.25	-6.16

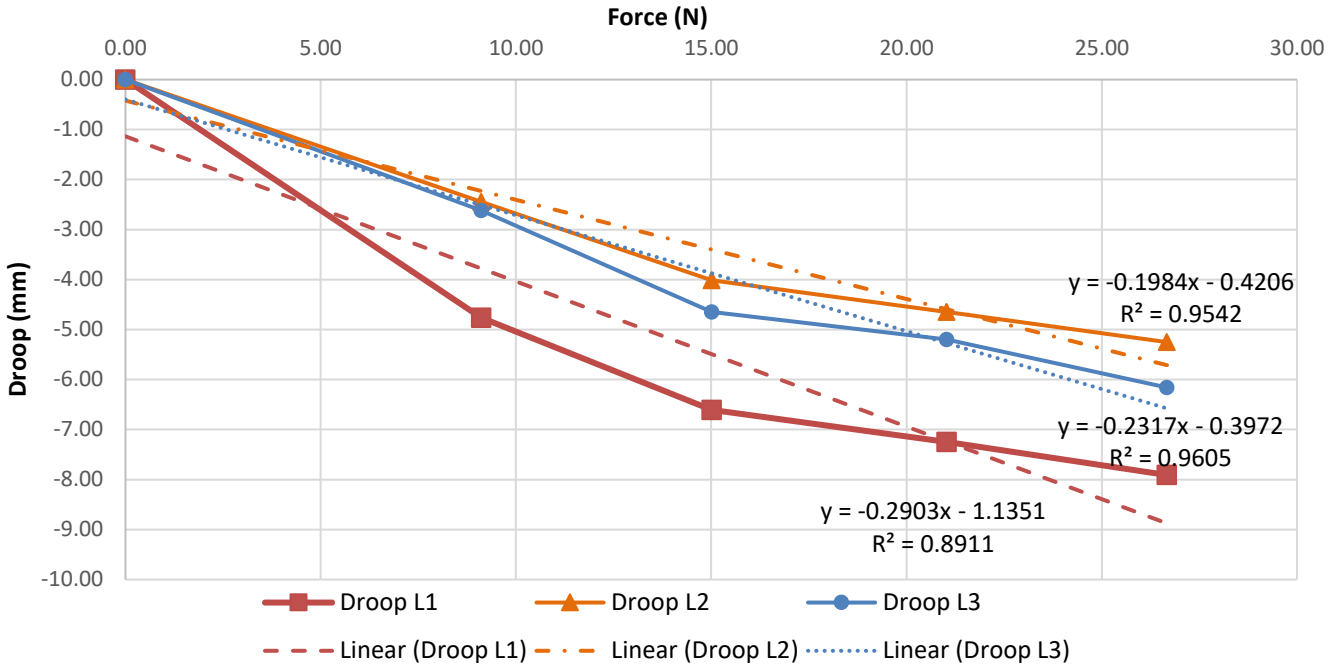

		Droop at 2.5 N (mm)	Droop at 5N (mm)	Droop at 7.5N (mm)	Droop at 10N (mm)	Droop at 12.5N (mm)
	L1	-2.03	-3.15	-4.27	-5.39	-6.51
	L2	-1.97	-3.04	-4.11	-5.18	-6.25
Heart 1	L3	-0.11	-0.29	-0.47	-0.65	-0.83
	L1	-0.54	-1.45	-2.35	-3.26	-4.16
	L2	-1.01	-1.64	-2.27	-2.90	-3.53
Heart 2	L3	-0.70	-1.10	-1.50	-1.89	-2.29
	L1	0.00	0.00	0.00	0.00	0.00
	L2	0.00	0.00	0.00	0.00	0.00
Heart 3	L3	0.00	0.00	0.00	0.00	0.00
	L1	-1.75	-2.80	-3.85	-4.90	-5.96
	L2	-1.71	-2.70	-3.69	-4.68	-5.67
Heart 4	L3	-1.01	-1.64	-2.27	-2.90	-3.53
	L1	-0.49	-0.98	-1.47	-1.97	-2.46
	L2	-0.41	-0.79	-1.17	-1.55	-1.93
Heart 5	L3	-0.27	-0.59	-0.91	-1.23	-1.55
	L1	-0.74	-1.44	-2.15	-2.85	-3.55
	L2	-0.38	-0.88	-1.37	-1.87	-2.36
Heart 6	L3	-0.69	-1.37	-2.04	-2.72	-3.39
	L1	1.35	-0.97	-3.28	-5.59	-7.91
	L2	-1.89	-3.40	-4.90	-6.41	-7.91
Heart 7	L3	-3.71	-4.66	-5.62	-6.58	-7.53
	L1	-1.27	-2.07	-2.87	-3.67	-4.46
	L2	0.00	0.00	0.00	0.00	0.00
Heart 8	L3	-2.00	-3.26	-4.52	-5.79	-7.05
	L1	-1.72	-2.97	-4.23	-5.48	-6.74
	L2	-0.97	-1.46	-1.96	-2.46	-2.96
Heart 9	L3	-0.87	-1.30	-1.72	-2.15	-2.57
	L1	-0.91	-1.70	-2.50	-3.29	-4.09
	L2	-0.71	-1.43	-2.16	-2.88	-3.60
Heart 10	L3	-0.51	-1.09	-1.67	-2.26	-2.84
	L1	-1.81	-2.25	-2.70	-3.14	-3.58
	L2	-1.99	-2.56	-3.13	-3.69	-4.26
Heart 11	L3	-1.48	-1.98	-2.47	-2.97	-3.46
	L1	-1.70	-2.41	-3.12	-3.84	-4.55
Heart 12	L2	-1.32	-1.79	-2.26	-2.73	-3.20

	L3	-0.59	-0.82	-1.05	-1.28	-1.50
	L1	-1.66	-2.59	-3.51	-4.44	-5.37
	L2	-0.45	-0.64	-0.83	-1.02	-1.20
Heart 13	L3	-1.12	-1.85	-2.58	-3.31	-4.05
	L1	-0.60	-1.20	-1.80	-2.39	-2.99
	L2	0.00	0.00	0.00	0.00	0.00
Heart 14	L3	-0.47	-0.84	-1.20	-1.56	-1.92
	L1	-0.86	-1.67	-2.47	-3.28	-4.09
	L2	-1.59	-3.07	-4.55	-6.03	-7.50
Heart 15	L3	-0.69	-1.47	-2.25	-3.03	-3.80
	L1	-0.55	-0.89	-1.24	-1.58	-1.92
	L2	-0.67	-1.16	-1.65	-2.14	-2.62
Heart 16	L3	-0.78	-1.43	-2.08	-2.72	-3.37
	L1	-1.18	-2.00	-2.81	-3.63	-4.45
	L2	-0.29	-0.62	-0.94	-1.26	-1.58
Heart 17	L3	-0.26	-0.68	-1.09	-1.51	-1.92
	L1	-2.11	-3.11	-4.11	-5.11	-6.11
	L2	-0.56	-0.98	-1.40	-1.82	-2.23
Heart 18	L3	-1.95	-2.82	-3.70	-4.58	-5.45
	L1	-0.98	-1.91	-2.84	-3.77	-4.71
	L2	0.00	0.00	0.00	0.00	0.00
Heart 19	L3	-0.94	-1.49	-2.04	-2.58	-3.13
	L1	-0.52	-0.96	-1.40	-1.83	-2.27
	L2	0.00	0.00	0.00	0.00	0.00
Heart 20	L3	-1.14	-2.32	-3.51	-4.69	-5.88
	L1	-1.80	-2.67	-3.54	-4.41	-5.28
	L2	-2.83	-3.85	-4.86	-5.87	-6.89
Heart 21	L3	0.00	0.00	0.00	0.00	0.00
	L1	-1.13	-1.93	-2.73	-3.53	-4.33
	L2	-0.61	-0.97	-1.33	-1.69	-2.05
Heart 22	L3	-0.59	-0.90	-1.20	-1.50	-1.80
	L1	-1.14	-1.81	-2.47	-3.13	-3.80
	L2	-0.72	-1.22	-1.73	-2.23	-2.73
Heart 23	L3	-0.42	-0.77	-1.13	-1.49	-1.85
	L1	-0.98	-1.78	-2.59	-3.40	-4.21
	L2	-0.30	-0.64	-0.98	-1.33	-1.67
Heart 24	L3	-0.48	-0.81	-1.13	-1.46	-1.79
Heart 25	L1	-0.46	-0.71	-0.95	-1.20	-1.44

	L2	-1.02	-1.37	-1.71	-2.06	-2.41
	L3	-0.68	-1.17	-1.67	-2.16	-2.65
	L1	-0.94	-1.73	-2.51	-3.29	-4.07
	L2	-0.36	-0.68	-1.00	-1.33	-1.65
Heart 26	L3	-0.61	-1.18	-1.75	-2.32	-2.89
	L1	-1.01	-1.49	-1.96	-2.44	-2.91
	L2	-0.95	-1.50	-2.04	-2.58	-3.12
Heart 27	L3	-0.63	-0.91	-1.20	-1.48	-1.76
	L1	-1.98	-2.74	-3.50	-4.26	-5.02
	L2	-0.91	-1.20	-1.49	-1.78	-2.06
Heart 28	L3	-1.80	-2.34	-2.88	-3.41	-3.95
	L1	-2.70	-3.27	-3.85	-4.43	-5.00
	L2	0.00	0.00	0.00	0.00	0.00
Heart 29	L3	-1.89	-2.30	-2.70	-3.10	-3.51
	L1	-2.40	-3.34	-4.29	-5.23	-6.18
	L2	-0.46	-0.89	-1.33	-1.76	-2.19
Heart 30	L3	-1.14	-1.85	-2.57	-3.28	-3.99
	L1	-0.16	-0.29	-0.42	-0.55	-0.67
	L2	0.02	-0.08	-0.19	-0.29	-0.39
Heart 31	L3	-0.76	-1.28	-1.80	-2.32	-2.84
	L1	-2.06	-2.66	-3.27	-3.87	-4.47
	L2	-0.68	-0.97	-1.25	-1.53	-1.81
Heart 32	L3	-1.73	-2.09	-2.46	-2.82	-3.19
	L1	0.00	0.00	0.00	0.00	0.00
	L2	-3.12	-3.87	-4.63	-5.38	-6.14
Heart 33	L3	-2.75	-3.38	-4.02	-4.65	-5.29
	L1	-1.58	-2.54	-3.51	-4.48	-5.44
	L2	-1.18	-1.98	-2.78	-3.58	-4.38
Heart 34	L3	-0.73	-1.46	-2.18	-2.90	-3.62
	L1	-1.65	-2.90	-4.15	-5.40	-6.65
	L2	-0.09	-0.20	-0.32	-0.44	-0.55
Heart 35	L3	-1.26	-2.09	-2.92	-3.75	-4.57
	L1	-0.69	-1.13	-1.57	-2.01	-2.45
	L2	-0.43	-0.56	-0.69	-0.81	-0.94
Heart 36	L3	-0.68	-1.24	-1.80	-2.37	-2.93
	L1	-2.28	-3.18	-4.08	-4.98	-5.88
	L2	0.00	0.00	0.00	0.00	0.00
Heart 37	L3	-1.85	-2.34	-2.84	-3.34	-3.84

	L1	-0.69	-1.02	-1.35	-1.68	-2.01
	L2	-0.75	-1.19	-1.64	-2.08	-2.52
Heart 38	L3	-0.68	-0.96	-1.25	-1.54	-1.82
	L1	-1.19	-1.78	-2.37	-2.95	-3.54
	L2	0.00	0.00	0.00	0.00	0.00
Heart 39	L3	-0.40	-0.67	-0.94	-1.21	-1.48
	L1	-0.35	-1.32	-2.30	-3.28	-4.26
	L2	-0.19	-0.89	-1.59	-2.29	-2.99
Heart 40	L3	-0.17	-0.62	-1.07	-1.53	-1.98
	L1	-1.53	-2.25	-2.97	-3.68	-4.40
	L2	-1.48	-2.10	-2.72	-3.35	-3.97
Heart 41	L3	-0.74	-1.09	-1.43	-1.78	-2.13
	L1	-0.90	-1.49	-2.09	-2.68	-3.28
	L2	0.00	0.00	0.00	0.00	0.00
Heart 42	L3	-0.51	-0.85	-1.18	-1.51	-1.84
	L1	-1.81	-2.33	-2.86	-3.38	-3.91
	L2	-0.07	-0.26	-0.44	-0.63	-0.81
Heart 43	L3	-0.21	-0.57	-0.93	-1.29	-1.65
	L1	-1.46	-1.97	-2.47	-2.98	-3.49
	L2	-1.38	-2.01	-2.63	-3.25	-3.88
Heart 44	L3	0.00	0.00	0.00	0.00	0.00
	L1	-0.63	-0.88	-1.14	-1.40	-1.66
	L2	-5.44	-6.87	-8.30	-9.73	-11.17
Heart 45	L3	-1.05	-1.51	-1.96	-2.41	-2.86
	L1	-1.89	-2.27	-2.64	-3.01	-3.38
	L2	0.00	0.00	0.00	0.00	0.00
Heart 46	L3	-1.06	-1.30	-1.54	-1.78	-2.02
	L1	-1.97	-2.70	-3.42	-4.15	-4.87
	L2	0.00	0.00	0.00	0.00	0.00
Heart 47	L3	-1.30	-2.05	-2.80	-3.55	-4.30
	L1	-0.69	-1.25	-1.81	-2.37	-2.93
	L2	0.00	0.00	0.00	0.00	0.00
Heart 48	L3	-0.46	-0.79	-1.13	-1.46	-1.80
	L1	-1.57	-2.02	-2.47	-2.92	-3.37
	L2	0.00	0.00	0.00	0.00	0.00
Heart 49	L3	-0.81	-1.11	-1.41	-1.71	-2.02
	L1	-1.86	-2.59	-3.31	-4.04	-4.76
Heart 50	L2	-0.92	-1.41	-1.91	-2.40	-2.90

	L3	-0.98	-1.56	-2.13	-2.71	-3.29

The upper and lower tolerance interval range was drawn per force, in blue at a proportion of 0.8 and in red 0.9 for p = 0.05. The upper and lower tolerance interval can be seen below.

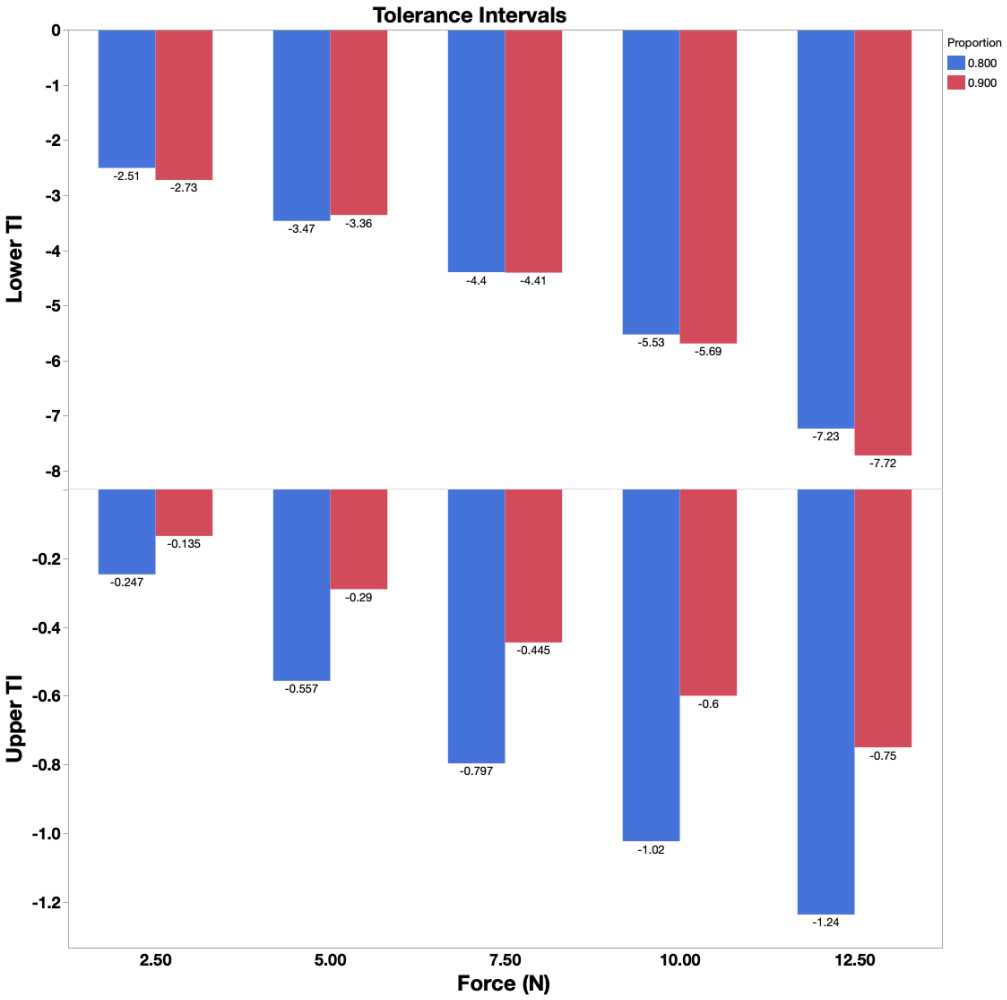

The values used can be seen in the table below.

Table	Force (N)	Y	Proportion	Lower TI	Upper TI	1-Alpha	Actual Confidence
Data2	2.50	Droop	0.8	-2.03	-0.27	0.95	0.954423601
Data2	5.00	Droop	0.8	-3.15	-0.62	0.95	0.954423601
Data2	7.50	Droop	0.8	-4.15	-0.94	0.95	0.954423601
Data2	10.00	Droop	0.8	-5.38	-1.23	0.95	0.954423601
Data2	12.50	Droop	0.8	-6.51	-1.5	0.95	0.958178013
Data2	2.50	Droop	0.9	-2.7	-0.11	0.95	0.954402826
Data2	5.00	Droop	0.9	-3.38	-0.29	0.95	0.954402826
Data2	7.50	Droop	0.9	-4.55	-0.44	0.95	0.954402826
Data2	10.00	Droop	0.9	-5.79	-0.63	0.95	0.954402826
Data2	12.50	Droop	0.9	-7.5	-0.81	0.95	0.956889662

The tolerance interval range was drawn per leaflet, in blue at a proportion of 0.8 and in red 0.9 for p = 0.05. The upper and lower tolerance interval can be seen below.

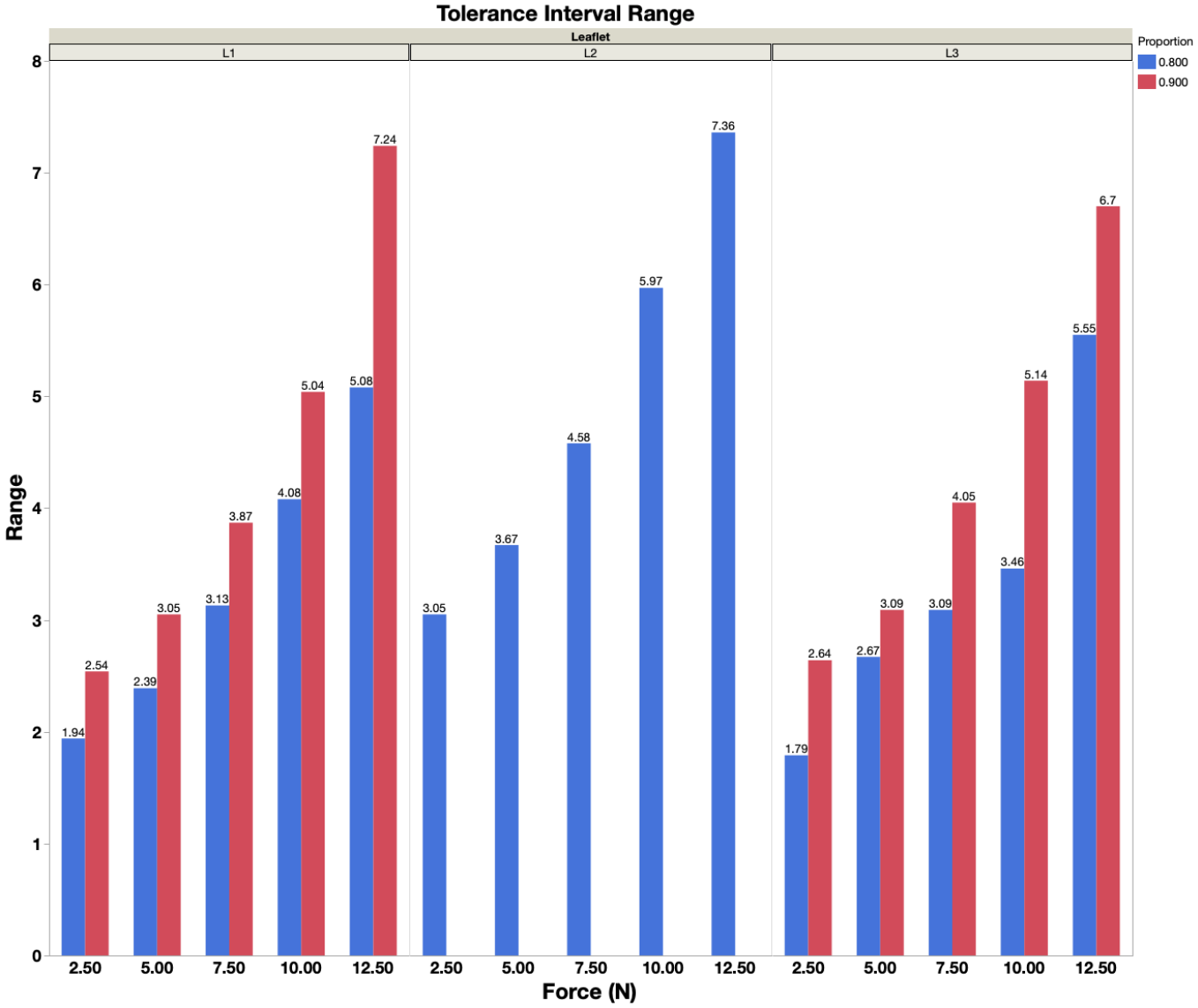
Tolerance Interval Range
Leaflet
L1
L2
L3
Proportion
0.800
0.900
Range
Force (N)
2.50
5.00
7.50
10.00
12.50
1.94
2.54
2.39
3.05
3.13
3.87
4.08
5.04
5.08
7.24
3.05
3.67
4.58
5.97
7.36
1.79
2.64
2.67
3.09
3.09
4.05
3.46
5.14
5.55
6.7

The values used can be seen in the table below.

Table	Force (N)	Leaflet	Y	Proportion	Lower TI	Upper TI	1-Alpha	Actual Confidence	Range
Data2	2.50	L1	Droop	0.8	-2.4	-0.46	0.95	0.975161	1.94
Data2	5.00	L1	Droop	0.8	-3.27	-0.88	0.95	0.975161	2.39
Data2	7.50	L1	Droop	0.8	-4.27	-1.14	0.95	0.975161	3.13
Data2	10.00	L1	Droop	0.8	-5.48	-1.4	0.95	0.975161	4.08
Data2	12.50	L1	Droop	0.8	-6.74	-1.66	0.95	0.975161	5.08
Data2	2.50	L2	Droop	0.8	-3.12	-0.07	0.95	0.983977	3.05
Data2	5.00	L2	Droop	0.8	-3.87	-0.2	0.95	0.983977	3.67
Data2	7.50	L2	Droop	0.8	-4.9	-0.32	0.95	0.983977	4.58
Data2	10.00	L2	Droop	0.8	-6.41	-0.44	0.95	0.983977	5.97
Data2	12.50	L2	Droop	0.8	-7.91	-0.55	0.95	0.983977	7.36
Data2	2.50	L3	Droop	0.8	-2	-0.21	0.95	0.966834	1.79
Data2	5.00	L3	Droop	0.8	-3.26	-0.59	0.95	0.966834	2.67
Data2	7.50	L3	Droop	0.8	-4.02	-0.93	0.95	0.966834	3.09
Data2	10.00	L3	Droop	0.8	-4.69	-1.23	0.95	0.966834	3.46
Data2	12.50	L3	Droop	0.8	-7.05	-1.5	0.95	0.971276	5.55
Data2	2.50	L1	Droop	0.9	-2.7	-0.16	0.95	0.959703	2.54
Data2	5.00	L1	Droop	0.9	-3.34	-0.29	0.95	0.959703	3.05
Data2	7.50	L1	Droop	0.9	-4.29	-0.42	0.95	0.959703	3.87
Data2	10.00	L1	Droop	0.9	-5.59	-0.55	0.95	0.959703	5.04
Data2	12.50	L1	Droop	0.9	-7.91	-0.67	0.95	0.959703	7.24
Data2	2.50	L2	Droop	0.9			0.95		
Data2	5.00	L2	Droop	0.9			0.95		
Data2	7.50	L2	Droop	0.9			0.95		
Data2	10.00	L2	Droop	0.9			0.95		
Data2	12.50	L2	Droop	0.9			0.95		
Data2	2.50	L3	Droop	0.9	-2.75	-0.11	0.95	0.951996	2.64
Data2	5.00	L3	Droop	0.9	-3.38	-0.29	0.95	0.951996	3.09
Data2	7.50	L3	Droop	0.9	-4.52	-0.47	0.95	0.951996	4.05
Data2	10.00	L3	Droop	0.9	-5.79	-0.65	0.95	0.951996	5.14
Data2	12.50	L3	Droop	0.9	-7.53	-0.83	0.95	0.956011	6.7

Oneway Analysis of Droop By Leaflet Force (N)=2.50

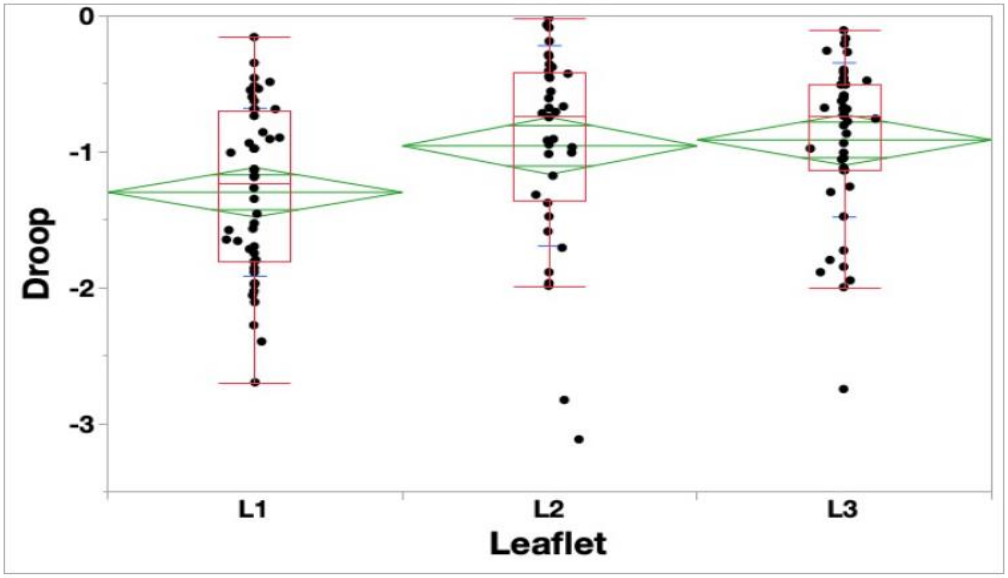

Wilcoxon / Kruskal-Wallis Tests (Rank Sums)

Level	Count	Score Sum	Expected Score	Score Mean	(Mean-Mean0)/Std0
L1	48	2450.50	3144.00	51.0521	-3.343
L2	36	2674.00	2358.00	74.2778	1.642
L3	46	3390.50	3013.00	73.7065	1.836

1-Way Test, ChiSquare Approximation

ChiSquare	DF	Prob>ChiSq
11.1996	2	0.0037*

Oneway Analysis of Droop By Leaflet Force (N)=5.00

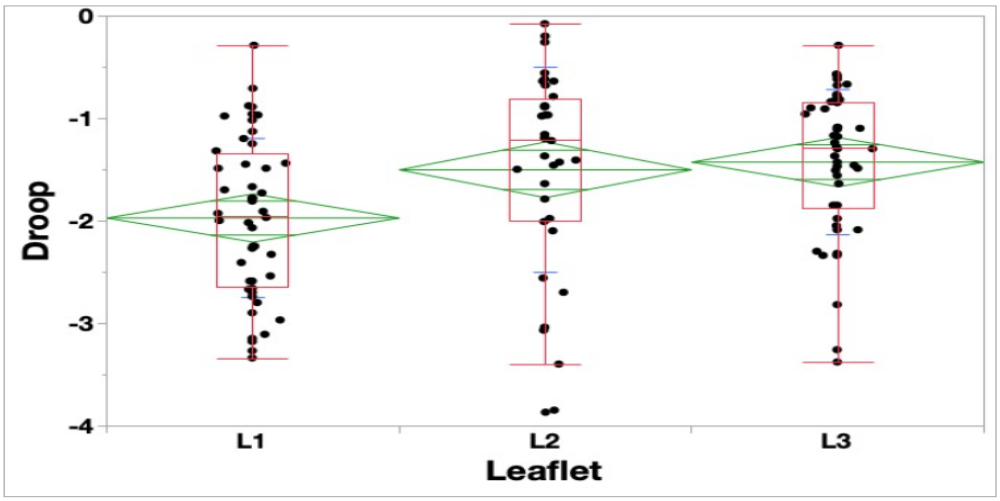

Wilcoxon / Kruskal-Wallis Tests (Rank Sums)

Level	Count	Score Sum	Expected Score	Score Mean	(Mean-Mean0)/Std0
L1	48	2383.00	3144.00	49.6458	-3.669
L2	36	2682.00	2358.00	74.5000	1.683
L3	46	3450.00	3013.00	75.0000	2.125

1-Way Test, ChiSquare Approximation

ChiSquare	DF	Prob>ChiSq
13.4828	2	0.0012*

Oneway Analysis of Droop By Leaflet Force (N)=7.50

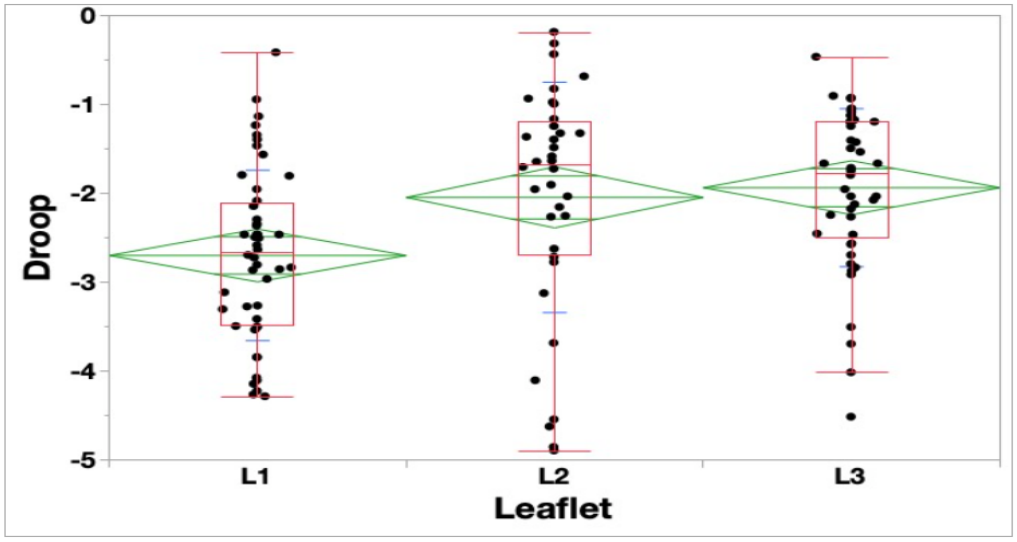

Wilcoxon / Kruskal-Wallis Tests (Rank Sums)

Level	Count	Score Sum	Expected Score	Score Mean	(Mean-Mean0)/Std0
L1	48	2294.00	3144.00	47.7917	-4.098
L2	36	2703.50	2358.00	75.0972	1.795
L3	46	3517.50	3013.00	76.4674	2.454

1-Way Test, ChiSquare Approximation

ChiSquare	DF	Prob>ChiSq
16.8440	2	0.0002*

Oneway Analysis of Droop By Leaflet Force (N)=10.00

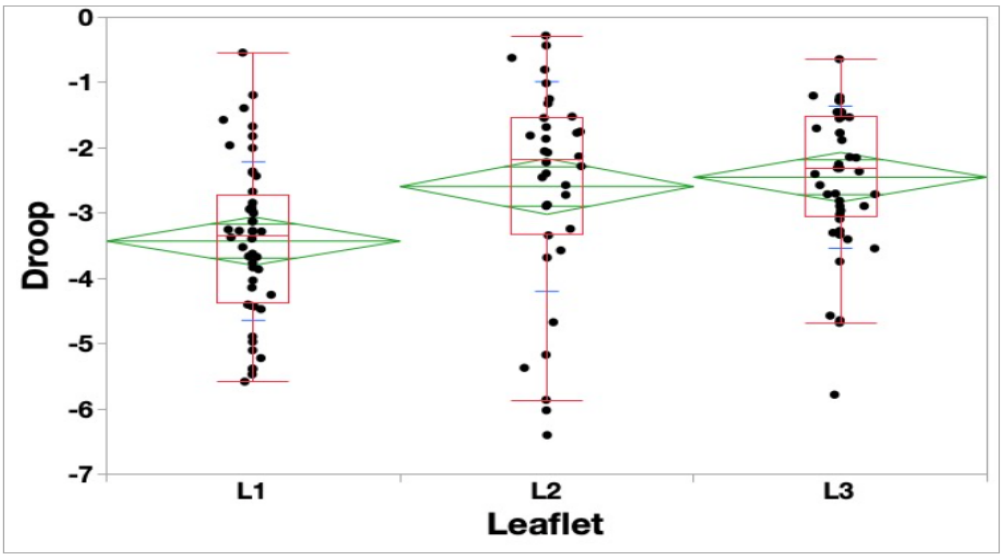

Wilcoxon / Kruskal-Wallis Tests (Rank Sums)

Level	Count	Score Sum	Expected Score	Score Mean	(Mean-Mean0)/Std0
L1	48	2270.50	3144.00	47.3021	-4.212
L2	36	2703.00	2358.00	75.0833	1.792
L3	46	3541.50	3013.00	76.9891	2.571

1-Way Test, ChiSquare Approximation

ChiSquare	DF	Prob>ChiSq
17.8102	2	0.0001*

Oneway Analysis of Droop By Leaflet Force (N)=12.50

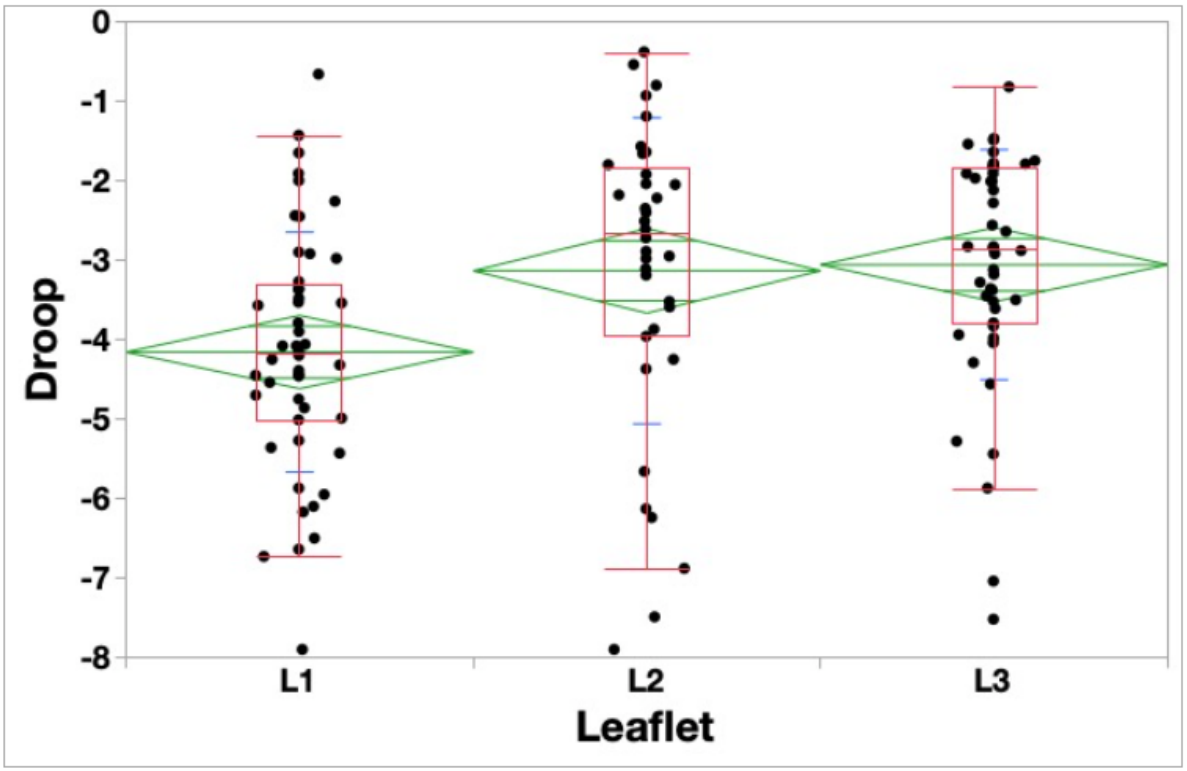

Wilcoxon / Kruskal-Wallis Tests (Rank Sums)

Level	Count	Score Sum	Expected Score	Score Mean	(Mean-Mean0)/Std0
L1	48	2302.50	3168.00	47.9688	-4.132
L2	36	2736.50	2376.00	76.0139	1.856
L3	47	3607.00	3102.00	76.7447	2.421

1-Way Test, ChiSquare Approximation

ChiSquare	DF	Prob>ChiSq
17.1015	2	0.0002*

Appendix D : Detail Drawings

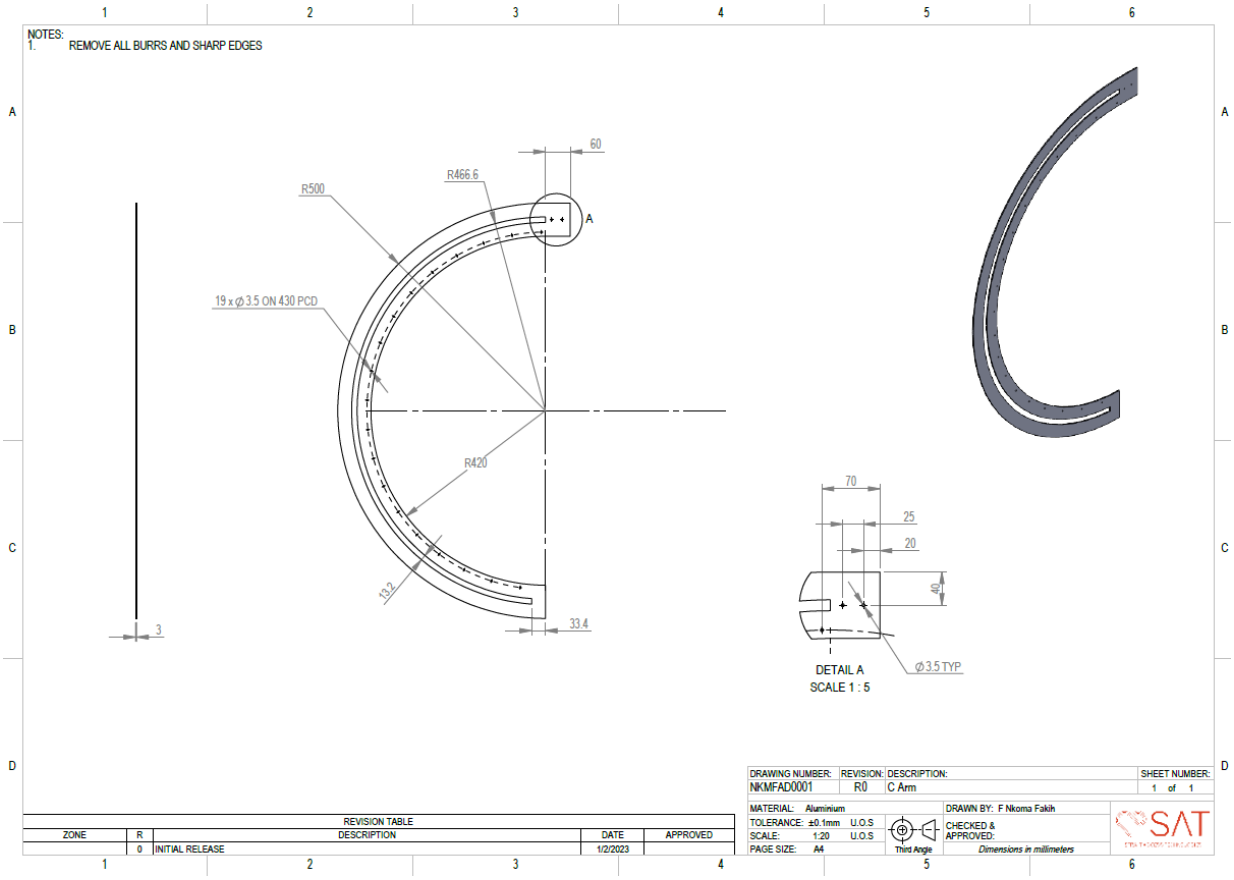

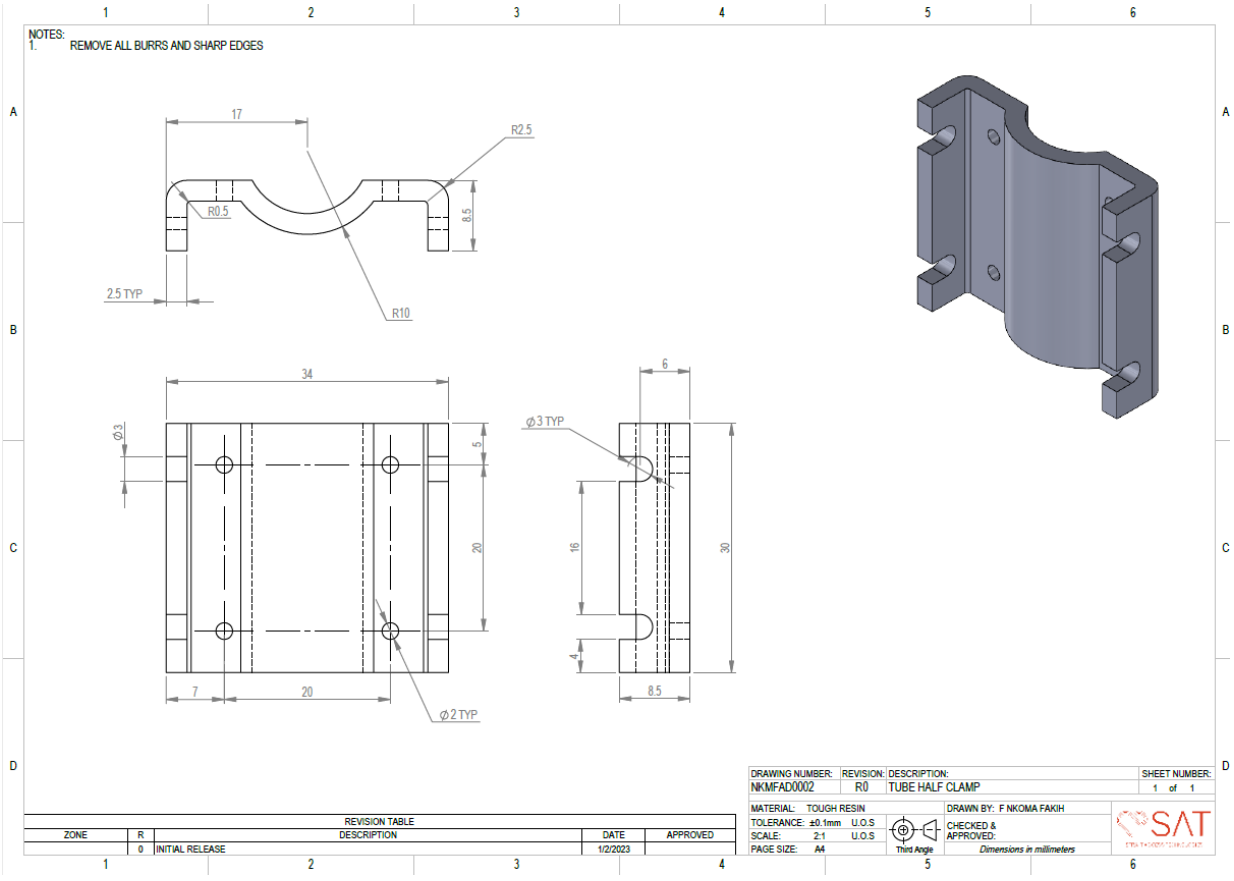
NOTES:
1. REMOVE ALL BURRS AND SHARP EDGES
17
R2.5
R0.5
8.5
2.5 TYP
R10
34
Ø3
5
20
7
20
Ø2 TYP
6
Ø3 TYP
16
30
4
8.5
DRAWING NUMBER: NKMFAD0002
REVISION: R0
DESCRIPTION: TUBE HALF CLAMP
SHEET NUMBER: 1 of 1
MATERIAL: TOUGH RESIN
TOLERANCE: ±0.1mm U.O.S
SCALE: 2:1 U.O.S
PAGE SIZE: A4
DRAWN BY: F NKOMA FAKIH
CHECKED & APPROVED:
Third Angle
Dimensions in millimeters
REVISION TABLE
ZONE | R | DESCRIPTION | DATE | APPROVED
0 | INITIAL RELEASE | 1/2/2023

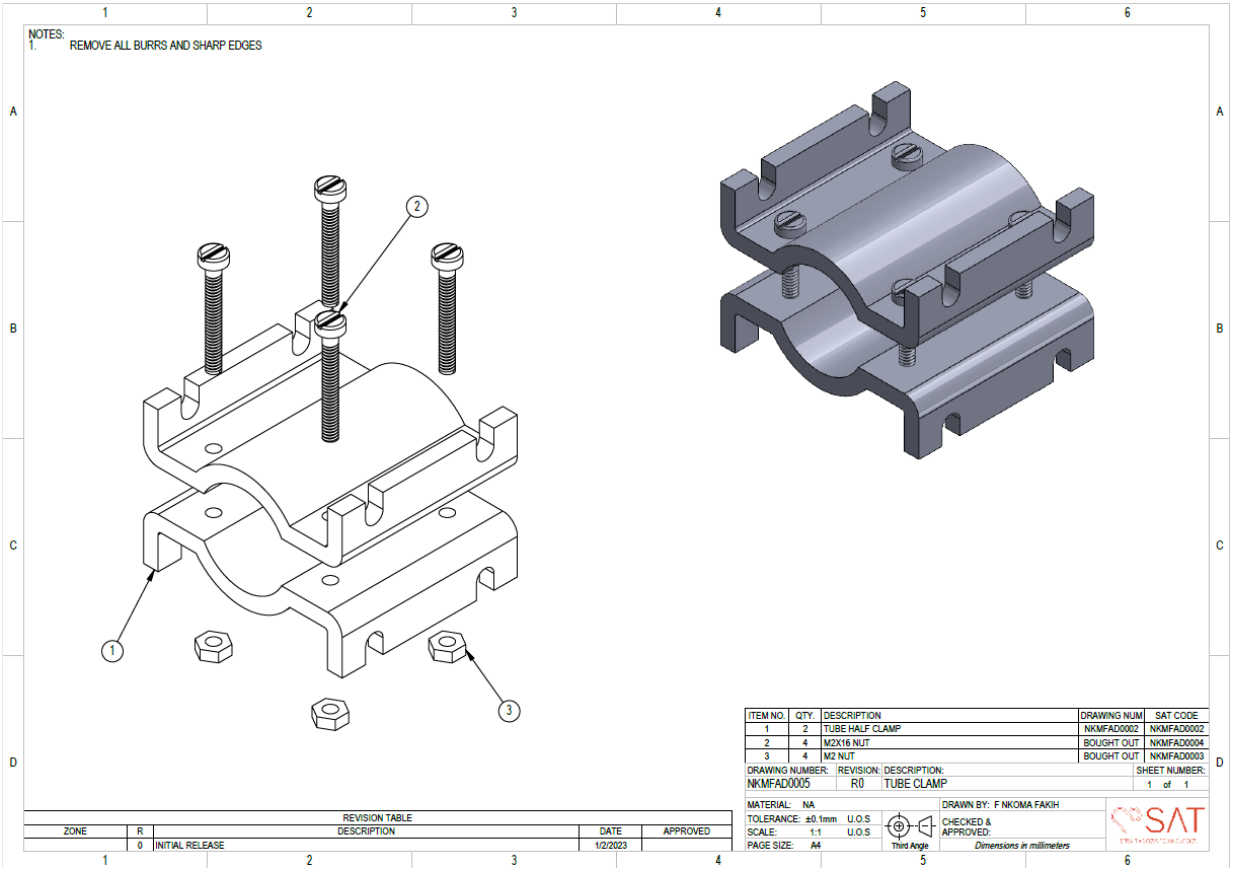
NOTES:
1. REMOVE ALL BURRS AND SHARP EDGES
1
2
3
ITEM NO. | QTY. | DESCRIPTION | DRAWING NUM | SAT CODE
1 | 2 | TUBE HALF CLAMP | NKMFAD0002 | NKMFAD0002
2 | 4 | M2X16 NUT | BOUGHT OUT | NKMFAD0004
3 | 4 | M2 NUT | BOUGHT OUT | NKMFAD0003
DRAWING NUMBER: NKMFAD0005
REVISION: R0
DESCRIPTION: TUBE CLAMP
SHEET NUMBER: 1 of 1
MATERIAL: NA
TOLERANCE: ±0.1mm U.O.S
SCALE: 1:1 U.O.S
PAGE SIZE: A4
DRAWN BY: F NKOMA FAKIH
CHECKED & APPROVED:
Third Angle
Dimensions in millimeters
REVISION TABLE
ZONE | R | DESCRIPTION | DATE | APPROVED
0 | INITIAL RELEASE | 1/2/2023

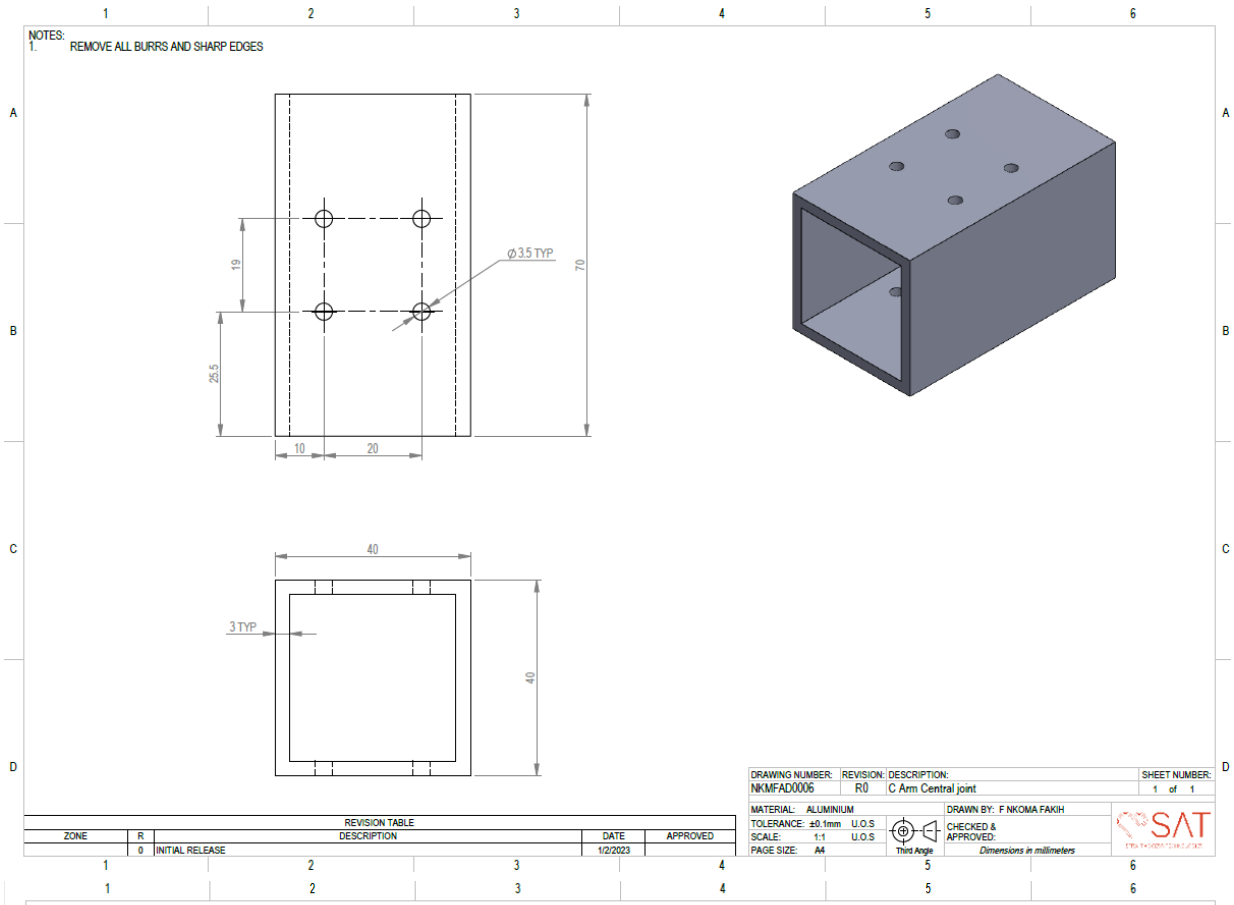
NOTES:
1. REMOVE ALL BURRS AND SHARP EDGES
Ø 3.5 TYP
19
25.5
70
10
20
40
3 TYP
40
DRAWING NUMBER: NKMFAD0006
REVISION: R0
DESCRIPTION: C Arm Central joint
SHEET NUMBER: 1 of 1
MATERIAL: ALUMINIUM
TOLERANCE: ±0.1mm U.O.S
SCALE: 1:1 U.O.S
PAGE SIZE: A4
DRAWN BY: F NKOMA FAKIH
CHECKED & APPROVED:
Third Angle
Dimensions in millimeters
REVISION TABLE
ZONE | R | DESCRIPTION | DATE | APPROVED
0 | INITIAL RELEASE | 1/2/2023

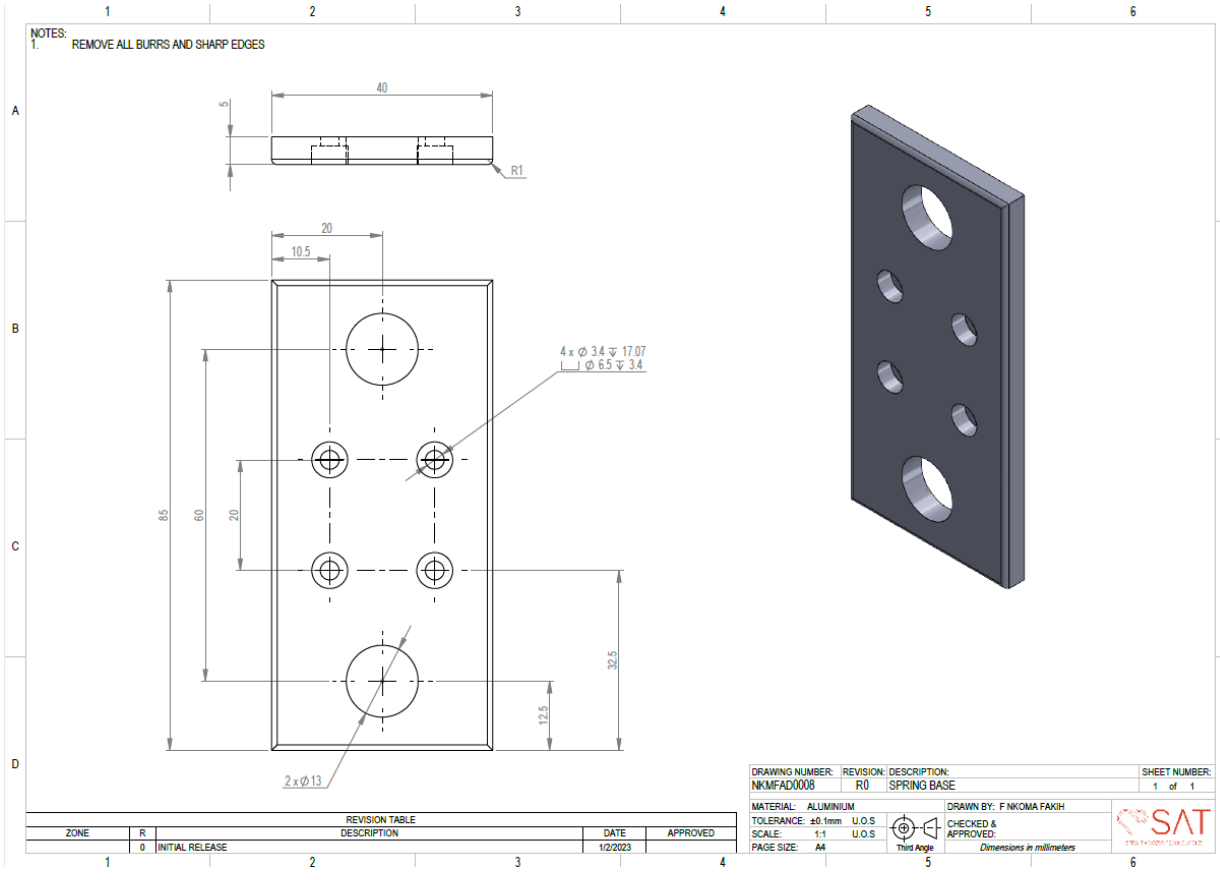
NOTES:
1. REMOVE ALL BURRS AND SHARP EDGES
40
5
R1
20
10.5
4 x Ø 3.4 ↧ 17.07
⌴ Ø 6.5 ↧ 3.4
85
60
20
32.5
12.5
2 x Ø 13
DRAWING NUMBER: NKMFAD0008
REVISION: R0
DESCRIPTION: SPRING BASE
SHEET NUMBER: 1 of 1
MATERIAL: ALUMINIUM
TOLERANCE: ±0.1mm U.O.S
SCALE: 1:1 U.O.S
PAGE SIZE: A4
DRAWN BY: F NKOMA FAKIH
CHECKED & APPROVED:
Third Angle
Dimensions in millimeters
REVISION TABLE
ZONE | R | DESCRIPTION | DATE | APPROVED
0 | INITIAL RELEASE | 1/2/2023

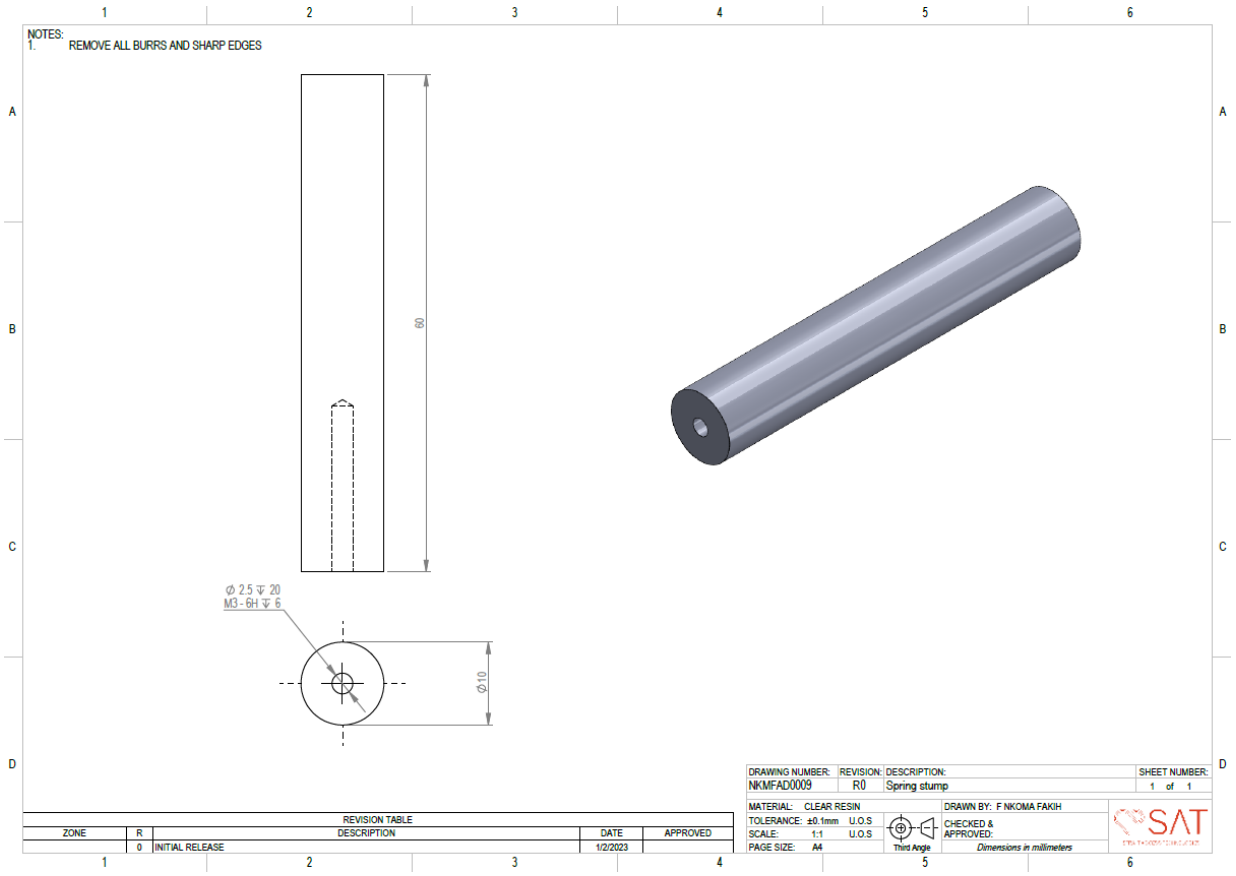
NOTES:
1. REMOVE ALL BURRS AND SHARP EDGES
60
Ø 2.5 ↧ 20
M3 - 6H ↧ 6
Ø10
REVISION TABLE
ZONE | R | DESCRIPTION | DATE | APPROVED
0 | INITIAL RELEASE | 1/2/2023
DRAWING NUMBER: NKMFAD0009
REVISION: R0
DESCRIPTION: Spring stump
SHEET NUMBER: 1 of 1
MATERIAL: CLEAR RESIN
TOLERANCE: ±0.1mm U.O.S
SCALE: 1:1 U.O.S
PAGE SIZE: A4
DRAWN BY: F NKOMA FAKIH
CHECKED & APPROVED:
Third Angle
Dimensions in millimeters

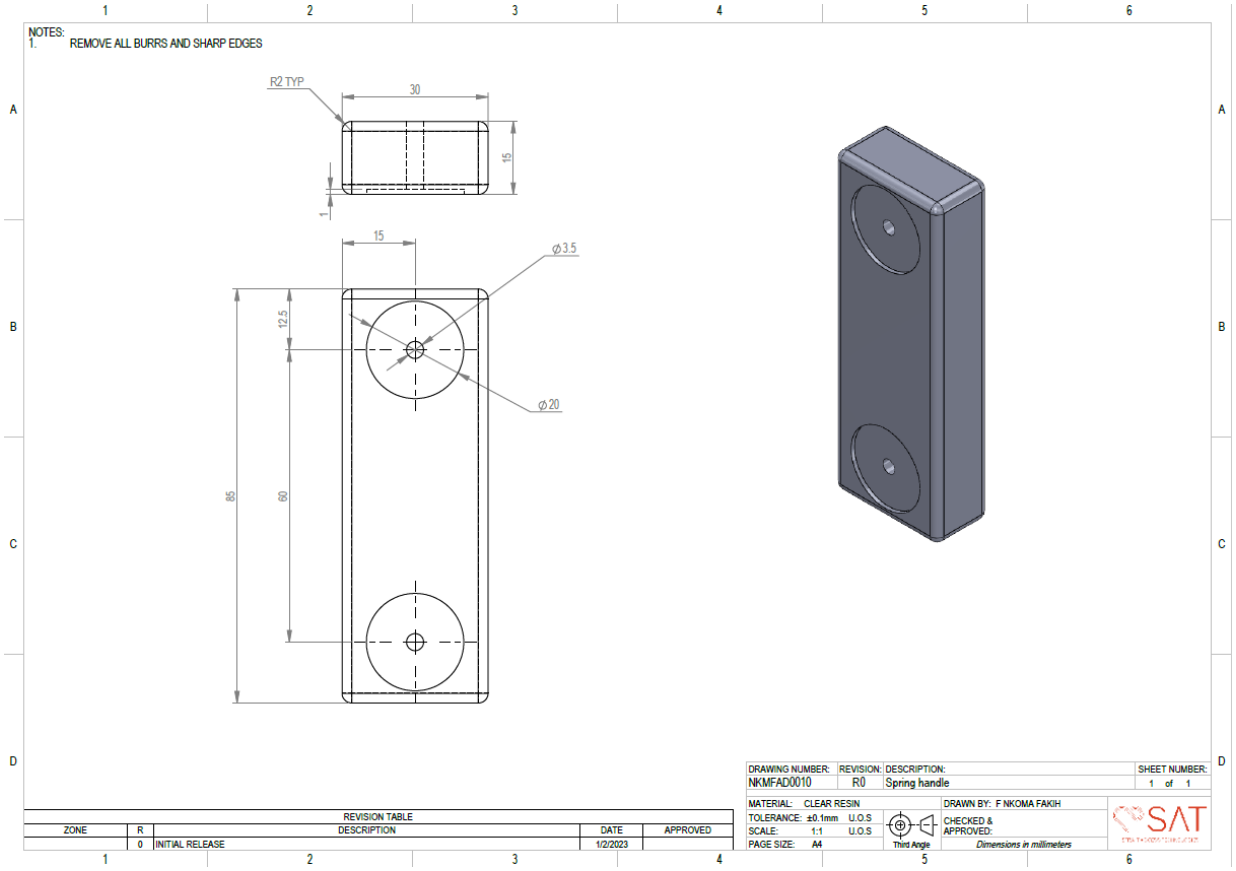
NOTES:
1. REMOVE ALL BURRS AND SHARP EDGES
R2 TYP
30
15
1
15
Ø3.5
12.5
Ø20
85
60
REVISION TABLE
ZONE | R | DESCRIPTION | DATE | APPROVED
0 | INITIAL RELEASE | 1/2/2023
DRAWING NUMBER: NKMFAD0010
REVISION: R0
DESCRIPTION: Spring handle
SHEET NUMBER: 1 of 1
MATERIAL: CLEAR RESIN
TOLERANCE: ±0.1mm U.O.S
SCALE: 1:1 U.O.S
PAGE SIZE: A4
DRAWN BY: F NKOMA FAKIH
CHECKED & APPROVED:
Third Angle
Dimensions in millimeters

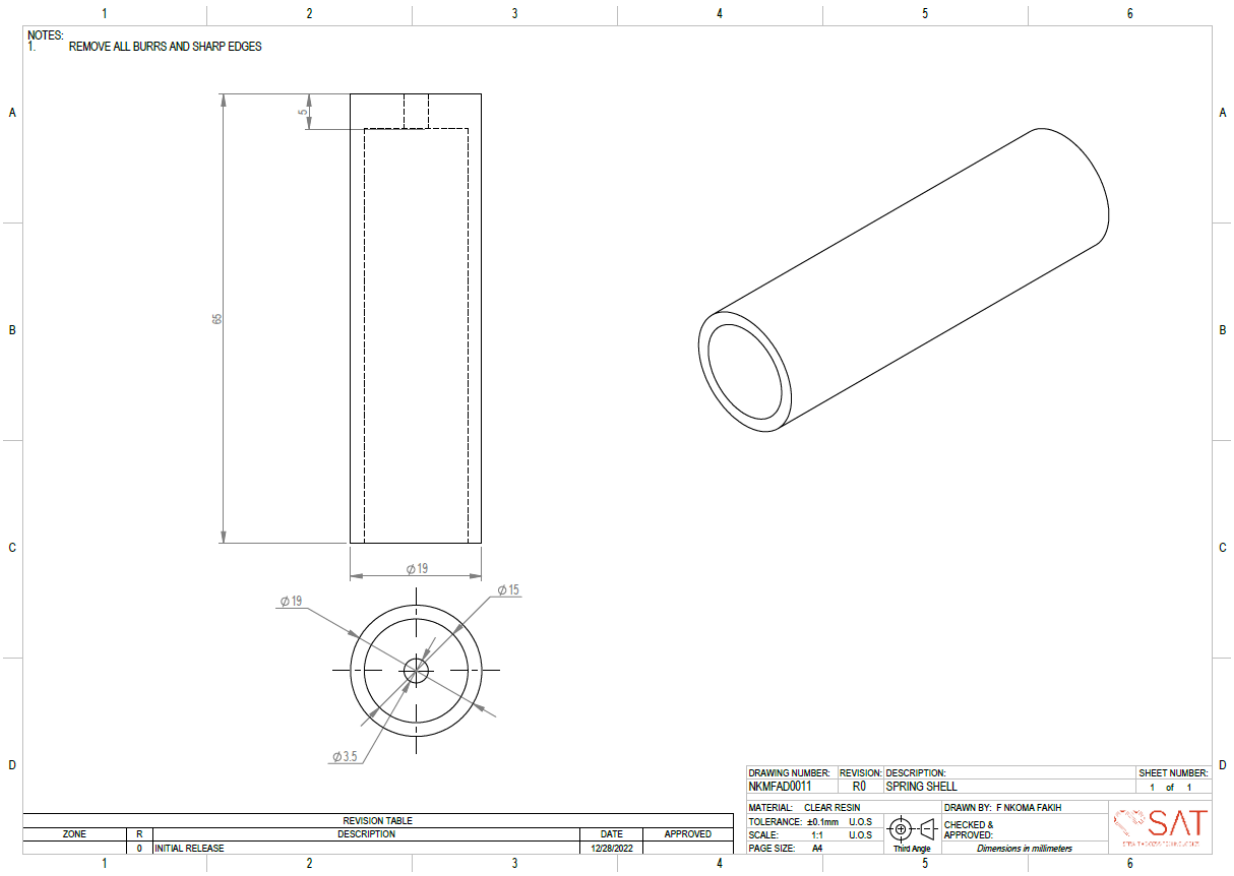
NOTES:
1. REMOVE ALL BURRS AND SHARP EDGES
5
65
Ø 19
Ø 19
Ø 15
Ø 3.5
DRAWING NUMBER: NKMFAD0011
REVISION: R0
DESCRIPTION: SPRING SHELL
SHEET NUMBER: 1 of 1
MATERIAL: CLEAR RESIN
TOLERANCE: ±0.1mm U.O.S
SCALE: 1:1 U.O.S
PAGE SIZE: A4
Third Angle
DRAWN BY: F NKOMA FAKIH
CHECKED & APPROVED:
Dimensions in millimeters
REVISION TABLE
ZONE | R | DESCRIPTION | DATE | APPROVED
0 | INITIAL RELEASE | 12/28/2022

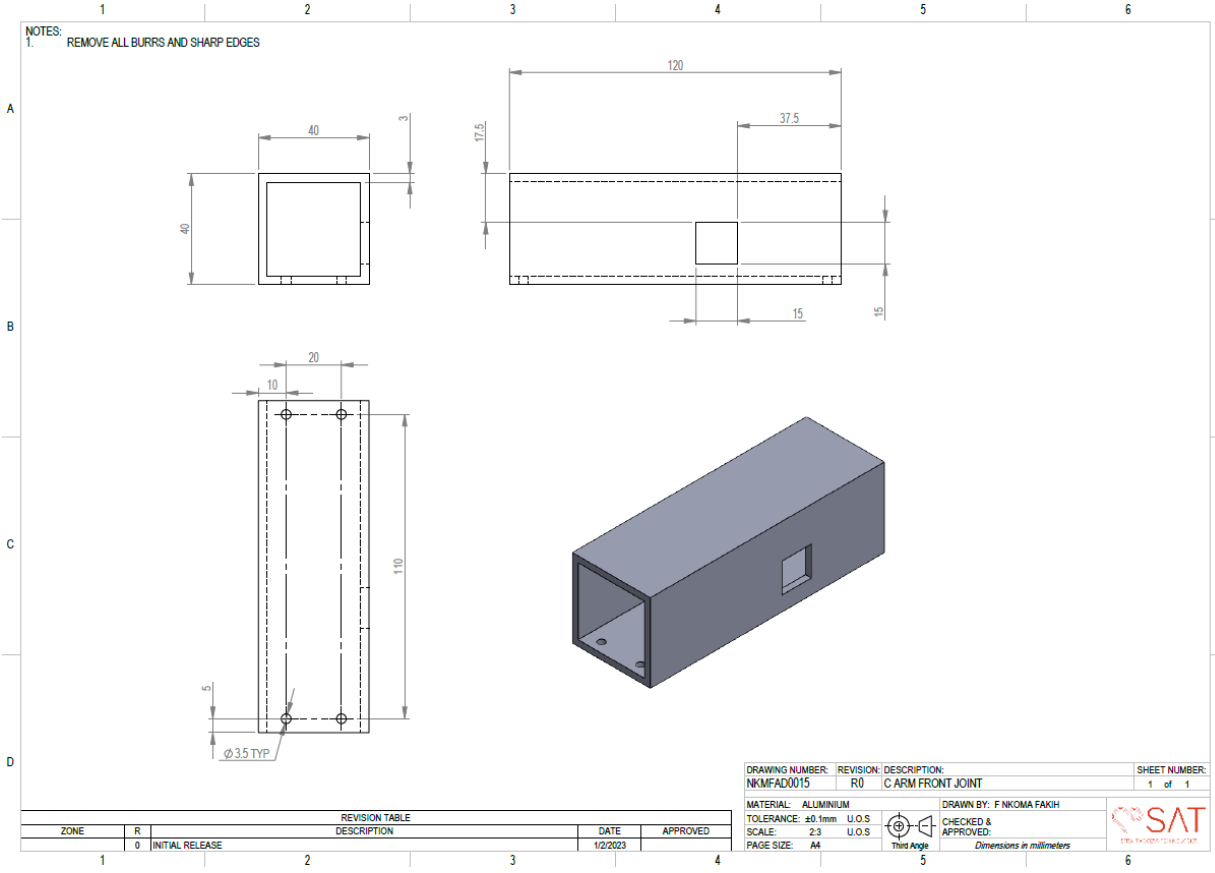
NOTES:
1. REMOVE ALL BURRS AND SHARP EDGES
120
37.5
17.5
40
40
3
15
15
20
10
110
5
Ø 3.5 TYP
DRAWING NUMBER: NKMFAD0015
REVISION: R0
DESCRIPTION: C ARM FRONT JOINT
SHEET NUMBER: 1 of 1
MATERIAL: ALUMINIUM
TOLERANCE: ±0.1mm U.O.S
SCALE: 2:3 U.O.S
PAGE SIZE: A4
Third Angle
DRAWN BY: F NKOMA FAKIH
CHECKED & APPROVED:
Dimensions in millimeters
REVISION TABLE
ZONE | R | DESCRIPTION | DATE | APPROVED
0 | INITIAL RELEASE | 1/2/2023

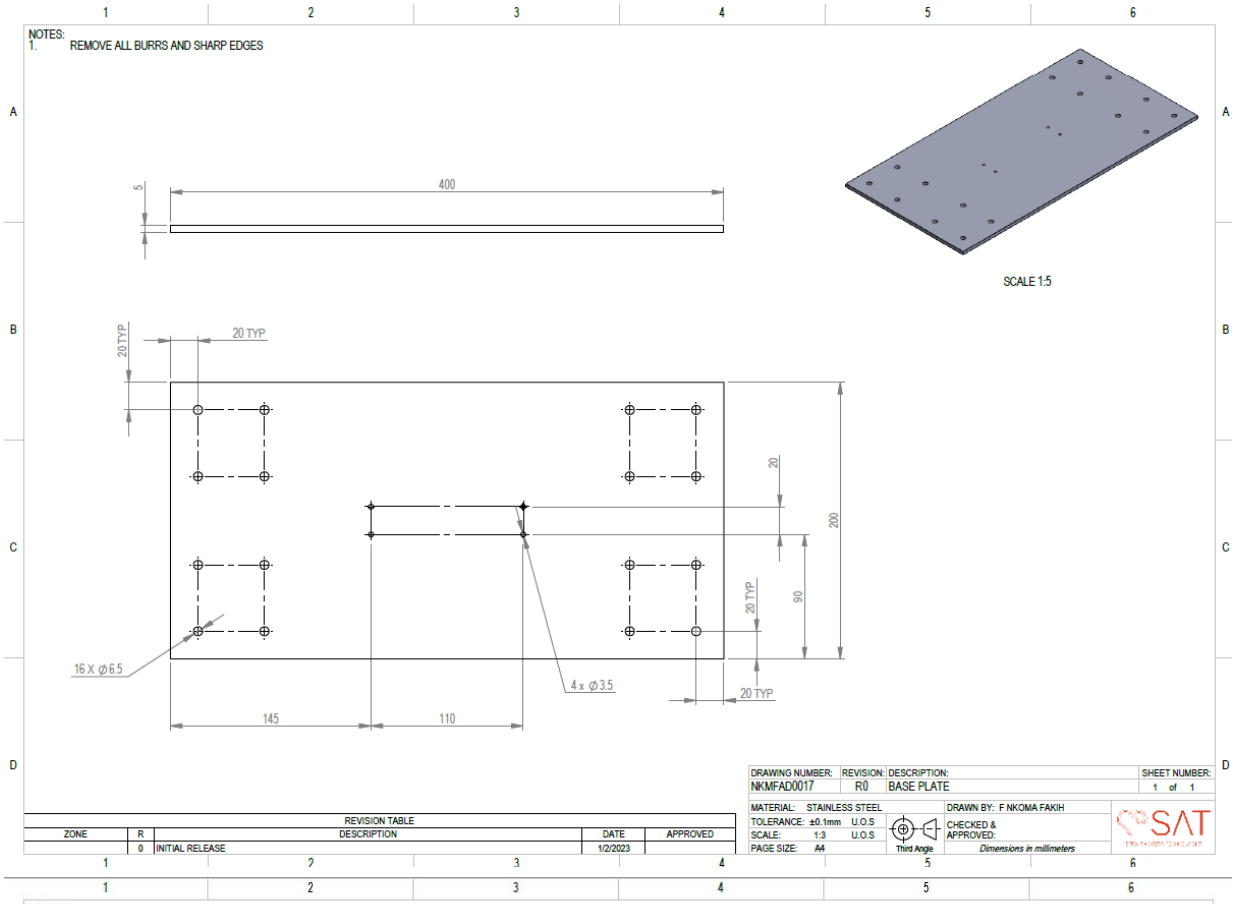
NOTES:
1. REMOVE ALL BURRS AND SHARP EDGES
400
5
SCALE 1:5
20 TYP
20 TYP
20
200
90
20 TYP
20 TYP
16 X Ø6.5
4 x Ø3.5
145
110
DRAWING NUMBER: NKMFAD0017
REVISION: R0
DESCRIPTION: BASE PLATE
SHEET NUMBER: 1 of 1
MATERIAL: STAINLESS STEEL
TOLERANCE: ±0.1mm U.O.S
SCALE: 1:3 U.O.S
PAGE SIZE: A4
DRAWN BY: F NKOMA FAKIH
CHECKED & APPROVED:
Third Angle
Dimensions in millimeters
REVISION TABLE
ZONE | R | DESCRIPTION | DATE | APPROVED
0 | INITIAL RELEASE | 1/2/2023

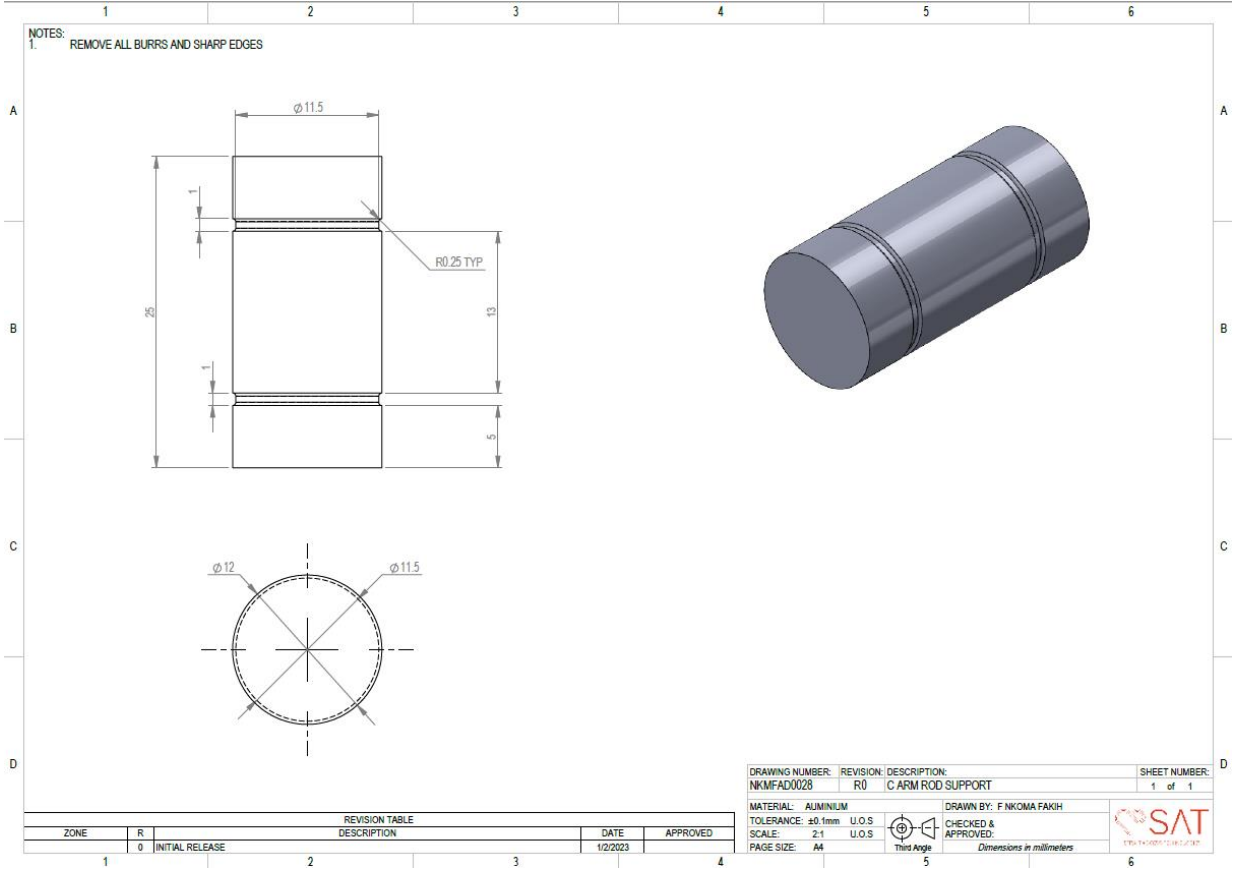
NOTES:
1. REMOVE ALL BURRS AND SHARP EDGES
Ø11.5
1
R0.25 TYP
25
13
1
5
Ø12
Ø11.5
DRAWING NUMBER: NKMFAD0028
REVISION: R0
DESCRIPTION: C ARM ROD SUPPORT
SHEET NUMBER: 1 of 1
MATERIAL: AUMINIUM
TOLERANCE: ±0.1mm U.O.S
SCALE: 2:1 U.O.S
PAGE SIZE: A4
DRAWN BY: F NKOMA FAKIH
CHECKED & APPROVED:
Third Angle
Dimensions in millimeters
REVISION TABLE
ZONE | R | DESCRIPTION | DATE | APPROVED
0 | INITIAL RELEASE | 1/2/2023

NOTES:
1. REMOVE ALL BURRS AND SHARP EDGES

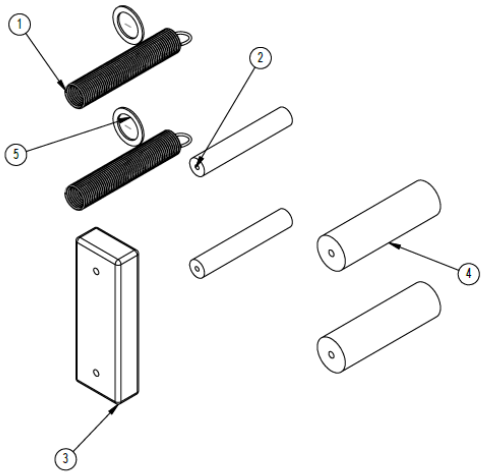

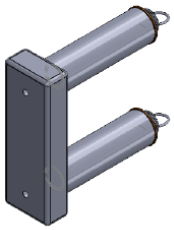

ITEM NO.	QTY.	DESCRIPTION	DRAWING NUM	ITEM NUM
1	2	SPRING	BOUGHT OUT	NKMFAD0007
2	2	SPRING STUMP	NKMFAD0009	NKMFAD0009
3	1	Spring handle	NKMFAD0010	NKMFAD0010
4	2	SPRING SHELL	NKMFAD0011	NKMFAD0011
5	2	RUBBER RING	BOUGHT OUT	NKMFAD0012

DRAWING NUMBER:	REVISION:	DESCRIPTION:	SHEET NUMBER:
NKMFAD0030	R0	HANDLE SUB ASSEMBLY	1 of 1

MATERIAL: NA		DRAWN BY: F NKOMA FAKIH
TOLERANCE: ±0.1mm	U.O.S	CHECKED & APPROVED:
SCALE: 1:2	U.O.S	Third Angle
PAGE SIZE: A4		Dimensions in millimeters

REVISION TABLE				
ZONE	R	DESCRIPTION	DATE	APPROVED
	0	INITIAL RELEASE	1/2/2023	

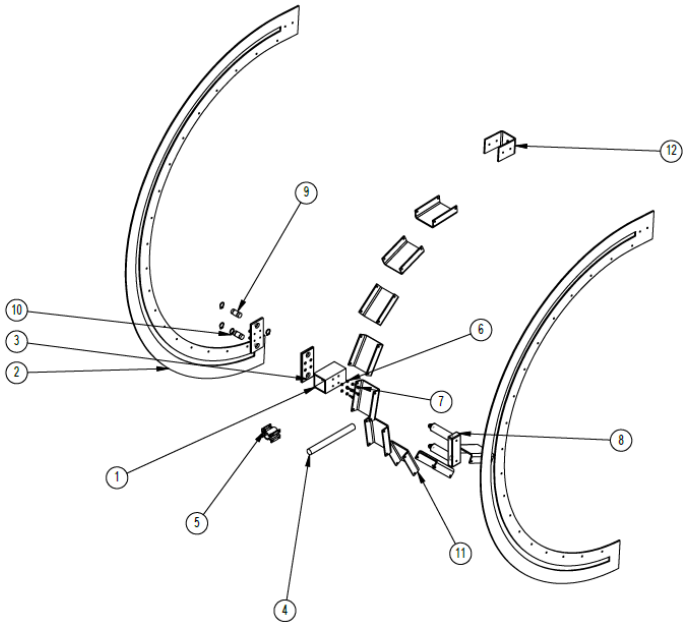

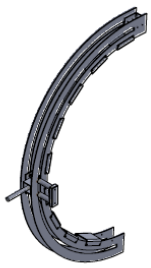

ITEM NO.	QTY.	DESCRIPTION	DRAWING NUM	ITEM NUM
1	1	C Arm Central joint	NKMFAD0006	NKMFAD0006
2	2	C Arm	NKMFAD0001	NKMFAD0001
3	2	SPRING BASE	NKMFAD0008	NKMFAD0008
4	1	HORIZONTAL SHAFT	BOUGHT OUT	NMFAD0014
5	1	TUBE CLAMP	NKMFAD0005	NKMFAD0005
6	8	M3 NUT SS	BOUGHT OUT	NKMFAD0019
7	8	M3x 10 SLOTTED CHEESE SS	BOUGHT OUT	NKMFAD0020
8	1	HANDLE SUB ASSEMBLY	NKMFAD0030	NKMFAD0030
9	2	C ARM ROD SUPPORT	NKMFAD0028	NKMFAD0028
10	4	CIRCLIP	BOUGHT OUT	NKMFAD0029
11	9	C ARM CONNECTOR	NKMFAD0032	NKMFAD0032
12	1	CAMERA STAND	NKMFAD0033	NKMFAD0033

DRAWING NUMBER:	REVISION:	DESCRIPTION:	SHEET NUMBER:
	R0		1 of 1

MATERIAL: NA		DRAWN BY: F NKOMA FAKIH
TOLERANCE: ±0.1mm	U.O.S	CHECKED & APPROVED:
SCALE: 1:10	U.O.S	Third Angle
PAGE SIZE: A4		Dimensions in millimeters

REVISION TABLE				
ZONE	R	DESCRIPTION	DATE	APPROVED
	0	INITIAL RELEASE	1/2/2023	

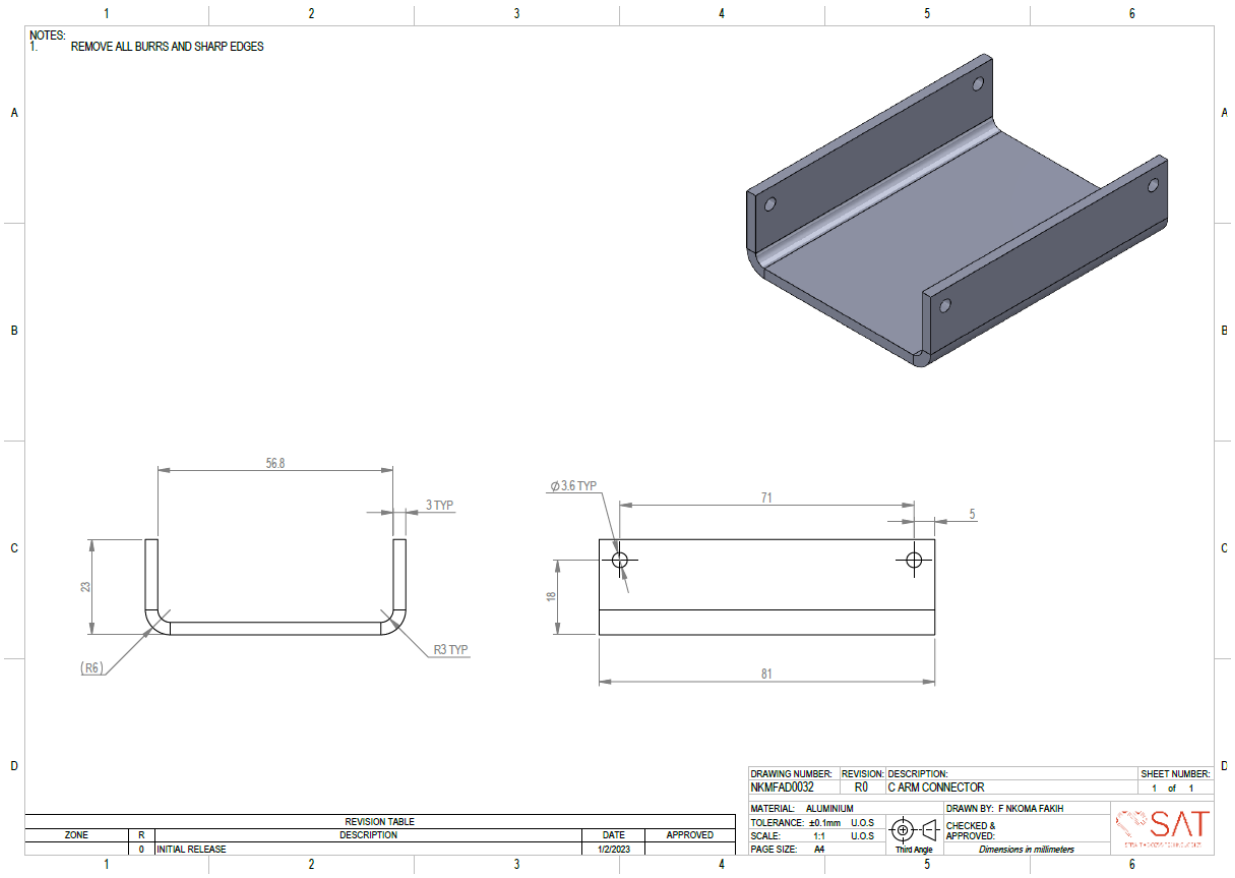
NOTES:
1. REMOVE ALL BURRS AND SHARP EDGES
56.8
3 TYP
23
R3 TYP
(R6)
Ø3.6 TYP
71
5
18
81
DRAWING NUMBER: NKMFAD0032
REVISION: R0
DESCRIPTION: C ARM CONNECTOR
SHEET NUMBER: 1 of 1
MATERIAL: ALUMINIUM
TOLERANCE: ±0.1mm U.O.S
SCALE: 1:1 U.O.S
PAGE SIZE: A4
Third Angle
DRAWN BY: F NKOMA FAKIH
CHECKED & APPROVED:
Dimensions in millimeters
REVISION TABLE
ZONE | R | DESCRIPTION | DATE | APPROVED
0 | INITIAL RELEASE | 1/2/2023

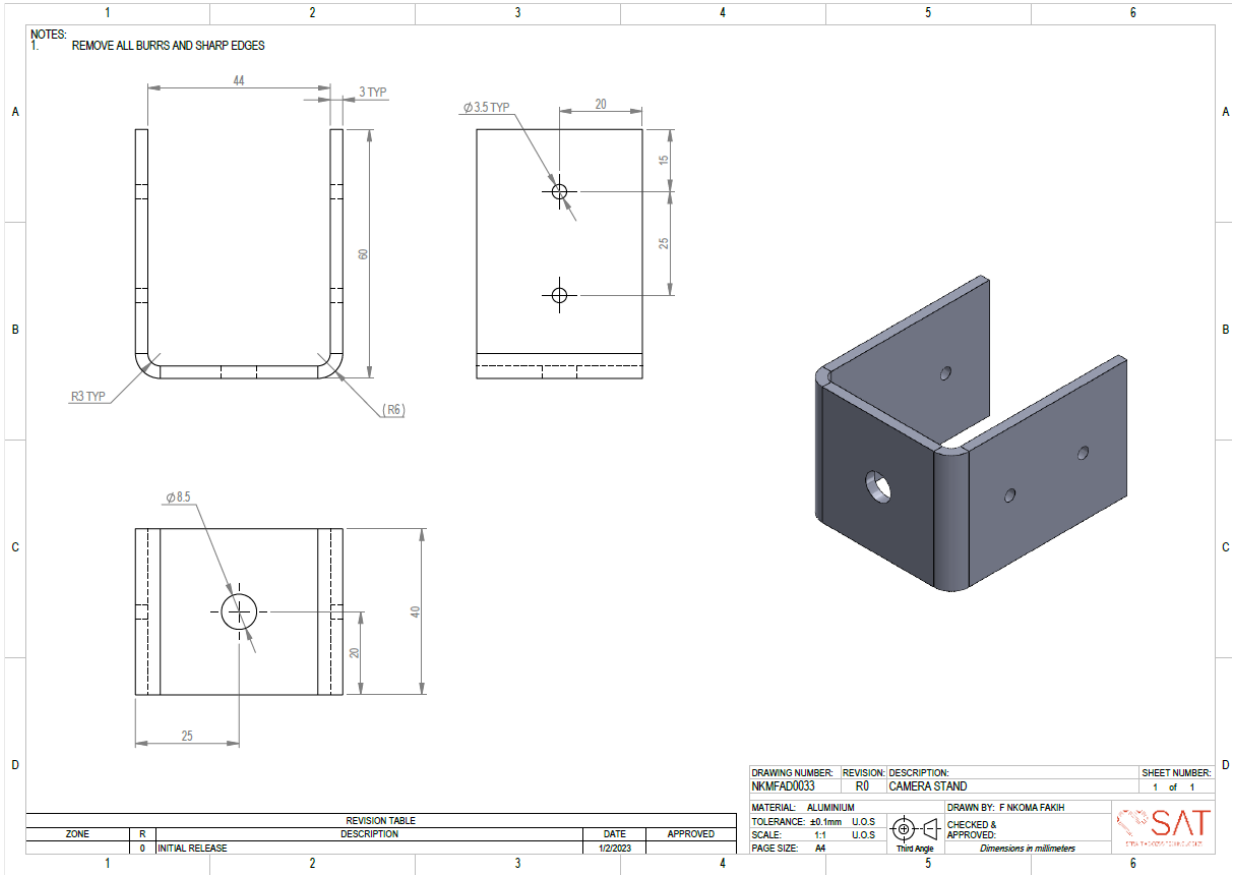
NOTES:
1. REMOVE ALL BURRS AND SHARP EDGES
44
3 TYP
60
R3 TYP
(R6)
Ø3.5 TYP
20
15
25
Ø8.5
40
20
25
DRAWING NUMBER: NKMFAD0033
REVISION: R0
DESCRIPTION: CAMERA STAND
SHEET NUMBER: 1 of 1
MATERIAL: ALUMINIUM
TOLERANCE: ±0.1mm U.O.S
SCALE: 1:1 U.O.S
PAGE SIZE: A4
Third Angle
DRAWN BY: F NKOMA FAKIH
CHECKED & APPROVED:
Dimensions in millimeters
REVISION TABLE
ZONE | R | DESCRIPTION | DATE | APPROVED
0 | INITIAL RELEASE | 1/2/2023

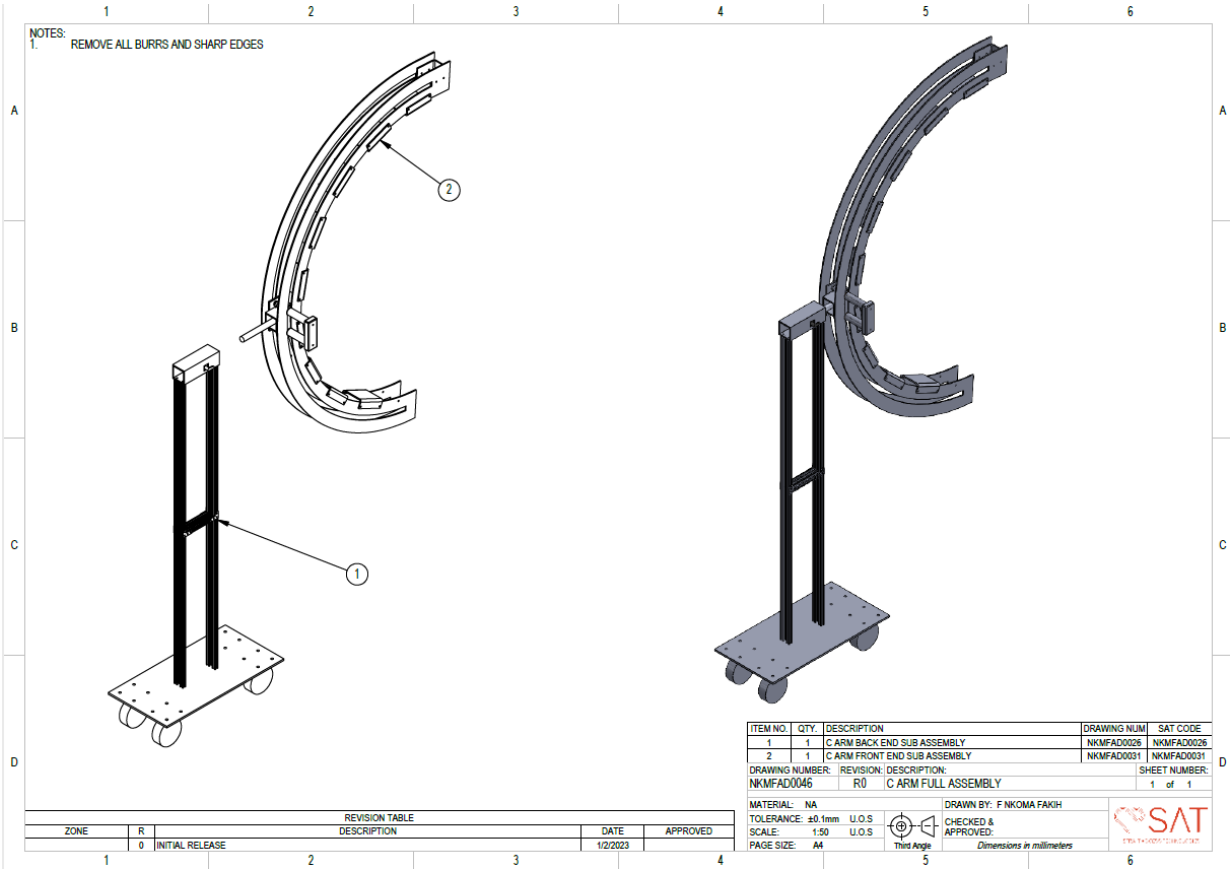
NOTES:
1. REMOVE ALL BURRS AND SHARP EDGES
2
1
ITEM NO. | QTY. | DESCRIPTION | DRAWING NUM | SAT CODE
1 | 1 | C ARM BACK END SUB ASSEMBLY | NKMFAD0026 | NKMFAD0026
2 | 1 | C ARM FRONT END SUB ASSEMBLY | NKMFAD0031 | NKMFAD0031
DRAWING NUMBER: NKMFAD0046 | REVISION: R0 | DESCRIPTION: C ARM FULL ASSEMBLY | SHEET NUMBER: 1 of 1
MATERIAL: NA
TOLERANCE: ±0.1mm U.O.S
SCALE: 1:50 U.O.S
PAGE SIZE: A4
Third Angle
DRAWN BY: F NKOMA FAKIH
CHECKED & APPROVED:
Dimensions in millimeters
REVISION TABLE
ZONE | R | DESCRIPTION | DATE | APPROVED
0 | INITIAL RELEASE | 1/2/2023

Appendix E: Arduino Code for the force sensor

```
#include <TimeLib.h>
#include <Arduino.h>


//PCB Mark   Arduino Pin
//D0   (0)
//D1   (1)
//NA   (2)
//NA   (3)
//D4   (4)
//D5   (5)
//D6   (6)
//D7   (7)
//D8   (8)
//D9   (9)
//D10  (10)
//D11  (11)
//D12  (12)
//D13  (13)
//A0   (14)
#define SENSOR
//A1   (15)
#define Red_LED 15
//A2   (16)
#define Green_LED 16
//A3   (17)
#define Blue_LED 17
//A4   (18)
//A5   (19)
//SDA  (20)
//SCL  (21)
//MISO (22)
//MOSI (23)
//SCK  (24)



//--------------------------------
// Heartbeat LED Variables
//--------------------------------
long last_sensor_time = 0;
long sensor_cycle_time = 100;
boolean sensor_pwm_direction = false;
//--------------------------------

int sensorValue = 0;
int sensorValueOld = 0;

void setup() {


  //============================================================
  // UART Setup
  //------------------------------------------------------------
  // put your setup code here, to run once:
  Serial.begin(9600);
 // while (!Serial);
  //============================================================
  // Analog & Digital I/O Setup
  //------------------------------------------------------------
  pinMode(A0, INPUT);
  pinMode(Red_LED, OUTPUT);
  pinMode(Blue_LED, OUTPUT);
  pinMode(Green_LED, OUTPUT);
//============================================================
```

```
  digitalWrite(Red_LED, LOW);
  digitalWrite(Green_LED, LOW);
  digitalWrite(Blue_LED, LOW);

}

void loop()
{
  yield();
  read_sensor();
}

void read_sensor()
{
  long current_sensor_time = millis();

  if ((current_sensor_time - last_sensor_time) >= sensor_cycle_time)
  {
    Serial.println("-");
    last_sensor_time = current_sensor_time;
    analogReadResolution(12);
    sensorValue = analogRead(A0);



    if(sensorValue > 4095)
    {
      sensorValue = 0;
    }

     if(sensorValue != sensorValueOld)
     {
      sensorValueOld = sensorValue;

      float Vref = 3.3;
      float SensorRange = 4095;
      float sensorValueFlt = float(sensorValue);
      float base = ((Vref*30000)/((sensorValueFlt/SensorRange)*Vref)) - 30000;
      float exponent = 0 - 1.34;
      float power_result = pow(base,exponent);
      float ForceN = (140235.1236)*(power_result);

      Serial.println("Sensor Value: " +String(sensorValueFlt));
      Serial.println("Force (N): " + String(ForceN));

        int Blue_Value = 0;
        int Green_Value = 0;
        int Red_Value = 0;

      if(ForceN <= 7.39)
      {
        // Blue
        Blue_Value = 128;
        Green_Value = 0;
        Red_Value = 0;
      }
      else if(ForceN <= 17.96)
      {
        //Green
        Blue_Value = 0;
        Green_Value = 128;
        Red_Value = 0;
      }
      else if(ForceN > 17.96)
      {
        //Red
        Blue_Value = 0;
        Green_Value = 0;
        Red_Value = 128;
      }
        analogWrite(Blue_LED, Blue_Value);
```

```
      analogWrite(Green_LED, Green_Value);
      analogWrite(Red_LED, Red_Value);
    }
  }
}
```